

# **ANALYSIS OF PENETRATION, MICROSTRUCTURE AND MECHANICAL PROPERTIES OF SOME NON – FERROUS ALLOYS USING GTAW PROCESS**

A THESIS SUBMITTED IN FULFILLMENTS OF REQUIREMENTS FOR THE AWARD OF THE  
DEGREE OF

**DOCTOR OF PHILOSOPHY**

*BY*

**PAWAN KUMAR**

*SUPERVISION OF*

**DR. C. K. DATTA**



**DEPARTMENT OF PRODUCTION AND INDUSTRIAL ENGINEERING  
FACULTY OF TECHNOLOGY, UNIVERSITY OF DELHI  
DELHI – 110042 (INDIA)**

**2012**

## **CERTIFICATE**

This is to certify that the thesis entitled “**ANALYSIS OF PENETRATION, MICROSTRUCTURE AND MECHANICAL PROPERTIES OF SOME NON FERROUS ALLOYS USING GTAW PROCESS**” being submitted by Mr. Pawan Kumar, to the Department of Production and Industrial Engineering, Faculty of Technology, University of Delhi, in fulfillment of the requirements for the award of the degree of “**DOCTOR OF PHILOSOPHY**”, is a record of bonafide research work carried out by him. He has worked under my guidance and supervision, and has fulfilled the requirements for submission of this thesis, which has reached the requisite standard required for a Ph.D degree of the University of Delhi. The results obtained in this thesis have not been submitted, in part or in full, to any other university or institute for the award of any degree or diploma.

Dr. C. K. Datta, Professor  
Department of Production and Industrial Engineering  
Delhi College of Engineering,  
Delhi - 110042

**Supervisor**

Prof. Raj Senani  
Head, Department of Production and Industrial Engineering,  
Faculty of Technology,  
University of Delhi, Delhi

## **ACKNOWLEDGEMENTS**

1. I would like to express my sincere gratitude to Dr. C K Datta, Professor Department of Production Engg, Delhi College of Engineering for his unstinted, wholehearted support and able guidance coupled with moral support throughout the entire period of my research work, without which it would not have been possible to accomplish this work. I am also extremely grateful to all faculty and staff members of the Mechanical Engineering Department of the college, especially to Dr. S K Garg and Dr. B D Pathak for their continual guidance and encouragement during some trying moments of this study.
2. I would also like to place on records my sincere appreciation and gratitude to Mr. R C Singh, Mr. Sanjay Kumar Singh, Dr. Kishor P Kolhe, Mr. Vinay Bhardwaj, Mr. S P Sharma and Mr. KB Gondhale for extending all the assistance in conducting various associated experiments. I will also like to thank all other research scholars of Delhi College of Engineering for their encouragement and cooperation during this research work. I am also grateful to all the respondents, who spared their valuable time and effort to not only, respond to the exhaustive questionnaires designed for this study, but also for their valuable suggestions and benevolent critique.
3. I would like to express my gratitude to Sh. Manmohan Singh, Director VRDE for his wholehearted support, guidance and encouragement. I cannot forget the contributions of Dr. S B Singh—Principal Associate Director who constantly motivated me and gave valuable inputs towards my project work. I would also like to thank Col G S Radkar, Mr. R Ranjan, Mr. P K Verma, Mr. D S Bhujbal and also the other staff members of VRDE (Defence Research and Development Orgn) Ahmednagar, who assisted me especially for experimentation, testing and thesis writing for this work.
4. Lastly but not the least I would like to thank my family members for their untiring patience, understanding, encouragement and support in my research work.

**(Pawan Kumar)**

## **ABSTRACT**

Gas Tungsten Arc Welding process (GTAW) is the best preferred welding process for high strength aluminium and titanium alloys due easier adaptability and better economy. In pulse GTAW process, the current is supplied in pulses rather than at constant amplitude. Arc pulsing is mainly used for achieving better penetration without excessive heat built-up and joining of lesser thickness plates. The better heat input control of pulsing makes this process best suitable for welding of precision parts.

The pulse process parameters like pulse current, base current, pulse frequency and pulse duty cycle, have the most important role for optimizing the bead geometry characteristics and mechanical properties of the weld. The pulses of higher current are found to generate a large variation of pressure in the arc. The arc pressure causes the turbulence in the weld pool, which allows the heat to penetrate deeper into the base metal. The amount of the base current affects the rate of cooling and solidification. Higher pulse duty cycle indicates the tendency towards continuous current. Arc pulsation is the most responsible factor for grain refinement, lesser risk of cracking, reduction in width of HAZ and less distortion. The present research work replicates the application of GTAW process for joining of aluminium and titanium alloys with sinusoidal AC wave.

Aluminium alloy 7039 (AA7039) is a heat treatable and weldable aluminium-4.5% Zinc-2.5% magnesium alloy. A demand for lighter and stronger aluminium armor for protection against high explosive shell fragments in the early 1960s led to the introduction of this alloy. Magnesium is alloyed with aluminium for increasing mechanical properties, corrosion resistance and easy machinability. Zinc is usually added to improve mechanical properties through formation of hard intermediate phase, such as  $Mg_2Zn$ . AA7039 aluminium alloys are widely used in aircraft structural applications and are susceptible to localized corrosion in chloride environments.

AA6061 aluminium alloy (Al-Mg-Si alloy) has gathered wide acceptance in fabrication of food equipments, chemical containers, passenger cars, road tankers and railway transportation systems. In any structural application of this alloy consideration its weldability is of utmost importance as welding is largely used for joining of structural components. The preferred welding process of aluminium alloy is frequently Pulsed GTAW due to its comparatively easier applicability and better economy. Pulsed parameters improve the mechanical properties of the welds of this alloy due to grain refinement occurring in the fusion zone.

Titanium has high melting point and can be alloyed with Al, Sn, V, Mo etc. Some of which are known as Alpha-stabilizing elements and others as Beta-stabilizing elements. However Titanium is an expensive metal. Titanium and its alloys have been considered as one of the best engineering metals for industrial applications due to the excellent combination of properties such as elevated strength to weight ratio, high toughness, excellent resistance to corrosion and good fatigue properties. Titanium alloy grade-5 (Ti-6Al-4V) has gathered wide acceptance in fabrication of vessels, blades, discs, military vehicle armors, airframes, rings, fasteners, forgings and biomedical implants.

In this research work, the effects of various current and frequencies of GTAW process on bead geometry (bead penetration, bead width and bead height) and mechanical properties (UTS, microhardness and percentage elongation) of AA7039 have been studied. Also optimization of pulse process parameters with and without gas mixtures have carried out for bead geometry and mechanical properties of AA7039, AA6061 and Ti alloy Grade-5. Also variation of microhardness and metallurgical studies of the above welded alloys have been carried out at various process parameters.

# ***CONTENTS***

| <b>Chapter</b>   | <b>Page No.</b>    |
|--|--------------------|
| Acknowledgement  | i                  |
| Abstract   | iii                |
| Contents   | v                  |
| List of Nomenclature                                       | ix                 |
| List of Tables   | xiii               |
| List of Figures  | xvii               |
| <br><b>Chapter – 1: Introduction</b>                       | <br><b>1 - 20</b>  |
| 1.1 GTAW Process   | 1                  |
| 1.2 Aluminium Alloys                                       | 5                  |
| 1.2.1 Characteristics of Aluminium and Aluminium Alloys    | 8                  |
| 1.2.2 Temper Designations of Aluminium Alloys              | 8                  |
| 1.2.3 Aluminium Alloy Designation System                   | 10                 |
| 1.2.4 Heat Treatability of Aluminium Alloys                | 11                 |
| 1.2.5 Characteristics of Principal Aluminium Alloys Groups | 12                 |
| 1.3 Titanium and Titanium Alloys                           | 13                 |
| 1.4 Selection of Welding Processes                         | 16                 |
| 1.5 Bead Geometry Studies                                  | 18                 |
| 1.6 Mechanical Properties Studies                          | 20                 |
| 1.7 Metallurgical Studies                                  | 20                 |
| <br><b>Chapter – 2: Review of Literature</b>               | <br><b>21 - 56</b> |
| 2.1 Introduction   | 21                 |
| 2.2 Welding of Aluminium Alloys                            | 21                 |
| 2.3 Welding of Titanium Alloys                             | 25                 |
| 2.4 Pulsed GTAW Process Parameters and Their Relationship  | 28                 |
| 2.5 Bead Geometry and Shape Relationship                   | 32                 |

|  |   |                 |
|--|---|-----------------|
| 2.6  | Mechanical Properties and Metallurgical Transformation          | 38              |
| 2.7  | Objective of Present Thesis                                     | 56              |
| <b>Chapter – 3: Experimental Details</b>                         |   | <b>57 - 75</b>  |
| 3.1  | Introduction  | 57              |
| 3.2  | The Process   | 57              |
| 3.3  | Equipment Used  | 59              |
| 3.4  | Base Metal  | 62              |
| 3.5  | Filler Metal  | 62              |
| 3.6  | Shielding Gases   | 63              |
| 3.7  | Bead Geometry Measurement                                       | 64              |
| 3.8  | Hardness Measurement  | 66              |
| 3.9  | Measurement of Tensile Strength and Percentage Elongation       | 68              |
| 3.10   | Metallographic Examination                                      | 71              |
| <b>Chapter – 4: Parametric Study of Gas Tungsten Arc Welding</b> |   | <b>77 - 93</b>  |
| 4.1  | Introduction  | 77              |
| 4.2  | Experimental Procedure  | 79              |
| 4.2.1  | Experimentation on Aluminium Alloy 7039 (Without Pulsing)       | 80              |
| 4.2.2  | Experimentation on Aluminium Alloy 7039 (With Pulsing)          | 82              |
| 4.2.3  | Experimentation on Aluminium Alloy 6061                         | 84              |
| 4.2.4  | Experimentation on AA 6061 and AA 7039 (With Gas Mixtures)      | 89              |
| 4.2.5  | Experimentation on Titanium Alloy Grade – 5 (With Gas Mixtures) | 92              |
| <b>Chapter – 5: Results and Discussion</b>                       |   | <b>95 - 155</b> |
| 5.1  | Introduction  | 95              |
| 5.2  | Experimentation on Aluminium Alloy 7039 (Without Pulsing)       | 95              |
| 5.3  | Experimentation on Aluminium Alloy 7039 (With Pulsing)          | 105             |
| 5.4  | Experimentation on Aluminium Alloy 6061                         | 118             |

|   |   |                  |
|---|---|------------------|
| 5.4.1   | Bead Geometry – Experimental Results and Analysis             | 118              |
| 5.4.2   | Mechanical Properties – Experimental Results and Analysis     | 121              |
| 5.5   | Experimentation on Aluminium Alloy 6061 with Gas Mixtures     | 127              |
| 5.5.1   | Bead Geometry – Experimental Results and Analysis             | 127              |
| 5.5.2   | Mechanical Properties – Experimental Results and Analysis     | 131              |
| 5.6   | Experimentation on Aluminium Alloy 7039 with Gas Mixtures     | 136              |
| 5.6.1   | Bead Geometry – Experimental Results and Analysis             | 136              |
| 5.6.2   | Mechanical Properties – Experimental Results and Analysis     | 140              |
| 5.7   | Experimentation on Titanium Alloy Grade - 5 with Gas Mixtures | 147              |
| 5.7.1   | Bead Geometry – Experimental Results and Analysis             | 147              |
| 5.7.2   | Mechanical Properties – Experimental Results and Analysis     | 150              |
| <b>Chapter – 6: Conclusions and Scope of the Future Study</b> |   | <b>157 - 160</b> |
| A.  | Conclusions   | 157              |
| B.  | Scope of the Future Study                                     | 160              |
| <b>References</b>   |   | <b>161 - 169</b> |

## ***List of Nomenclature***

|      |  |
|------|--|
| GTAW | Gas Tungsten Arc Welding   |
| GMAW | Gas Metal Arc Welding  |
| TIG  | Tungsten Inert Gas   |
| MIG  | Metal Inert Gas  |
| AC   | Alternating Current  |
| Al   | Aluminium  |
| AA   | Aluminium Alloy  |
| Ti   | Titanium   |
| SS   | Stainless Steel  |
| Mg   | Magnesium  |
| Si   | Silicon  |
| Zn   | Zinc   |
| Cu   | Copper   |
| V    | Vanadium   |
| Mn   | Manganese  |
| DC   | Direct Current   |
| DCEN | Direct Current Electrode Negative                                      |
| DCEP | Direct Current Electrode Positive                                      |
| AWS  | American Welding Society   |
| ISO  | International Organization of Standardization                          |
| DIN  | Deutsches Institute fur Normung (German Institute for Standardization) |
| Ar   | Argon  |
| He   | Helium   |
| eV   | Electron Volt  |
| EC   | Electric-Conductor   |
| ASTM | American Society for Testing and Materials                             |
| ANSI | American National Standards Institute                                  |

|            |  |
|------------|--|
| SAE        | The Society of Automotive Engineers              |
| P          | Pulse / Peak Current                             |
| B          | Base / background / secondary current            |
| F          | Frequency / Pulse Frequency                      |
| T          | Pulse Duty Cycle                                 |
| X          | Percentage of Helium in Argon–Helium mixture     |
| DP         | Double Pulse                                     |
| p          | Bead penetration                                 |
| b          | Bead width                                       |
| h          | Bead height                                      |
| b/p (WPSF) | Weld penetration shape factor                    |
| MTM        | Modified Taguchi Method                          |
| FZ         | Fusion Zone                                      |
| HAZ        | Heat Affected Zone                               |
| A / Amp    | Ampere   |
| UTS        | Ultimate Tensile Strength                        |
| UTM        | Universal Testing Machine                        |
| MPa        | Mega Pascal                                      |
| Hz         | Hertz  |
| VPN / VHN  | Vickers Pyramid Number / Vickers Hardness Number |
| HV         | Vickers Hardness                                 |
| PWHT       | Post Weld Heat Treatment                         |
| EWTh       | Thoriated Tungsten type Electrode                |
| TWB        | Tailor Welded Blank                              |
| DSAW       | Double Sided Arc Welding                         |
| ANOVA      | Analysis of variance                             |
| PMZ        | Partially Melted Zone                            |
| GB         | Grain Boundaries                                 |
| FB         | Fusion Boundary                                  |

|      |                              |
|------|------------------------------|
| Fig  | Figure                       |
| s    | Second                       |
| EDA  | Energy Dispersive Analysis   |
| SEM  | Scanning Electron Microscope |
| Kgf  | Kilogram force               |
| g/cc | Gram / Cubic Centimeter      |
| HF   | High Frequency               |
| DOE  | Design of Experiment         |
| OA   | Orthogonal Array             |
| S/N  | Signal to Noise Ratio        |
| AHP  | Analytical Hierarchy Process |
| μm   | Micrometer                   |

## ***List of Tables***

| <b>Table No.</b> | <b>Title of Table</b>   | <b>Page No.</b> |
|------------------|---|-----------------|
| Table 1.1        | Recommended Filler Metals for Various Al Alloys                     | 17              |
| Table 3.1        | Composition and Properties of AA6061                                | 63              |
| Table 3.2        | Composition and Properties of AA7039                                | 63              |
| Table 3.3        | Composition and Properties of Ti Alloy Gr-5                         | 63              |
| Table 3.4        | Chemical Composition of Filler Metals                               | 64              |
| Table 3.5        | Grain Size Measurement Method                                       | 75              |
| Table 4.1        | Recommended Tungsten Electrode Diameters                            | 78              |
| Table 4.2        | Experimental Layout for AA7039 (Without Pulsing)                    | 81              |
| Table 4.3        | Experimental Layout for AA7039 (With Pulsing)                       | 82–84           |
| Table 4.4        | Process Parameters and their limiting Values                        | 88              |
| Table 4.5        | Experimental Layout using L16 Orthogonal Array                      | 88              |
| Table 4.6        | Process Parameters and their limiting Values<br>(With Gas Mixtures) | 90              |
| Table 4.7        | Experimental Layout using L25 Orthogonal Array                      | 91              |
| Table 4.8        | Process Parameters and their limiting Values for Ti alloy           | 93              |
| Table 5.1        | Experimental results for the bead geometry of AA6061                | 119             |
| Table 5.2        | Weighted response for the bead geometry of AA6061                   | 119             |
| Table 5.3        | Results of analysis of variance for bead geometry of<br>AA6061      | 119             |
| Table 5.4        | Response table for the weld bead properties of AA6061               | 120             |
| Table 5.5        | Confirmation test results for bead geometry of AA6061               | 120             |
| Table 5.6        | Experimental results for the mechanical properties of<br>AA6061     | 122             |
| Table 5.7        | Weighted response for the mechanical properties of<br>AA6061        | 123             |
| Table 5.8        | Results of ANOVA for the mechanical properties of AA6061            | 123             |
| Table 5.9        | Response table for the mechanical properties of AA6061              | 123             |

|            |   |     |
|------------|---|-----|
| Table 5.10 | Confirmation test results for the mechanical properties of AA6061                   | 124 |
| Table 5.11 | Experimental results for the bead geometry of AA6061 with Gas mixtures              | 128 |
| Table 5.12 | Weighted response for the bead geometry of AA6061 with Gas mixtures                 | 129 |
| Table 5.13 | Results of ANOVA for bead geometry of AA6061 with Gas mixtures                      | 130 |
| Table 5.14 | Response table for the weld bead properties of AA6061 with Gas mixtures             | 130 |
| Table 5.15 | Confirmation test results for bead geometry of AA6061 with Gas mixtures             | 130 |
| Table 5.16 | Experimental results for the mechanical properties of AA6061 with gas mixtures      | 132 |
| Table 5.17 | Weighted response for the mechanical properties of AA6061 with gas mixtures         | 133 |
| Table 5.18 | Results of ANOVA for the mechanical properties of AA6061 with gas mixtures          | 133 |
| Table 5.19 | Response table for the mechanical properties of AA6061 With gas mixtures            | 133 |
| Table 5.20 | Confirmation test results for the mechanical properties of AA6061 with gas mixtures | 135 |
| Table 5.21 | Experimental results for the bead geometry of AA7039 with Gas mixtures              | 137 |
| Table 5.22 | Weighted response for the bead geometry of AA7039 with Gas mixtures                 | 137 |
| Table 5.23 | Results of ANOVA for bead geometry of AA7039 with Gas mixtures                      | 138 |
| Table 5.24 | Response table for the weld bead properties of AA7039 with Gas mixtures             | 138 |

|            |   |     |
|------------|---|-----|
| Table 5.25 | Confirmation test results for bead geometry of AA7039 with Gas mixtures             | 138 |
| Table 5.26 | Experimental results for the mechanical properties of AA7039 with gas mixtures      | 141 |
| Table 5.27 | Weighted response for the mechanical properties of AA7039 with gas mixtures         | 142 |
| Table 5.28 | Results of ANOVA for the mechanical properties of AA7039 With gas mixtures          | 142 |
| Table 5.29 | Response table for the mechanical properties of AA7039 With gas mixtures            | 143 |
| Table 5.30 | Confirmation test results for the mechanical properties of AA7039 with gas mixtures | 143 |
| Table 5.31 | Experimental results for the bead geometry of Ti Alloy Gr-5                         | 147 |
| Table 5.32 | Weighted response for bead geometry of Ti Alloy Grade-5                             | 148 |
| Table 5.33 | Results of analysis of variance for bead geometry of Ti Alloy Grade - 5             | 148 |
| Table 5.34 | Response table for the weld bead properties of Ti Alloy Gr – 5                      | 148 |
| Table 5.35 | Confirmation test results for the weld bead properties of Ti Alloy Grade – 5        | 149 |
| Table 5.36 | Experimental results for mechanical properties of Ti Alloy Gr – 5                   | 151 |
| Table 5.37 | Weighted response for mechanical properties of Ti Alloy Gr – 5                      | 152 |
| Table 5.38 | Results of ANOVA for mechanical properties of Ti Alloy Gr – 5                       | 153 |
| Table 5.39 | Response table for mechanical properties of Ti Alloy Gr-5                           | 153 |
| Table 5.40 | Confirmation test results for mechanical properties of Ti Alloy Grade – 5           | 153 |

## ***List of Figures***

| <b>Figure No</b> | <b>Title of Figures</b>   | <b>Page No</b> |
|------------------|---|----------------|
| Fig 1.1          | Schematic Diagram of GTAW Process                                       | 2              |
| Fig 2.1          | Conventional and Pulsed current transients for GTAW process             | 30             |
| Fig 2.2          | Pulsed GTAW Waveforms   | 31             |
| Fig 2.3          | Schematic Diagram of Bead Profile                                       | 36             |
| Fig 2.4          | Cross Sectional Area for measurement of Bead Profile                    | 36             |
| Fig 2.5          | Nomenclature for various welding regions                                | 50             |
| Fig 2.6          | Weld Hardness Distribution of Heat Treatable Al Alloy                   | 54             |
| Fig 2.7          | Grain Growth in HAZ   | 55             |
| Fig 2.8          | Effect of Heat Input per unit length of weld                            | 55             |
| Fig 2.9          | Effect of welding on AA6061-T6 age-hardened alloy                       | 56             |
| Fig 3.1          | Schematic Diagram of GTAW Process                                       | 57             |
| Fig 3.2          | Circuit Diagram of GTAW Process   | 58             |
| Fig 3.3          | TRITON 220 AC / DC (Pulsed GTAW Machine)                                | 58             |
| Fig 3.4          | Characteristics of TRITON 220 AC / DC                                   | 60             |
| Fig 3.5          | Welding Torch / Gun of GTAW process                                     | 61             |
| Fig 3.6          | Mould Sample for Bead Geometry Measurement and Microstructural Analysis | 65             |
| Fig 3.7          | Automatic Polishing Machine   | 65             |
| Fig 3.8          | Bead Geometry Macrograph of samples                                     | 66             |
| Fig 3.9          | Surface Plate with Measuring Instruments                                | 66             |
| Fig 3.10         | Vickers Hardness Indentation  | 67             |
| Fig 3.11         | Digital Vickers Microhardness Tester                                    | 68             |
| Fig 3.12         | Computerized Universal Testing Machine                                  | 69             |
| Fig 3.13         | Digital Ultrasonic Flaw Detector  | 70             |
| Fig 3.14         | Ultrasonic Testing of Welded Samples                                    | 71             |
| Fig 3.15         | Metallurgical Microscope with Image Analyzer Software                   | 73             |

|          |   |     |
|----------|---|-----|
| Fig 3.16 | Microstructure showing Hardness Indenter                              | 74  |
| Fig 4.1  | Recommended Tungsten Electrode Shape                                  | 78  |
| Fig 4.2  | Bead-On-Plate sample  | 80  |
| Fig 4.3  | Dimensions of single “V” butt joint configuration                     | 86  |
| Fig 5.1  | Schematic Diagram of Weld Bead  | 95  |
| Fig 5.2  | Weld bead width at various currents and keeping frequencies Constant  | 96  |
| Fig 5.3  | Weld bead width at various frequencies and keeping Currents constant  | 96  |
| Fig 5.4  | Bead height at various currents and keeping frequencies Constant      | 96  |
| Fig 5.5  | Bead height at various frequencies and keeping currents constant      | 97  |
| Fig 5.6  | Bead penetration at various currents and keeping frequencies Constant | 97  |
| Fig 5.7  | Bead Penetration at various frequencies and keeping Currents constant | 97  |
| Fig 5.8  | Schematic Diagram for measurement of Microhardness for samples        | 99  |
| Fig 5.9  | Variation of Microhardness at 90 Amp                                  | 100 |
| Fig 5.10 | Variation of Microhardness at 120 Amp                                 | 100 |
| Fig 5.11 | Variation of Microhardness at 150 Amp                                 | 100 |
| Fig 5.12 | Variation of Microhardness at 180 Amp                                 | 101 |
| Fig 5.13 | Variation of Microhardness at 50 Hz                                   | 101 |
| Fig 5.14 | Variation of Microhardness at 100 Hz                                  | 101 |
| Fig 5.15 | Variation of Microhardness at 150 Hz                                  | 102 |
| Fig 5.16 | Variation of Microhardness at 200 Hz                                  | 102 |
| Fig 5.17 | Microstructure of Weld Zone, Fusion Boundary and HAZ                  | 103 |
| Fig 5.18 | Microstructure of HAZ of welded AA7039                                | 104 |
| Fig 5.19 | Microstructure of Base Metal of AA7039                                | 104 |

|          |  |     |
|----------|--|-----|
| Fig 5.20 | Effect of Pulse Duty Cycle on Bead Penetration at various Frequencies  | 105 |
| Fig 5.21 | Effect of Pulse Frequency on Bead Penetration at various Duty Cycles   | 105 |
| Fig 5.22 | Effect of Pulse Current on Bead Penetration at various Base Current    | 106 |
| Fig 5.23 | Effect of Base Current on Bead Penetration at various Pulse Current    | 106 |
| Fig 5.24 | Effect of Pulse Duty Cycle on p / b ratio at various Frequencies       | 106 |
| Fig 5.25 | Effect of Pulse Frequency on p / b ratio at various Duty cycles        | 107 |
| Fig 5.26 | Effect of Pulse Current on p / b ratio at various Base Current         | 107 |
| Fig 5.27 | Effect of Base Current on p / b ratio at various Pulse currents        | 107 |
| Fig 5.28 | Variation of Microhardness in Weld Zone at T = 50 % and F = 50 Hz      | 110 |
| Fig 5.29 | Variation of Microhardness in Weld Zone at P = 150A and B = 120 Amp    | 110 |
| Fig 5.30 | Variation of Microhardness at various Pulse Duty Cycles and F = 50 Hz  | 110 |
| Fig 5.31 | Variation of Microhardness at various Pulse Duty Cycles and F = 100 Hz | 111 |
| Fig 5.32 | Variation of Microhardness at various Pulse Duty Cycles and F = 150 Hz | 111 |
| Fig 5.33 | Variation of Microhardness at various Pulse Duty Cycles and F = 200 Hz | 111 |
| Fig 5.34 | Variation of Microhardness at various Pulse Duty Cycles and F = 250 Hz | 112 |

|          |   |     |
|----------|---|-----|
| Fig 5.35 | Variation of Microhardness at various Pulse Frequencies<br>and T = 10 % | 112 |
| Fig 5.36 | Variation of Microhardness at various Pulse Frequencies<br>and T = 30 % | 112 |
| Fig 5.37 | Variation of Microhardness at various Pulse Frequencies<br>and T = 50 % | 113 |
| Fig 5.38 | Variation of Microhardness at various Pulse Frequencies<br>and T = 70 % | 113 |
| Fig 5.39 | Variation of Microhardness at various Pulse Frequencies<br>and T = 90 % | 113 |
| Fig 5.40 | Variation of Microhardness at various Base Current and<br>P = 125 Amp   | 114 |
| Fig 5.41 | Variation of Microhardness at various Base Current and<br>P = 150 Amp   | 114 |
| Fig 5.42 | Variation of Microhardness at various Base Current and<br>P = 175 Amp   | 114 |
| Fig 5.43 | Variation of Microhardness at various Base Current and<br>P = 200 Amp   | 115 |
| Fig 5.44 | Variation of Microhardness at various Base Current and<br>P = 220 Amp   | 115 |
| Fig 5.45 | Variation of Microhardness at various Pulse Current and<br>B = 40 Amp   | 115 |
| Fig 5.46 | Variation of Microhardness at various Pulse Current and<br>B = 60 Amp   | 116 |
| Fig 5.47 | Variation of Microhardness at various Pulse Current and<br>B = 80 Amp   | 116 |
| Fig 5.48 | Variation of Microhardness at various Pulse Current and<br>B = 100 Amp  | 116 |
| Fig 5.49 | Variation of Microhardness at various Pulse Current and<br>B = 120 Amp  | 117 |

|          |   |     |
|----------|---|-----|
| Fig 5.50 | Microstructure of Pulsed GTA Welded AA7039                                  | 117 |
| Fig 5.51 | Weld Zone Microstructure (Pulsed GTA Welded – AA7039)                       | 118 |
| Fig 5.52 | Response Graph for Bead Geometry Properties of AA6061                       | 120 |
| Fig 5.53 | Response Graph for Mechanical Properties of AA6061                          | 124 |
| Fig 5.54 | Microstructures of weld zone of GTA welded AA6061                           | 126 |
| Fig 5.55 | Microstructures of HAZ and weld zone of GTA welded AA6061                   | 126 |
| Fig 5.56 | Schematic Diagram of Weld Groove and Bead                                   | 127 |
| Fig 5.57 | Response Graph for Bead Geometry Properties of AA6061 With gas mixtures     | 131 |
| Fig 5.58 | Response Graph for Mechanical Properties of AA6061 With gas mixtures        | 135 |
| Fig 5.59 | Response Graph for Bead Geometry Properties of AA7039 With gas mixtures     | 139 |
| Fig 5.60 | Response Graph for Mechanical Properties of AA7039 With gas mixtures        | 143 |
| Fig 5.61 | Microstructure of welded AA7039 at HAZ, Fusion Boundary and Weld Zone       | 144 |
| Fig 5.62 | Microstructure of HAZ of welded AA7039 (100x)                               | 145 |
| Fig 5.63 | Grain Size ( $\mu\text{m}$ ) Frequency Distribution of HAZ of welded AA7039 | 145 |
| Fig 5.64 | Microstructure of welded AA7039 at Weld Zone                                | 146 |
| Fig 5.65 | Grain Size ( $\mu\text{m}$ ) Frequency Distribution of AA7039 at Weld Zone  | 146 |
| Fig 5.66 | Response Graph for Bead Geometry Properties of Ti Alloy Gr–5                | 149 |
| Fig 5.67 | Response Graph for Mechanical Properties of Ti Alloy Grade–5                | 154 |
| Fig 5.68 | Optical micrographs of Ti Alloy Grade – 5 at Fusion Zone                    | 155 |

## **Chapter 1**

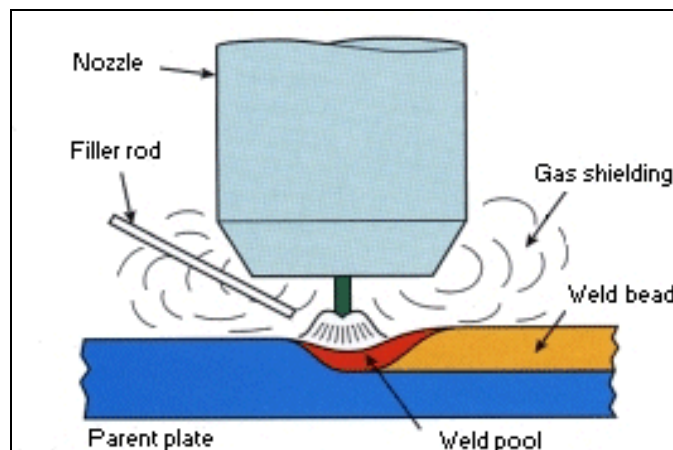
### **INTRODUCTION**

#### **1.1 GTAW Process**

Gas Tungsten Arc Welding (GTAW), also known as Tungsten Inert Gas (TIG) welding, is an arc welding process that uses a non consumable tungsten electrode to produce the weld. The weld area is protected from atmospheric contamination by a shielding gas (usually an inert gas such as argon) and a filler metal is normally used. A constant-current welding power supply produces energy which is conducted across the arc. Arc is an important ingredient in electric circuit of welding and the portion of circuit in which temperature is generated and transferred to workpiece [1].

The preferred polarity of the GTAW system depends largely on the type of metal being welded. Direct current with a negatively charged electrode (DCEN) is often employed when welding steels, nickel, titanium, and other metals. It can also be used in GTA welding of aluminum or magnesium when helium is used as a shielding gas. The negatively charged electrode generates heat by emitting electrons which travel across the arc, causing thermal ionization of the shielding gas and increasing the temperature of the base material. The ionized shielding gas flows toward the electrode, not the base material. Direct current with a positively charged electrode (DCEP) is less common in welding and is used primarily for shallow welds since less heat is generated in the base material. Instead of flowing from the electrode to the base material, as in DCEN, electrons go the other direction, causing the electrode to reach very high temperatures. For maintaining good weld geometry and prevent softening, a larger diameter electrode is generally preferred. As the electrons flow toward the electrode, ionized shielding gas flows back toward the base material, cleaning the weld by removing oxides and other impurities and thereby improving its quality and appearance.

Alternating current (AC), commonly used for welding of aluminium and magnesium, combines the two direct currents by making the electrode and base material alternate between positive and negative charge. This causes the electron flow to switch directions constantly, preventing the tungsten electrode from overheating while maintaining the heat in the base material. Surface oxides are still removed during the electrode-positive portion of the cycle and the base metal is heated more deeply during the electrode-negative portion of the cycle. At the highest welding currents, the maximum temperature occurs at an intermediate point between the electrode tip and collet [2].



**Fig 1.1: Schematic Diagram of GTAW Process**

The electrode used in GTAW is made of tungsten or a tungsten alloy, because tungsten has the highest melting temperature (3422 °C) among pure metals [3]. As a result, the electrode is not consumed during welding, though some erosion (called burn-off) can occur. Electrodes can have either a clean finish or a ground finish, clean finish electrodes have been chemically cleaned, while ground finish electrodes have been ground to a uniform size and have a polished surface, making them optimal for heat conduction. The diameter of the electrode can vary between 0.5 and 6.4 mm and their length can range from 75 to 610 mm [4].

A number of tungsten alloys have been standardized by the International Organization for Standardization and the American Welding Society in ISO

6848 and AWS A5.12, respectively. Cerium oxide (or ceria) as an alloying element improves the arc stability and the ease of starting while decreasing burn-off. Using an alloy of lanthanum oxide (or lanthana) has a similar effect. Thorium oxide (or thoria) alloy electrodes were designed for DC applications and can withstand somewhat higher temperatures while providing many of the benefits of other alloys.

Filler metals are also used in nearly all applications of GTAW, the major exception being the welding of thin materials. Filler metals are available with different diameters and are made of a variety of materials. In most cases, the filler metal in the form of a rod is added to the weld pool manually, but some applications call for an automatically fed filler metal, which often are stored on spools or coils. If no filler metals are added, the type of welding is autogenous weld.

Shielding gases are necessary in GTAW to protect the welding area from atmospheric gases such as nitrogen and oxygen, which can cause fusion defects, porosity and weld metal embrittlement if they come in contact with the electrode, the arc, or the welding metal. The gas also transfers heat from the tungsten electrode to the metal and it helps in starting and maintaining a stable arc.

The selection of a shielding gas depends on several factors, including the type of material being welded, joint design and desired final weld appearance. Argon (Ar) is the most commonly used shielding gas for GTAW process when using with AC because of easier initiation of arc, greater arc cleaning action, high weld quality and lower porosity levels [5]. Another common shielding gas – helium (He), is the most often used to increase the weld penetration in a joint, to increase the welding speed and to weld metals with high heat conductivity, such as copper and aluminum. The disadvantage of the helium gas is that in the absence of arc cleaning, the edges of the weld pool are not clearly delineated and the joint faces must be carefully cleaned prior to welding to reduce the attendant risk of oxide inclusions and porosity [6].

Argon-helium mixtures are also frequently utilized in GTAW, since they can increase control of heat input while maintaining the benefits of using argon. These mixtures increase the speed and quality of the AC welding of aluminum, and also make it easier to strike an arc [7]. The weld penetration was increased with gases having a high first ionization potential, because of voltage and thus heat input was increased. Helium, due to its high first ionization potential (24.5 eV), produced deeper fusion zones than argon (15.9 eV). When 1% hydrogen was added to either Ar or He, the fusion zones were more penetrating with the monatomic gases only. Minor additions of hydrogen to Ar or He could be recommended to increase melting [8].

Excessive flow rates of shielding gases cause turbulence in gas stream, which may aspirate atmospheric contamination into the weld pool. Turbulence in gas flow system can cause instabilities in the welding arc. Sharp bends, sharp edges and massive volume change in the gas supply system may cause turbulence in the gas flow. A good rule of thumb is to have approximately 5:1 reduction ratio between the inlet diameters of the supply line to the outlet diameter to the torch hose to ensure a laminar flow [9].

Aluminum is most often welded using alternating current GTAW but the use of direct current is also possible, depending on the properties desired. Before welding, the work area should be cleaned and may be preheated to 175 to 200 °C to improve penetration and increase travel speed. AC current can provide a self-cleaning effect, removing the thin refractory aluminium oxide (sapphire) layer that forms on aluminium metal within minutes of exposure to air. This oxide layer must be removed for welding to occur. When AC is used, pure tungsten electrodes or zirconiated tungsten electrodes are preferred to thoriated electrodes, as the latter are more likely to spit electrode particles across the welding arc into the weld. Blunt electrode tips are preferred and pure argon shielding gas should be employed for thin workpieces. Introducing helium allows for greater penetration in thicker workpieces, but can make arc starting difficult.

Nonferrous alloys are alloys that are the byproducts of nonferrous metals such as aluminum, cobalt, lead, magnesium, titanium and zinc. By definition, a nonferrous alloy is an alloy that does not intentionally contain iron. In general, nonferrous alloys are invested with non-magnetic properties, have better strength, lightweight and resistant to chemical and atmospheric corrosion. These properties make them a favored choice for several commercial and non-commercial uses, including automobile and aircraft parts, communication equipment, water valves, musical instruments and the manufacturing of flammables and explosives.

Aluminum alloys are preferred for use around flammable and explosive substances due to their non-sparking and non-magnetic characteristics. Also, the alloy's good malleability makes it an excellent industrial use product. The high melting point of this nonferrous alloy makes it further suited for electrical uses. Resistance to oxidizing acids, chlorine gas, sodium hypochlorite and seawater makes titanium alloys perfect products for aircraft part manufacturing. Further, properties like high strength and low weight impart them with an edge over other alloys. Titanium alloys usually are considered having good weldability, except that due to their extreme reactivity, unusual precautions must be taken to shield the molten pool and the hot metal from contact with air. Always clean the metal with utmost care and chemically pickle or at least stainless steel wire brush.

## **1.2 Aluminium Alloys**

Pure aluminum is a silver-white metal characterized by a slightly bluish cast. It has a specific gravity of 2.70, resists the corrosive effects of many chemicals and has a malleability approach. When alloyed with other metals, numerous properties are obtained that make these alloys useful over a wide range of applications. Aluminium is a ductile member of the boron group of chemical elements. It has the symbol Al and its atomic number is 13. It is not soluble in water under normal circumstances. Aluminium is chemically too reactive to occur in nature as a free metal.

Aluminum alloys are light in weight compared with steel, brass, nickel or copper; can be fabricated by all common processes; are available in a wide range of sizes, shapes, and forms; resist corrosion; readily accept a wide range of surface finishes; have good electrical and thermal conductivities; and are highly reflective to both heat and light.

Aluminum is one of the two common metals having an electrical conductivity high enough to use as an electric conductor. The conductivity of electric-conductor (EC) grade is about 62% that of the International Annealed Copper Standard. Aluminum has non-sparking and nonmagnetic characteristics that make the metal useful for electrical shielding purposes such as enclosures for other electrical equipment and inflammable or explosive substances. Almost all methods of joining are applicable to aluminum – riveting, welding or brazing.

Aluminium is a soft, durable, lightweight, malleable metal with appearance ranging from silvery to dull gray, depending on the surface roughness. The yield strength of pure aluminium is 7.0–11.0 MPa, while the aluminium alloys have yield strength ranging from 200 MPa to 650 MPa. Aluminium has about one-third the density and stiffness of steel. In the Earth's crust, aluminium is the most abundant (8.3% by weight) metallic element and the third most abundant of all elements (after oxygen and silicon). Pure aluminium has a low tensile strength, but when combined with thermo-mechanical processing, aluminium alloys display a marked improvement in mechanical properties, especially when tempered. Aluminium alloys form vital components of aircrafts and rockets due to their high strength-to-weight ratio. Aluminium readily forms alloys with many elements such as copper, zinc, magnesium, manganese and silicon.

Some of the many uses for aluminium are in:

- Transportation (automobiles, aircraft, railway cars and marine vessels)
- Packaging
- Construction (windows, doors, siding, building wire)

- Electrical transmission lines for power distribution
- Aluminium can be reacted with hydrochloric acid to form hydrogen gas.

Aluminium was first produced in 1825 (in an impure form) by Danish physicist and chemist Hans Christian Orsted. Further, Pierre Berthier discovered aluminium in bauxite ore and successfully extracted it. Frenchman Henri Etienne Sainte-Claire Deville improved Wohler's method in 1846 and described his improvements in a book in 1859. Aluminium was selected as the material to be used for the apex of the Washington Monument in 1884 [11]. The Cowles companies supplied aluminium alloy in quantity in the United States and England using smelters like the furnace of Carl Wilhelm Siemens by 1886. Charles Martin Hall of Ohio in the U.S. and Paul Héroult of France independently developed the Hall-Héroult electrolytic process that made extracting aluminium from minerals cheaper and is now the principal method used worldwide.

The strength and durability of aluminium alloys varies widely, not only because of the components of the specific alloy, but also as a result of heat treatments and manufacturing processes. Aluminium alloy compositions are registered with “The Aluminum Association”. Many organizations publish more specific standards for the manufacture of aluminium alloy, including the Society of Automotive Engineers (SAE) standards organization, specifically its aerospace standards subgroups and ASTM (American Society for Testing and Materials) International. Alloy systems are classified by a number system (ANSI - American National Standards Institute) or by names indicating their main alloying constituents (DIN and ISO). Selecting the right alloy for a given application entails considerations of strength, ductility, formability, workability, weldability and corrosion resistance to name a few [12]. Wrought and cast aluminium alloys use different identification systems. Wrought aluminium is identified with a four digit number which identifies the alloying elements. Cast aluminium alloys use a four to five digit number with a decimal point. The digit in the hundreds place indicates the alloying elements, while the digit after the decimal point indicates the form (cast shape or ingot).

### **1.2.1 Characteristics of Aluminum and Aluminum Alloys**

Aluminum and its alloys lose their strength at elevated temperatures, although some alloys retain good strength at temperatures from 200 to 250 °C. When aluminum surfaces are exposed to the atmosphere, a thin invisible oxide skin forms immediately, that protects the metal from further oxidation. This self-protecting characteristic gives aluminum its high resistance to corrosion. Aluminum can be cast by any method known. It can be rolled to any desired thickness down to foil thinner than paper and in sheet form can be stamped, drawn, spun or roll-formed. The metal may be extruded into a variety of shapes.

### **1.2.2 Temper Designations of Aluminum Alloys**

The temper designation system adopted by “The Aluminum Association” and used in industry pertains to all forms of wrought and cast aluminium, and aluminium alloys except ingot. It is based on the sequences of basic treatments used to produce the various tempers. Temper designation follows the alloy designation, being separated by a dash.

Basic temper designations consist of letters. Subdivisions of the basic tempers, where required, are indicated by one or more digits following the letter. These digits designate specific sequences of basic treatments, but only operations recognized as significantly influencing the characteristics of the product are indicated.

The basic temper designations and subdivisions are as follows:

- F, as fabricated.
- O, annealed, recrystallized (wrought products only).
- H, strain-hardened (wrought products only): Applies to products that have their strength increased by strain-hardening.

The -H is always followed by two or more digits.

-H1, strain-hardened only: Applies to strain-hardened products to obtain the desired mechanical properties without supplementary thermal treatment.

-H2, strain-hardened and then partially annealed: Applies to products that are strain-hardened more than the desired final amount and then reduced in strength to the desired level by partial annealing.

-H3, strain-hardened and then stabilized: Applies to products which are strain-hardened and then stabilized by a low-temperature heating to slightly lower their strength and increase ductility.

The second digit following the designations -H1, -H2, and -H3 indicates the final degree of strain-hardening. Numeral 8 has been assigned to indicate tempers having a final degree of strain-hardening equivalent to that resulting from approximately 75% reduction of area.

Tempers between -O (annealed) and 8 (full hard) are designated by numerals 1 through 7. Material having an ultimate strength about midway between that of the -O temper and that of the 8 temper is designated by the numeral 4 (half hard).

-T, thermally treated to produce stable tempers other than -F, -O, or -H: Applies to products that are thermally treated, with or without supplementary strain-hardening and to produce stable tempers. The -T is always followed by one or more digits.

-T1, naturally aged to a substantially stable condition.

-T2, annealed (cast products only): Designates a type of annealing treatment used to improve ductility and increase dimensional stability of castings.

-T3, solution heat-treated and then cold-worked: Applies to products that are cold-worked to improve strength.

-T4, solution heat-treated and naturally aged to a substantially stable condition: Applies to products that are not cold-worked after solution heat treatment.

-T5, artificially aged only: Applies to products that are artificially aged after an elevated-temperature rapid-cool fabrication process.

-T6, solution heat-treated and then artificially aged: Applies to products that are not cold-worked after solution heat-treatment.

-T7, solution heat-treated and then stabilized: Applies to products that are stabilized to carry them beyond the point of maximum hardness.

-T8, solution heat-treated, cold-worked and then artificially aged: Applies to products that are cold-worked to improve strength.

-T9, solution heat-treated, artificially aged and then cold-worked: Applies to products that are cold-worked to improve strength.

-T10, artificially aged and then cold-worked: Applies to products that are artificially aged after an elevated-temperature rapid-cool fabrication process.

Additional digits may be added to designations -T1 through -T10 to indicate a variation in the treatment that significantly alters the characteristics of the product.

### **1.2.3 Aluminum Alloy Designation System**

A system of four-digit numerical designations for wrought aluminum and wrought aluminum alloys was adopted by “The Aluminum Association” in 1954. This system is used by the commercial producers and is similar to the one used by the SAE; the difference being the addition of two prefixes letters.

The first digit of the designation identifies the alloy type:

- 1) Indicating an aluminum of 99.00 % or greater purity (1xxx series)
- 2) Copper (2xxx series)
- 3) Manganese (3xxx series)
- 4) Silicon (4xxx series)
- 5) Magnesium (5xxx series)
- 6) Magnesium and silicon (6xxx series)
- 7) Zinc (7xxx series)
- 8) Some element other than those aforementioned (8xxx series)
- 9) Unused (not assigned at present) (9xxx series)

If the second digit in the designation is zero, it will indicate that there is no special control on individual impurities; integers 1 through 9 indicate special control on one or more individual impurities.

In the 2xxx to 8xxx series groups the last two of the four digits have no significance but are used to identify different alloys in the group. At the time of adoption of this designation system, most of the existing commercial designation numbers were used for these last two digits. When new alloys are developed and are commercially used, these last two digits are assigned consecutively beginning with -01, skipping any numbers previously assigned at the time of initial adoption.

#### **1.2.4 Heat Treatability of Aluminum Alloys**

In high-purity form, aluminum is soft and ductile. Most commercial uses, however, require greater strength than pure aluminum affords. This extra strength is achieved in aluminum first by the addition of other elements to produce various alloys, which singly or in combination impart strength to the metal. Further strengthening is possible by the means that classify the alloys roughly into two categories, non-heat-treatable and heat-treatable.

**Non-heat-treatable alloys:** The initial strength of alloys in this group depends upon the hardening effect of elements such as manganese, silicon, iron and magnesium, singly or in various combinations. The non-heat-treatable alloys are usually designated in the 1000, 3000, 4000 or 5000 series. These alloys are work-hardenable, so further strengthening is made possible by various degrees of cold working, denoted by the "H" series of tempers.

**Heat-treatable alloys:** The initial strength of alloys in this group is enhanced by the addition of alloying elements such as copper, magnesium, zinc and silicon. These elements singly or in various combinations show increasing solid solubility in aluminum with increasing temperature, so it is possible to subject them to thermal treatments that will impart pronounced strengthening.

The first step, called heat-treatment or solution heat-treatment, is an elevated-temperature process designed to put the soluble element in solid solution. This step is followed by rapid quenching, usually in water, which momentarily freezes the structure and for a short time renders the alloy very workable.

Some fabricators retain this more workable structure by storing the alloys at below freezing temperatures until they can be formed. At room or elevated temperatures the alloys are not stable after quenching, however, and precipitation of the constituents from the supersaturated solution begins. After a period of several days at room temperature, termed aging or room-temperature precipitation, the alloy is considerably stronger. Many alloys approach a stable condition at room temperature, but some alloys, particularly those containing Mg and Si or Mg and Zn, continue to age-harden for long periods of time at room temperature.

Heating for a controlled time at slightly elevated temperatures provides even further strengthening and properties are stabilized. This process is called artificial aging or precipitation hardening. By application of the proper combination of solution heat-treatment, quenching, cold working and artificial aging, the highest strengths are obtained.

### **1.2.5 Characteristics of Principal Aluminum Alloys Groups**

**1000 series:** These alloys are characterized by high corrosion resistance, high thermal and electrical conductivity, low mechanical properties and good workability.

**2000 series:** Copper is the principal alloying element in this group. These alloys require solution heat-treatment to obtain optimum properties; in the heat-treated condition mechanical properties are similar to, and sometimes exceed, those of mild steel. In some instances artificial aging is employed to further increase the mechanical properties. This treatment increases yield strength with loss in elongation and does not affect on tensile strength.

**3000 series:** Manganese is the major alloying element of alloys in this group, which is generally non-heat-treatable.

**4000 series:** The major alloying element of this group is silicon, which can be added in sufficient quantities to cause substantial lowering of the melting point without producing brittleness in the resulting alloys. For these reasons

aluminum-silicon alloys are used in welding wire and as brazing alloys where a lower melting point than that of the parent metal is required. Most of the alloys are non-heat-treatable.

**5000 series:** Magnesium is one of the most effective and widely used alloying elements for aluminum. When it is used as the major alloying element or with manganese, the result is a moderate to high strength non-heat-treatable alloy. Magnesium is considerably more effective than manganese as a hardener, about 0.8 per cent magnesium being equal to 1.25 per cent manganese, and it can be added in considerably higher quantities.

**6000 series:** Alloys in this group contain silicon and magnesium in approximate proportions to form magnesium silicates, thus making them capable of being heat-treated. The major alloy in this series is 6061, one of the most versatile of the heat-treatable alloys. Though less strong than most of the 2000 or 7000 alloys, the magnesium - silicon alloys possess good formability and corrosion resistance. Alloys in this heat-treatable group may be formed in the -T4 temper (solution heat-treated but not artificially aged) and then reach full -T6 properties by artificial aging.

**7000 series:** Zinc is the major alloying element in this group and when coupled with a smaller percentage of magnesium, results in heat-treatable alloys of very high strength. Other elements such as copper and chromium are usually added in smaller quantities. A notable member of this group is 7075, which is among the highest strength aluminum alloys available and is used in air-frame structures and for highly stressed parts.

### **1.3 Titanium and Titanium Alloys**

Titanium is a gray, light metal with a better strength-to-weight ratio than any other metal at room temperature and is used in corrosive environments or in applications that take advantage of its light weight, good strength and nonmagnetic properties.

Titanium is an element with the symbol Ti and atomic number 22. Sometimes called the 'space age metal'. It has a low density and is a strong, lustrous and corrosion resistant transition metal. Titanium can be alloyed with iron, aluminium, vanadium, molybdenum etc. to produce strong lightweight alloys for aerospace (jet engines, missiles and spacecraft), military, industrial processes (chemicals and petro-chemicals, desalination plants, pulp and paper), automotive, agri-food, medical prostheses, orthopedic implants, dental and endodontic instruments, dental implants, sporting goods, jewelry, mobile phones and other applications. Titanium was discovered in England by William Gregor in 1791 and named by Martin Heinrich Klaproth for the Titans of Greek mythology.

The processes required to extract titanium from its various ores are laborious and costly. Pure metallic titanium (99.9%) was first prepared in 1910 by Matthew A. Hunter at Rensselaer Polytechnic Institute by heating  $\text{TiCl}_4$  with sodium at 700–800 °C. Titanium metal was not used outside the laboratory until 1932 when William Justin Kroll proved that it could be produced by reducing titanium tetrachloride ( $\text{TiCl}_4$ ) with calcium. Eight years later he refined this process (known as the Kroll process) by using magnesium and even sodium. Although research continues into more efficient and cheaper processes (e.g. FFC Cambridge), the Kroll process is still used for commercial production [13].

In the 1950s and 1960s the Soviet Union pioneered the use of titanium in military and submarine applications as a part of programs related to the Cold War. Around 50 grades of titanium and titanium alloys are designated and currently used, however only a couple of dozen are readily available commercially.

Commercially pure titanium contains acceptable mechanical properties and has been used for orthopedic and dental implants. For most applications titanium is alloyed with small amounts of aluminium and vanadium, typically 6% and 4% respectively, by weight. This mixture has a solid solubility which

varies dramatically with temperature, allowing it to undergo precipitation strengthening. This heat treatment process is carried out after the alloy has been worked into its final shape but before it is used.

Titanium is available commercially in many alloys but multiple requirements can be met by a single grade of the commercially pure metal. The alloys of titanium are of three metallurgical types: alpha, alpha-beta and beta, with these designations referring to the predominant phases present in the microstructure.

Ti Grade-5, also known as Ti-6Al-4V, is the most commonly used alloy. It has a chemical composition of 6% Aluminium, 4% Vanadium, 0.25% (max) iron, 0.2% (max) oxygen, and the remainder titanium. It is used extensively in aerospace, medical, marine and chemical processing. It is significantly stronger than commercially pure titanium while having the same stiffness and thermal properties. This grade is an excellent combination of strength, corrosion resistance, weld and fabricability. In consequence, its uses are numerous such as for military aircraft or turbines. It is also used in surgical implants.

Titanium has a strong affinity for hydrogen, oxygen and nitrogen gases, which tend to embrittle the material; carbon is another embrittling agent. Nearly all non-aircraft applications take advantage of this corrosion resistance. It is used in aircraft engine compressors and in airframe structures.

Generally, titanium is welded by GTAW or plasma arc techniques and the key to successful welding lies in proper cleaning and shielding. The alpha-beta titanium alloys can be heat treated for higher strength but they are not easily welded. Beta and alpha-beta alloys are designed for formability; they are formed in the soft state and then heat treated for high strength.

Followings are some famous commercial Ti alloys:

**Ti Grade-1:** Lower strength, softest, unalloyed Ti grade with highest ductility, cold formability, impact toughness and high weldability.

**Ti Grade-2:** Moderate strength, unalloyed Ti with excellent weldability and formability.

**Ti Grade-5:** (Ti-6Al-4V) alloyed, heat treatable, high strength, most commercially available, offering an excellent combination of high strength, toughness and ductility along with the good weldability at a temperature of up to 400 °C.

#### **1.4 Selection of Welding Processes**

The welding processes for Al alloys include AC/DC GTAW, Laser Beam Welding (LBW), Electron Beam Welding (LBW) and Friction Stir Welding (FSW); amongst these, the AC GTAW is the most frequently used process for welding of aluminum, especially for lesser thickness. GTAW is the number one process chosen by professional welders for welding of lower thick metals. The pure aluminum has melting point less than 650 °C and does not exhibit the color changes before melting. The oxide or skin that forms so rapidly on its surface has a melting point almost three times as high (1800°C). The oxide is also heavier than aluminum and tends to be trapped in the molten aluminum. Luckily, maximum penetration is achieved when 50% of the AC cycle is spent on electrode negative polarity and maximum cleaning of oxides (ahead of the weld) is achieved when 50% of the cycle is spent on electrode positive polarity [14].

If a DC voltage is used to drive the arc between the tungsten electrode and workpiece, the oxide film on the weld pool will not broken down, with the eventual result of a poor weld. For this reason, an AC arc is used normally, at mains frequency of 50 Hz. The oxide removal action will take place only during the portion of the current cycle when the electrode is positive. To continue the maintenance of the arc cycle, the power source must either has a high enough open-circuit voltage (100 V RMS for argon and 150 V RMS for helium), or a high voltage at high frequency must be impressed on the arc gap at the time when the current passes through the zero and the electrode becomes positive [15].

Aluminum is an excellent conductor of heat. It requires large heat inputs when welding is begun, since much heat is lost in heating the surrounding base metal. After welding has progressed a while, much of this heat has moved ahead of the arc and pre-heated the base metal to a temperature requiring less welding current than the original cold plate. If the weld is continued further on to the end of the two plates where there is nowhere for this pre-heat to go, it can pile up to such a degree as to make welding difficult unless the current is decreased.

The correct choice of a filler rod significantly affects the strength, ductility, corrosion resistance and chances of cracking. The table 1.1 shows the various recommendations of aluminium alloy fillers for the maximum strength and maximum elongation. Maximum weld quality can be obtained if the filler material is clean and of high quality.

**Table 1.1: Recommended Filler Metals for Various Aluminium Alloys**

| Base Metal | Recommended Filler Metal |                        |
|------------|--------------------------|------------------------|
|            | For Maximum Strength     | For Maximum Elongation |
| 1100       | 1100                     | 1100, 4043             |
| 3003       | 5183, 5356               | 1100, 4043             |
| 3004       | 5554, 5356               | 5183, 4043             |
| 5005       | 5183, 4043, 5356         | 5183, 4043             |
| 5050       | 5356, 5183               | 5183, 5356, 5654       |
| 5052       | 5554, 5356               | 5356                   |
| 5083       | 5356, 5554               | 5554, 5356             |
| 5086       | 5556                     | 5183, 5356             |
| 6061       | 4043, 5183               | 5356                   |
| 6063       | 4043, 5183               | 5356                   |
| 7005       | 5356, 5183               | 5183, 5356             |
| 7039       | 5356, 5183               | 5183, 5356             |

Titanium is not a difficult material to weld but strict precautions must be taken to guard against contamination at the high temperatures. This applies not only to the atmospheric gases (oxygen, nitrogen and water vapour) but also to any dirt or other surface layer on the metal. Fusion welding techniques must be aimed, therefore, at the exclusion of atmospheric contamination by welding in argon, helium or vacuum, following careful cleaning and edge preparation of the areas to be joined. All heated surfaces, both front and back, must be equally protected. Titanium can be joined by fusion, resistance, flash-butt, explosion and friction welding. Plasma Arc Welding (PAW), GTAW, GMAW and Electron Beam Welding (EBW) are all suitable for the material, but techniques such as oxyacetylene, carbon arc and atomic hydrogen cause contamination to the titanium, so they should not be used.

The method which is most commonly used for the welding of titanium is GTAW although plasma is growing in importance, particularly where thick plate is to be welded and where automatic techniques are applicable. In GTAW process, cleanliness is vital, both with respect to the metal adjacent to where the weld is to be made and also to the welding shop. Any thick oxide layer must be removed from the titanium surface by grit blasting and / or pickling. In addition, materials to be welded, filler wire, welding equipment and clamps must all be absolutely dry, since small amounts of moisture can result in severe contamination.

## **1.5 Bead Geometry Studies**

GTAW is a commonly used for welding hard-to-weld metals, such as Al, SS, Mg and Ti alloys, because of its possible heat input control. This control can be utilized through a good selection of the process variables, which in turn results in optimizing the bead dimensions. GTA weld quality is strongly characterized by the weld bead geometry. This is because the weld bead geometry plays an important role in determining the mechanical properties of the weld. Therefore, it is very important to select the welding process parameters for obtaining optimal weld bead geometry. To study the effect of

GTAW process parameters on weld bead dimensions, suitable combinations of process variables can lead to optimum bead dimensions. With AC polarity, a weld bead may be formed on these alloy sheets [16].

It is widely understood that the GTA welding of titanium alloy exhibits columnar grains in the weld pool, which often results in inferior mechanical properties and may lead to hot cracking. Current pulsing technique was attempted by many researchers to great success, resulting in grain refinement of fusion zone. It was reported that substantial grain refinement was possible in the case of Al and Ti alloys [17, 18].

The Taguchi method is a powerful tool for the design of high-quality systems. It provides a simple, efficient, and systematic approach to optimize designs for performance, quality, and cost. The methodology is valuable when process parameters are qualitative and discrete. Taguchi method can optimize the quality characteristics through the settings of process parameters reduce the sensitivity of the system performance to the sources of variation [19].

Modified Taguchi Method (MTM) was adopted to analyze the effect of each GTAW process parameter on the weld pool geometry and to determine the process parameters with the optimal weld pool geometry. Experimental results had shown that the front height, front width, back height and back width of the weld pool in the GTA welding of stainless steel are greatly improved by using this approach [20].

The strength of welded joint depends upon the weld bead dimensions and shape relationships which include penetration ( $p$ ), weld bead width ( $b$ ), height of reinforcement ( $h$ ) and weld penetration shape factor ( $b/p$ ). These weld bead dimensions and shape relationships are controlled by the welding variables. The important process parameters which affects the bead profile are pulse current, secondary current (base / background current), pulse frequency, pulse duty cycle, welding voltage, welding speed and gas flow rate. It was therefore, decided to study the effects of these pulse parameters on the weld bead dimensions, by developing the design matrix on bead-on-plate weld.

## **1.6 Mechanical Properties Studies**

During welding, melting occurs and heat transfer takes place through conduction into the base material adjacent to the weld. Typically, the completed weldment is divided into three distinct areas: the weld metal, the heat-affected zone (HAZ) adjacent to the weld and the base material beyond the HAZ that has been unaffected by the welding operation. Because the HAZ will experience cycles of heating and cooling during the welding operation, arc welding on materials which have been strengthened by work hardening or precipitation hardening, will change its properties and may be extremely different than that of the original base alloy and the unaffected area of the base material. Therefore effect of various process parameters and gas mixtures on mechanical properties (like Ultimate Tensile Strength–UTS, percentage elongation and hardness) of aluminium and titanium alloys has been carried out and optimized. Study of microhardness has been carried at different locations of weld zone and HAZ.

## **1.7 Metallurgical Studies**

It has been recognized that one of the major problem associated with fabrication by welding, arise from the inability to obtain uniform mechanical properties through out the weldment as well as bead of the weldment. The overall mechanical properties of a weldment are therefore, determined by the microstructure of the weld zone and HAZ. Owing to vastly different structures of these zones, it is obvious that the strength of the weldment depends upon the strength of the weakest zone. As the strength of welding is determined by its microstructure, it is therefore, essential to have adequate knowledge about the micro-constituents and phases of welding. Therefore microstructural study of welded Al and Ti alloys has been carried out.

## **Chapter 2**

### **REVIEW OF LITERATURE**

#### **2.1 Introduction**

Review of the available published literature on any specific area of research is essential to get a feedback about the present status of particular area of research. In this chapter, the effort is made to present the review of the available literature and the relevant information on the different aspects of investigation is undertaken in the present research work. The literature reviewed as follows.

- [1] Welding of Aluminium Alloys
- [2] Welding of Titanium Alloys
- [3] Pulsed GTAW process parameters and their relationship
- [4] Bead Geometry and Shape relationships
- [5] Mechanical properties and Metallurgical transformation

#### **2.2 Welding of Aluminum Alloys**

GTAW is an arc-welding process that produces coalescence of metals by heating them with an arc between a non-consumable tungsten electrode and the base metal. This process was originally developed for hard-to-weld and lightweight metals such as aluminum, magnesium and titanium. Many delicate components in aircraft and nuclear reactors are GTA welded and therefore the weld quality is of extreme importance.

The specific properties that affect welding of aluminum and its alloys are its oxide characteristics, lack of color change when heated, wide range of mechanical properties and melting temperatures, and its thermal, electrical and nonmagnetic characteristics.

Aluminum oxide melts at about 2050 °C which is much higher than the melting point of the base alloy. If the oxide is not removed or displaced, the result will be incomplete fusion. In some joining processes, chlorides and fluorides are used in order to remove the oxide. Chlorides and fluorides must be removed after the joining operation to avoid a possible corrosion problem in service.

**AC Power to Weld Aluminum:** For the most GTAW applications, AC power is used for the very practical reason of oxide removal or cleaning action in aluminum welding. If GTAW with DC power is used on aluminum, which has not been chemically and / or mechanically cleaned immediately before welding, the thick and porous oxide layer of  $\text{Al}_2\text{O}_3$  can have a detrimental effect on both integrity and acceptability of the joint. When aluminum alloys are welded, a strong cleaning action is achieved by using AC power and DCEP (Direct Current Electrode Positive). During GTAW, electrical charge builds up below and above the oxide layer, which is an electrical insulator. When the  $\text{Al}_2\text{O}_3$  (Aluminium Oxide) layer accumulates sufficient electrical charge, it physically explodes leaving a clean surface protected by the argon shielding gas. This action not only takes place above the melting point of aluminum (660°C) but also below its melting point. In fact, the HAZ of the aluminum weld is usually completely cleaned by this action. This dynamic cleaning action is clearly visible by the welder during the welding operation. After the weld is finished, the weld and HAZ areas are smooth and brightly cleaned.

**DCEP (Direct Current Electrode Positive) to Weld Aluminum:** The great advantage of GTAW of aluminum with DCEP is the maximum possible cleaning effect. Unfortunately, 70% of the heat generated by the arc is delivered to the tungsten electrode while using DCEP. This results in spitting and melting of the tungsten electrode even at very low current settings. Furthermore, weld penetration with DCEP is very shallow. Thus, the only limited use of DCEP is for welding thin sheets, where the current is low enough to prevent melting of the tungsten electrode.

**DCEN (Direct Current Electrode Negative) to Weld Aluminum:** Although the great majority of GTAW is conducted by using AC power, aluminum can be welded with DCEN current using 100% helium and thoriated tungsten electrodes. The disadvantage of DCEN current is the total absence of cleaning action. The great advantage of GTAW with DCEN current is the substantial increase in penetration. A further advantage is that smaller diameter electrodes can be used, because 30% of the heat is used to heat the tungsten electrode with DCEN. Compared to AC welding, DCEN can provide a deeper and narrower weld pool. Unlike AC welding, preheating of thicker aluminum section is not necessary. In addition, less edge preparation is needed and the groove can be reduced in size so that less filler metal is consumed. Since the heat intensity is greater with DCEN, the weld pool is formed faster resulting in less distortion of the base metal than with AC. DCEN can also be used for welding thin aluminum at faster travel speeds than with AC.

During AC welding due to different abilities to emit electrons of tungsten and the weld metal, wave rectification is used. The tungsten electrode emits electron more readily because it attains a much high temperature than metal being welded. Thus current amplitude during half cycle, when the electrode is negative, is greater than the amplitude during the half cycle, when the electrode is positive. To obtain balanced current flow, DC suppressor is used [21].

Aluminum possesses a number of properties like high thermal conductivity, high thermal expansion coefficient, low melting temperature and absence of color change as temperature approaches the melting point. Lack of weld fusion is normally seen especially at the start of weld. When alum becomes more sluggish and have low fluidity, aluminum can be easily welded in all positions with spray and pulsed mode. In contrast to steel, the high conductivity of aluminum acts as a heat sink, and makes weld fusion and weld penetration more difficult to achieve on parts having thickness more than 4.0

mm. However on thin parts, the rapid build up of heat in the alum parts may increase high weld fluidity and chances of burn-through.

While considering the welding of aluminum alloys, typically a variety of filler alloys are available which may be used to join any given base alloy. However, there are a number of variables associated with the selection of the most suitable filler alloy to be used for any base alloy or alloy combination. In some cases, we may find ourselves in a trade off situation, where it is required to choose between different characteristics of the weld. Some considerations for the selection of a filler alloy are typically ease of welding, strength of welded joint, ductility, corrosion resistance, sustained temperature service, color match and post weld heat treatment (PWHT).

6xxx series (Al–Mg–Si alloy) are principally used in automotive, pipe, structural, railings and extruded parts. This series can be prone to hot cracking, but this problem can be overcome by the correct type of joint, filler metal used and weld procedure that minimize weld heat input. As many of the 6xxx series alloys have 1.0% magnesium silicide ( $Mg_2Si$ ), these alloys are sensitive for cracking and can not be arc welded successfully without filler alloy. This series are usually welded with filler material of type Al–5%Mg and less commonly, with Al–5%Si, neither of which respond to a post weld aging treatment. Filler which are age hardenable and at the same time also resist hot cracking have also been suggested and occasionally used.

With non-heat treatable aluminum alloys, the reduction of the HAZ tensile strength is typically predictable under normal weld conditions. In contrast the HAZ strength with heat treatable alloy can be reduced below the minimum tensile strength required for the parts when the welding heat is excessive during the weld. Higher tensile strength from the filler and reduced strength from the part influenced by the annealing effect of the weld and hot cracking may occur in the HAZ of the base metal.

Also, special techniques such as synchronous rolling and the use of trailing heat sink have been suggested for reducing tensile welding stresses and

hence hot cracking of high strength aluminium alloys during fusion welding [22]. Yang *et al.* [23] reported that with the help of a trailing heat sink in GTA welding of aluminum alloys, the mechanical strain associated with hot cracking can be significantly reduced particularly in the brittle temperature region (between the weld pool and heat sink). With a proper combination of the distance (between the welding torch and trailing heat sink) and cooling intensity, hot cracking can be eliminated. Also microstructural refinement and more favorable grain orientation were observed.

Hydrogen dissolves very rapidly in molten aluminum. However, hydrogen has almost no solubility in solid aluminum and it has been determined as the primary cause of porosity in aluminum welds. High temperature of the weld pool allows a large amount of hydrogen to be absorbed and as the pool solidifies, the solubility of hydrogen is greatly reduced. Also hydrogen can be derived during welding from base metal contaminants hydrocarbons, lubricant, grease, moisture, paints and compressed air. Cleaning and degreasing with stainless wire brushes / carbide wheels are done to minimize hydrogen and weld porosity during welding.

It is widely recognized that hydrogen is the dominant cause of porosity in aluminum welds. Gases such as oxygen and nitrogen present lower solubility in molten aluminum in comparison to hydrogen [24] and they usually do not play any important role in porosity generation. However, in a micro gravity environment with vacuum, these gases can assume importance. In a study on aluminum welding in this environment, Fujii *et al.* [25] carried out experiments with GTAW processes and some unexpected results emerged. These workers report that in all runs, several pores were observed. This porosity was linked to the formation of  $\text{Al}_2\text{O}_3$  gas bubbles at high vacuum (the oxygen come from the superficial oxide layer).

### **2.3 Welding of Titanium Alloys**

Welding of titanium alloys has the greatest potential for affecting material properties. In all types of welds, contamination by interstitial impurities, such

as oxygen and nitrogen must be minimized to maintain useful ductility in the weldment. Alloy composition, welding procedure and subsequent heat treatment are highly important in determining the final properties of welded joint.

Some general principles can be summarized as follows:

- Welding generally increases strength and hardness.
- Welding generally decreases tensile strength and bend ductility.
- Welds in unalloyed titanium grades 1, 2 and 3 do not require PWHT unless the material will be highly stressed in a strongly reducing atmosphere.
- Welds in more beta-rich and alpha-beta alloys such as Ti-6Al-6V-2Sn have a high likelihood of fracturing with little or no plastic straining.

Titanium and titanium alloys are heat treated for the following purposes:

- To reduce residual stresses developed during fabrication.
- To produce an optimal combination of ductility, machinability, and dimensional and structural stability (annealing).
- To increase strength (solution treating and aging).
- To optimize special properties such as fracture toughness, fatigue strength, and high-temperature creep strength.

Commercially pure titanium and titanium alloys are welded by adopting the procedures and equipments used in welding of stainless steel and aluminum. Because of the high reactivity of the alloy at temperatures above 550°C, additional precautions must be taken to shield the weldment from air. Further titanium base metal and filler metal must be cleaned to avoid contamination during welding. Unalloyed titanium and all alpha titanium alloys are weldable. Alpha-beta alloy Ti-6Al-4V and other beta-stabilized alloys are also weldable. All grades are usually welded in the annealed condition. Welding of cold-worked alloys anneals the HAZ and eliminates the strength produced by cold working.

GTAW is the most widely used process for joining titanium and titanium alloys except the parts with thick sections. Square-groove butt joints can be welded without filler metal up to 2.5 mm thick base metal. For thicker base metals, the joint should be grooved and filler metal is required. The heated weld metal in the weld zone must be shielded from the atmosphere to prevent contamination with oxygen, nitrogen and carbon, which will degrade the weldment ductility.

A conventional power supply, AC and DCEN are used for GTA welding while reverse polarity (DCEP) is used for GMA welding of titanium alloys. A water-cooled welding torch, equipped with a 3/4-inch ceramic cup and a gas lens are recommended for GTA welding of titanium. The conventional thoriated tungsten types of electrodes (EWTh-1 or EWTh-2) are used for titanium. To improve arc initiation and control the spread of the arc, the electrode should be ground to a point. The electrode may extend one and half times the size of the diameter beyond the end of the nozzle.

Shielding gases used in welding of titanium and titanium alloys are only argon and helium, and occasionally mixtures of these two gases. Jonsson *et al.* [26] reported that the addition of up to 5% oxygen to an argon shielded gas was found to be affecting the characteristics of the arc column to small extent only. Onsoien *et al.* [27] also reported that the hydrogen addition to shielding gas changed the arc characteristics and increased the arc resistance in GTAW, thus increasing the heat input and decreasing the depth-to-width ratio of the weld. It can also achieve 50% more penetration.

Ti-6Al-4V (ASTM Grade 5) alloy can be welded in the annealed condition or in the solution-treated and partially aged condition, with completion of ageing during post weld stress relieving. Ti-6Al-4V has weld zone hardness and strength almost similar to that of parent metal but ductility and bend performance are inferior. For maximum toughness and ductility in Grade-5 joints produced by GTAW, it is preferable to use commercially pure, similar, matching or Ti-3%Al-2.5%V (ASTM Grade 9) filler wire.

Titanium weld colors have some significant meanings. Discoloration of titanium from the heat of welding is caused by oxidation and different colors are caused by varying thickness of oxide layers. The colors such as blue, violet, green, gray and white all occur at gradually higher temperatures. The first titanium weld color is straw, followed by brown, then brownish blue, purple blue, green and blue, dull salmon pink, gray and white oxide. Titanium begins to discolor at around 250 °C. To a certain extent the quality of the weld can be judged by its coloring. Yellowish to bluish colors indicate slight hardening of the weld, which are however acceptable. Dark blue color or a gray oxide layer indicates the embrittlement of the weld through oxygen and / or nitrogen pickup. The hardness of a good weld should not exceed that of the fully recrystallized base metal by more than 50 points.

#### **2.4 Pulsed GTAW process parameters and their relationship**

GTAW process originally was created in the 1940s to weld magnesium and aluminum alloys for aircraft applications. Besides the equipment, the most important aspect of the GTAW process is the welding parameters used. A change in any parameter will have an effect on the final weld quality. For welding in many precision or high-purity applications, the recommended welding parameters are arc length, welding speed, welding current, gas flow rate and arc pulsing.

**Arc Length:** The arc length (sometimes called the arc gap) is the distance from the electrode tip to the part to be welded. This setting is dependent on weld current, arc stability and part concentricity / ovality. The welding engineer's objective is to keep the electrode at a constant distance from the part surface with a sufficient gap to avoid stubbing out.

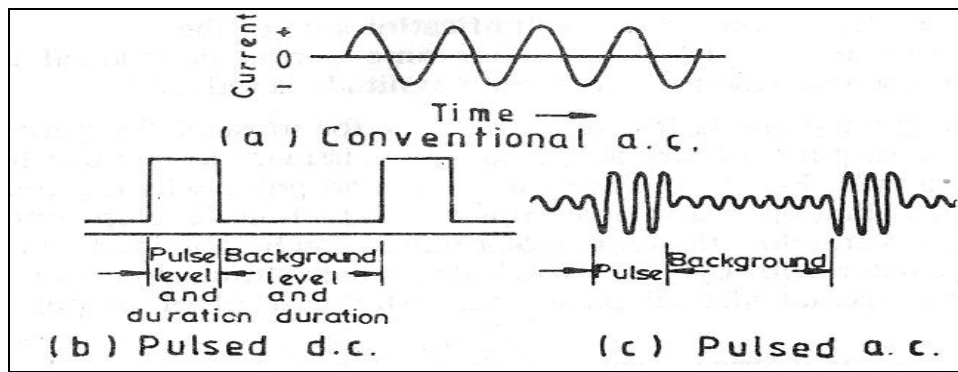
**Welding Speed:** The weld speed is defined as the speed of travel of the torch over the part which depends on the flow rate of the material to be welded and the material thickness. This is very dominating factor in defining the geometry of the bead. With increase in welding speed, the heat per unit length decreases, and hence the weld width and penetration are reduced.

**Welding Current:** The welding current corresponds to the amount of heat applied to affect the weld and depends on the material to be welded, material thickness, welding speed and shielding gas. The objective is to achieve defect-free welds with the required penetration. The number of levels of welding current needed depend greatly on the welding application and the associated welding speed.

**Gas Flow Rate:** When the gas flow rate is very high, spattering takes place and irregular shape is obtained. With increase in gas flow rate, penetration and weld width increases initially, and then reduce due to increasing heat losses by radiation and convection.

**Arc Pulsing:** Arc pulsing involves the use of welding power supply to alternate the weld current rapidly from a high peak / pulse current to a low background / base current value. This technique reduces the overall heat input to the base material and also can allow for increase in weld speed. In the basic-current phase, the low temperature causes a decrease in the volume of the molten pool. Thus the heat input is reduced and optimum control of the molten bath is ensured. The predominant factors which are having greater influence on the fusion zone grain refinement of pulsed current GTAW process have been identified from the literature survey [28–31]. They are peak current  $P$ , background current  $B$ , pulse duty cycle  $T$  and pulse frequency  $F$ , shown in Fig 2.1 and 2.2. Kumar P *et al* [32–35] reported that pulse current, base current, pulse frequency, pulse duty cycle and gas mixture (Ar + He) plays an important role for optimizing the weld bead geometries and mechanical properties of aluminium and titanium alloys. Also arc pulsing significantly improves the grain structure.

- **Pulse Current:** The pulses of higher current are found to generate a large variation of pressure in the arc. Arc pressure causes the turbulence in the weld pool, which allows the heat to penetrate deeper into the base metal. Increased current produces higher weld pool temperature resulting in more fluidity hence the spreading of the weld bead occurs.



**Fig 2.1: Conventional and Pulsed current transients for GTAW process**

- **Back Ground Current:** The value of back ground current decides heat input to the work piece if the pulse current is constant. This current affects rate of cooling and solidification.
- **Pulse Duty Cycle:** It can be defined as fraction of time period of the pulse.

$$\text{Pulse Duty Cycle} =$$

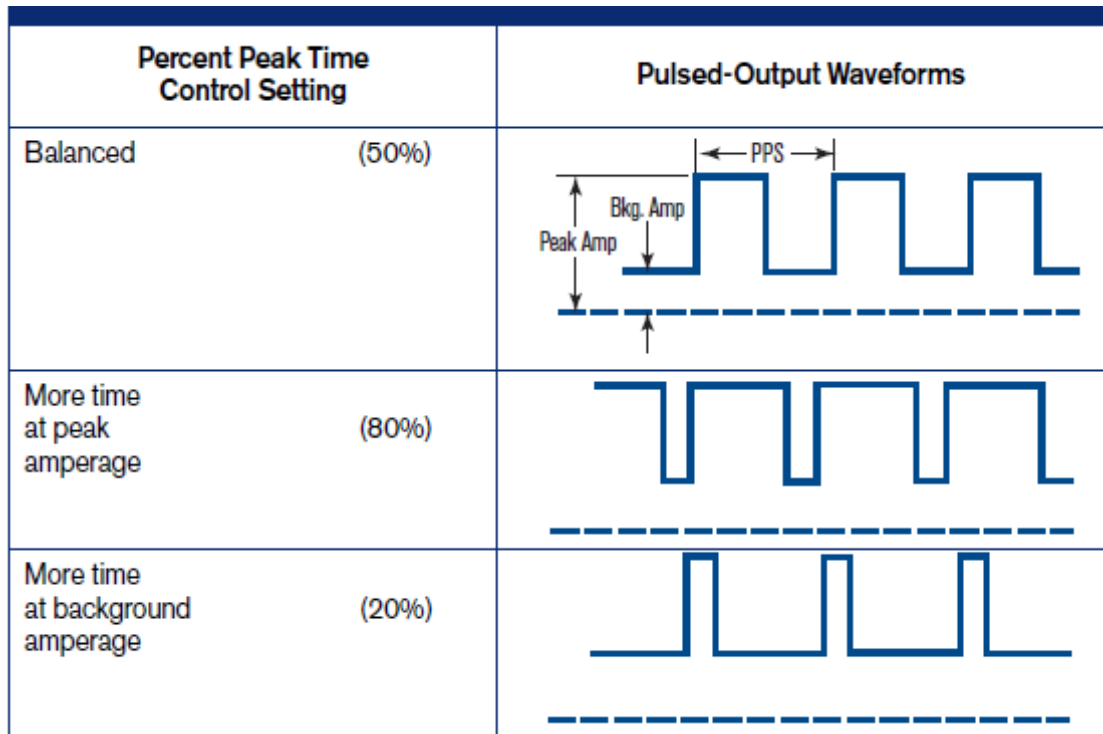
$$\frac{\text{Pulse Current Time}}{(\text{Pulse Current time} + \text{Base Current Time})}$$

Higher pulse duty cycle indicates the tendency towards continuous current. Increase in pulse duty cycle cause increase in heat input resulting deeper penetration and wider weld bead.

- **Pulse Frequency:** When the number of pulse is increased the pulse time reduces. This will reduce the radiation loss per pulse. However the total radiation losses per second shall be the product of the heat loss per pulse multiplied by number of pulses. The total radiation and convection losses increase with increasing frequency. This will reduce penetration and weld width, and increase the width of HAZ.

In pulsed GTAW process, the current is supplied in pulses rather than at constant magnitude. This is because the conventional GTAW when used for thin sheets requires very low current, which depends on the nature of the current. Stability of the arc can be achieved in such cases if the current is supplied in pulses. The main aim of pulsing is to achieve maximum penetration without excessive heat built-up by using the high current pulses to penetrate deeply and then allowing the weld pool to dissipate some of the

heat during a proportionately longer arc period at a lower current. In contrast to constant current welding, the heat energy required to melt the base material is supplied only during peak current pulses for brief intervals of time allows heat to dissipate into the base material leading to a narrower HAZ. Another advantage of pulsing is the action of bringing the impurities to the weld surface by pulse action agitating / stirring the weld pool [36].



**Fig 2.2: Pulsed GTAW Waveforms**

Backer *et al.* [37] reported that heat input can be significantly reduced by proper selection of pulsing conditions. Lietner *et al.* reported that the use of any combination of pulsation parameter will result in a weld with deeper penetration and greater depth to width ratio that can not be obtained by a conventional GTA weld of the same heat input. Omar *et al.* [38] reported that lower the pulse frequency narrower the HAZ and wider the fusion zone. The narrowest HAZ was found to be at pulse frequency of 1 Hz for high peak currents and short pulse duration.

Birman *et al.* [39] reported that when pulsed arc welding is adopted, there is a less risk of hot cracking than with conventional use. Vainarman *et al.* [40]

reported that use of pulsed arc welding increases output by 200 – 400%, reduces consumption of argon by three to ten times and also reduces the cost of 1 m weld deposition by three to five times with respect to conventional GTAW process. Kozakov [41] reported that the quality of welded joint between components with different thickness made by pulsed TIG welding is governed by the dimensions and structure of the HAZ in thinner component.

Buchinski, *et al.* [42] demonstrated that the joints made by pulsed GTAW method have the same properties as by normal argon metal arc method with less distortion of the product. Ramesh, V.R. [43] reported that pulsed current automatic GTAW shows increased arc stability particularly at low current and arc blow effects are eliminated. Karnad, S.S. [44] observed that pulsed GTAW process can more easily cope up with variations in joint geometry, clamping of fit-up and can weld very thin sheets with precision, which can not be welded by conventional GTAW.

Balasubramanian V *et al.* [45] studied the effect of pulsing current on GTA welded Ti-6Al-4V alloy. He observed that the effect of pulsing frequency and peak current had two regions with initially increasing and then decreasing the tensile properties irrespective of changes in base current and pulse-on-time. Because of grain refinement and equiaxed large beta grain size in the fusion zone, the tensile properties found to have a slight increase in the weld fusion zone. It has been understood that there is a value of optimum frequency at which the tensile properties are maximum. Sundaresan *et al.* [46] justified the use of current pulsing by improving the weld metal properties. Current pulsing has been used by several investigators to obtain grain refinement in weld fusion zones and improvement in weld mechanical properties.

## **2.5 Bead Geometry and Shape Relationships**

The mechanical properties and weld quality of GTA welded joint largely depend on the weld bead dimensions and shape relationships which in turn are influenced by welding variables like welding current, arc voltage and welding speed [47]. The bead geometry is specified by the depth of

penetration ( $p$ ), bead width ( $b$ ), reinforcement height ( $h$ ), the ratio of weld width to penetration ( $b/p$ ), known as weld penetration shape factor (WPSF), dilution and contact angle.

**Penetration:** Penetration is considered as one of the most important dimensions of a weld, as it determines the stress carrying capacity of a welded joint [48]. It has been well established that penetration is influenced by current, voltage and welding speed [49, 50]. The relationship between voltage and penetration shows that there is an optimum voltage at which penetration is highest. Increasing or decreasing arc voltage from this point reduces penetration [51]. Gunnert [52] reported a decrease in penetration, with increase in voltage. It has been reported that penetration increases as welding speed decreases [49–52]. A relatively straight-line relationship exists between weld travel speed and penetration.

Saedi *et al.* [53] reported that high frequency current pulsing increases the electromagnetic stirring force in the weld pool and therefore, increases the weld depth independent of top width, resulting in a different pool shape. Thus current pulsing can be used to control the weld pool geometry in GTAW.

Kumar Rakesh *et al.* [54] reported that by changing the EN (Electrode Negative) ratio, the depth of penetration can be controlled. Increase in the EN ratio results in shallow penetration, which resulted excellent welds of thin sheets. Use of AC wave pulse welding gave high quality appearance to bead shape, which is preferred especially for aluminium welding. Kumar P *et al* [55] also reported that penetration of weld bead increases with increase in current and slightly increases with increase in frequency.

**Bead width:** Bead width is an important characteristic of a weld particularly when using automatic equipment to fill up a weld groove. Increase in arc voltage results in the longer arc, which causes wide bead [52]. Gurave and Stout [56] reported that bead width increases with increase of heat input to the work i.e. with either increase in welding current or decrease in welding speed. The bead width increases with increase in current until a critical value is

reached, after that further increase in welding current produces a decrease in width [57–59]. Welding speed has straight line relationship, as weld travel speed increases the weld width decreases. However, Houldcraft and John [60] reported that a very high current would give digging arc and narrow weld bead.

**Reinforcement:** Reinforcement height is reported to be inversely proportional to the welding speed [58]. A straight-line relationship exists between welding current and reinforcement height [59, 61]. Reinforcement should usually be 20% of the plate thickness [62]. Excessive reinforcement not only increases electrode consumption but also owns the sharp changes in the plate thickness which leads to the failure of welded joint due to notch effect. Reinforcement height may be the most effectively controlled by welding speed, due to straight-line the relationship between them. As welding speed increases the reinforcement height decreases [60].

**Dilution:** The study of dilution helps in evaluating not only the proportion of the weld metal deposited but also in ascertaining the stress concentration due to excessive convexity of bead shape up to some extent [63]. The dilution of base metal in molten pool is reported to increase with the increase in welding speed [64].

**Weld penetration shape factor (WPSF):** The ratio of weld width to the penetration is known as weld penetration shape factor (WPSF) or coefficient of internal shape [64]. Quintino and Allum [60] reported that WPSF increases with the increase in welding current as well as with the increase in arc voltage. He also reported that WPSF improved with nozzle angle change from trailing to leading position. The limits of WPSF were reported to be different for each welding process [64]. In case of assembly welding operation the range of WPSF is 0.5 – 5.0 and the nominal value is in range of 1.20 – 3.50. A sound weld is obtained by choosing nominal value.

**Contact Angle:** Contact angle is an angle between the tangent to the weld metal at the point where the weld metal meets the base metal and the base

metal line. The contact angle influences bead shape, undercuts and overlapping. Konkai and Koons [65] reported that the contact angle decreases by decreasing current and electrode sickout, and by increasing the voltage and travel speed.

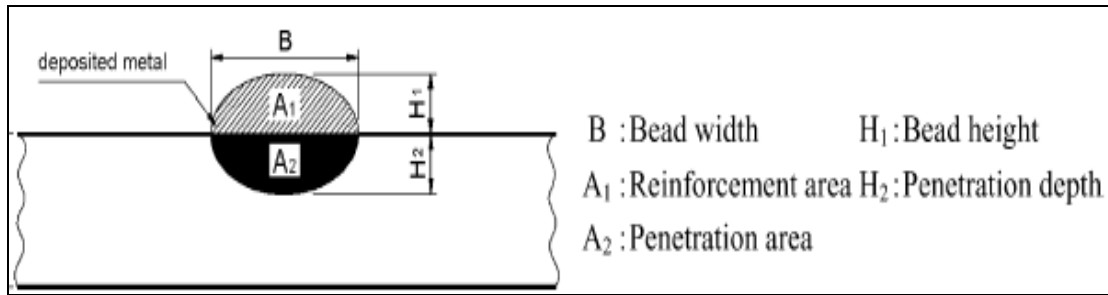
Pulse process variables are controlling factors for heat input which in turn leads to grain refinement in fusion zone, width reduction of HAZ, segregation of alloying elements, reduction in hot cracking sensitivity and residual stresses [16, 66]. Improved mechanical properties of welds are achieved by using current pulsing due to the grain refinement occurring in the fusion zone. The use of high current pulses is to penetrate deep and cater for longer arc period at lower current. Deep penetration in pulsed current welding is produced by arc pressure at peak for longer durations [12, 67, 68].

Heat input is the sole variable on the variation of bead characteristics and correlated with welding variables. On increasing current, bead width, height and penetration increases, while on increasing voltage, bead width increases but bead height and penetration increased up to a limit and then remain constant. With increased travel speed, bead width and penetration increases, while height decreases. However a linear relationship exists between heat input of a weld and maximum temperature at a given distance from the weld centre line. It shows that pulsed arc welds are cooler and exhibit less thermal distortion than conventional GTA welds of the same penetration [69]. Heat input is typically calculated as follows:

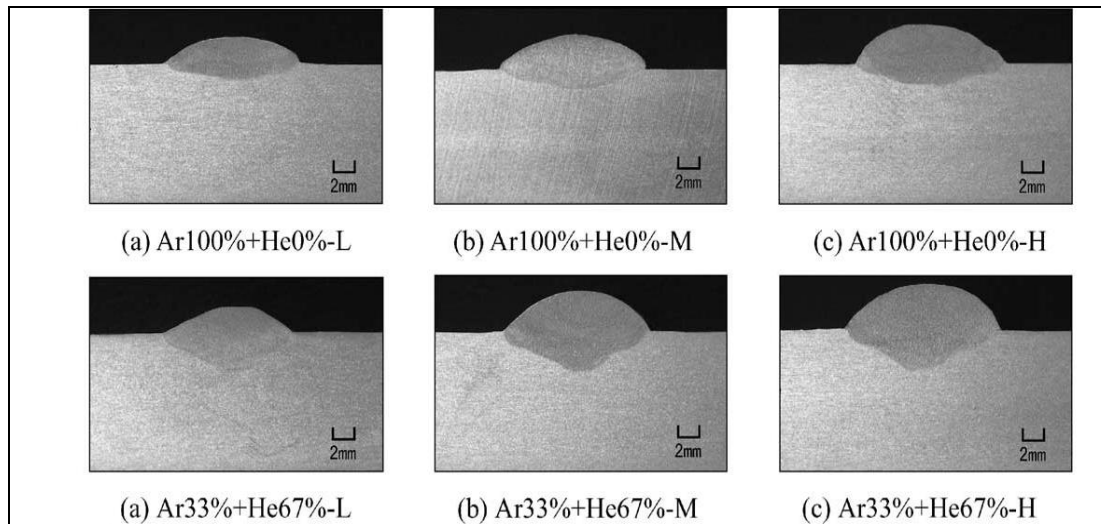
$$H = [60 E I] / 1000 S$$

Where H = Heat Input (kJ/mm), E = Arc Voltage (Volts), I = Current (Amps) and S = Travel Speed (mm/min).

Maximum bead width was achieved by using pure argon shielding gas during the pulsed GMA welding of aluminum alloy 5083 (Fig 2.3 and 2.4). But the penetration depth, weld area and dilution were greatest with Ar-33% + He-67% gas mixture [70].



**Fig 2.3: Schematic Diagram of Bead Profile**



**Fig 2.4: Cross Sectional Area for measurement of Bead Profile**

[L: Low Heat Input, M: Medium Heat Input and H: High Heat Input]

Goyal *et al.* [71] developed a model for predicting the penetration and width of fusion of the base plate and consequently the weld pool geometry of pulsed GMA welded aluminium and its alloys. However, the application of the model with an accuracy of  $\pm 10\%$  is limited to prediction of the weld geometry at mean current above 150 A.

Esme *et al.* [72] developed a systematic approach to the optimization of GTAW process parameters. The mathematical relationship between input control variables and weld pool quality parameters were obtained using the results of experiments. Six nonlinear and five multi-objective mathematical models are constructed and solved under the predetermined limits of the input control variables using the obtained mathematical relationships as objective functions.

Moulton *et al.* [73] studied the double sided arc welding (DSAW) of AA5083 aluminium alloy for Tailor Welded Blank (TWB) application and observed the hydrogen porosity in the weld metal even with cathodic cleaning of the oxide by the AC welding arc. The hydrogen porosity was significantly reduced by stainless steel wire brushing the weld surfaces prior to welding. DSAW improved the consistency of the weld bead geometries and facilitated an increase in the maximum welding speed of about 20%; however, there was little or no change in the transverse tensile strength with reduced hydrogen porosity. Zhang *et al.* [74–79] have examined the feasibility of using the DSAW process to make uphill, keyhole-mode welds in 6 to 12 mm thick plain carbon steel, stainless steel or aluminum alloy plates.

Weld pool oscillation behavior of GTAW has been studied extensively by many researchers [80–84]. Kotecki *et al.* [80] reported the presence of weld pool oscillation while investigating ripple formation during solidification of GTAW spot welds. Renwick and Richardson [81] using a linear constant current power source measured the arc voltage ripple to determine the weld pool oscillation frequency for a stationary weld pool. They discovered that the oscillation frequency was strongly dependent on weld pool geometry, which correlated well with inverse of square root of the pool mass. Alternatively Deam [82] estimated the oscillation frequency by measuring the radiated arc light which was proportional to the arc length, except at very low currents. Sorensen and Eager [83] developed a theoretical model for a stationary weld pool, which incorporated weld pool size, shape, density and surface tension. They validated this model against the resonant natural frequency of the weld pool, derived from the voltage and current spectra using Fourier Transform techniques.

Giridharan *et al.* [85] developed a mathematical model for correlating weld bead properties to pulsed GTAW process parameters with high accuracy. They also concluded that welding speed is the most important and pulse current the next important influencing process variable on bead geometry, while pulse current duration is the least important.

Balasubramanian *et al.* [86] reported that a five-level factorial technique can be employed effectively for developing mathematical models to predict weld pool geometry within the region of control process parameters. They optimized pulsed current GTAW process parameters to attain optimal weld pool geometry in titanium alloy using statistical tools such as design of experiments, ANOVA and multi-objective optimization tool namely, lexicographic method. The optimal weld pool geometry was obtained at a peak current of 84 Amp, background current of 36 Amp, pulse frequency of 6.3 Hz and pulse on time of 44%.

## **2.6 Mechanical properties and Metallurgical transformation**

The transverse groove weld tensile strength of aluminum alloys is a property which often used for evaluating the performance of groove welds while conducting welding procedure qualification test. The transverse tensile strength of an arc welded aluminum groove weld in the as-welded condition is contingent on the tensile strength of the HAZ of the weld. The HAZ is the area of base material immediately adjacent to the weld whose mechanical properties or microstructure transform by the heat of the welding. In the non-heat treatable aluminum alloys, the HAZ is near the annealed condition of the base alloy. In the heat treatable alloys, the HAZ will typically become partially annealed and over aged, depending on the original temper of the base alloy prior to welding and the heat input during welding.

Ductility is influenced by chemistry of the aluminum alloy and thermal strain is influenced by welding process, heat input, joint configuration and fixturing [87]. Aluminium alloys are sensitive to solidification and liquation cracks, which can be attributed to relatively high thermal expansion of aluminium, its large change in volume upon solidification and its wide solidification temperature range. Al alloys with greater amounts of alloying additions are more sensitive to weld cracking [88–89]. To minimize it, filler wire having higher level of solute and lower melting point than the parent metal is selected, which provides sufficient eutectic liquid for back filling of tears during

the solidification. In the family of Al–Cu alloys, AA2219 exhibits low sensitivity to hot cracking [89–91]. Pumphry and Lyons [92] demonstrated the relative crack sensitivity of Al–Cu alloy with different copper content in Al alloy, where sensitivity is very low at greater than 6% Cu and it shows very good weldability.

Guitterez *et al.* [93] reported that the strength of GTA welded joints can be influenced by modified welding parameters, which reduce the softening of precipitation-hardenable materials in HAZ. But the potential to improve the welding factor by parameter optimization is limited.

The superior tensile properties of post weld aged and pulsed GTAW joints of Al–Zn–Mg–Cu alloys are mainly due to the following reasons: (i) finer grains in the weld metal region in the order of 20  $\mu\text{m}$  (ii) more grain boundary area due to fine grains (iii) uniform distribution of precipitates all over the matrix (enhances resistance to indentation) and (iv) higher amount of precipitates in the weld region [94].

Tveiten *et al.* [95] reported that aluminium alloy welded joints having relatively poor mechanical properties have good fatigue strength. This effect is most likely caused by the strong compressive stresses near the welds that are effectively blocking crack initiation at the base of the fillet welds. Furthermore, since fatigue is dominated by crack propagation, the effect of the reduced mechanical properties at the point of failure are negligible compared to the important residual stresses caused by the welding procedure.

Padmanabham *et al.* [96] reported that increase in pulse frequency with same mean current and welding speed reduced the yield strength of the joint due to coarsening of weld microstructure. Percentage elongation seems to be increasing slightly, but this may be due to the increase in difference between yield stress and stress at fracture. Fracture in tensile specimens occurred mostly through the first fill pass and weld interface of the root pass. The fractographs on the weld interface indicates that the fracture could be through the fine equiaxed grain zone or the PMZ.

Myhr *et al.* [97] have presented a numerical solution, capable of handling nucleation, growth and coarsening and likewise dissolution of hardening precipitates in Al–Mg–Si alloys during ageing, welding and PWHT. Gaofeng *et al.* [98] have studied the softening of HAZ of pulsed current GMA welded Al–Zn–Mg alloy. They reported that the HAZ hardness can be recovered by PWHT and artificial aging more effectively than natural aging considering the recovery of the hardness.

During welding of dissimilar Al alloys (AA6061 & AA6063), there is a small decrease in microhardness near the weld interface in the 6063 alloy at different distances from the weld centre line but a significant microhardness drop was seen near the weld interface in the 6061 alloy [99]. Kumar P *et al* [100–102] also reported that the microhardness reduces in the particular area of the heat affected zone due to grain coarsening and precipitation hardening. Also, the drop in the microhardness shifts away from weld centre towards the unaffected base metal due to the increase in heat input as current and frequency are increased.

Softening and subsequent natural ageing (as a function of temperature and hold time) has to be conducted for getting the information needed to predict the hardness after welding. Also this highlighted the evolution of microstructure and yield properties which occurs in aluminium alloys during the weld thermal cycle [103].

In the GTA welding of AA6061 alloys, peak current and pulse frequency are having directly proportional relationship with the tensile properties of the welded joint, i.e. if the peak current is increased, the tensile strength will increasing and the similar effect is observed when the frequency is increased. However, base current and pulse duty cycle is having inversely proportional relationship with the tensile strength, i.e. if the base current is raised, the tensile strength will decreasing and the similar influence is noticed when pulse duty cycle is increased [104, 168].

Geoffroy *et al.* [105] reported that during GMA welding of AA6082-T5 aluminium alloy, there is a significant strength reduction near the welds due to over-aging but the size of the HAZ is small (less than 10 mm). The compressive residual stresses near the fillet welds had a strong positive influence on the fatigue life.

Cold worked aluminium alloys like 5xxx when subjected to high heat during welding suffers from hot cracking, which results from liquation cracking in the HAZ and solidification cracking in the weld [106]. Gambrell *et al.* [107] reported that material behavior in thick Al welded joints is highly complex, nonuniform and generally nonlinear on a point to point basis.

Kumar *et al.* [108–109] studied the influence of pulsed welding parameters (such as peak current, base current, welding speed and frequency) and magnetic arc oscillation on mechanical properties like UTS, yield strength, percent elongation and hardness of AA 5456 aluminum alloy weldments. The behavior of the welded joints at the optimum condition of process parameters is attributed to increase an amount of  $Mg_2Al_3$  precipitates that are formed in the aluminum matrix. In addition, the metallographic analysis reveals a fine grain structure at the weld centre, which results in higher mechanical properties. It is observed that, there is 10–15% improvement in mechanical properties after planishing.

Koteswara Rao *et al.* [110] reported that small addition of scandium (Sc) through filler resulted in fine equiaxed grain structure in 2219 aluminum alloy weld metals and have increased hardness values of weld metals. Sound welds could be obtained when weld metal Mg content was kept low, with addition of small amount of Sc. Addition of 0.25% Sc to Al-Cu filler did not result in improvement of strength of the weld metal. However, addition of 0.4% Mg to Al-Cu-Sc filler improved the strength significantly. Scandium addition in general resulted in significant increase in percent elongation. Huang *et al.* [111] also reported that addition of scandium with 7A52 (Al-Zn-Mg) aluminium alloy leads to very significant grain refinement in the fusion

zone, which leads to a reduction in solidification cracking tendency. There are obviously two soft areas in the welded joint, welding seam and over-aging zone.

Squillace *et al.* [112] reported that in AA2024-T3 aluminium alloy, the micro-hardness along with the thickness of GTA weld joint has the general decay of mechanical properties – in both weld bead and HAZ, related to phase transformation induced by high temperatures experienced by material.

Neutron and synchrotron X-ray measurements of welded aluminium alloy 2024 indicates that near the start (approximately 50 mm) of the weld, the maximum tensile stresses are approximately 60% of the original yield stress for the plate and are situated approximately 5–6 mm laterally from the weld line [113].

Balasubramanian *et al.* [114–115] reported that the superior mechanical properties (higher yield strength and hardness), preferred microstructures in the weld metal region (very fine equi-axed grains with higher amount of precipitates) and favorable residual stress field in the weld metal region (large magnitude of compressive stress) are the reasons for better fatigue performance of the post weld aged pulsed current GTAW joints of aluminum alloy 7075.

Ghosh *et al.* [116] and Patluri NB *et al.* [117] observed that the refinement of microstructure due to the pulsed current welding of 7xxx aluminum alloy results in a uniform distribution of the fine precipitates more effectively governed by its zinc pick up, enhancing the amount of precipitates in the matrix. Hardness in the fusion zone is the lowest due to the as-cast nature of the microstructure, which is characterized by coarse dendritic grains, interdendritic segregate phases and the lack of strengthening phases. Hardness is slightly higher in pulsed current welds as compared to continuous current welds and this could be due to the refined microstructure and low segregation of strengthening phases. The moderately higher hardness of pulsed current welds close to the fusion boundary is possibly due to a large

fraction of alloying elements in solid solution at the end of the weld thermal cycle, thereby giving conditions for extensive age hardening [118].

Balasuramanian *et al.* [119] reported that in AA7075 aluminium alloys, the hardness is lower in weld metal region compared to partially melted zone (PMZ), HAZ and base metal regions irrespective of welding technique. Very low hardness is recorded in constant current GMAW joints (70 VHN) and the maximum hardness is recorded in pulsed current GTAW joints (100 VHN). The simple aging treatment applied to the joints increased the weld metal hardness irrespective of welding processes and the increase in hardness is 15 – 20%.

The PMZ is the region immediately outside the fusion zone, where liquation occurs during welding because of heating above the eutectic temperature (or the solidus temperature), if the workpiece is completely solutionized before welding [120].

GTAW process has received considerable attention for the welding of 2xxx aerospace alloys. Much of the problem with weldability lies with the large gap between solidus and liquidus which can lead to liquation cracking in the HAZ or coarse segregated microstructures in the weld metal itself [121]. Some improvement in weldability has been achieved by careful control of the weld metallurgy, most notably through the use of scandium to refine the microstructure and greater weldability is achieved in the 6xxx and 7xxx alloys [122–123].

Prasad Rao K *et al.* [124] reported that AA6061–T4 alloys have relatively less PMZ cracking susceptibility with respect to T6 during GTAW irrespective of filler material used and highest cracking resistance when the AA4043 fillers containing 0.5% Sc was used. The increase in PMZ cracking resistance obtained by grain refiner fillers was attributed to lower silicon / magnesium segregation at grain boundaries and also to a ductile fusion zone.

Huang and Kou [125 –129] studied PMZ liquation in the welds of Alloys 2219, 2024, 6061 and 7075, including the liquation mechanisms, GB (grain boundaries) solidification, GB segregation and PMZ weakening caused by GB segregation.

Haung *et al.* [130] reported that the liquation cracking can be severe in welding of Al-Mg-Si alloys when the weld-metal solute content is low and much lower than the base-metal solute content. This cracking may be caused by the tensile strains, induced in the solidifying PMZ by the solidifying and contracting weld metal, that exceed the PMZ resistance to cracking. Liquation cracking initiates at or in the PMZ near the outer edge of the weld and propagates along the outer edge.

Haung *et al.* [131] also reported that aluminium alloy 2219, which is a simple binary Al-Cu alloy easy to understand, was welded with filler metals of various Cu and Si contents, including 1100, 2319, 4145, 4047 and 2319 plus extra Cu. Liquation cracking near the weld root was examined in the transverse and longitudinal macrographs. The PMZ grain boundaries (GB) near the weld root immediately behind the oscillating penetration in front of the weld pool are subjected to GB liquation and tensile stress / strain, and liquation cracking can occur.

Almost all the heat treatable aluminium alloys are unfortunately prone to hot cracking. The susceptibility to solidification cracking is greatly influenced by the composition of the weld metal hence the proper choice of filler material is an important aspect in controlling solidification cracking. The use of non-heat treatable fillers which can resist hot cracking is more meaningful in welding 7xxx series alloys. In these alloys, as long as the weld metal contains 3% Mg or more, hot cracking is not a serious problem. Coarse columnar grains are often more susceptible to solidification cracking than fine equi-axed grains. This may be because fine equi-axed grains can deform to accommodate contraction strains more easily [22].

Prior thermal temper and the welding techniques plays important role in the liquation of PMZ of the heat treatable aluminium alloy (AA2219) welds [132]. PMZ extends usually one or two grains into the HAZ relative to the fusion line. It is characterized by grain boundary liquation, which may result in liquation cracking [133].

The prominent factors which are having greater influence on fusion zone grain refinement are pulse current, back ground current, pulse frequency and pulse duty cycle [134]. An increase in the pulse frequency refines grain structure of weld metal using pulses of short duration. At a given frequency, long pulse duration produces coarser grain structure than shorter pulse duration. Further increase in the peak current leads to coarseness of grain structure [135].

The main problems in welding 7xxx series alloys are: (i) hot cracking (solidification cracking) in the weld and (ii) excessive micro-fissuring due to hot tearing in the PMZ of the HAZ. The 7075 alloy possess a substantial amount of copper (around 1.75 %) has a wide melting range with a low solidus temperature and is extremely sensitive to weld cracking when fusion welded [136]. Solidification cracking in welds is influenced by a combination of mechanical, thermal and metallurgical factors. Heat treatable filler alloys can be used in combination with current pulsing techniques to enhance solidification cracking resistance of fusion zone only, if the alloy is not sensitive to liquation cracking in the HAZ [137].

In welding 7075 aluminium alloy, solidification and liquation cracking can be avoided by using non-heat treatable filler alloys such as AA4043 and AA5356. To overcome liquation cracking in HAZ, fillers for welding heat treatable aluminium alloys should have a lower melting temperature than the base alloy. By allowing the low melting point constituents of the base alloy adjacent to the weld to solidify before the weld metal, stresses are minimized on the base metal during its hot short conditions and tendencies for intergranular cracking are greatly reduced [138]. Another way of controlling solidification cracking is to refine the fusion zone grain structure.

By selecting matching filler composition with AA7075 alloy and using pulse GTAW, enhanced solidification cracking resistance is obtained in fusion zone by refining grain size. However, the cracking still persists in HAZ, it is inferred that current pulsing is still inadequate to counter cracking tendency in weldments by using heat treatable filler alloys [139]. A non-heat treatable filler alloy of AA5356 (Al–5%Mg) is used to weld AA7075 to improve the mechanical properties of welds by the means of pulsed current welding and PWHT.

Another way of reducing the susceptibility to solidification cracking is through fusion zone grain refinement, which confers the further benefit that the weld metal mechanical properties are improved. Various grain refinement techniques have been discussed in the literature for aluminum alloy welds, e.g. electromagnetic stirring, current pulsing, torch vibration and inoculation. Of these, pulsed current welding technique has gained wide popularity because of its striking promise and the relative ease with which these techniques can be applied to actual industrial situations with only minor modification to the existing welding equipment [140].

The 7xxx series of alloys can also be separated into two groups as far as weldability is concerned. These are the Al-Zn-Mg and the Al-Zn-Mg-Cu types. Al-Zn-Mg Alloys such as 7005 will resist hot cracking better and exhibit better joint performance than the Al-Zn-Mg-Cu alloys such as 7075. The Mg content in this group (Al-Zn-Mg) of alloys would generally increase the cracking sensitivity. However, Zn is added to refine grain size and this reduces the cracking tendency effectively. This alloy group is easily welded with the high magnesium filler alloys such as 5356, which ensures that the weld contains sufficient magnesium to prevent cracking. Silicon based filler alloys such as 4043 are not generally recommended for these alloys because the excess Si introduced by the filler alloy can result in the formation of excessive amounts of brittle  $Mg_2Si$  particles in the weld.

The evolution of microstructure in weld fusion zone is influenced by current pulsing and cyclic variations of energy input into the weld pool causing thermal fluctuations / oscillation. Consequently this leads to periodic interruption in solidification process. As pulse peak current decays, solid–liquid interface advances towards the arc and increasingly becomes vulnerable to any disturbances in the arc formation. As current increases again in the subsequent pulse, the growth is arrested and remelting of the growing of dendrites can also occur. Current pulsing also results in periodic variations of the arc forces resulting in additional fluid flow which lowers the temperature in front of the solidifying interface. Furthermore, the temperature fluctuations inherent in pulsed welding leads to a continual change in the weld pool size and shape favoring growth of new grains. It is to be understood that effective heat input for unit volume of weld pool should be considerably less in pulse current welds, thus expecting the average weld pool temperatures to be low [134,140–141].

Weld fusion zones typically exhibit coarse columnar grains because of the prevailing thermal conditions during weld metal solidification. This often results inferior weld mechanical properties and poor resistance to hot cracking. While it is thus highly desirable to control solidification structure in welds, such control is often very difficult because of the higher temperatures and higher thermal gradients in welds in relation to castings and the epitaxial nature of the growth process [142]. Nevertheless, several methods for refining weld fusion zones were tried with some success: inoculation with heterogeneous nucleants, microcooler additions, surface nucleation induced by gas impingement and introduction of physical disturbance through techniques such as torch vibration and current pulsing [143].

A weldment basically consists of five microstructurally distinct regions normally identified as fusion zone, unmixed region, partially melted region, HAZ and unaffected base metal. The HAZ is the portion of weld joint which experiences peak temperatures high enough to produce solid-state microstructural changes but they are too low to cause any melting. Every

point of the weldment in the HAZ relative to the fusion line is subjected to unique thermal experience during welding, in terms of both maximum temperature and cooling rate. Thus, each point has its own microstructural features and corrosion susceptibility.

The weld pool solidification during fusion welding begins with the epitaxial growth of grains from PMZ grains along the fusion boundary, at the interface between the base metal and fusion zone. The partially melted grains provide excellent sites for growth with the growth rate exceeding the nucleation in this region. Epitaxial growth across the weld pool results in long and oriented columnar grains. The epitaxial grains are the end result of continuing growth of the partially melted grains from the fusion boundary. To initiate nucleation in the weld deposit and concurrently promote epitaxial grain refinement, it is essential to either increase the driving force, i.e. degree of undercooling or reduce the free energy barrier by introducing trace amounts of zirconium or titanium to the aluminum weld pool [118].

The microstructure of AA6061 exhibits intermetallics and strengthening particles. The intermetallics are formed during casting and ingot homogenization due to interaction between alloying elements and impurities present in the alloy. In AA6061 the  $Mg_2Si$  intermetallics undergo phase transformation and change their morphology during ingot homogenization, but they are not affected by solution heat treatment and aging of the alloy. The strengthening particles have composition  $Mg_2Si$  and size in the nanometer range. Their precipitation in the matrix during aging provides strength to the alloy [144].

Grain refinement in the pulse current GTAW takes place due to effects of pulsing on the weld pool shape, fluid flow and temperatures. The continual change in the weld pool shape is particularly important. As the direction of maximum thermal gradient at the solid–liquid interface changes continuously, newer grains successively become favorably oriented. Thus, while each grain

grows only a small distance, more grains grow resulting in a fine grained structure [145].

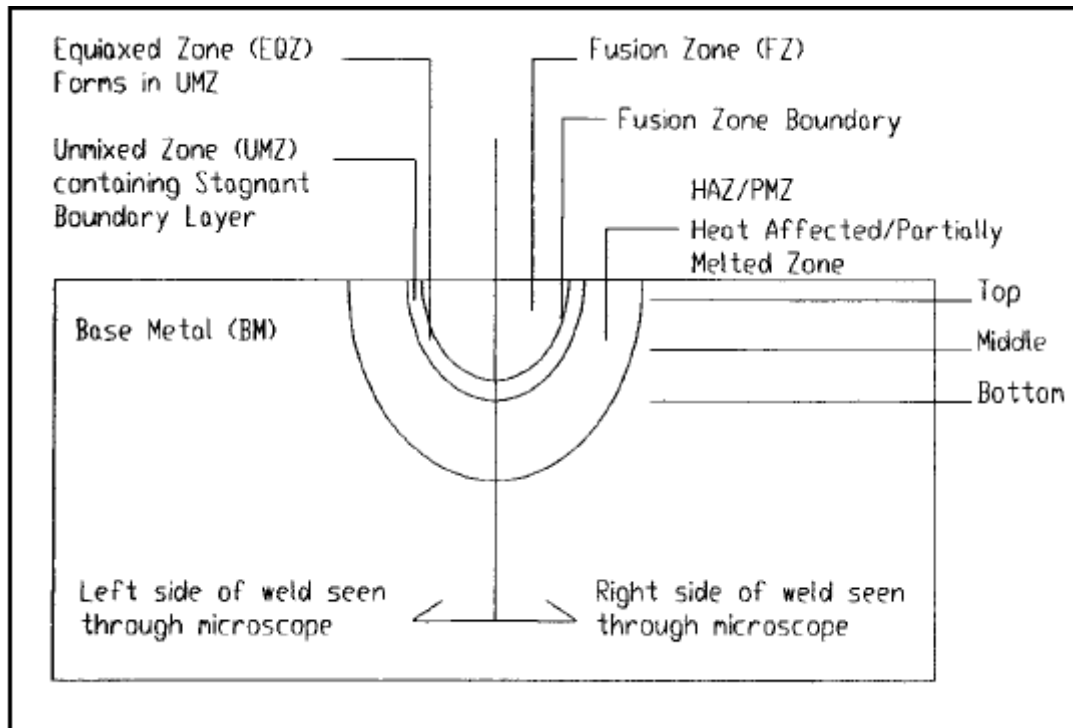
Mechanical properties and solidification cracking tendency of the Al-Mg-Si weld joint are largely governed by its microstructural characteristics apart from the mechanical constraints. The microstructure includes types of phases, their relative amounts and distribution besides grain structure. The grain structure of the weld metal shows the size, shape and the distribution of phases in the alloy. Coarse columnar grains with a large amount of low melting phases along the grain boundary increase solidification cracking tendency over the fine equiaxed grains with well distributed second phase particles [146].

Rao *et al.* [147] studied the influence of arc manipulation techniques (pulse current welding and magnetic arc oscillation) on the grain structure and tensile properties of Al-Cu alloy (2219) weld joints produced by GTAW and they found that 4–6 Hz pulse frequency is effective to control the grain structure. Fine and equiaxed grains obtained by arc manipulation improve the tensile strength and ductility.

Heat transfer experienced by the weldment during welding can alter the microstructure and the property of the weldment. Therefore the heat transfer and fluid flow in the weld pool can significantly influence factors such as weld pool geometry, temperature gradient local cooling rates and solidification structure [136].

The metallurgical features directly affected by heat input rate are the grain size in the HAZ and weld metal. Grains in the solidifying weld metal grow coherently with grains in the solid metal at the fusion boundary. Therefore the longer the time spent above the grain coarsening temperature of the alloy, the coarser the structure in HAZ and weld metal [64–65]. Aidun and Dean [148] reported the nomenclature for various welding regions (Fig 2.5) to postulate the effects of enhanced convection on fluid flow, heat transfer and their impact on solidification morphology as well as compositional homogeneity in fusion zone (FZ).

In multi layer welds partial or complete re-crystallization of weld metal occurs, depending upon the heat input, bead dimensions and the time interval between successive depositions, with the exception of final layer, the structure is refined with a corresponding improvement in ductility and toughness [149–150].



**Fig 2.5: Nomenclature for various welding regions**

Mendes da Silva *et al.* [151] concluded that the double pulsed GMAW (DP-GMAW) technique does not increase the porosity susceptibility in aluminum welding, when compared with the pulsed GMAW technique.

Grossbeck *et al.* [152] reported that oxygen and hydrogen are important impurities in order to weld vanadium alloys and must be controlled. Hydrogen results mostly from decomposition of water vapor by the welding arc, even at low concentrations.

Current pulsing has been used by few investigators [153–155] to obtain grain refinement in weld fusion zones and improvement in weld mechanical properties. Significant refinement of the solidification structure has been reported in aluminium alloys and titanium alloys. Most of the reported literatures are focused on the effect of pulsed current welding on grain refinement in fusion zone microstructure and tensile properties.

Acoff *et al.* [167] investigated the effects of PWHT thermal cycles on the fusion zone properties of  $\alpha_2$  titanium aluminide, Ti–14%Al–21%Nb. The as-welded  $\omega$ -type phase microstructure had tweed like molted appearance, which produced a microhardness that was approximately 100 VHN higher than the as received microhardness. PWHT at 650 °C eliminates the  $\omega$ -type phase.

Arenas *et al.* [156] also reported that the mechanical properties of the GTA welded Ti-48Al-2Cr-2Nb were decreased relative to the base metal, indicated by microhardness measurements and tensile testing. A significant increase in microhardness was observed in the fusion zone.

Choi *et al.* [157] investigated the effect of welding conditions on mechanical properties of pure titanium. The amount of shielded gas - 25 liter / min, the specimen showed the highest tensile strength and elongation. The cooling time after welding did not significantly affect the tensile strength and elongation. The hardness was the highest in HAZ and the difference in the hardness between HAZ and other zones was a major cause of the reduction of fatigue life of the welded zone.

Winco K.C *et al.* [158] reported that for Ti-64 alloy, welds of acceptable visual quality were produced by pulsed GTAW with welding currents of between 45 to 235 A, welding speeds of 0.26 - 1.27 mm sec and pulse-on times of 0.25 - 0.50. The best strength of the welds achieved was 1048 MPa, which was only 3.2 % lower than that of parent metal. The ductility of the as-welded weld metal of Ti-64 was lower than that of the parent metal.

Balasubramanian *et al.* [159] reported the impact toughness of pulsed current GTA welded  $\alpha$ - $\beta$  titanium alloy joints is having inversely proportional relationship to grain size. Peak current and pulse frequency are having profound influence on the effect of grain size on impact toughness. The effect of pulsing current increases the impact toughness up to a particular frequency (6 Hz) and then drops down.

In continuous current welding  $\alpha$ - $\beta$  Ti-6Al-4V alloy, the microhardness study of the welded joints revealed largest grains with highest hardness and had columnar grain morphology. Zhou Wei and Chew [160] found that significant improvement in impact toughness was shown to be due to the much reduced amount of primary  $\alpha$  grain in the weld metal. Senthil Kumar *et al.* and Balasubramanian *et al.* [28–30] have recently demonstrated the effectiveness of the pulsed current in refining the grain size by modeling and optimization.

Inoue *et al.* [161] reported that the solute micro-segregation occurring in Ti-6Al-4V during welding solidification was not significant due to the large solute back-diffusion in the solid. After solidification, there was a rapid dispersion in the matrix and a homogenization at an early stage of weld cooling.

Keshava Murthy *et al.* [162] reported that autogenous GTA welding of Ti-6Al-4V alloy reduces its ductility but raises the fracture toughness. Increase in fracture toughness attributable to a lamellar intragranular microstructure. PWHT at 900 °C / 4 hours improves fusion zone ductility and further increases fracture toughness.

Balasubramanian *et al.* [163] conducted an experimental study to understand the effect of process parameters of pulsed current GTA welding on titanium alloy weldments. Four important process parameters of pulsed current GTAW were used to optimize the three quality characteristics of tensile properties. Modified taguchi method [MTM] was used with success to identify the optimum parameters. Experimental results coupled with ANOVA results proved that pulse frequency is having pronounced effect on the multiple quality characteristics of tensile properties.

Balasubramanian *et al.* [164] also studied the effect of pulsing current on corrosion rate of GTA welded titanium alloy. It was observed that the effect of pulsing frequency and peak current had two regions with initially decreasing the corrosion rate and then increasing the corrosion rate irrespective of changes in base current and pulse on time. Current pulsing in GTAW has lead to relatively finer and more equi-axed grain structure. It has been understood that there is a value of optimum frequency at which the corrosion rate is minimum. The grain refinement due to the current pulsing has resulted in increase in corrosion resistance. Of the four pulsed parameters, peak current and pulse frequency are having predominant effect on corrosion properties.

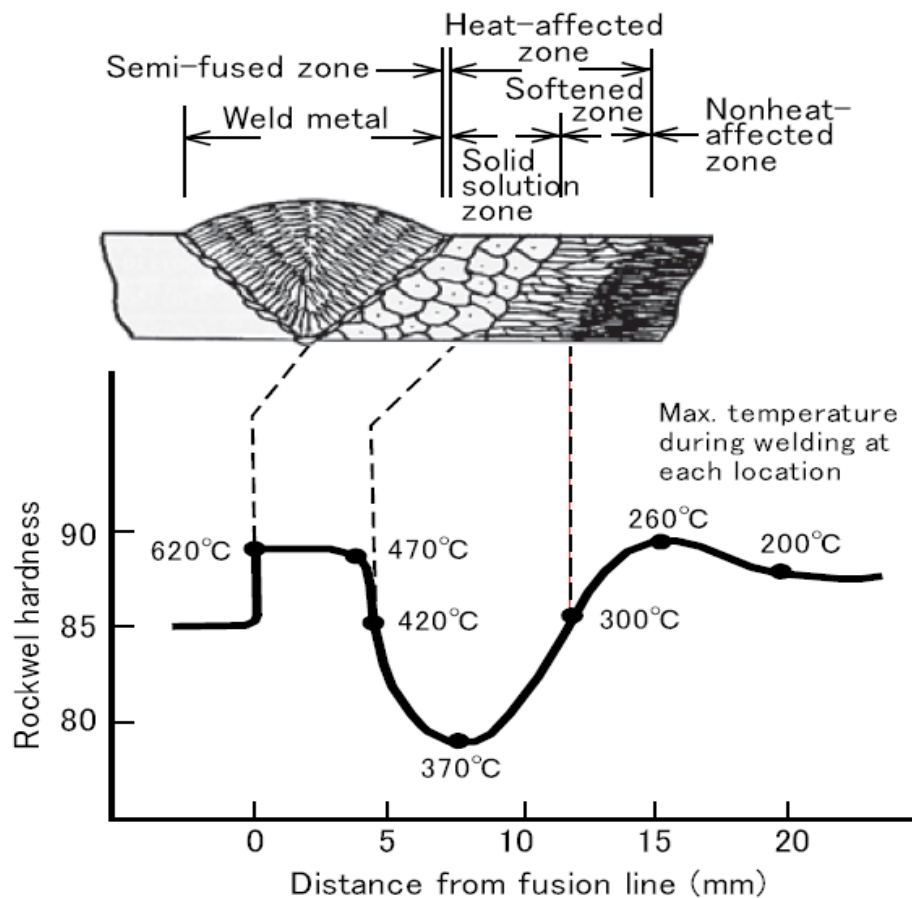
GTA welding of Ti-6Al-4V alloy has an undesirable effect on the corrosion behavior of the weldment and causes the fusion zone to act as anode during corrosion process. Also the distribution of  $\beta$ -phase as random, isolated and nodular particles in a predominantly  $\alpha$  matrix (microstructure of base metal) exhibits the best corrosion resistance. Weldment corrosion behavior is improved appreciably by subjecting it to a solutionizing and aging treatment [165].

Wang and Wei [166] described that the microstructure of Ti-6Al-4V alloy consists of a mixture of  $\alpha$  and  $\beta$  phase and measured volume fraction of  $\alpha$  and  $\beta$  phase is about 65% and 35% respectively. They reported that the mixed fine elongated  $\alpha$  and  $\beta$  phases have a grain size of about 5–20  $\mu\text{m}$ .

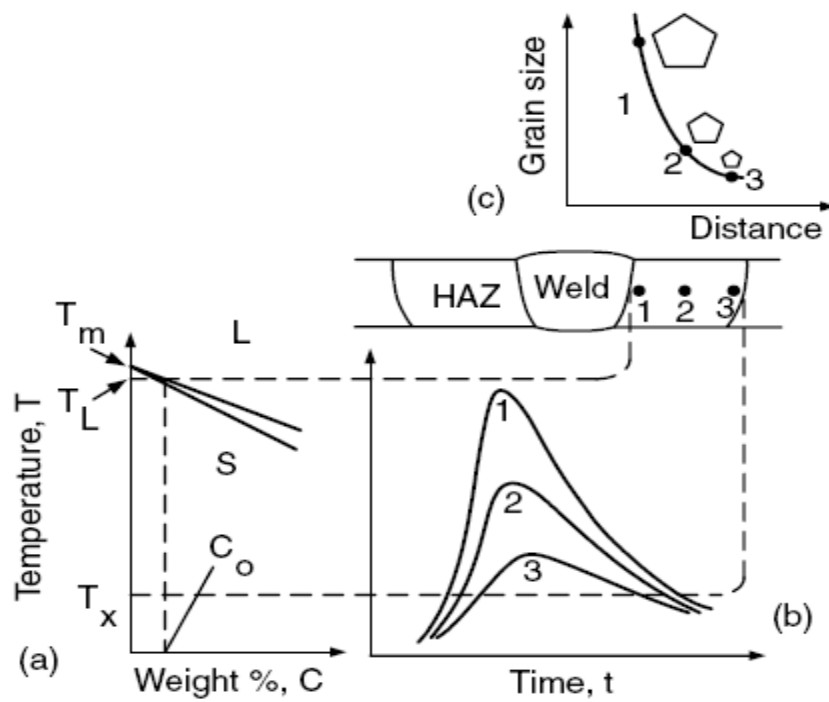
In the case of heat treatable aluminium alloys, the weld hardness exhibits a complicated distribution as shown in Fig 2.6 [175], which is due to the microstructural change affected by the temperature of individual zone. Softening in the HAZ is found to occur above a peak temperature of about 200  $^{\circ}\text{C}$ . It was found that the HAZ of an Al-Mg-Zn alloy can be divided into two sub-zones according to their different mechanism of softening: the dissolution zone and the over-ageing zone. The dissolution zone is characterized by dissolution of precipitates and covers the peak temperature range above 380 $^{\circ}\text{C}$ . The over-ageing zone is characterized by growth of precipitates and

covers the peak temperature range between 230 and 380 °C. The hardness in the heat-affected zone can be recovered by post-weld heat treatment, especially in the dissolution zone [98].

Sindo Kou [176] explains the grain growth of heat treatable aluminium alloys with the help of Fig 2.7, which indicates the increase in heat input (higher ratio of heat input to welding speed) increases the width of HAZ and comparatively coarse grains are developed. He also suggested the deterioration of strength and hardness in HAZ of heat treatable Al alloys by increasing the heat input and coarsening of grains with the help of Fig 2.8. The losses in mechanical properties of 6xxx and 7xxx series aluminium alloys after welding due to coarsening / over-aging of the precipitates are illustrated in Fig 2.9 [176].

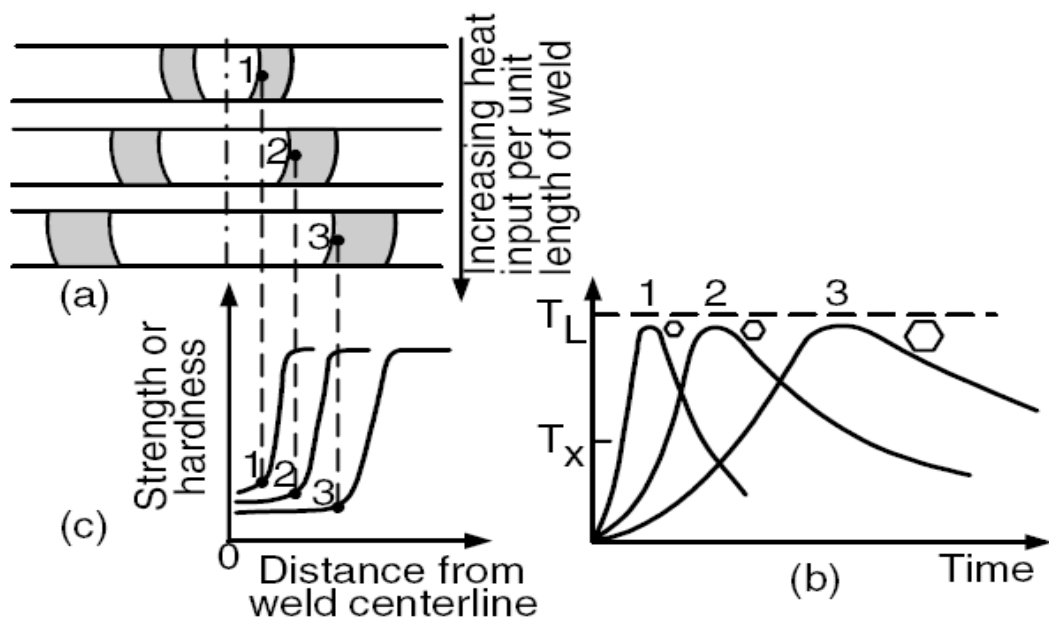


**Fig 2.6: Weld Hardness Distribution of Heat Treatable Aluminum Alloys** (230 A and welding speed 60 cm/min, after aging)



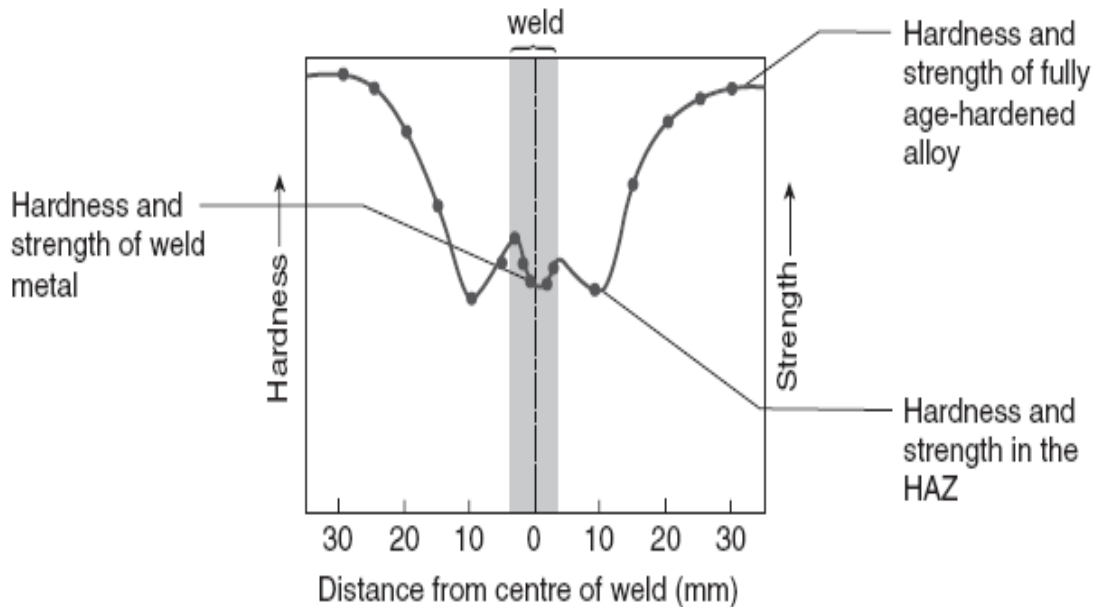
**Fig 2.7: Grain Growth in HAZ**

(a) Phase Diagram (b) Thermal cycles (c) Grain Size Variations,  
Suggested by Sindo Kou [176]



**Fig 2.8: Effect of heat input per unit length of weld on (a) Width of HAZ**

(Shaded), (b) Thermal Cycles near Fusion Boundary, (c) Strength and Hardness Profiles



**Fig 2.9: Effect of welding on AA6061-T6 age-hardened alloy – as welded**

## 2.7 Objectives of Present Thesis

None of the researcher has described / discussed in details, the optimization of bead geometry and mechanical properties of aluminium alloys AA7039 and AA6061, and Titanium alloy Grade-5. This research study describes the affects and optimization of various process parameters on the bead geometry and mechanical properties of the GTA welds. The objectives of the present thesis are as given below.

1. To study the effect of current and frequency of GTAW process on **bead geometry and mechanical properties of Aluminium alloys.**
2. To select the appropriate pulsed GTAW process parameters, like pulse current, base current, pulse frequency and pulse duty cycle for optimizing **bead geometry and mechanical properties of Aluminium alloys.**
3. To select the appropriate pulsed GTAW process parameters, like pulse current, base current, pulse frequency and pulse duty cycle with **gas mixtures** for optimizing **bead geometry and mechanical properties of Aluminium and Titanium alloys.**
4. To get improved bead geometry and mechanical properties of Al & Ti alloys.
5. To carry out Metallographic investigation and microhardness of Al and Ti alloys welded joint.

## Chapter 3

### EXPERIMENTAL DETAILS

#### 3.1 Introduction

This chapter describes the process, the capabilities of the equipments / machines / power source and the properties of selected base and filler alloys used in present study. The methods used for testing and measuring the properties of the GTA welded alloys are also described.

#### 3.2 The Process

In the GTAW process, an electrical arc is established between a non consumable tungsten electrode and the part to be welded. To start the arc, a high voltage is used to break down the insulating gas between the electrode and the part. Current is then transferred through the electrode to create an electrode arc. The metal to be welded is melted by the intense heat of the arc and is fused together either with or without a filler material.

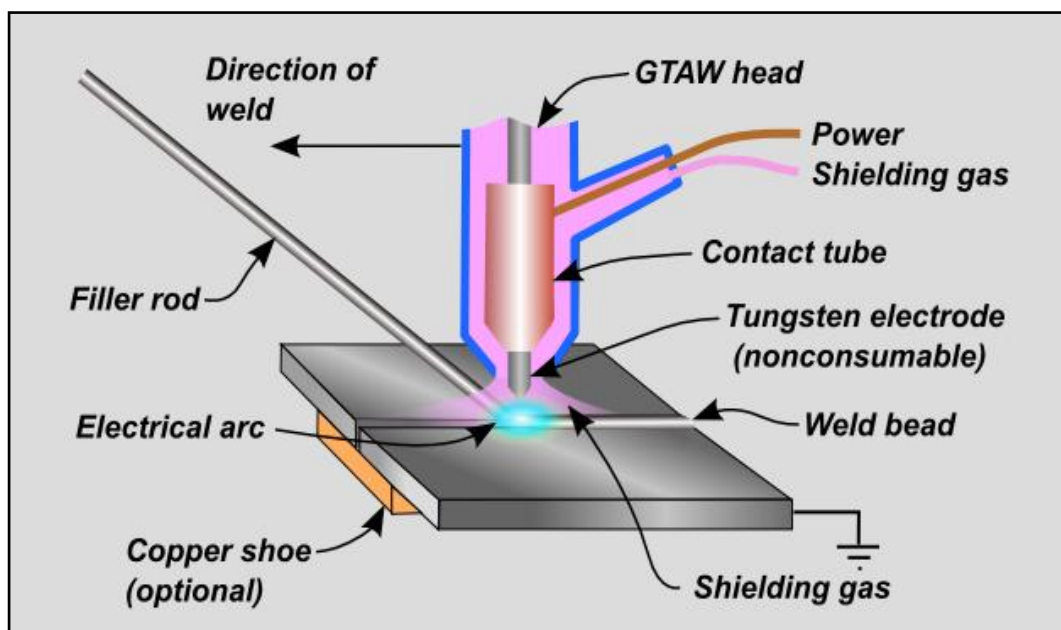
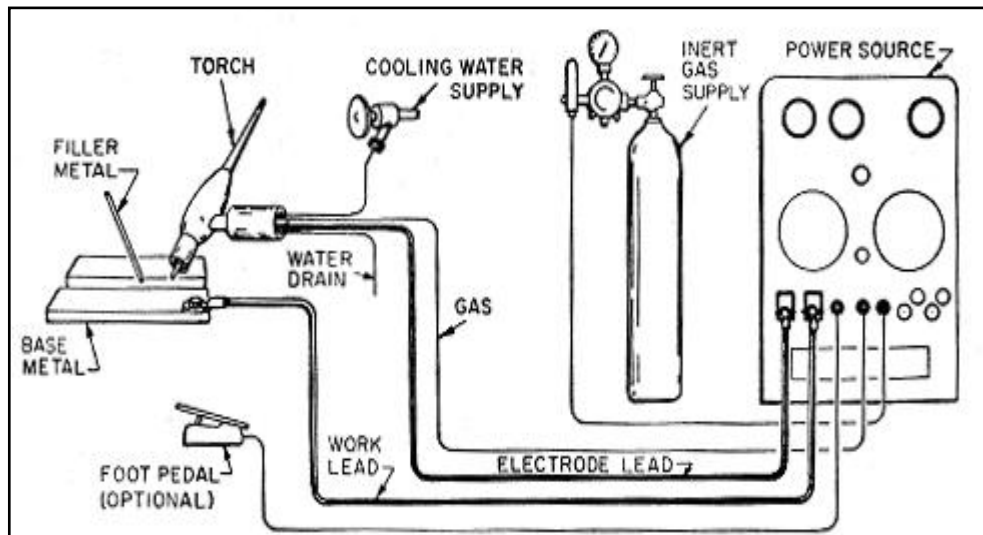


Fig 3.1: Schematic Diagram of Gas Tungsten Arc Welding (GTAW) Process

The arc zone is shielded with an inert gas to protect the tungsten electrode and molten material from oxidation and to provide a conducting path for the arc current. Shield gases used are argon, helium or mixtures of argon and helium. Schematic diagram and Circuit diagram of GTAW process is shown in Fig 3.1 and 3.2 respectively.



**Fig 3.2: Circuit Diagram of GTAW Process**



**Fig 3.3: TRITON 220 AC / DC (Pulsed GTAW Machine)**

### 3.3 Equipment Used

The equipment used includes a power supply, a welding torch, a non-consumable tungsten electrode and a gas shielding system. A digital Pulse GTAW TRITON – 220 AC/DC welding machine (Fig 3.3) was used for depositing the welds. Some important AC features of this machine are:

- Safe welding of different sheet thickness using the 'AC special' function
- Different AC curve shapes for all applications
- Sinus shape (silence arc) exceptionally low noise level
- Trapezoidal shape (medium arc) the all-rounder for most applications
- Rectangle shape (power arc) - for complex jobs
- Optimum ignition and arc stabilization as well as optimum ball formation by specifying the tungsten electrode diameter
- Optimization of the cleaning effect and fusion penetration characteristics by the adjustable balance
- Arc modification for different welding tasks by the adjustable frequency

Following are the ranges of main characteristics of TRITON 220 and the display screen is shown in Fig 3.4:

- Welding current / Voltage : 5A – 220A / 10.1V – 18.8V
- Open Circuit Voltage : 45V
- Frequency : 50 – 200 Hz
- Ambient temperature : - 10<sup>0</sup>C to + 40<sup>0</sup>C
- Tungsten electrode diameter : 1.0 – 4.0 mm
- AC balance : -30% to +30%
- Gas Pre-flow time : 0.1 – 5.0s, 0.1s increment.
- Ignition current : 0 – 100% of main current,  
1% increment
- Upslope time : 0.1 – 20.0s, 0.1s increment
- Pulse time : 0.01 – 10.0s, 0.01s increment
- Secondary current : 0 – 100% of main current,  
1% increment

- Pulse pause time : 0.01 to 10.0s, 0.01s increment
- Down slope time : 0.10 to 20.0s, 0.1s increment
- End crater current: : 0 –100% of main current,  
1% increment
- Gas post flow time : 0.10 – 20.0s, 0.1s increment

Pulse GTAW machine has power source with following facilities:

- Microprocessor controlled technology
- Advanced soft switching inverter technology
- Adjustable Pre-flow and Post-flow of shielding gas
- Up-Slope and Down-Slope rate of current
- Digital display of current with precise preset function
- High Switching Frequency, hence low volume and weight
- Built in High Frequency
- Pulsation controls to regulate intensity and duration

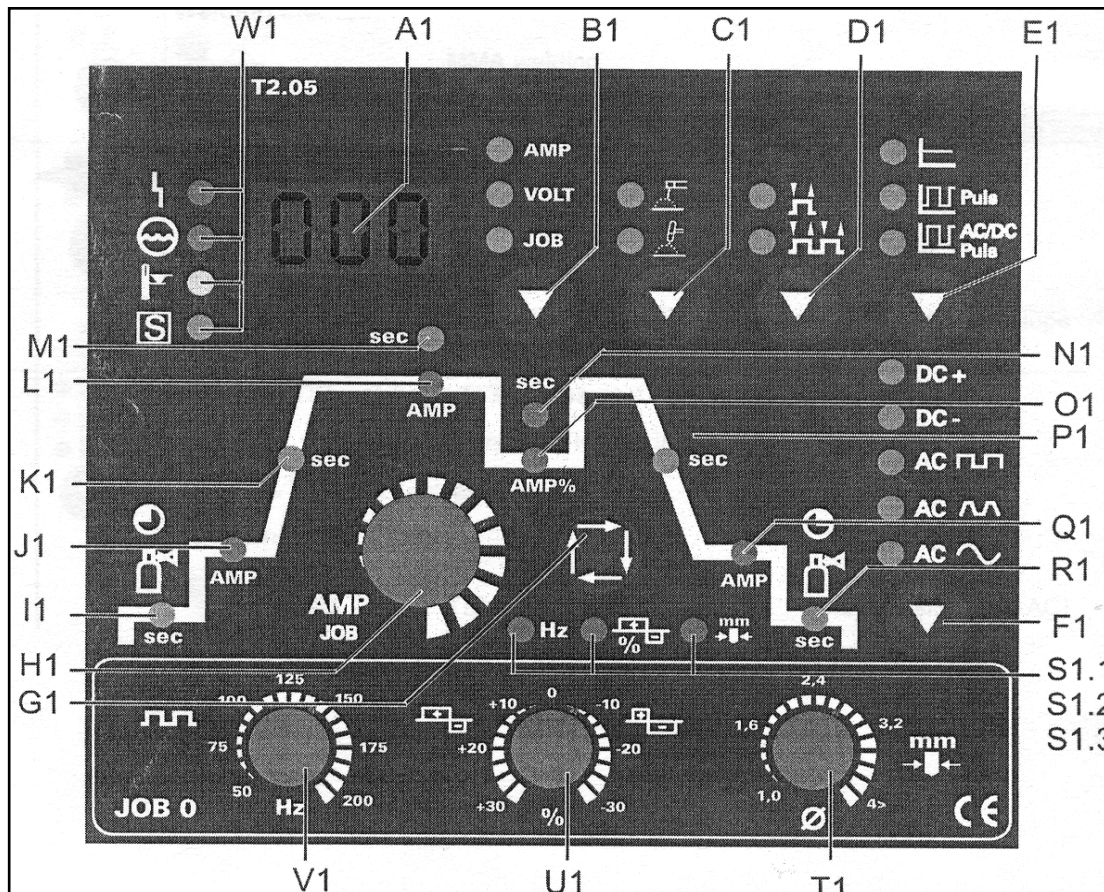
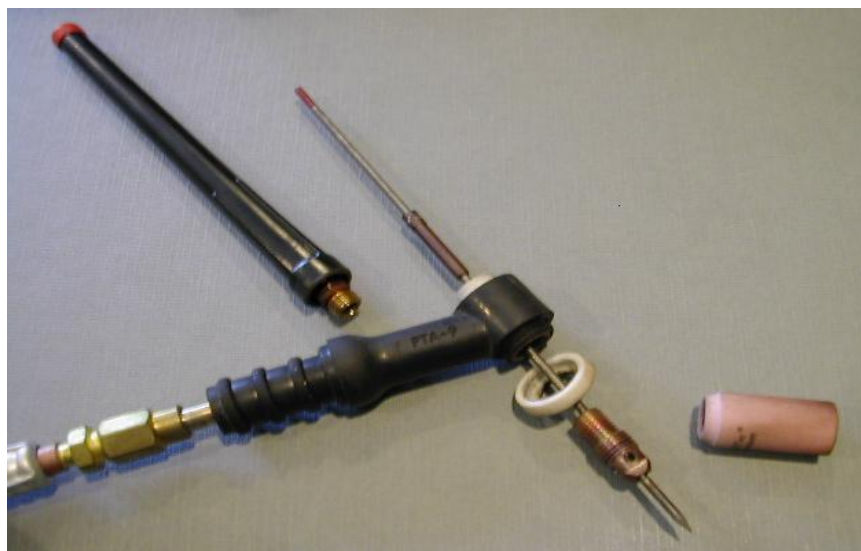


Fig 3.4: Characteristics of TRITON 220 AC / DC

**Welding Torch:** The torch of TRITON – 220 AC / DC GTAW machine is compact, light weight and fully insulated (Fig 3.5). It has a handle for holding it, a means for conveying the shielding gas to the arc area and a collet, chuck or other means for securing the tungsten electrode and suitable cables for conducting welding current to it. The torches may be air cooled or water cooled depending upon the current carrying capacity. Air cooled torch is used for welding of alloys which has a maximum current carrying capacity of 220A. Water cooled torches have a current carrying capacity more than 220A, which can be used for continuous welding operation.

**Nozzle:** Ceramic nozzle was used for the welding torch of GTAW machine. Ceramic nozzles become brittle after continuous use and must be replaced when the lip of nozzle becomes rough and uneven. A rough and uneven lip interferes with the flow of shielding gas and causes non uniform coverage of the weld area. A small size nozzle helps in maintaining a stable arc, permits welding in more restricted areas and give better vision of the weld. Larger size of nozzles gives better shielding – gas blankets at a slower gas discharge rate than smaller size nozzles. For metals such as titanium that are sensitive at elevated temp to contamination from the ambient atmosphere, larger size nozzles are safer. The shape of the nozzle is cylindrical with tapered inner surface.



**Fig 3.5: Welding Torch / Gun of GTAW process**

**Electrodes:** Tungsten, which has the high melting point 3422 °C and strong electron emitting capacity, has proved to be the best material for non consumable electrodes. Tungsten of commercial purity (99.5% W) and tungsten alloyed with either thoria or zirconia are the electrode material used in virtually all applications of GTAW. Tungsten electrodes with 1 to 2 % thoria (EWTh -1 and EWTh – 2) are superior to pure tungsten electrodes. They have improved electron emissivity, current carrying capacity, longer life and greater contamination resistance [38].

**Welding cables** links the power source to the torch and workpiece. Cables are normally made of copper or aluminium and consist of fine standard wires enclosed in insulated casing of natural and synthetic rubber. Cable must be kept to a minimum length and must be of ample size to carry the welding current without overheating. **Shielding gases** are generally stored in cylinders. Gas flow is controlled by flow meters and regulators. The shielding gas is brought to the welding torch through hoses, which may be connected straight to the torch or through the power supply or to an inert gas attachment to the torch.

### **3.4 Base Metal**

The experiments were conducted on Aluminium Alloys (AA6061 and AA7039) and Titanium Alloy Grade–5. The plate thickness selected for Al alloys 6061 & 7039 were 5.0 and 6.0 mm respectively for the present work. Also titanium alloy selected for experimentation was 2.5 mm thick. The compositions of the selected alloys are as per “The Aluminium Association (AA)” and “The International Alloy Designation System”. The chemical compositions and properties of base metals are shown in tables 3.1 – 3.3.

### **3.5 Filler Metal**

The filler metal rods consumed in this experimentation on GTAW process are of either 2.00 mm or 3.15 mm diameter. Fillers recommended for welding of aluminium alloys AA6061 and AA7039 base plates are aluminium alloys

AA5183, 5356 or 4043 and AA 5183 or 5356 respectively. In this study AA5356 filler rods were used for welding of AA7039 and AA5183 were used for welding of AA6061. For welding of Ti Grade–5 alloy, the matching filler rods (Ti Gr–5 alloy) were used. The chemical compositions of filler metals are shown in tables 3.4.

**Table 3.1: Composition and Properties of Aluminum Alloy 6061**

|                                  |                                     |                        |
|----------------------------------|-------------------------------------|------------------------|
| Al = 95.8 – 98.6 %               | Mg = 0.8 – 1.2 %                    | Si = 0.40 – 0.80%      |
| Cu = 0.15 – 0.40                 | Other each = 0.05                   | OTHER TOTAL = Max 0.15 |
| Density = 2.70 g/cc              | Yield Tensile Strength = 276 MPa    |                        |
| Hardness, Vicker's = 107 VPN     | Ultimate Tensile Strength = 310 MPa |                        |
| Melting Point = 582 – 651.7 °C   | Elongation at Break = 12%           |                        |
| Thermal Conductivity = 180 W/m-K | Modulus of Elasticity = 68.9 GPa    |                        |

**Table 3.2: Composition and Properties of Aluminum Alloy 7039**

|                                  |                                     |                        |
|----------------------------------|-------------------------------------|------------------------|
| Al = 90.45 – 90.50               | Mg = 2.30 -3.30                     | Zn = 3.50 – 4.50       |
| Cr = 0.15 – 0.25                 | Other each = 0.40                   | OTHER TOTAL = Max 0.50 |
| Density = 2.74 g/cc              | Yield Tensile Strength = 330 MPa    |                        |
| Hardness, Vicker's = 125 VPN     | Ultimate Tensile Strength = 400 MPa |                        |
| Melting Point = 482 - 638 °C     | Elongation at Break = 22%           |                        |
| Thermal Conductivity = 140 W/m-K | Modulus of Elasticity = 69.6 GPa    |                        |

**Table 3.3: Composition and Properties of Titanium Alloy Grade - 5**

|                                |                                     |           |
|--------------------------------|-------------------------------------|-----------|
| Ti = 90.0 %                    | Al = 06.0 %                         | V = 4.0 % |
| Density = 4.43 g/cc            | Yield Tensile Strength = 880 MPa    |           |
| Hardness, Vicker's = 349 VPN   | Ultimate Tensile Strength = 950 MPa |           |
| Melting Point = 1604 – 1660 °C | Elongation at break = 14.0 %        |           |

### 3.6 Shielding Gas

Argon as a shielding gas with 99.9% purity was used to weld the aluminium alloys. Also argon-helium mixtures were used to weld the Al and Ti alloys. The

different mixture (Ar + He) compositions are: 90% + 10%, 80% + 20%, 70% + 30%, 60% + 40% and 50% + 50%. In the case of aluminium, argon offers a stable arc, however it has lower penetration intensity and its security against porosity (due to hydrogen) is not as resistant as argon-helium mixtures. Effective combinations of helium and argon have been found to lie between 30-70% of each respective gas. Most commonly used is a mixture of 50% argon and 50% helium.

**Table 3.4: Chemical Composition of Filler Metals**

|               |   |
|---------------|---|
| Al Alloy 5356 | Al 92.90 – 95.30 %, Mg 4.50 – 5.50 %                  |
| Al Alloy 5183 | Al 91.20 – 95.20 %, Mg 4.30 – 5.20 %, Mn 0.50 – 1.0 % |
| Ti Alloy Gr-5 | Ti – 90%, Al – 6%, V – 4%                             |

Due to the higher ionization energy of helium compared to argon, a greater welding voltage (approximately 75% greater) provides the same amount of amperage and this leads to a higher thermal input into the workpiece. The higher heat conductivity of helium is another advantage compared to the argon. From an economical point of view it also has to be considered that helium is more expensive than argon. In addition, due to its lower specific weight, comparatively more helium than argon has to be used for gas shielding purposes. The higher energy input by helium results in an increased welding speed, lower pre-heat temperatures at the same penetration and a lower tendency for porosity by a hotter weld pool with lower viscosity and better degasification possibilities.

### **3.7 Bead Geometry Measurement**

The bead-on-plate welds were performed as per the design of experiment (DOE) discussed in chapter 4. Bead samples were cut into the suitable sizes from the middle of the welded samples and mould of the samples were prepared as shown in Fig: 3.6. The mould samples were polished on Automatic Polisher (Fig: 3.7) with the help of different grit size of abrasive papers and diamond powders. All samples were then etched in the suitable

chemicals and prepared for the weld bead geometry measurement and microstructural analysis. With the help of polishing and etching, bead geometry samples were able for differentiating the weld zone with the base metal as shown in Fig 3.8.

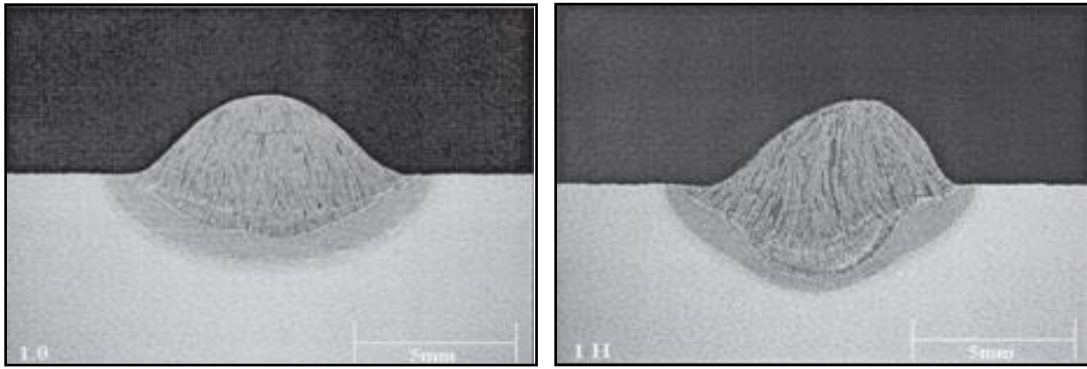


**Fig 3.6: Mould Sample for Bead Geometry Measurement and Microstructural Analysis**



**Fig 3.7: Automatic Polishing Machine**

(Base/Head: 8 inch, Pneumatically Force Application, Variable reversible speed 40 -500 RPM, CCW / CW wheel rotation and Color display touch pad)



**Fig 3.8: Bead Geometry Macrograph of samples**



**Fig 3.9: Surface Plate with Measuring Instruments**

With the help of magnifying glasses and various instruments (with surface plate), shown in Fig 3.9, the bead geometry parameters like penetration ( $p$ ), width ( $b$ ) and reinforcement height ( $h$ ) were measured.

### **3.8 Hardness Measurement**

The Vickers hardness test method consists of indenting the test material with a diamond indenter, in the form of a right pyramid with a square base and an angle of  $136^\circ$  between opposite faces subjected to a load of 1 to 100 kgf (shown in Fig 3.10). The full load is normally applied for 10 to 15 seconds. The two diagonals of the indentations left in the surface of the material after removal of the load are measured using a microscope and their average is

calculated. The area of the sloping surface of the indentation is calculated. The Vickers hardness is the quotient obtained by dividing the kgf load by the square mm area of indentation.

$$HV = \frac{2F \sin \frac{136^\circ}{2}}{d^2} \quad HV = 1.854 \frac{F}{d^2} \text{ approximately}$$

F= Load in kgf, d = Arithmetic mean of the two diagonals, d1 and d2 in mm

HV = Vickers hardness

When the mean diagonal of the indentation has been determined, the Vickers hardness may be calculated from the formula, but it is more convenient to use conversion tables. The Vickers hardness should be reported like 800 HV/10, which means a Vickers hardness of 800 was obtained using a 10 kgf force. The advantages of the Vickers hardness test are that extremely accurate readings can be taken and just one type of indenter is used for all types of metals and surface treatments.

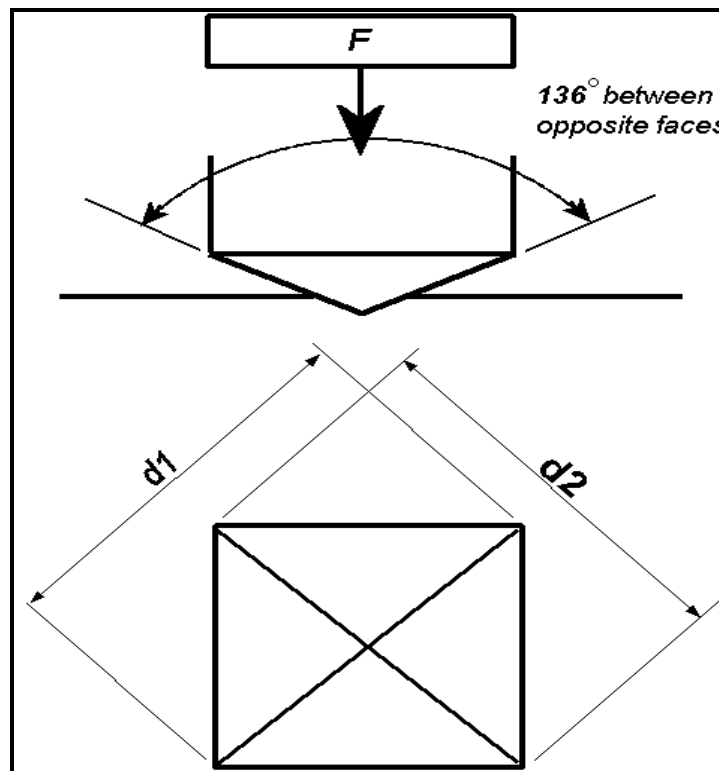


Fig 3.10: Vickers Hardness Indentation



**Fig 3.11: Digital Vickers Microhardness Tester**

(Load range – 10 to 1000 grams, Loading mechanism – Automatic, Load Duration – 5 to 60 seconds Max, Sample Size – 90 mm Height, Magnification – 100X and 500X)

Microhardness testing as per ASTM E-384 gives an allowable range of loads for testing with a diamond indenter; the resulting indentation is measured and converted to a hardness value. The actual indenters used are Vickers (more common; a square base diamond pyramid with an apical angle of  $136^\circ$ ). The result for Vickers microhardness is reported in  $\text{kg/cm}^2$  and is proportional to the load divided by the square of the diagonal of the indentation measured from the test. The load on the Vickers microhardness indenter usually ranges from a few grams to several kilograms. The indentations should be as large as possible, within the confines of sample geometry, to minimize errors in measuring the indentation. A Digital Vickers Microhardness Tester is shown in Fig 3.11. The test samples should have a smooth surface and be held perpendicular to the indenter.

### **3.9 Measurement of Tensile Strength and Percentage Elongation**

Tensile properties indicate how the material will react to forces being applied in tension. A tensile test is a fundamental mechanical test, where a carefully prepared specimen is loaded in a very controlled manner while measuring the

applied load and the elongation of the specimen over some distance. Tensile tests are carried out on Universal Testing Machine (UTM) and used to determine the modulus of elasticity, elastic limit, elongation and reduction in area, tensile strength, yield point, yield strength and other tensile properties. All tensile test of this study were performed on a computerized UTM (Fig 3.12). All welded samples should be defect free before tensile testing; therefore they were checked ultrasonically on Ultrasonic Flaw Detector (Fig 3.13 and 3.14).



**Fig 3.12: Computerized Universal Testing Machine**

(Loading capacity – 400 KN, Clearance for Test – 700 mm Max., Loading Speed – 1 mm / min, Graph facility – Online display of Load Vs Displacement)

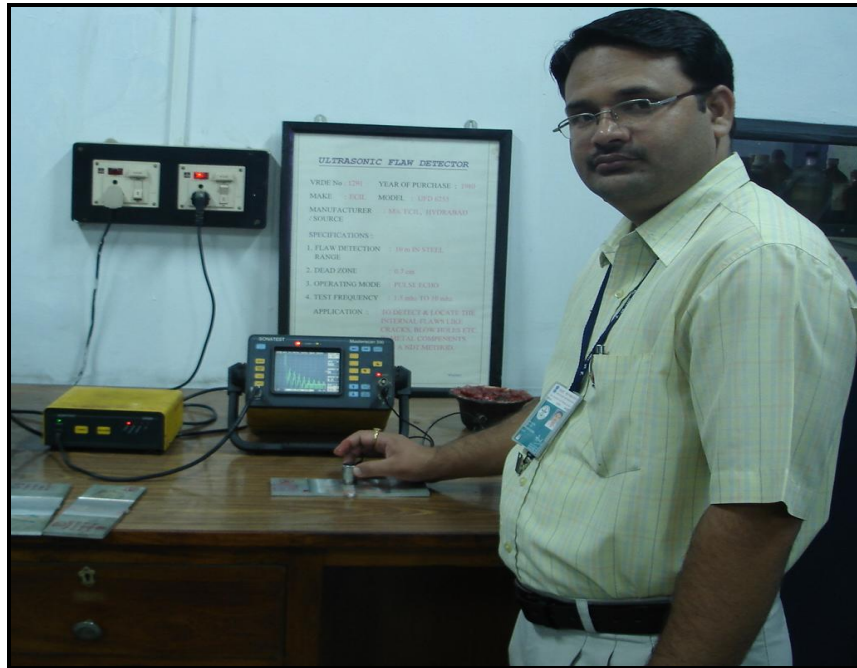
The ultimate tensile strength (UTS) or more simply the tensile strength is the maximum engineering stress level reached in a tension test. The strength of a material is its ability to withstand external forces without breaking. In brittle

materials, the UTS will be at the end of the linear-elastic portion of the stress-strain curve or close to the elastic limit. In ductile materials, the UTS will be well outside of the elastic portion into the plastic portion of the stress-strain curve. The main product of a tensile test is a load versus elongation curve which is then converted into a stress versus strain curve. The stress-strain curve relates the applied stress to the resulting strain and each material has its own unique stress-strain curve.



**Fig 3.13: Digital Ultrasonic Flaw Detector**  
(Test Range – Up to 10 m in steel, Test Mode – Pulse Echo,  
Frequency range – 1.5 to 10 MHz)

The ductility of a material is a measure of the extent to which a material will deform before fracture. The conventional measures of ductility are the engineering strain at fracture (usually called the elongation). It is obtained by fitting the specimen back together after fracture and measuring the change in length. Elongation is the change in axial length divided by the original length of the specimen or portion of the specimen. It is expressed in percentage.



**Fig 3.14: Ultrasonic Testing of Welded Samples**

### **3.10 Metallographic Examination**

The grains, grain boundaries and phases together are called the microstructure. These are distinguished and identified by suitable polishing and etching the alloy surface and examining it under a microscope at high magnification. This procedure is referred to as metallographic examination. It is one of the important methods of studying the characteristics of metals and alloys. The microstructure of an alloy is largely responsible for its physical and mechanical properties, and behavior in service.

Microstructural evaluation ranges from simple determination of certain parameters such as grain size and pores structure for full characterisation. A combination of techniques are used including optical and scanning electron microscopy (SEM), and Energy Dispersive Analysis (EDA) which provide both physical and chemical information, with sub-micron resolution.

Our wealth of expertise in materials can be accessed to solve problems with typical applications including: grain size measurement, identification of inclusions and specks, porosity and bonding evaluation, development of

interfaces on reaction, evaluation of material processing, performance evaluation and variability, Failure mechanisms and crack development, and evaluation of loci of failure.

Olympus make Inverted Metallurgical Microscope GX-51 was used for taking the microstructure of welded alloys for this study and the specifications of the same are as follows:

- Optical System – Universal Infinite System (UIS) 2
- Observation Method – Bright field, dark field, simple polarized light, differential interference contrast mode
- Focusing Part - Manual, Coarse and fine coaxial handle
- Imprinting of scale - All Ports, Reversed Position (up / down) from observation position seen through the eye
- Light Source - 100W halogen bulbs-2No
- Neutral density filter, 25% transmission, 25 mm dia
- Widefield binocular tube- U-B190, U-TR30H-2

Image recording equipment is attached with digital camera (Model DP 20) with 2.0 M Pixel CCD and driver software. The microscope is also attached with the computer. It consists of following specifications:

1. Inverted stand, complete with built-in glass refractor and built in power supply transformer, variable light intensity control, output sockets and fuse holder.
2. To meet high-magnification observation requirements, magnification settings extend from lower magnifications to higher magnification, when using eyepiece.
3. Suitable for both bright field and simple polarizing observations. The polarizer can be rotated through 90°, allowing optimum contrast control.
4. As well as it has the standard 6V, 30W halogen lamp, users can select a 100W fiber light source, high-brightness images even of dark samples.

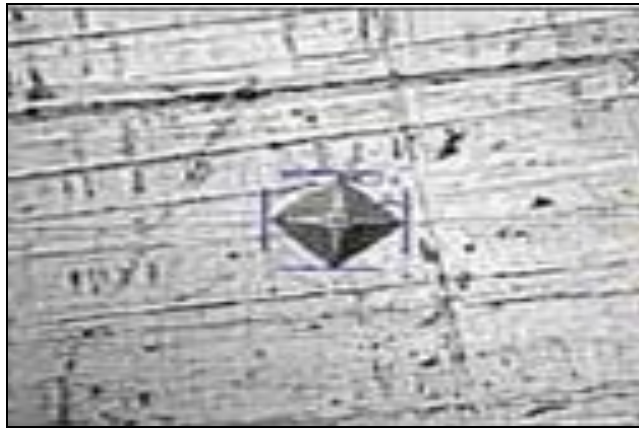
5. Reflected light illuminator with aperture stop. Optimum contrast is obtained according to objective magnification and observation method.

Fig 3.15 shows the experimental setup of image analysis software. The experimental setup divides part of interested area from one up and background area. This uses dialog box of phase, showing multiple binarizations. This multiphase fraction support multiple threshold ranges from setting up various phases. As per ASTM-E562 international standard phase analysis consists of following:

- 1) Low: Lower bound threshold linked lower bar of histogram viewer.
- 2) High: Higher bound of threshold linked higher bar of histogram viewer.
- 3) Phase consists of combo box, color button and name editing box to combo box.
- 4) Display all phases: display all phases with color and current phase display selected phase.
- 5) Table: contains ratio of phases like type of phase and analyzed surface (%) ratio of each phase computed.



**Fig 3.15: Metallurgical Microscope with Image Analyzer Software**  
(Make – Olympus Corporation Japan, Magnification – 50X TO 1000X,  
Image Analyzer Software – Inclusion inspector)



**Fig 3.16: Microstructure showing Hardness Indenter**

**Grain Size Measurement Method:** There are two methods to measure grain content – Intercept method and Plani-metric method. Both are used to measure average grain size of the selected material as per ASTM-E112 standard. This method supports measuring function for average material grain size with method of intercept procedure. The size of grain with Intercept method as per ASTM-E112 was selected for further analysis. The detail of grain size measurements are given in table 3.5.






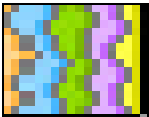
The microstructural quantity known as the ASTM Micro Grain Size number,  $n$ , is define by the following relationship:

$$N = 2^{n-1}$$

Where  $N$  is the number of grains per square inch, measured at a magnification of 100x. The most common methods of value of  $n$  are:

1. Comparison Method: The overall appearance of the microstructure is simply compared with a standard set of micrographs or 'plates' for which the ASTM Grain Size number has been determined.
2. Grain Counting Method: The number of grains per unit area is counted directly. The ASTM Grain Size number is then determined according to the definition.

**Table 3.5: Grain Size Measurement Method**

| Icon  | Name        | Processing  |
|---|-------------|---|
|    | Intercept   | Measure average grain size by intercept method.                           |
|    | Planimetric | Measure average grain size by planimetric method.                         |
|    | Phase       | Measure multi-phase fraction  |
|    | Graphite    | Measure nodularity and size distribution of graphite in nodular cast iron |
|   | Hardness    | Measure the micro-hardness of materials                                   |
|  | Thickness   | Measure the local thickness of metal and oxide coatings                   |

## **Chapter 4**

### **PARAMETRIC STUDY OF GAS TUNGSTEN ARC WELDING**

#### **4.1 Introduction**

In GTAW, the weld deposit quality is mainly dependent on the material to be welded, type of joint preparation, shielding gas used, filler metal selection, gas flow rates and other welding parameters, like welding current, current pulsing, arc voltage, speed of travel, size of electrode and heat input rate. The welding parameters should be selected properly for getting the optimum results, which have been already discussed in Chapter 2.

GTA welding of aluminium is normally performed using AC, where oxide film removal takes place on the electrode positive half cycle. However, the electrode cooling and weld bead penetration takes place on the electrode negative half cycle of the AC sine wave. The arc is extinguished and reignited every half cycle as the arc current passes through zero, on a 50Hz power supply requiring this to occur 100 times per second, twice on each power cycle. To achieve an instant arc re-ignition a high-frequency (HF), high-voltage current is applied to the arc, bridging the arc gap with a continuous discharge. This ionizes the gas in the arc gap, enabling the arc to reignite with a minimum delay. Aluminium is a poor emitter of electrons, meaning that it is more difficult to reignite the arc on the electrode positive half-cycle. If there is any delay in re-ignition then less current flows on the positive half cycle than on the negative half cycle.

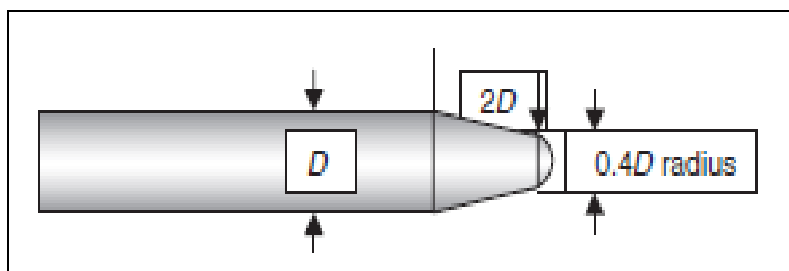
The power source controls should provide for both pre-flow and post-flow of the shield gas. A pre-flow is used to protect the electrode when the arc is established. Maintaining the flow of gas when the weld is terminated is also necessary to protect both the weld pool and the electrode from oxidation as they cool from welding temperature. Gas flow rates, ignition current, end crater current, 0 AC balance, up-slop time and down-slop time settings remain constant during all the experimentations.

The small diameter electrode leads to overheating and possibly melting, resulting in tungsten contamination of the weld pool. Nevertheless, the large diameter electrode resulted in arc stability problems and a very wide weld pool. Hence for getting the best results the recommended electrode diameters and welding currents are presented in Table 4.1. Before production welding is started, it is recommended that the electrode is preheated by forming an arc on an aluminium scrap piece. This enables the rounded tip to be formed, allows the welder to check that the electrode is performing correctly and enables the arc to be reignited on the production component with ease.

If the tip becomes contaminated or is damaged in any way, it should be reground and reformed. The electrode tip assumes a hemispherical shape during welding. It is important that this shape is maintained if a stable arc is to be achieved. The electrode tip should be lightly tapered to assist in the formation of the rounded tip as illustrated in Fig. 4.1.

**Table 4.1: Recommended Tungsten Electrode Diameters**

| Tungsten Electrode Diameter (mm) | Current (A) |
|----------------------------------|-------------|
| 1.0                              | 20 – 50     |
| 1.6                              | 50 – 80     |
| 2.4                              | 80 – 160    |
| 3.2                              | 160 - 225   |
| 4.0                              | 225 - 330   |
| 5.0                              | 330 – 400   |
| 6.0                              | 400 – 550   |



**Fig 4.1: Recommended Tungsten Electrode Shape**

The filler rod should be fed into the leading edge of the weld pool with a slow dabbing action at an angle of 10–20°. A steeper angle than 10–20° restricts the welder's view of the weld pool. The tip of the filler rod should be held inside the gas shield while it is hot to prevent oxidation. As the component thickness increases the filler rod diameter increases, necessitating an increase in arc length. Up to 3 mm thickness, the weld can be made without a weld preparation, but above this a V or U preparation will be necessary to achieve full fusion. The appearance of the weld pool is used to judge a full penetrated root bead by a skilled welder. When full penetration has been achieved the weld pool will sink and will have a bright shiny surface.

## **4.2 Experimental Procedure**

The experiments were performed on a digital Pulse GTAW TRITON–220 AC/DC welding machine with non-ferrous alloys. The non-ferrous alloys selected for experimentation was aluminium alloys (AA7039 and AA6061) in T6 condition and Ti Grade–5 titanium alloy. The plate thicknesses of the above alloys were as follows:

|                        |   |        |
|------------------------|---|--------|
| Aluminum alloy AA7039  | – | 6.0 mm |
| Aluminum alloy AA6061  | – | 5.0 mm |
| Titanium alloy Grade 5 | – | 2.5 mm |

The filler rods selected for welding the above alloys are as follows:

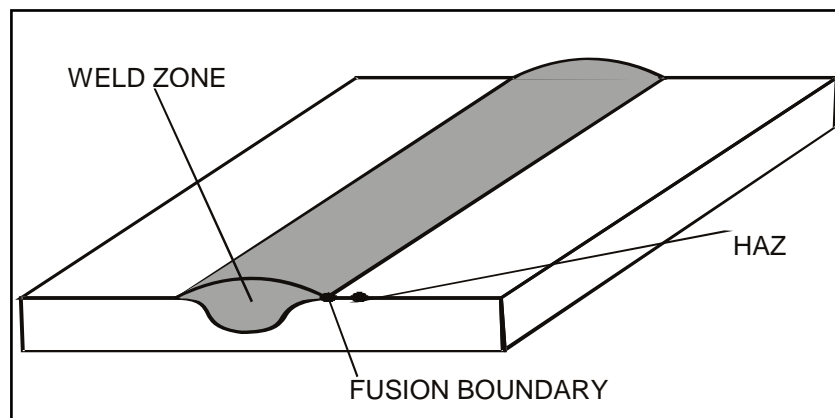
| <b>Base Metal</b>      | <b>Recommended Filler Rods</b>    |
|------------------------|-----------------------------------|
| Aluminium Alloy 7039   | AA5356 – 2.00 / 3.15 mm $\Phi$    |
| Aluminium Alloy 6061   | AA5183 – 2.00 / 3.15 mm $\Phi$    |
| Titanium Alloy Grade 5 | Ti Alloy Grade 5 – 2.00 mm $\Phi$ |

The experiments were done in various stages for analyzing the effects of GTAW process parameters on bead geometry and mechanical properties of Al and Ti alloys. Also experiments were done for optimization of pulsed GTAW process parameters and gas mixtures for bead geometry and mechanical properties of above alloys. The various stages of the experimental studies are illustrated as follows:

#### **4.2.1 Experimentation on Aluminium Alloy 7039 (Without Pulsing)**

The 6.0 mm thick samples of aluminium alloy 7039 were cut into the standard sizes (AWS Standard) of 80mm x 120mm (bead-on-plate) by shear and milling machines [12]. All samples and filler rods were cleaned by stainless steel wire brush / with acetone for removing the dust, oil, grease and thin oxide coating before welding. Weld beads along the length were deposited using 3.15mm diameter filler rods as shown in Fig 4.2. A non-consumable tungsten electrode of 2.4mm diameter was used with high purity (99.99%) argon as a shielded gas. Bead-on-plate samples welding have been carried out with AC sinusoidal wave at various currents and frequencies. These welded samples were used to measure the bead geometry parameters as well as for microhardness measurement in different zones of welding.

Design of Experiment (DOE) for the above study is given in Table 4.2. Parameters level / limiting values of current and frequencies were decided by performing large number of trial weld on the above plates. At lower current (below 90A), the heat input was not sufficient to melt the base metal and for higher current (above 150A), there was chances of burn through due to excessive heat input. Also at lower frequencies (less than 50Hz), bead contour and bead profile were not of good quality and at the same time at higher frequencies (above 200Hz), there was harsh sound in the welding machine.



**Fig 4.2: Bead-On-Plate sample**

**Table 4.2: Experimental Layout for AA7039 (Without Pulsing)**

| <b>Experiment No</b> | <b>Current (A)</b> | <b>Frequency (Hz)</b> | <b>Experiment No</b> | <b>Current (A)</b> | <b>Frequency (Hz)</b> |
|----------------------|--------------------|-----------------------|----------------------|--------------------|-----------------------|
| 1.                   | 90                 | 50                    | 29.                  | 90                 | 50                    |
| 2.                   | 100                | 50                    | 30.                  | 90                 | 75                    |
| 3.                   | 110                | 50                    | 31.                  | 90                 | 100                   |
| 4.                   | 120                | 50                    | 32.                  | 90                 | 125                   |
| 5.                   | 130                | 50                    | 33.                  | 90                 | 150                   |
| 6.                   | 140                | 50                    | 34.                  | 90                 | 175                   |
| 7.                   | 150                | 50                    | 35.                  | 90                 | 200                   |
| 8.                   | 90                 | 100                   | 36.                  | 120                | 50                    |
| 9.                   | 100                | 100                   | 37.                  | 120                | 75                    |
| 10.                  | 110                | 100                   | 38.                  | 120                | 100                   |
| 11.                  | 120                | 100                   | 39.                  | 120                | 125                   |
| 12.                  | 130                | 100                   | 40.                  | 120                | 150                   |
| 13.                  | 140                | 100                   | 41.                  | 120                | 175                   |
| 14.                  | 150                | 100                   | 42.                  | 120                | 200                   |
| 15.                  | 90                 | 150                   | 43.                  | 150                | 50                    |
| 16.                  | 100                | 150                   | 44.                  | 150                | 75                    |
| 17.                  | 110                | 150                   | 45.                  | 150                | 100                   |
| 18.                  | 120                | 150                   | 46.                  | 150                | 125                   |
| 19.                  | 130                | 150                   | 47.                  | 150                | 150                   |
| 20.                  | 140                | 150                   | 48.                  | 150                | 175                   |
| 21.                  | 150                | 150                   | 49.                  | 150                | 200                   |
| 22.                  | 90                 | 200                   | 50.                  | 180                | 50                    |
| 23.                  | 100                | 200                   | 51.                  | 180                | 75                    |
| 24.                  | 110                | 200                   | 52.                  | 180                | 100                   |
| 25.                  | 120                | 200                   | 53.                  | 180                | 125                   |
| 26.                  | 130                | 200                   | 54.                  | 180                | 150                   |
| 27.                  | 140                | 200                   | 55.                  | 180                | 175                   |
| 28.                  | 150                | 200                   | 56.                  | 180                | 200                   |

#### 4.2.2 Experimentation on Aluminium Alloy 7039 (With Pulsing)

Bead-on-plate samples were prepared and welded in the same manner as 4.2.1. The experimental layout for pulsed GTA welding on AA 7039 is given in Table 4.3. Parameters level / feasible working limits of pulsed current GTAW parameters like pulse / peak current (P), base / secondary current (B), pulse frequency (F) and pulse-on-time / pulse duty cycle (T) were decided by performing large number of trial welds. Different combinations of pulse current parameters were used to conduct the trial runs. The bead contour, bead appearance and weld quality were inspected to identify the welding parameters. From the above analysis, following observations were made:

- If the peak current (P) < 125 A, incomplete penetration and lack of fusion were observed. At the same time, if the P > 200 A, under cut, spatters and overheating were observed.
- If base current (B) < 40 A, arc length was found to be very short. On the other hand, B > 120 A, arc became unstable and arc length was increased.
- If the pulse frequency (F) < 50 Hz, the bead contour and bead appearance was not of good quality. However, if the F > 250 Hz, there was a harsh sound in welding machine.
- If the pulse duty cycle (T) < 10%, the heat input was very low which was not sufficient to melt the base metal. On the contrary, if the T > 90%, over melting of the base and filler metal, and overheating of tungsten electrode was noticed.

**Table 4.3: Experimental Layout for AA7039 (With Pulsing)**

| Experiment No | Base Current (A) | Pulse Current (A) | Pulse Frequency (Hz) | Pulse Duty Cycle (%) |
|---------------|------------------|-------------------|----------------------|----------------------|
| 1.            | 120              | 150               | 50                   | 10                   |
| 2.            | 120              | 150               | 50                   | 30                   |
| 3.            | 120              | 150               | 50                   | 50                   |

|            |     |     |     |    |
|------------|-----|-----|-----|----|
| <b>4.</b>  | 120 | 150 | 50  | 70 |
| <b>5.</b>  | 120 | 150 | 50  | 90 |
| <b>6.</b>  | 120 | 150 | 100 | 10 |
| <b>7.</b>  | 120 | 150 | 100 | 30 |
| <b>8.</b>  | 120 | 150 | 100 | 50 |
| <b>9.</b>  | 120 | 150 | 100 | 70 |
| <b>10.</b> | 120 | 150 | 100 | 90 |
| <b>11.</b> | 120 | 150 | 150 | 10 |
| <b>12.</b> | 120 | 150 | 150 | 30 |
| <b>13.</b> | 120 | 150 | 150 | 50 |
| <b>14.</b> | 120 | 150 | 150 | 70 |
| <b>15.</b> | 120 | 150 | 150 | 90 |
| <b>16.</b> | 120 | 150 | 200 | 10 |
| <b>17.</b> | 120 | 150 | 200 | 30 |
| <b>18.</b> | 120 | 150 | 200 | 50 |
| <b>19.</b> | 120 | 150 | 200 | 70 |
| <b>20.</b> | 120 | 150 | 200 | 90 |
| <b>21.</b> | 120 | 150 | 250 | 10 |
| <b>22.</b> | 120 | 150 | 250 | 30 |
| <b>23.</b> | 120 | 150 | 250 | 50 |
| <b>24.</b> | 120 | 150 | 250 | 70 |
| <b>25.</b> | 120 | 150 | 250 | 90 |
| <b>26.</b> | 40  | 125 | 50  | 50 |
| <b>27.</b> | 60  | 125 | 50  | 50 |
| <b>28.</b> | 80  | 125 | 50  | 50 |
| <b>29.</b> | 100 | 125 | 50  | 50 |
| <b>30.</b> | 120 | 125 | 50  | 50 |
| <b>31.</b> | 40  | 150 | 50  | 50 |
| <b>32.</b> | 60  | 150 | 50  | 50 |
| <b>33.</b> | 80  | 150 | 50  | 50 |
| <b>34.</b> | 100 | 150 | 50  | 50 |

|     |     |     |    |    |
|-----|-----|-----|----|----|
| 35. | 120 | 150 | 50 | 50 |
| 36. | 40  | 175 | 50 | 50 |
| 37. | 60  | 175 | 50 | 50 |
| 38. | 80  | 175 | 50 | 50 |
| 39. | 100 | 175 | 50 | 50 |
| 40. | 120 | 175 | 50 | 50 |
| 41. | 40  | 200 | 50 | 50 |
| 42. | 60  | 200 | 50 | 50 |
| 43. | 80  | 200 | 50 | 50 |
| 44. | 100 | 200 | 50 | 50 |
| 45. | 120 | 200 | 50 | 50 |
| 46. | 40  | 220 | 50 | 50 |
| 47. | 60  | 220 | 50 | 50 |
| 48. | 80  | 220 | 50 | 50 |
| 49. | 100 | 220 | 50 | 50 |
| 50. | 120 | 220 | 50 | 50 |

#### **4.2.3 Experimentation on Aluminium Alloy 6061**

**The Taguchi Experimental Design:** In any experiment the results and conclusions that can be drawn depends to a large extent on the manner in which the data were collected. Genichi Taguchi (a Japanese Engineer) contributed discipline and structure to the design of experiments. He simplified and standardized the fractional designs in such a manner that engineers conducting tests thousands of miles apart will always use similar design and tend to obtain similar results [161].

Taguchi constructed special set of orthogonal arrays (OAs) to layout experiments. The OAs are generalized Graeco – Latin squares. These OAs are standard ones that can be used for number of experimental situations. Each row represents a trial condition with factor levels indicated by the numbers in the row. The vertical column corresponds to the factors specified

in the study. The OA array facilitates the experiment design process. The arrays force all the experiments to design almost identical experiments [170]. In the taguchi method the results of the experiments are analyzed to achieve one or more the following objectives [171].

- To establish the best or the optimum condition for a production process.
- To estimate the contribution of individual parameters and interactions.
- To estimate the response under the optimum conditions.

Taguchi suggests two different routes to carry out the complete analysis of results. First the standard approach, where the results of single run or the repetitive runs, are processed through main effect and ANOVA (Analysis of Variance) analysis. The second approach which he strongly recommends for multiple runs, is to use signal to noise ratio (S/N) for the same steps in the analysis. S/N ratio indicates the scatter around the target value [169].

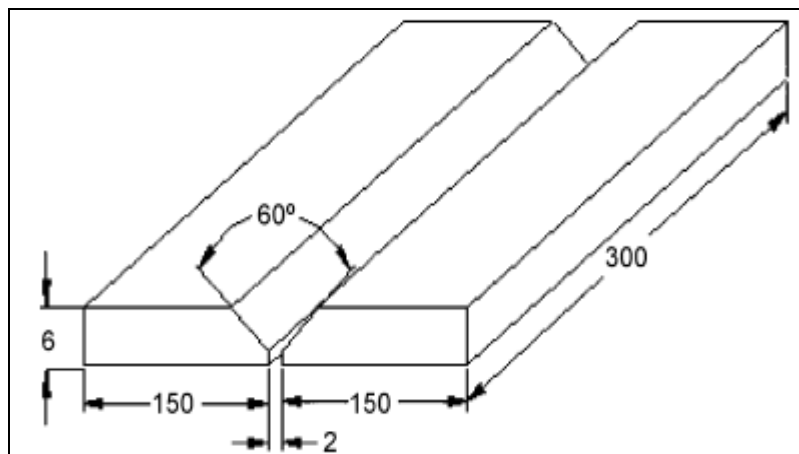
There are two types of process parameters / factors, independent parameters and parameters interacting with each others. The two parameters are said to be interacting with each other, if the effect of one factor upon the result is dependent on the condition of other. The taguchi technique also takes into account the effect of interactions of parameters on the result.

The effect of many different parameters on the performance characteristic in a condensed set of experiments can be examined by using the orthogonal array experimental design proposed by Taguchi. Once the parameters affecting a process that can be controlled have been determined, the levels at which these parameters should be varied must be determined. Determining what levels of a variable to test requires an in-depth understanding of the process, including the minimum, maximum, and current value of the parameter. If the difference between the minimum and maximum value of a parameter is large, the values being tested can be further apart or more values can be tested. If the range of a parameter is small, then less value can be tested or the values tested can be closer together.

Knowing the number of parameters and the number of levels, the proper orthogonal array can be selected. Using the array selector table, the name of the appropriate array can be found by looking at the column and row corresponding to the number of parameters and number of levels. Once the name has been determined (the subscript represents the number of experiments that must be completed), the predefined array can be looked up. These arrays were created using an algorithm developed, and allows for each variable and setting to be tested equally.

To study the entire process parameters with a small number of experiments, the taguchi technique is used. In fact taguchi technique has been designed to optimize a single quality characteristic. To consider several quality characteristics together in the selection of process parameters, the modified taguchi method (MTM) is used.

The 5mm thick samples of aluminium alloy 6061 were cut into the standard sizes of 80mm x 120mm for bead-on-plate (AWS Standard) and 300mm x 150mm coupon plate for tensile testing (ASTM standard–Fig 4.3) by shear and milling machines [12, 119]. All samples and filler rods were prepared as discussed in previous experiment and weld beads along the length were deposited using 3.15 mm diameter filler rods as shown in Fig 4.2. Coupon plates for tensile tests were welded using 2.00 / 3.15mm diameter filler rods.



**Fig 4.3: Dimensions of single “V” butt joint configuration**

All necessary care was taken to avoid joint distortion and the joints were made after clamping the plates with suitable clamps. A non-consumable tungsten electrode of 2.4mm diameter was used with high purity (99.99%) argon as a shielded gas. AC sinusoidal wave with various pulse process parameters was used to perform the above experiments. These welded samples were used for measurement of the bead geometry and mechanical properties of the welds.

The quality of weld is based on the process parameters such as peak current in the range of 120–150 A, the base current in the range of 80–110 A, the pulse frequency in the range of 50–125 Hz and the pulse on time / pulse duty cycle in a range of 30–75%. A large number of trial runs were carried out using 5mm-thick AA6061 samples to find out the feasible working limits of pulsed current GTAW parameters. Different combinations of pulse current parameters were used to conduct the trial runs. The bead contour, bead appearance and weld quality were inspected to identify the welding parameters. From the above analysis, following observations are made:

1. If the peak current (P) was less than 120 Amp, incomplete penetration and lack of fusion were observed. At the same time, if the pulse current exceeded 150 Amp, spatters and overheating were observed.
2. If base current (B) was lower than 80 Amp, arc length was found to be very short. On the other hand, if the background current was greater than 110 Amp, arc became unstable and arc length was increased.
3. If the pulse frequency (F) was less than 50 Hz, the bead contour and bead appearance was not of good quality. However, if the pulse frequency was greater than 125 Hz, there was a harsh sound in welding machine.
4. If the pulse duty cycle was lower than 30%, the heat input was very low which was not sufficient to melt the base metal. On the contrary, if the pulse duty cycle was greater than 75%, over melting of the base and filler metal and overheating of tungsten electrode was noticed.

**Table 4.4: Process Parameters and their limiting Values**

| Symbol | Process parameter  | Unit | Level 1 | Level 2 | Level 3 | Level 4 |
|--------|--------------------|------|---------|---------|---------|---------|
| P      | Pulse/Peak Current | Amp  | 120     | 130     | 140     | 150     |
| B      | Secondary Current  | Amp  | 80      | 90      | 100     | 110     |
| F      | Pulse Frequency    | Hz   | 50      | 75      | 100     | 125     |
| T      | Pulse Duty Cycle   | %    | 30      | 45      | 60      | 75      |

**Table 4.5: Experimental Layout using L16 Orthogonal Array**

| Experiment No | Levels of Process Parameters |                  |                     |                      |
|---------------|------------------------------|------------------|---------------------|----------------------|
|               | Peak Current (P)             | Base Current (B) | Pulse Frequency (F) | Pulse Duty Cycle (T) |
| 1.            | 1                            | 1                | 1                   | 1                    |
| 2.            | 1                            | 2                | 2                   | 2                    |
| 3.            | 1                            | 3                | 3                   | 3                    |
| 4.            | 1                            | 4                | 4                   | 4                    |
| 5.            | 2                            | 1                | 2                   | 3                    |
| 6.            | 2                            | 2                | 1                   | 4                    |
| 7.            | 2                            | 3                | 4                   | 1                    |
| 8.            | 2                            | 4                | 3                   | 2                    |
| 9.            | 3                            | 1                | 3                   | 4                    |
| 10.           | 3                            | 2                | 4                   | 3                    |
| 11.           | 3                            | 3                | 1                   | 1                    |
| 12.           | 3                            | 4                | 2                   | 2                    |
| 13.           | 4                            | 1                | 4                   | 2                    |
| 14.           | 4                            | 2                | 3                   | 1                    |
| 15.           | 4                            | 3                | 2                   | 4                    |
| 16.           | 4                            | 4                | 1                   | 3                    |

Process parameters and their experimental limiting values are tabulated in Table 4.4. Modified Taguchi Method (MTM) is used to find out the optimal process parameter mix to enhance the bead geometry and mechanical properties by conducting minimal experiments. In the study, four levels were

chosen for the four factors. There is 12 degree of freedom and hence L16 orthogonal array was used. The experimental layout for the experimentation is detailed in Table 4.5.

#### **4.2.4 Experimentation on AA 6061 and AA 7039 (With Gas Mixtures)**

The 5.0 mm thick samples of aluminium alloy 6061 and 6.0 mm thick samples of aluminium alloy 7039 were cut into the standard sizes (as mentioned in 4.2.3) by shear and milling machines. All samples and filler rods were prepared as discussed earlier and weld beads along the length were deposited using 3.15mm diameter filler rods as shown in Fig 4.2. Similarly all tensile coupons were welded with 2.00 / 3.15 mm diameter filler rods and necessary precaution was taken to avoid joint distortion. A non-consumable tungsten electrode of 2.4mm diameter was used with argon-helium gas mixture as a shielded gas. AC sinusoidal wave with various pulse process parameters was used to perform the experiments. These welded samples were used for measurement of the bead geometry and mechanical properties of the welds.

The quality of weld is based on the process parameters such as peak current in the range of 150–210 A, the base current in the range of 75–135 A, the pulse frequency in the range of 50–150 Hz, the pulse on time in a range of 30–90% and the percentage of helium with argon in a range of 10–50%. A large number of trial runs were carried out using 5mm–thick AA6061 samples and 6.0 mm thick AA7039 samples to find out the feasible working limits of pulsed current GTAW parameters and gas mixtures. Different combinations of pulse current parameters with various gas mixtures were used to conduct the trial runs. The bead contour, bead appearance and weld quality were inspected to identify the welding parameters. From the above analysis, following observations are made:

1. If the peak current ( $P$ ) < 150 A, incomplete penetration and lack of fusion were observed. At the same time, if the  $P$  > 210 A, under cut, spatters and overheating were observed.

2. If background current (B) < 75 A, arc length was found to be very short. On the other hand, B > 135 A, arc became unstable and arc length was increased.
3. If the pulse frequency (F) < 50 Hz, the bead contour and bead appearance was not of good quality. However, if the F > 150 Hz, there was a harsh sound in welding machine.
4. If the pulse duty cycle (T) < 30%, the heat input was very low which was not sufficient to melt the base metal. On the contrary, if the T > 90%, over melting of the base and filler metal, and overheating of tungsten electrode was noticed.
5. If the percentage of helium in argon (X) < 10%, the arc stability, bead penetration and bead appearance were poor. On the other hand if X > 50%, gas consumption gas mixture per kg weld deposition was very high.

Process parameters and their experimental limiting values are tabulated in Table 4.6. Modified Taguchi Method (MTM) is used to find out the optimal process parameter mix to enhance the bead geometry and mechanical properties by conducting minimal experiments. In the study, five levels were chosen for the five factors. There is 20 degree of freedom and hence L25 orthogonal array was used. The experimental layout for the experimentation is detailed in Table 4.7.

**Table 4.6: Process Parameters and their limiting Values (With Gas Mixtures)**

| Symbol | Process parameter             | Unit | Level 1 | Level 2 | Level 3 | Level 4 | Level 5 |
|--------|-------------------------------|------|---------|---------|---------|---------|---------|
| P      | Pulse Current                 | A    | 150     | 165     | 180     | 195     | 210     |
| B      | Base Current                  | A    | 75      | 90      | 105     | 120     | 135     |
| F      | Pulse Frequency               | Hz   | 50      | 75      | 100     | 125     | 150     |
| T      | Pulse Duty Cycle              | %    | 30      | 45      | 60      | 75      | 90      |
| X      | Percentage of Helium in Argon | %    | 10      | 20      | 30      | 40      | 50      |

**Table 4.7: Experimental Layout using L25 Orthogonal Array**

| <b>Experiment<br/>No</b> | <b>Levels of Process Parameters</b> |                             |                                |                                 |                                       |
|--------------------------|-------------------------------------|-----------------------------|--------------------------------|---------------------------------|---------------------------------------|
|                          | <b>Peak<br/>Current (P)</b>         | <b>Base<br/>Current (B)</b> | <b>Pulse<br/>Frequency (F)</b> | <b>Pulse Duty<br/>Cycle (T)</b> | <b>Percentage of<br/>He in Ar (X)</b> |
| 1.                       | 1                                   | 1                           | 1                              | 1                               | 1                                     |
| 2.                       | 1                                   | 2                           | 2                              | 2                               | 2                                     |
| 3.                       | 1                                   | 3                           | 3                              | 3                               | 3                                     |
| 4.                       | 1                                   | 4                           | 4                              | 4                               | 4                                     |
| 5.                       | 1                                   | 5                           | 5                              | 5                               | 5                                     |
| 6.                       | 2                                   | 1                           | 2                              | 3                               | 4                                     |
| 7.                       | 2                                   | 2                           | 3                              | 4                               | 5                                     |
| 8.                       | 2                                   | 3                           | 4                              | 5                               | 1                                     |
| 9.                       | 2                                   | 4                           | 5                              | 1                               | 2                                     |
| 10.                      | 2                                   | 5                           | 1                              | 2                               | 3                                     |
| 11.                      | 3                                   | 1                           | 3                              | 5                               | 2                                     |
| 12.                      | 3                                   | 2                           | 4                              | 1                               | 3                                     |
| 13.                      | 3                                   | 3                           | 5                              | 2                               | 4                                     |
| 14.                      | 3                                   | 4                           | 1                              | 3                               | 5                                     |
| 15.                      | 3                                   | 5                           | 2                              | 4                               | 1                                     |
| 16.                      | 4                                   | 1                           | 4                              | 2                               | 5                                     |
| 17.                      | 4                                   | 2                           | 5                              | 3                               | 1                                     |
| 18.                      | 4                                   | 3                           | 1                              | 4                               | 2                                     |
| 19.                      | 4                                   | 4                           | 2                              | 5                               | 3                                     |
| 20.                      | 4                                   | 5                           | 3                              | 1                               | 4                                     |
| 21.                      | 5                                   | 1                           | 5                              | 4                               | 3                                     |
| 22.                      | 5                                   | 2                           | 1                              | 5                               | 4                                     |
| 23.                      | 5                                   | 3                           | 2                              | 1                               | 5                                     |
| 24.                      | 5                                   | 4                           | 3                              | 2                               | 1                                     |
| 25.                      | 5                                   | 5                           | 4                              | 3                               | 2                                     |

#### **4.2.5 Experimentation on Titanium Alloy Grade–5 (With Gas Mixtures)**

The 2.5 mm thick samples of Ti alloy Gr-5 were cut into the standard sizes by shear and milling machines. Standard sizes of samples were 80mm x 120mm for bead-on-plate (AWS Standard) and 150mm x 100mm coupon plate for tensile testing (ASTM standard) [163]. All samples and filler rods were prepared as discussed above and weld beads along the length were deposited using 2.0 mm diameter filler rods. Similarly all tensile coupons were welded with necessary precautions to avoid joint distortion. A non-consumable tungsten electrode of 2.4 mm diameter was used with argon-helium mixture as a shielded gas. AC sinusoidal wave with various pulse process parameters was used to perform the experiments. These welded samples were used for measurement of the bead geometry and mechanical properties of the welds.

The quality of weld was based on the process parameters such as peak current in the range of 100–140 A, the base current in the range of 50–90 A, the pulse frequency in the range of 50–150 Hz, the pulse on time in a range of 40–80% and the percentage of helium in argon in a range of 10–50%. A large number of trial runs were carried out using 2.5 mm-thick Titanium Alloy Grade–5 samples to find out the feasible working limits of pulsed current GTAW parameters. Different combinations of pulse current parameters with argon-helium gas mixtures were used to conduct the trial runs.

The bead contour, bead appearance and weld quality were inspected to identify the welding parameters. From the above analysis, following observations were made:

1. If the peak current ( $P$ ) < 100 A, incomplete penetration and lack of fusion were observed. At the same time, if the  $P$  > 140 A, under cut, spatters and overheating were observed.
2. If background current ( $B$ ) < 50 A, arc length was found to be very short. On the other hand,  $B$  > 90 A, arc became unstable and arc length was increased.

3. If the pulse frequency ( $F$ )  $< 50$  Hz, the bead contour and bead appearance was not of good quality. However, if the  $F > 150$  Hz, there was a harsh sound in welding machine.
4. If the pulse duty cycle ( $T$ )  $< 40\%$ , the heat input was very low which was not sufficient to melt the base metal. On the contrary, if the  $T > 80\%$ , over melting of the base and filler metal, and overheating of tungsten electrode was noticed.
5. If the percentage of helium in argon ( $X$ )  $< 10\%$ , the arc stability, bead penetration and bead appearance were poor. On the other hand if  $X > 50\%$ , gas consumption gas mixture per kg weld deposition was very high.

Process parameters and their experimental limiting values are tabulated in Table 4.8. Modified Taguchi Method (MTM) is used to find out the optimal process parameter mix to enhance the bead geometry and mechanical properties by conducting minimal experiments. In the study, five levels were chosen for the five factors. There is 20 degree of freedom and hence L25 orthogonal array was used. The experimental layout for the experimentation is detailed in Table 4.7.

**Table 4.8: Process Parameters and their Limiting Values for Ti alloy**

| Symbol | Process parameter             | Unit | Level 1 | Level 2 | Level 3 | Level 4 | Level 5 |
|--------|-------------------------------|------|---------|---------|---------|---------|---------|
| P      | Pulse Current                 | A    | 100     | 110     | 120     | 130     | 140     |
| B      | Base Current                  | A    | 50      | 60      | 70      | 80      | 90      |
| F      | Pulse Frequency               | Hz   | 50      | 75      | 100     | 125     | 150     |
| T      | Pulse Duty Cycle              | %    | 40      | 50      | 60      | 70      | 80      |
| X      | Percentage of Helium in Argon | %    | 10      | 20      | 30      | 40      | 50      |

## Chapter 5

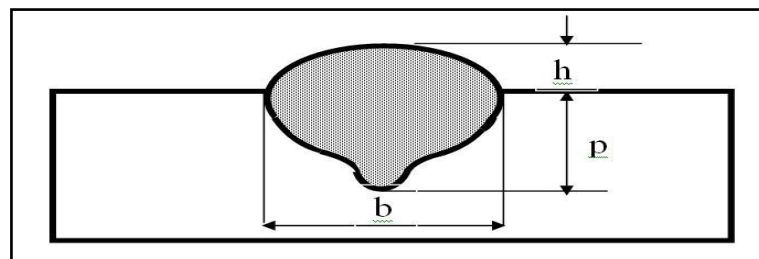
### RESULTS AND DISCUSSION

#### 5.1 Introduction

This chapter describes the results of the experiments, which were carried out / explained in the previous chapter. The experimental results are tabulated in various tables and accordingly graphs are plotted. Also analysis of results, with the help of various calculation methods followed by discussions has been carried out to optimize the GTAW process parameters.

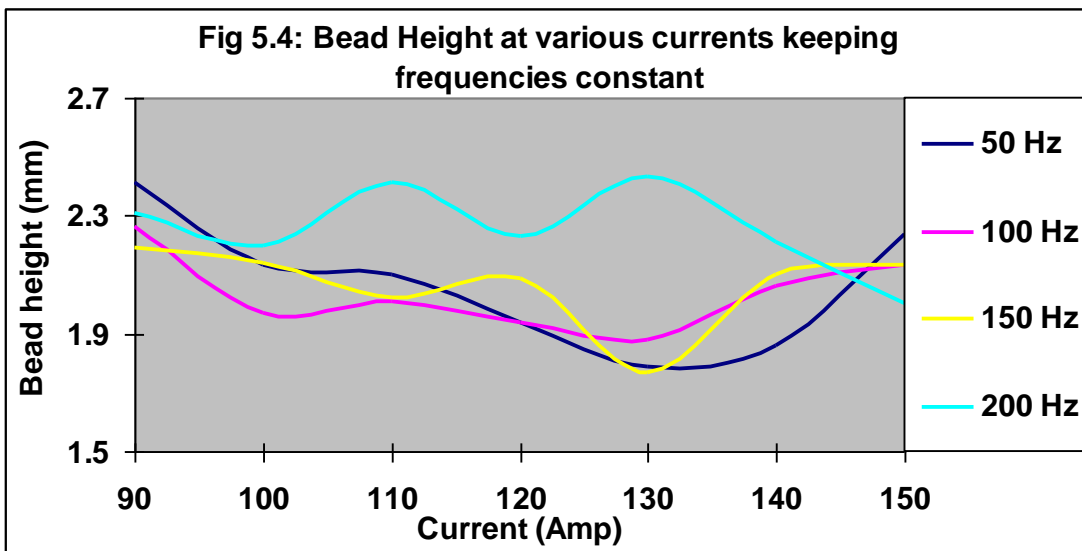
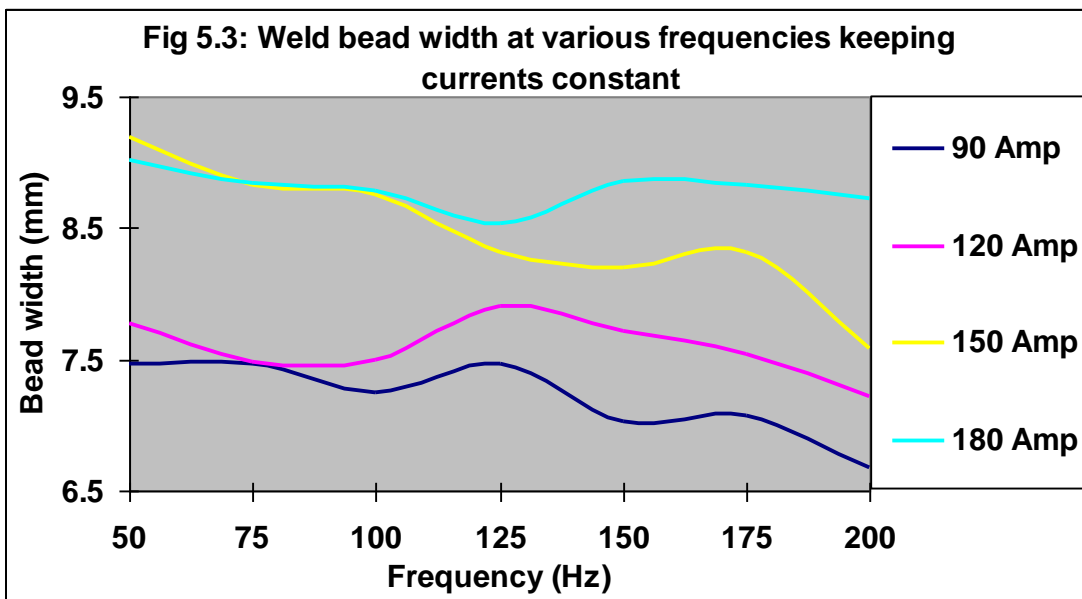
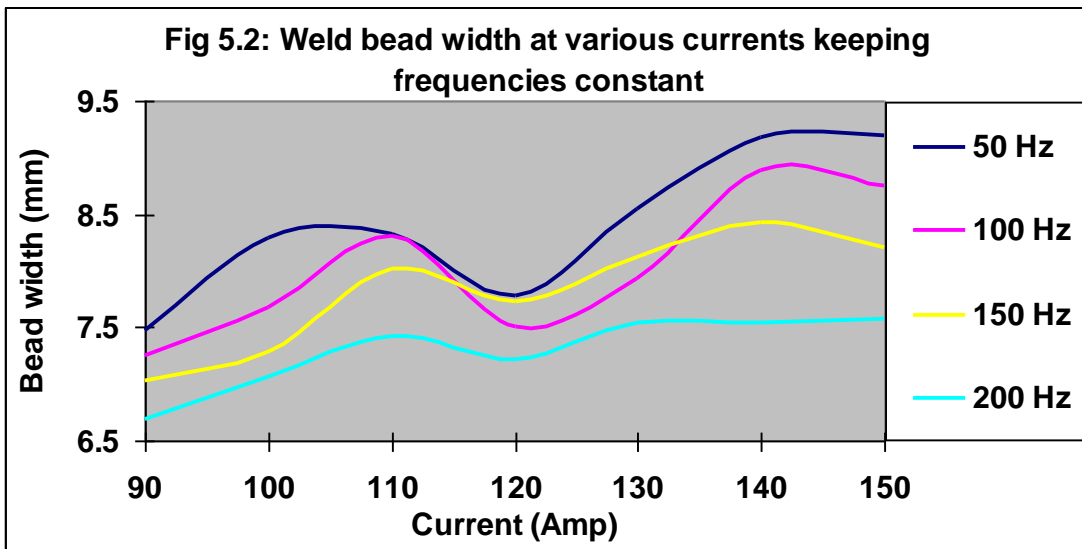
#### 5.2 Experimentation on Aluminium Alloy 7039 (Without Pulsing)

The tests were conducted as per the experimental layout decided in Table 4.2. After completion of bead-on-plate welding, suitable size samples were taken from the middle of the bead-on-plate. The samples were cut along the width (almost perpendicular to the length of the weld bead) so that the cross sectional area of the bead will be clearly visible. After polishing and some etching, the bead profile / geometry of welds can be easily measured with the help of magnifying glasses and vernier caliper. The bead geometry includes the penetration (p), bead width (b) and reinforcement height (h) as shown in Fig 5.1. The graphs of the various results measured are plotted and shown in Fig 5.2–5.7. In Al-Zn-Mg alloys, zinc in combination with magnesium will give improvements in strength and will assist in regaining some of the strength lost in welding.



p – Penetration      b – Bead Width      h – Bead Height

**Fig 5.1: Schematic Diagram of Weld Bead**



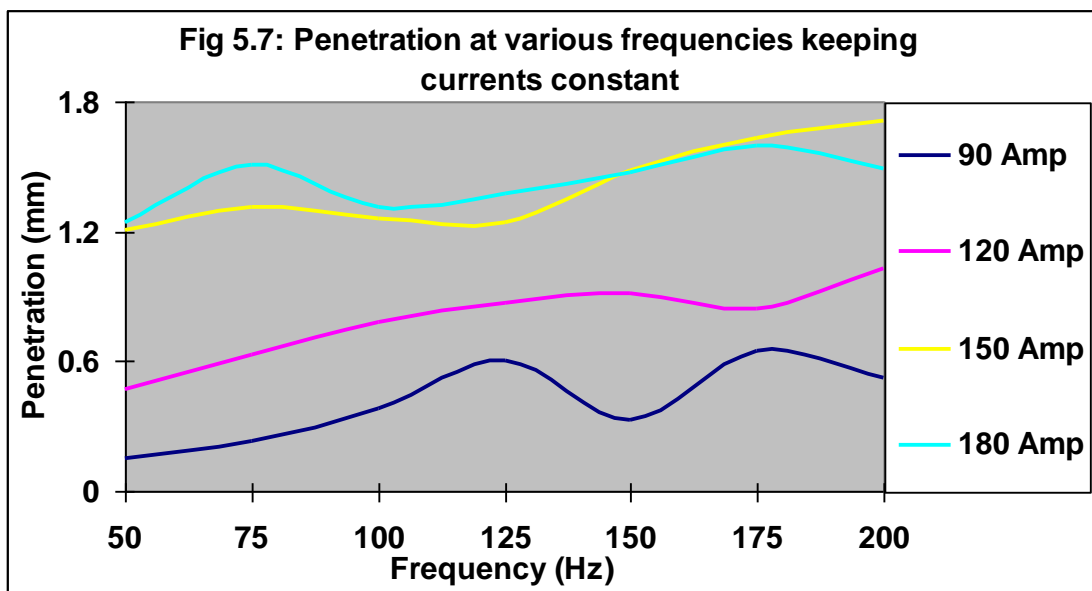
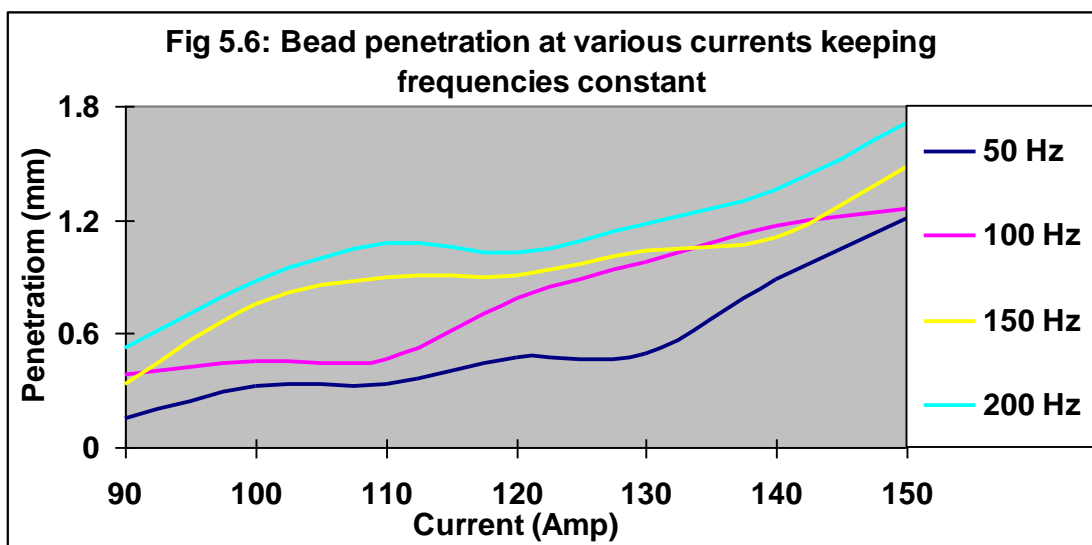
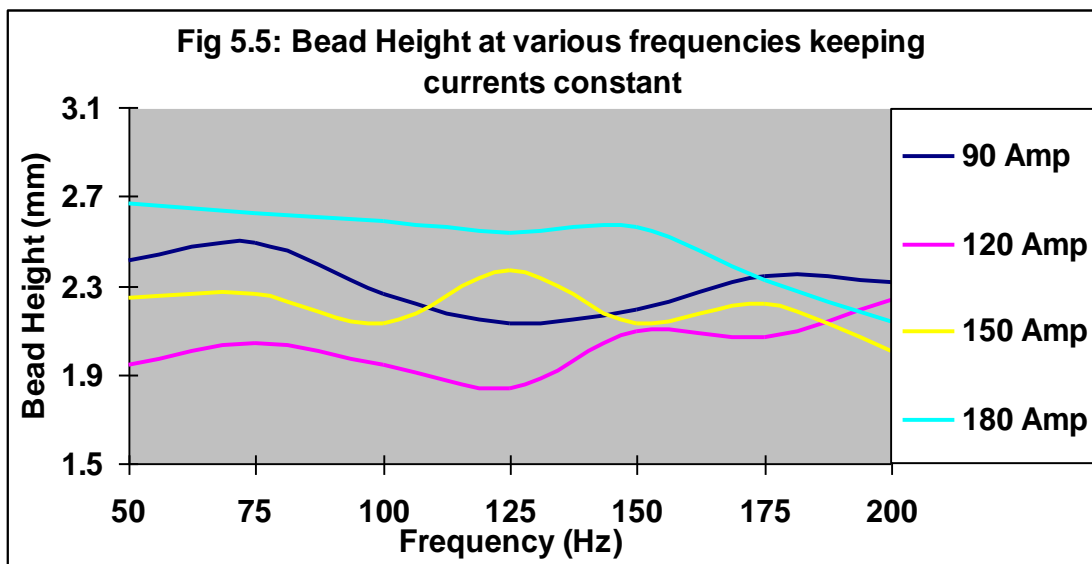
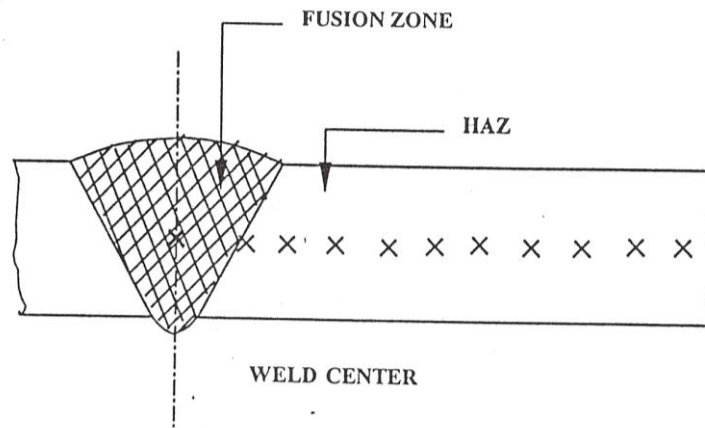


Fig 5.2 shows variation of weld bead width with current at various frequencies. It is clear that width of weld bead increases with current initially. Further increase in current decreases the width, which later increases as the current increases. But as the frequency of the welding current increases, the width of the weld bead decreases and similar results were concluded by Gurave and Stout [56].

Fig 5.3 shows variation of weld bead width with frequency at various current and indicates that width of weld bead very slightly decreases with increase in frequency of welding. Very similar results were concluded by Yarmuch and Patchett [10]. But as the current increases, the width increases. This is due to increase in radiation and convection losses at higher frequencies and at the same time electromagnetic stirring force increases in the weld pool, which increases the depth of penetration independent of top width as explained by Saedi et al [53].

Fig 5.4 and 5.5 shows the variation of weld bead height at various currents and frequencies. Here also it is clear that height of the weld bead does not follow any trend and shows that there is no correlation between height of weld bead with current and frequency of welding. It depends upon the amount of filler wire supplied and speed of welding as described by Quintino et al [60]. Fig 5.6 and 5.7 shows that penetration of weld bead increases with increase in current and frequency of welding due to increase in heat input as explained earlier by Lietner et al [69].

The measurements of microhardness were carried out on as-welded condition (Welded + Naturally aged 5 or 7 days) samples, from the weld centre line to unaffected base metal at an interval of 0.8 mm as shown in Fig 5.8. The variations in the measured microhardness of welded samples were plotted in the graphs Fig 5.9–5.16. The measured area covers the weld zone, fusion boundary, PMZ, HAZ and unaffected base metal. In aluminium alloys 7039, the weld hardness exhibits a complicated distribution as shown in Fig 2.6, which is due to the microstructural change affected by the temperature of individual zone.

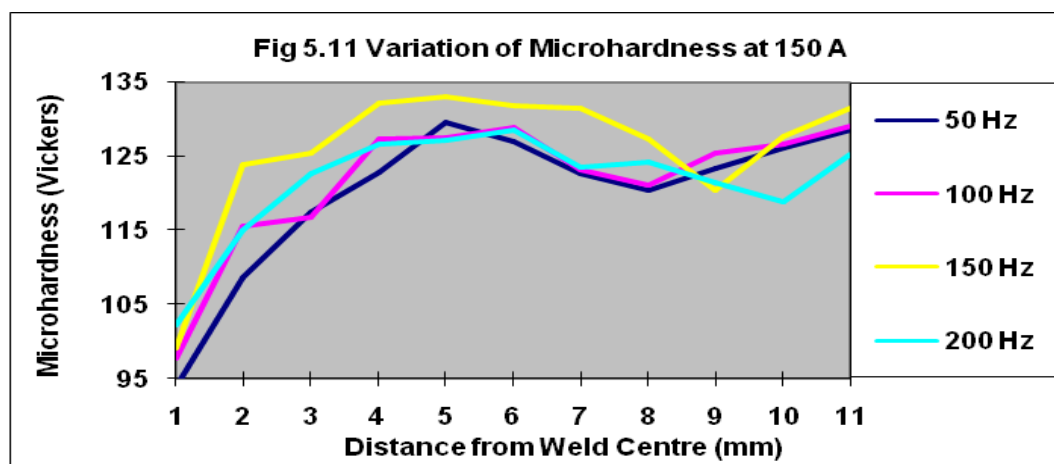
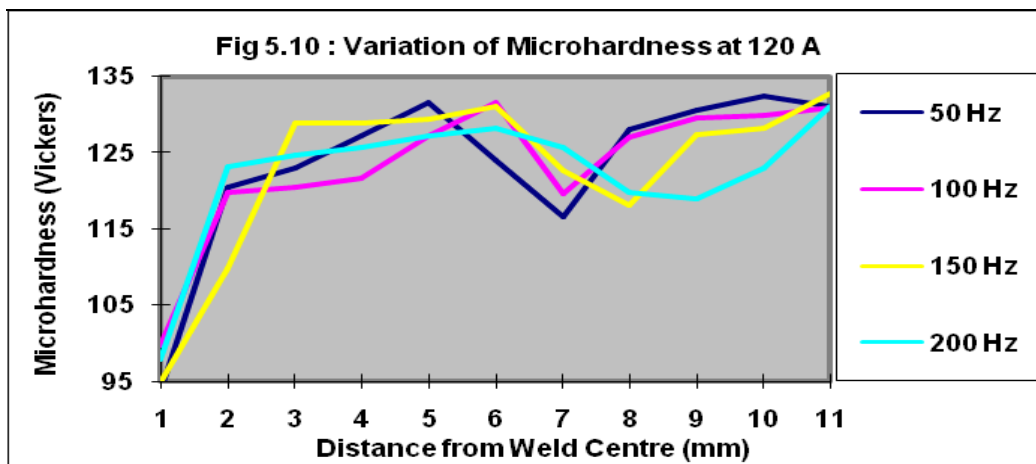
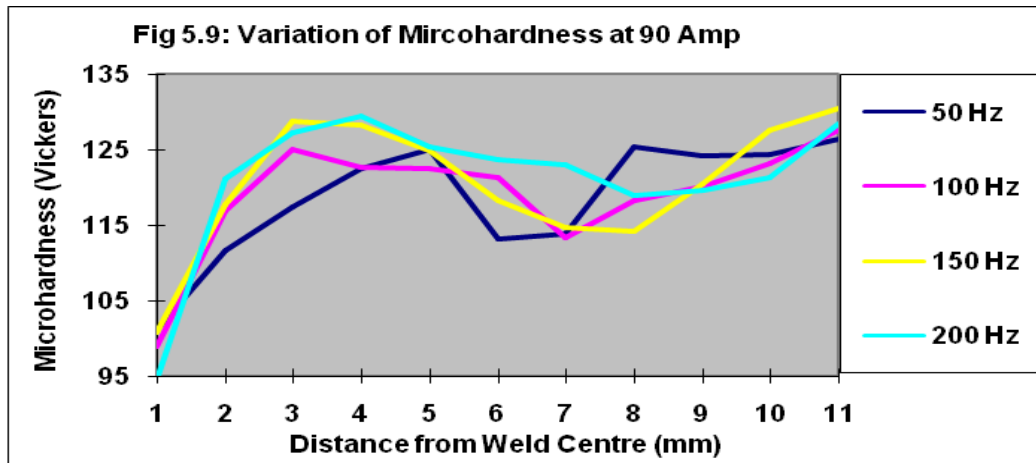


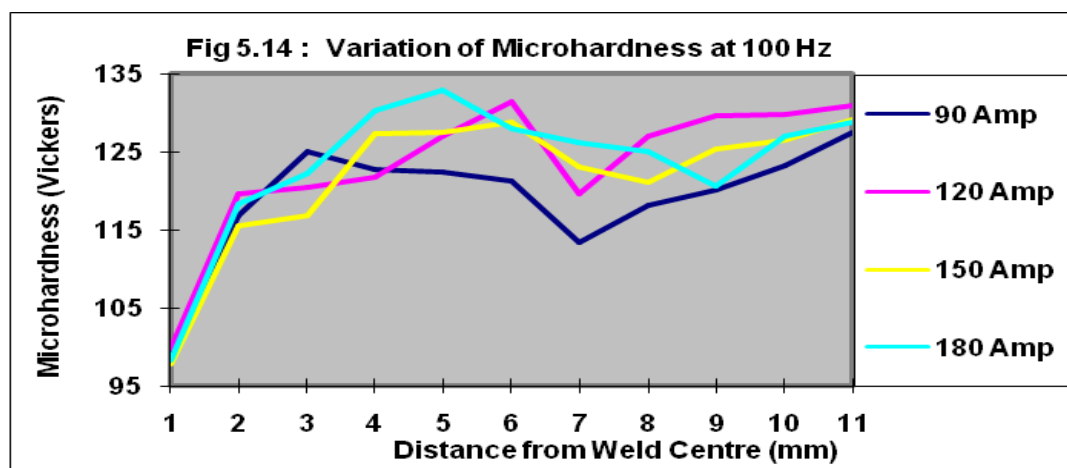
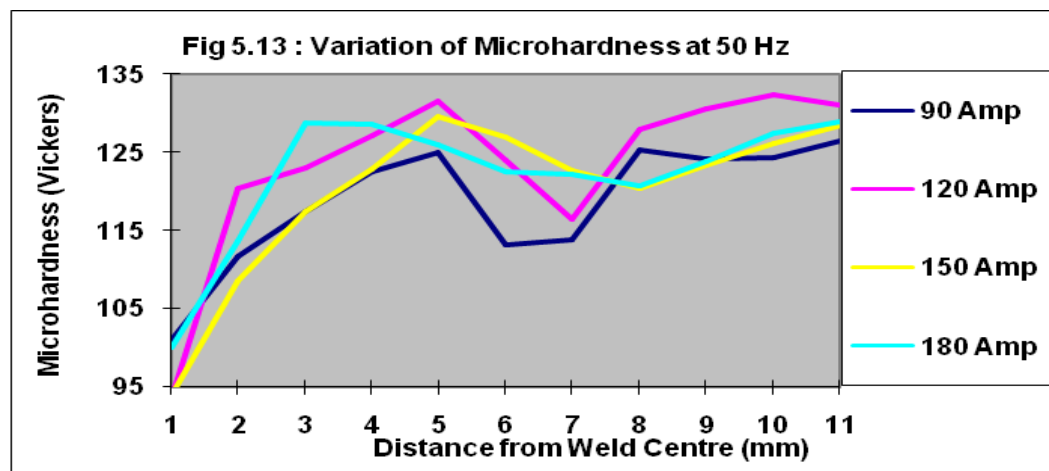
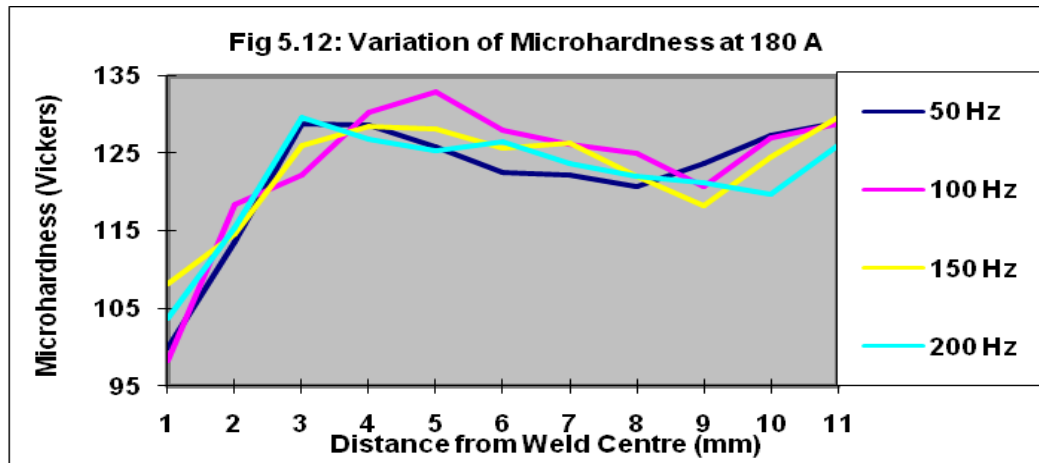
**Fig 5.8: Schematic Diagram for Measurement of Microhardness for Samples**

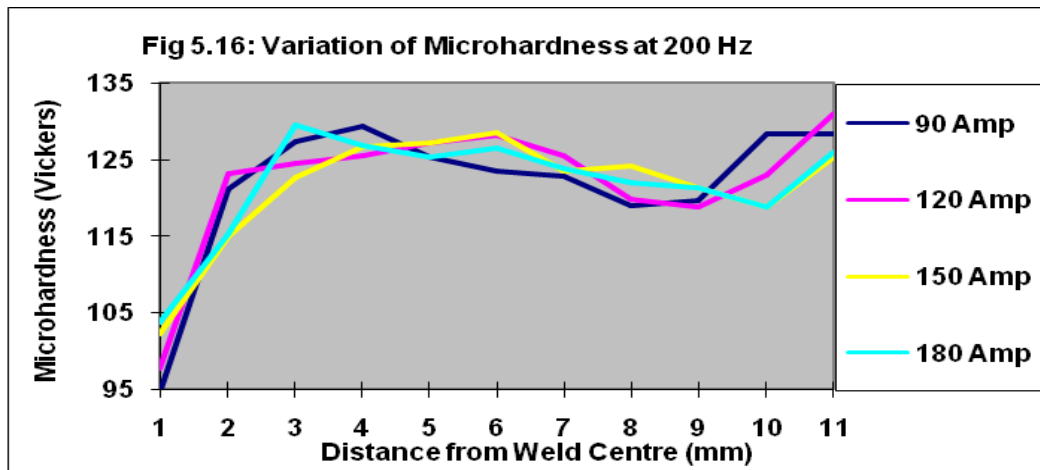
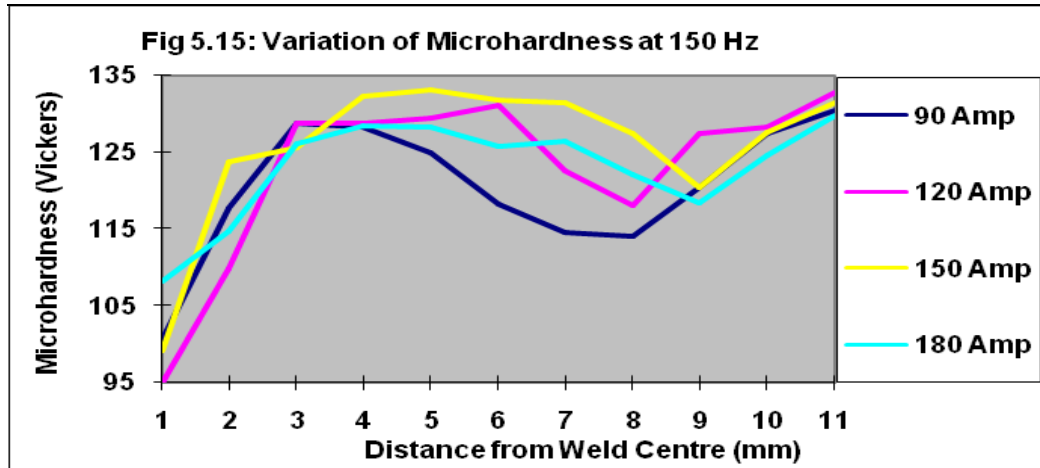
In general the microhardness in the weld zone is lowest due to as-cast nature of microstructure as shown in Fig 5.17, which is characterized by coarse grains and lack of strengthening phases. The similar results were explained by Barbosa et al [99]. A coarser grain size is normally regarded as undesirable from the point of view both mechanical properties as well as weldability.

As constitutional super-cooling increases, the solidification mode changes from planar to cellular and further to columnar as shown in Fig 5.17, which depends upon the  $G/R$  (Temperature Gradient/Growth Rate) ratio of the metal. Increase in super-cooling leads to increase in heterogeneous nucleation which promotes equiaxed grains in the fusion boundary. The reason for higher hardness in fine equiaxed grains is due to fine grains have more grain boundaries which serves as an effective barrier to the movement of dislocations.

At fusion boundary (Fig 5.17), precipitate dissolution occurs as the particles are exposed to temperatures higher than  $400^{\circ}\text{C}$  during heating and cooling as result of welding. Dissolution process enriches the solid solution of the aluminium matrix with Si and Mg. The closer metal to weld interface, the higher temperature, the higher amount of precipitates dissolved and the higher is the hardness.



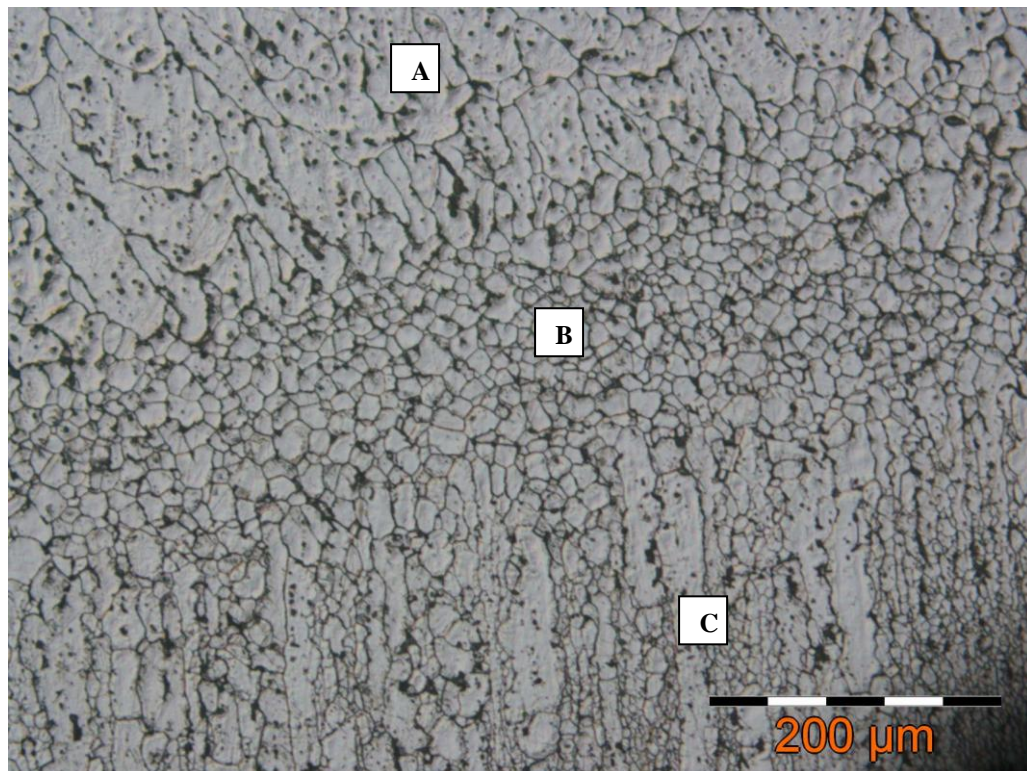




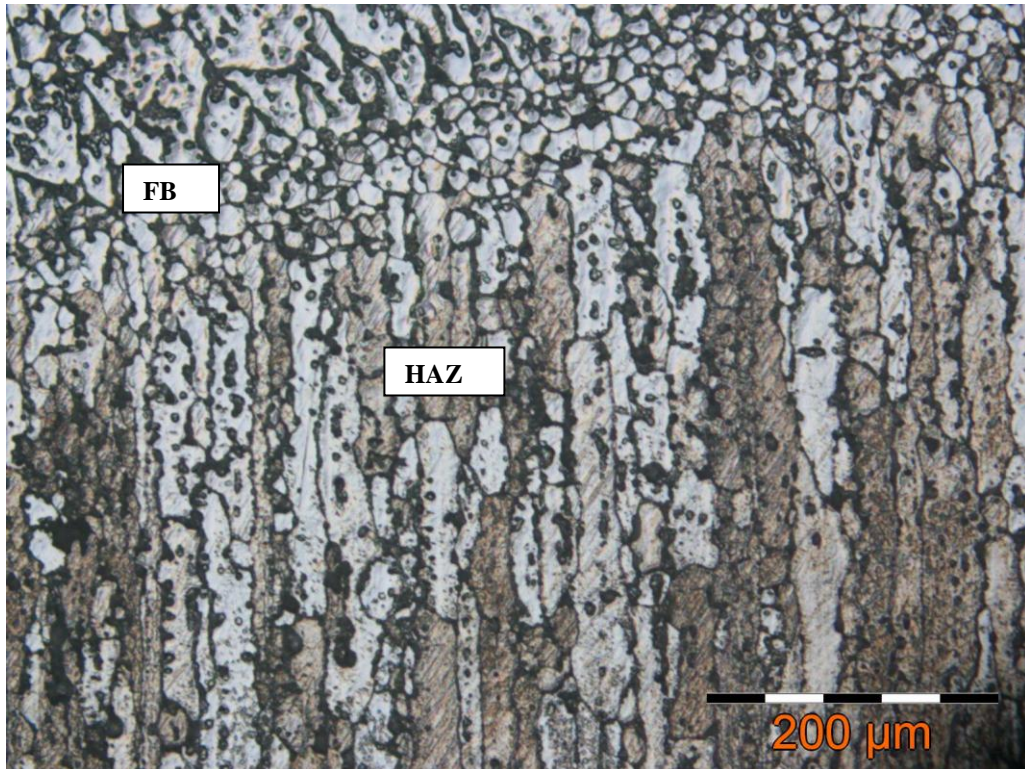
It has been observed from Fig 5.18 and 5.19 that the grains in the HAZ are coarser than base metal due to higher temperature near fusion boundary, which is responsible for this re-crystallization and grain growth. Grain growth in the HAZ can be explained with the help of thermal cycles in Fig 2.7. The higher hardness of the welds close to fusion boundary is possible due to large fraction of alloying elements in the solid solution at the end of the weld thermal cycle, thereby giving conditions for extensive age hardening at room temperature over a period of 5 to 7 days.

HAZ is quite wide because of the high thermal conductivity of the base metal. The microhardness decreases in a particular area (at 6 to 8 mm approximately) from fusion boundary, generally known as soft zone and shown in Fig 2.6. This gives a clear indication that a result of the welding technique / heat input the age-hardened parent metal has been overage. Soft regions are those which have hardness lower than 60% of base metal hardness.

The width of the soft zone depends on the peak temperature heating / cooling rate, dissolution and / or growth of precipitates and formation of stable phases. Loss of hardness and strength in HAZ is due to the dissolution and coarsening of  $Mg_2Si$  phase, the main strengthening phase in Al-Mg-Si alloys. Similar results were concluded by Borbosa et al [99] and Bradley et al [174]. In case of Al-Zn-Mg alloys, the weld soften area can be gradually recovered by increasing its hardness according to the time elapsed after welding due to excellent natural age hardening characteristics.



**Fig 5.17: Microstructure of Weld Zone (A), Fusion Boundary (B) and HAZ (C)**



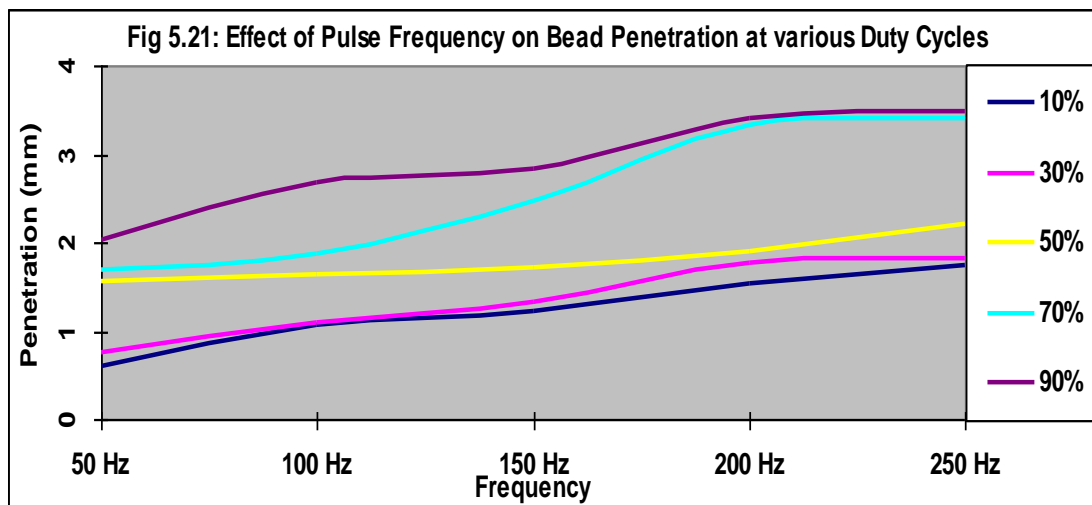
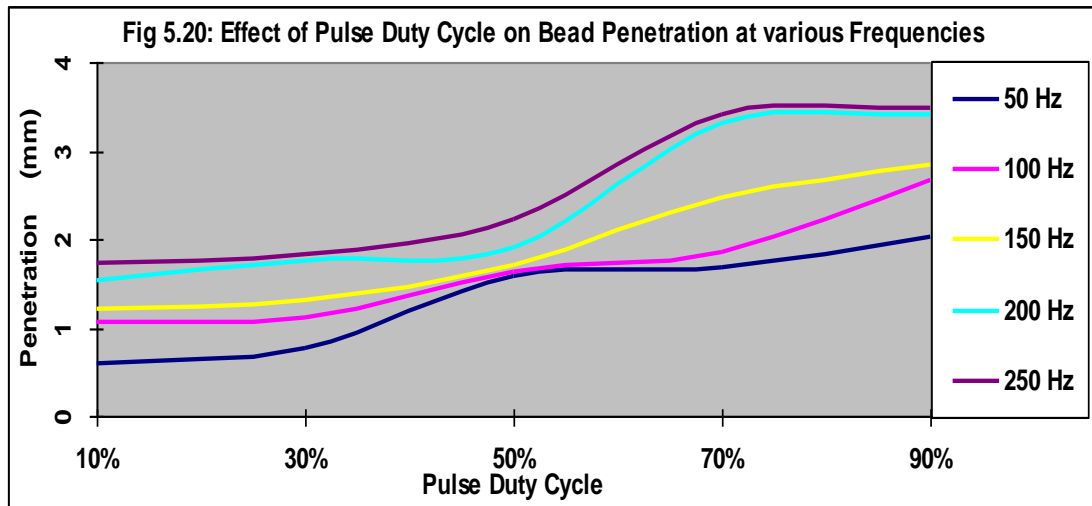
**Fig 5.18: Microstructure of HAZ of welded Al Alloy 7039**

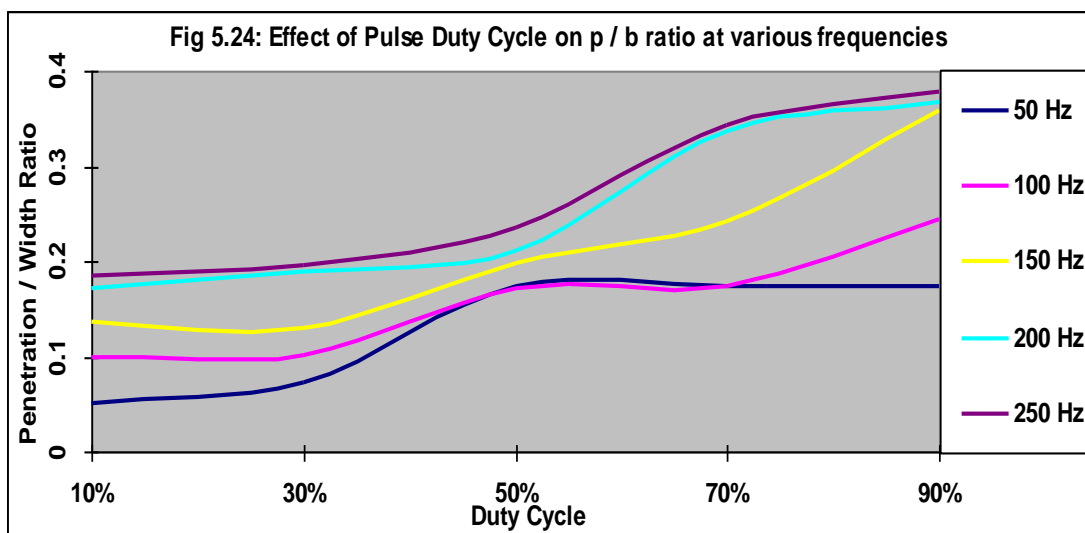
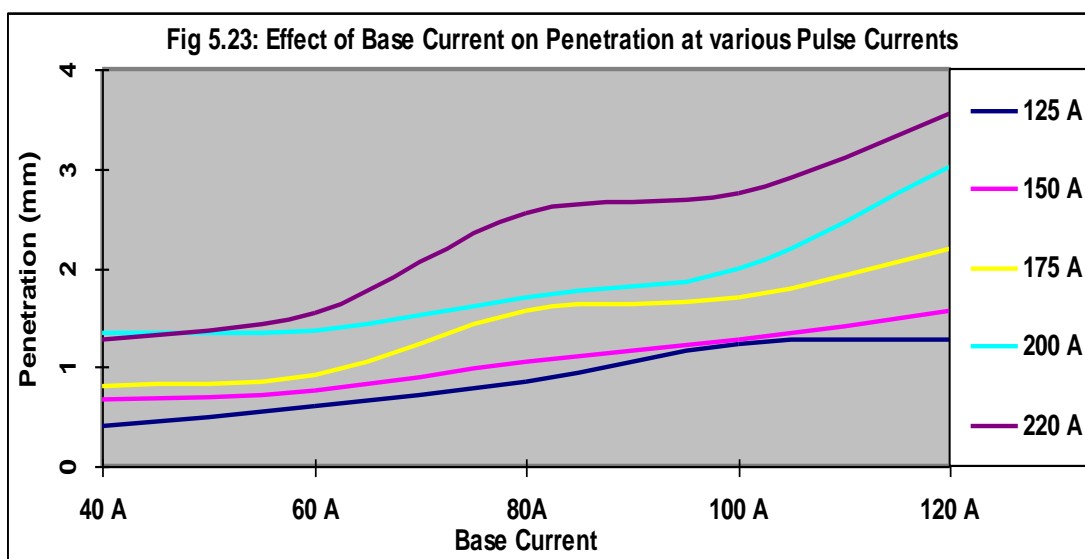
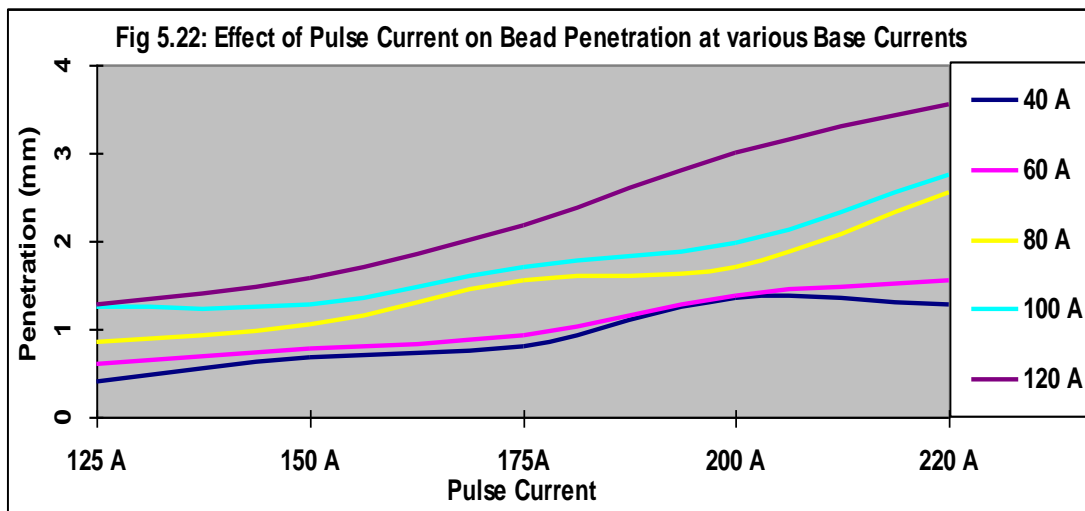


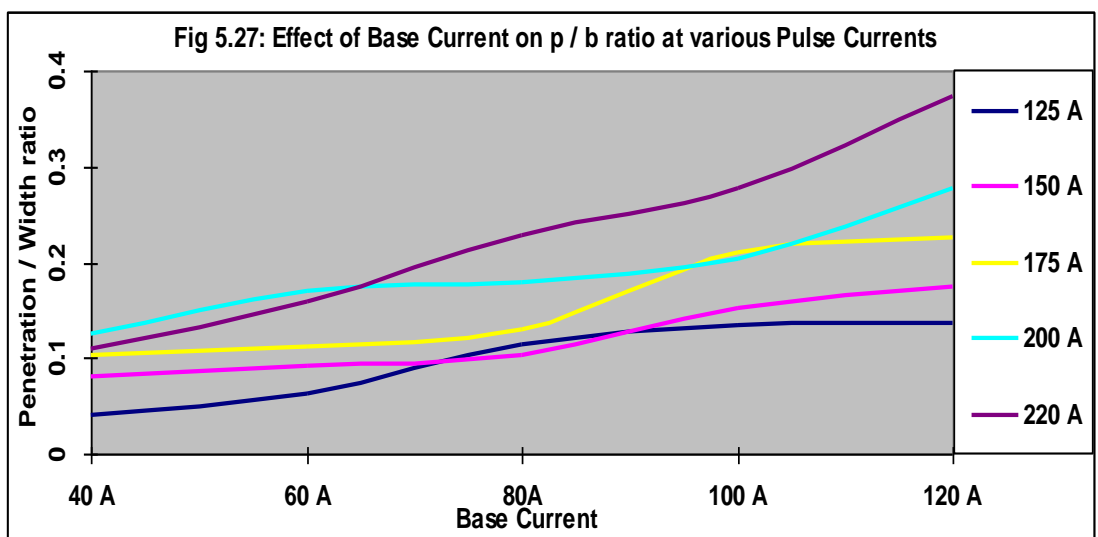
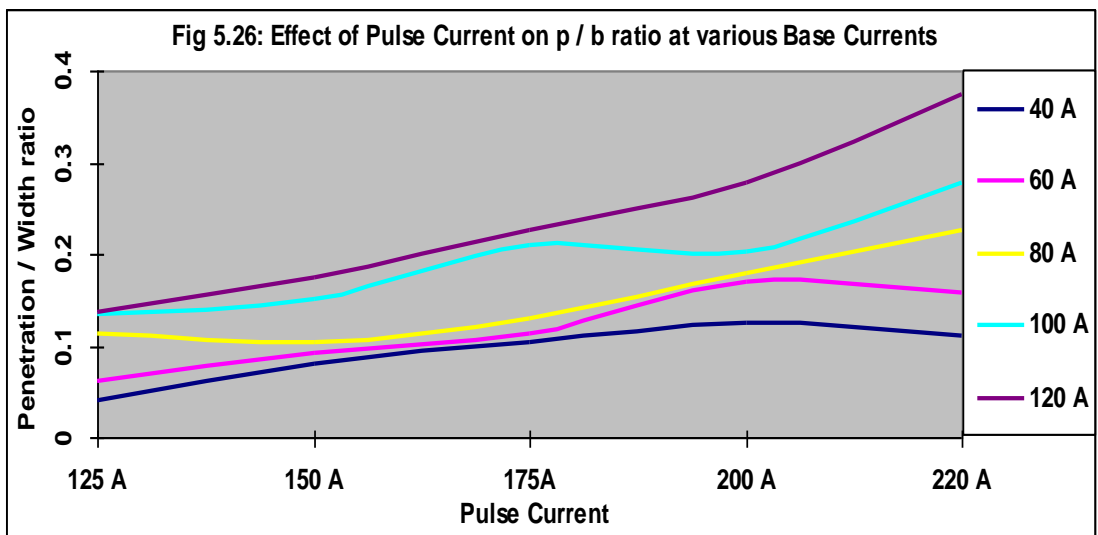
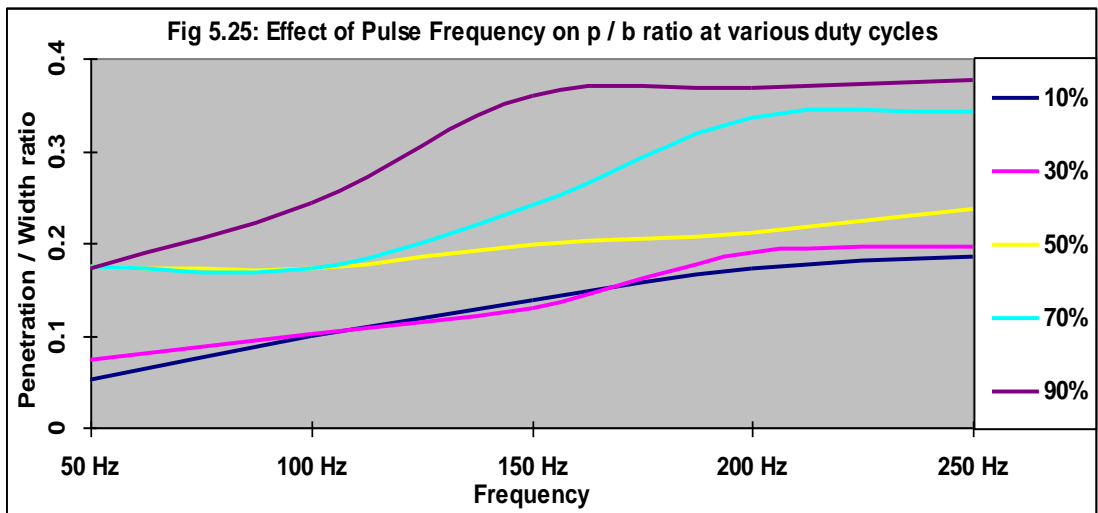
**Fig 5.19: Microstructure of Base Metal of Al Alloy 7039**

### 5.3 Experimentation on Aluminium Alloy 7039 (With Pulsing)

The tests were performed as per the experimental layout decided in Table 4.3. Bead geometry samples were prepared in similar manner as in 5.2 and the parameters like penetration, width and reinforcement height were measured. The graphs of the measured readings were plotted / shown in Fig 5.20–5.27 and following observations were made:







As the pulse duty cycle increases from 10% to 90% at various pulse frequencies, there is an increase in penetration and penetration / width (p/b) ratio due to increase in the duration of pulse current i.e. increase in heat input. The calculation of heat input for the pulsed current welding process can be done by mean current using the relationship  $I_m = [I_p t_p + I_b t_b] / t_T$ , where  $I_m$  = mean current,  $I_p$  = pulse current,  $t_p$  = time on peak pulse,  $I_b$  = base current,  $t_b$  = time on base current,  $t_T$  = total time. The heat input was calculated as approximately 300 J/mm for pulse current of 150A, base current of 120A, pulse frequency of 50 Hz, pulse duty cycle of 50%, Voltage of 13.5V, welding speed of 4.16 mm/s (constant for all experiments) and 70% efficiency of utilization of the heat generated.

As the pulse frequency increases from 50 to 250 Hz at various pulse duty cycles, there is also an increase in penetration and penetration / width (p/b) ratio due to increase in repetition of pulse current and similar results were also drawn by Qui et al [175]. At the same time when pulse current and base current increases, there is an increase in penetration and penetration / width (p/b) ratio due to increase in the amplitude of the pulse current i.e. increase in heat input as concluded by Lancaster [64] and Lietner et al [69].

The measurements of microhardness were carried out on as-welded condition (Welded + Naturally aged 7 days) samples in a similar manner as mentioned in without pulsing. The variations in the measured microhardness of welded samples were plotted in the graphs Fig 5.28–5.49. The comparison of hardness profiles of the CC (continuous current – Fig 5.9 to 5.16) and PC (Pulsed Current – Fig 5.28 to 5.49) fusion zone shows that hardness is slightly higher in PC welds and the magnitude of variation in hardness is less compared to CC welds. This could be due to the refined microstructure and low segregation of Si and Mg. Also width of HAZ is comparatively less in pulsed current welds.

It has been observed from Fig 5.28, 5.29 and 5.50 that the microhardness in fusion boundaries is highest due to the small grain size. As we proceed toward the weld centre, the microhardness of weld zone proportionally

decreases with distance to the minimum of 80 VHN and again increases in the same manner up to another end of fusion zone due to large columnar grains at weld centre and grain size proportionally decreases away from weld centre. Maximum temperature is in the centre of the weld pool and then decreases towards the fusion line. The cooling rate in the centre of weld zone is low and hence gives rise to coarse grains.

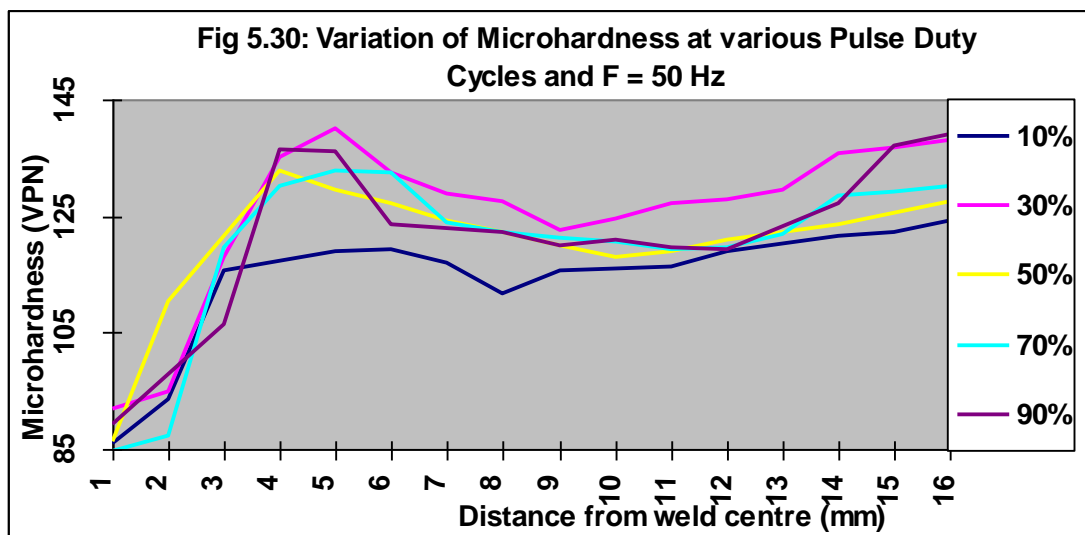
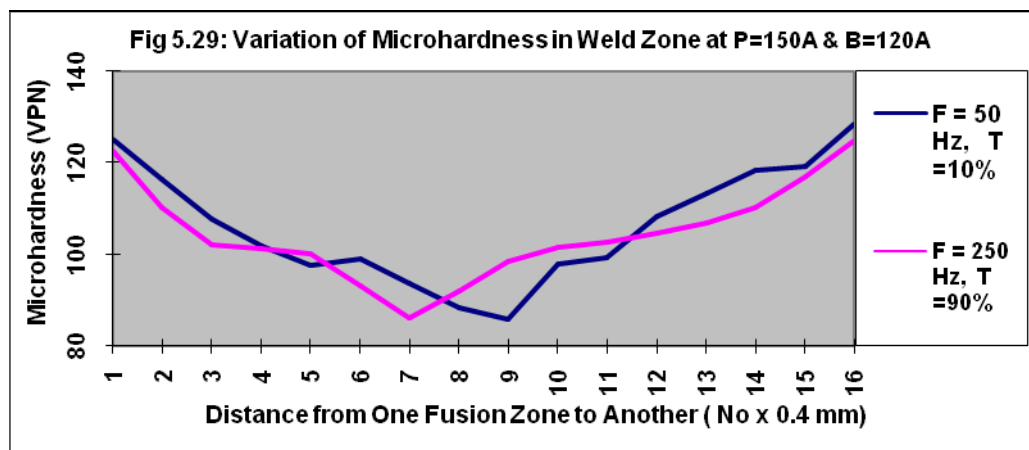
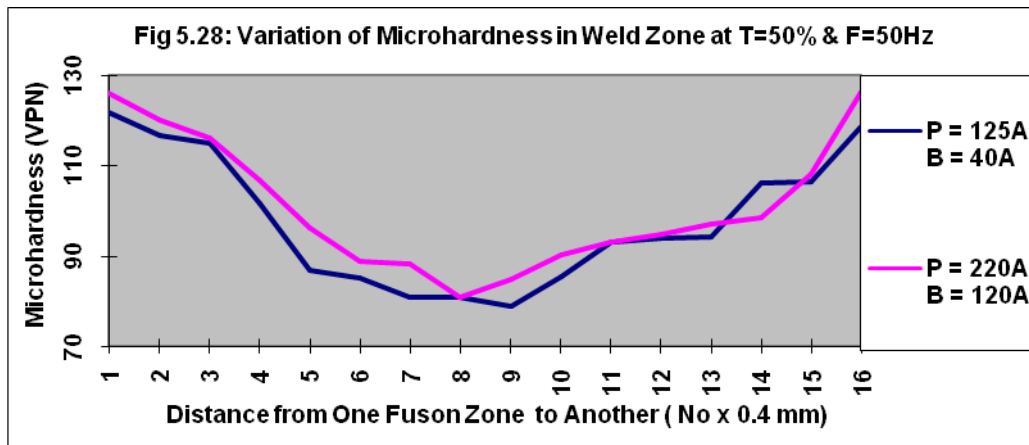
The microhardness in the weld zone is lowest due to as-cast nature of microstructures as shown in Fig 5.50 and 5.51, which is characterized by coarse grains and lack of strengthening phases. The similar results were explained by Barbosa et al [99].

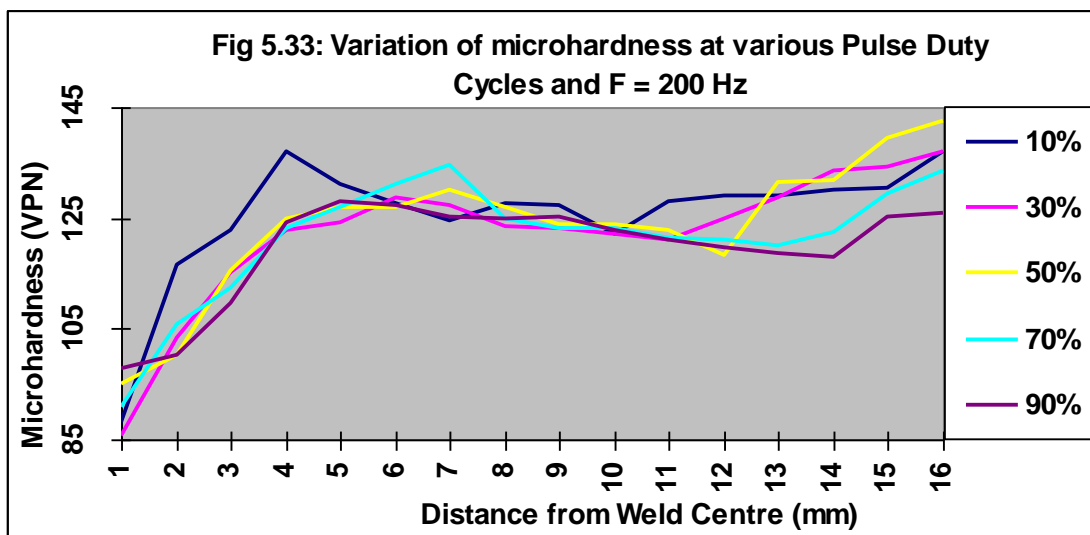
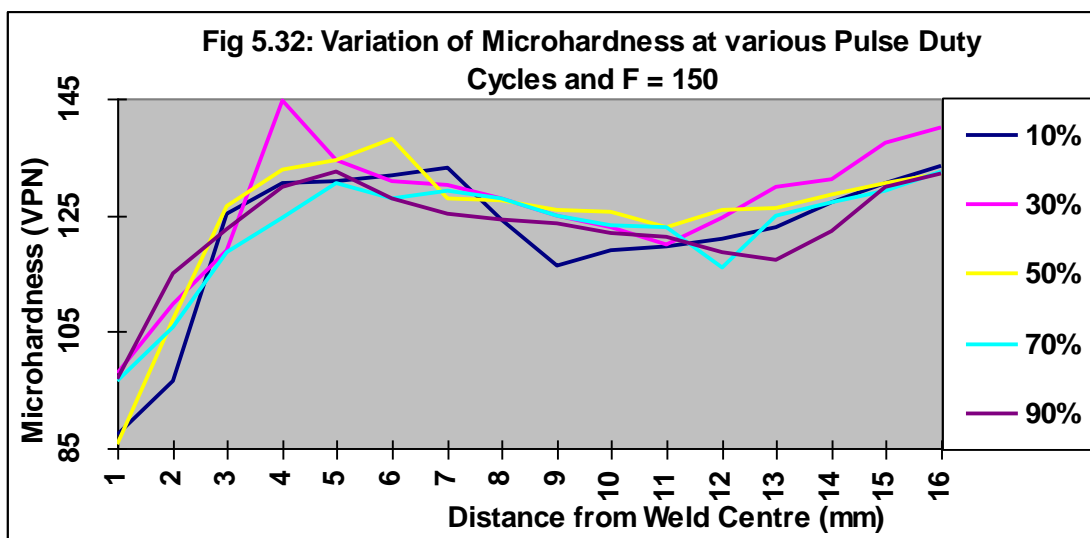
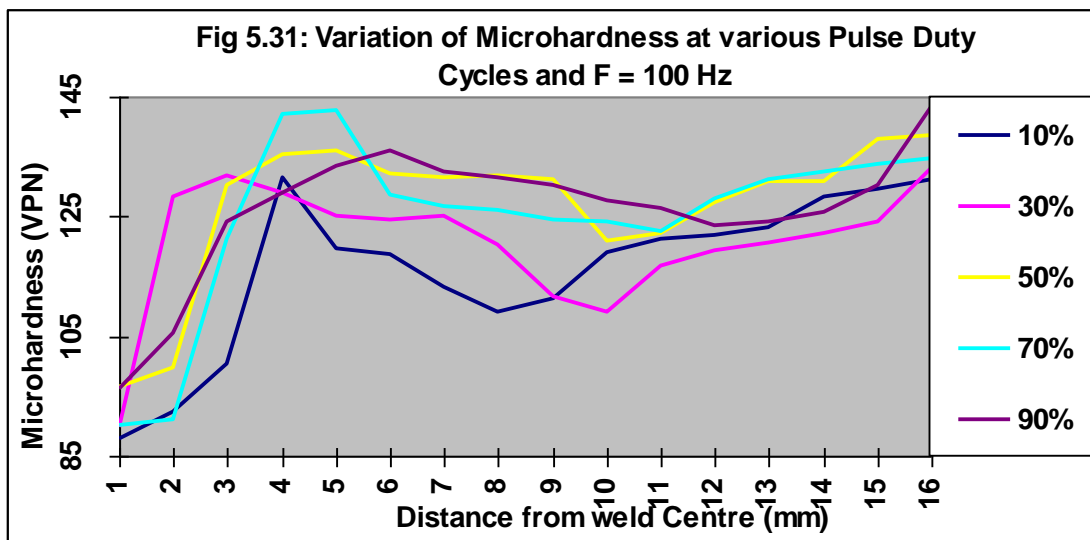
It is observed that as we move from the weld zone towards the unaffected base metal, the microhardness increases from 95 VHN to 145 VHN (approx) at fusion boundary. Increase in super-cooling leads to increase in heterogeneous nucleation which promotes fine equiaxed grains in the fusion boundary as shown in Fig 5.50. The reason for higher hardness in fine equiaxed grains is due to fine grains have more grain boundaries which serves as an effective barrier to the movement of dislocations.

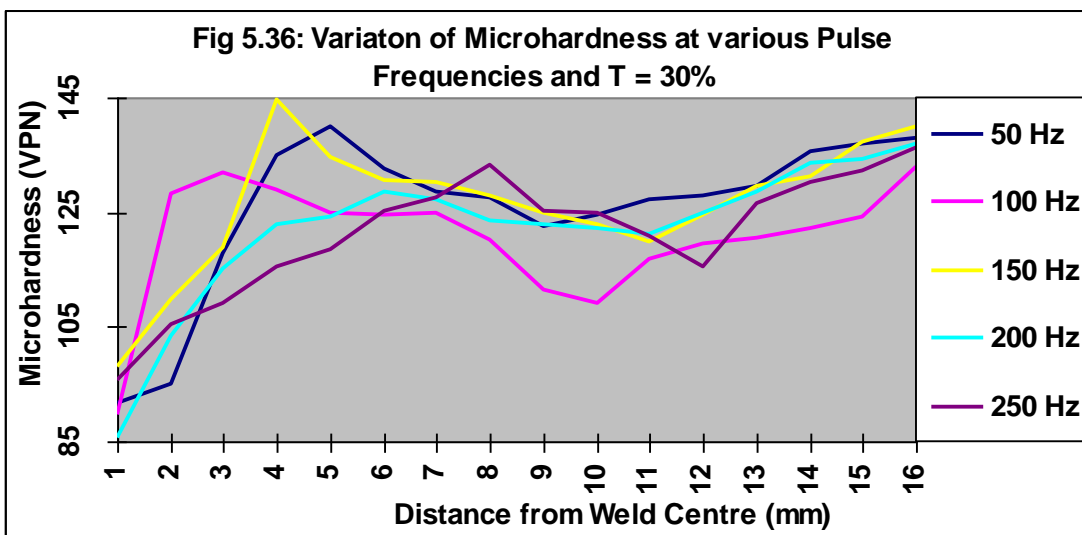
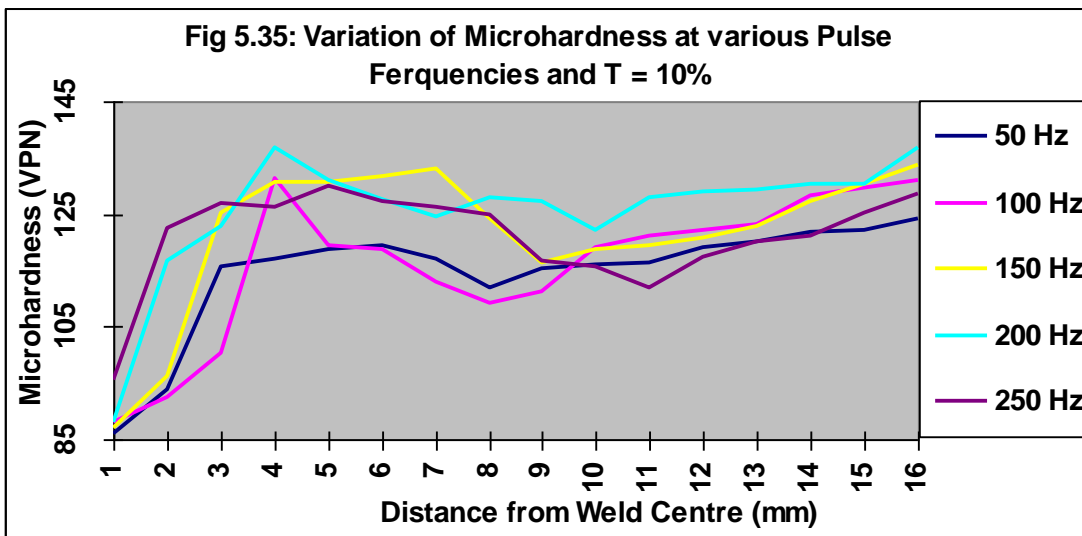
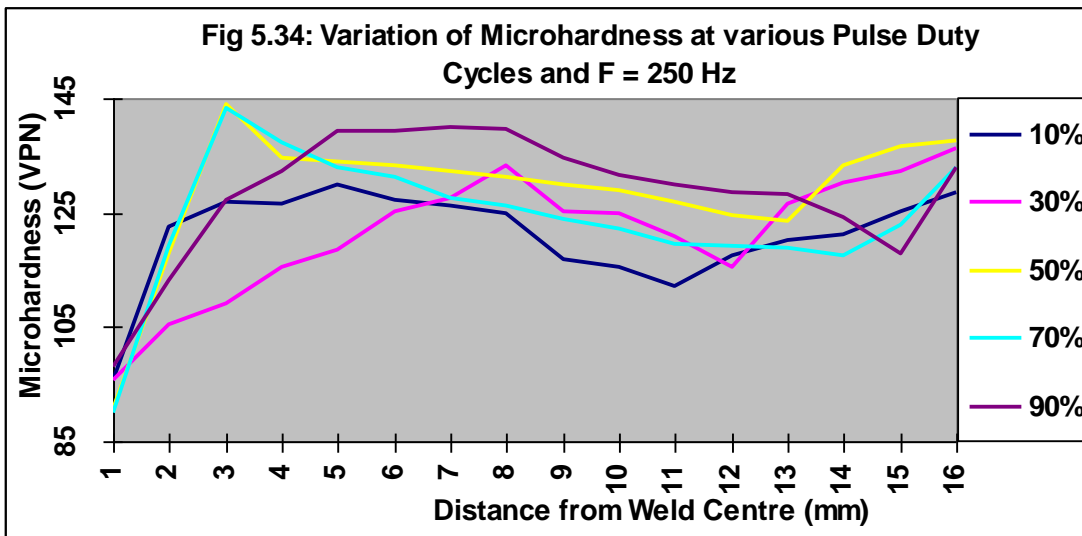
The higher hardness of the welds close to fusion boundary is possible due to large fraction of alloying elements in the solid solution at the end of the weld thermal cycle, thereby giving conditions for extensive age hardening at room temperature over a period of 5 to 7 days. At fusion boundary (Fig 5.50), precipitate dissolution occurs as the particles are exposed to temperatures higher than 400°C during heating and cooling as result of welding. Dissolution process enriches the solid solution of the aluminium matrix with Si and Mg.

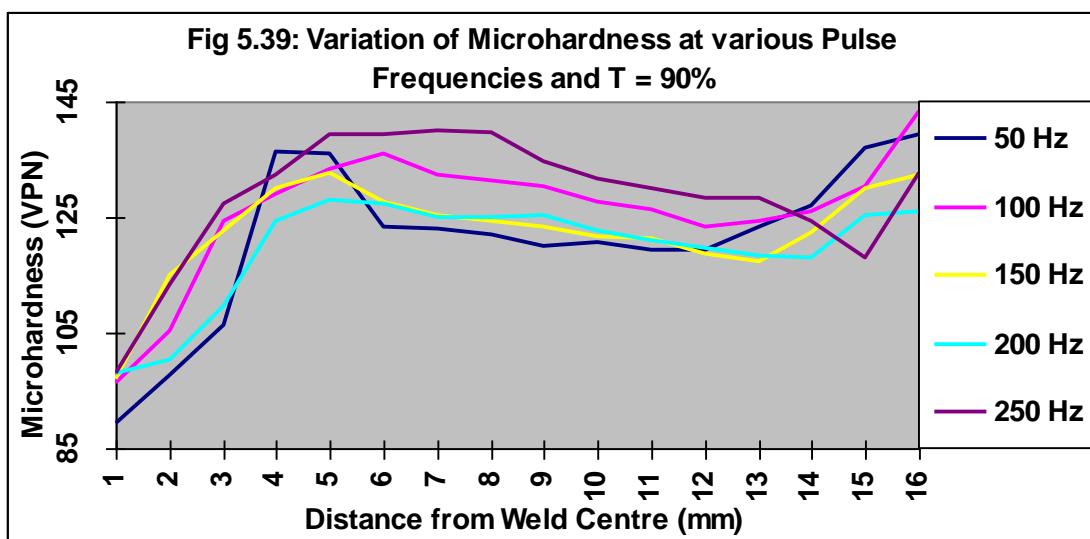
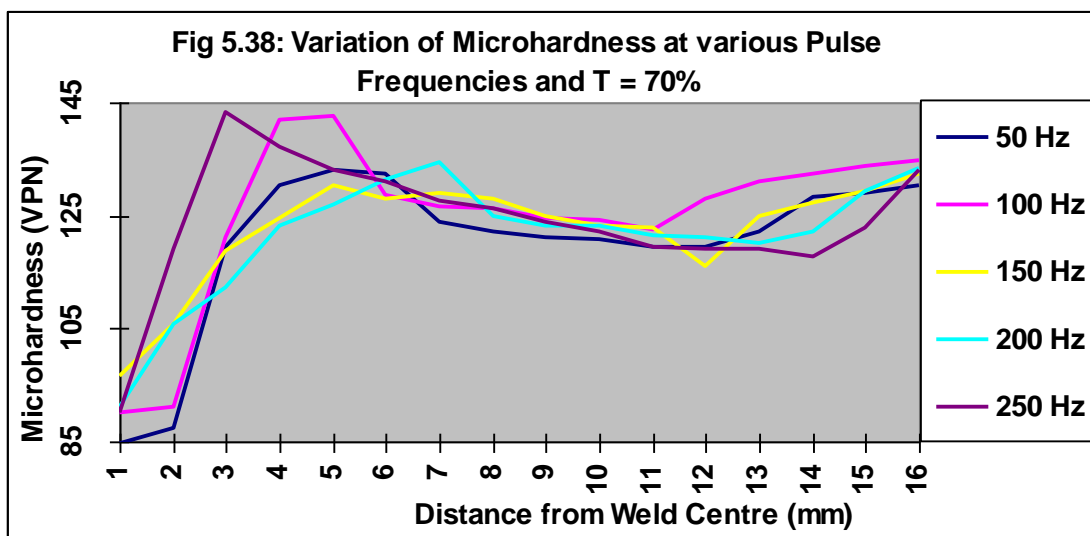
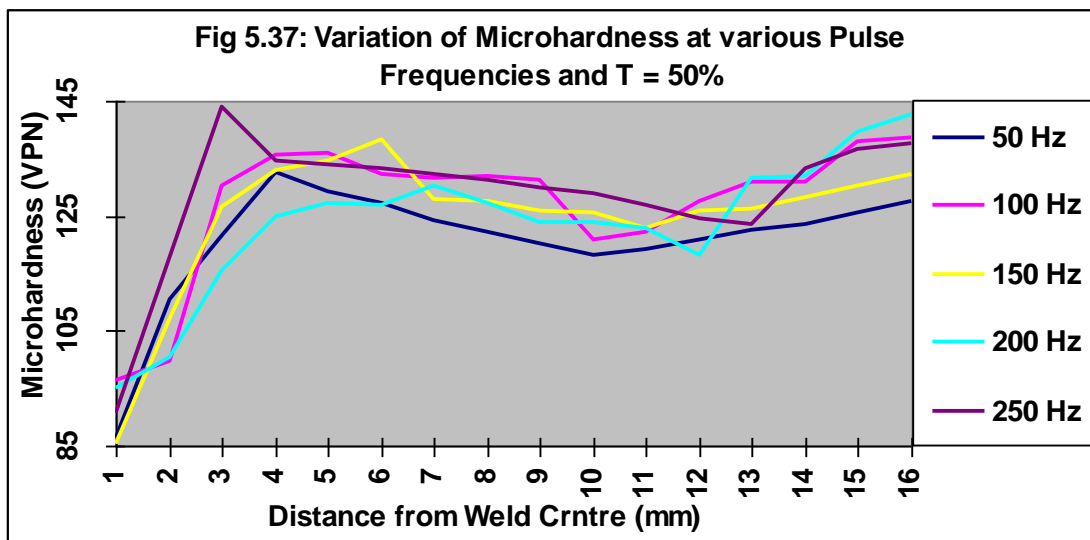
The microhardness decreases in a particular area (at 6 to 8mm approximately from the fusion boundary) in HAZ, which is known as soft zone as shown in Fig 2.6. The width of this soft zone depends on the peak temperature heating / cooling rate, dissolution or growth of precipitates and formation of stable phases. Loss of hardness and strength in HAZ is due to the dissolution and coarsening of  $Mg_2Si$  phase, the main strengthening phase in Al-Mg-Si alloys. After a particular drop in microhardness at HAZ, it again increases up to the

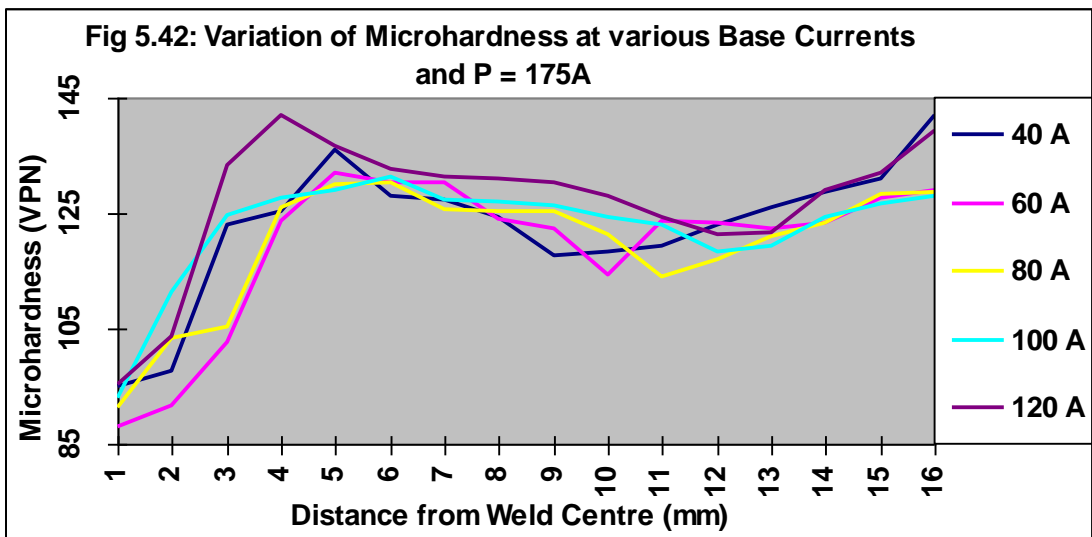
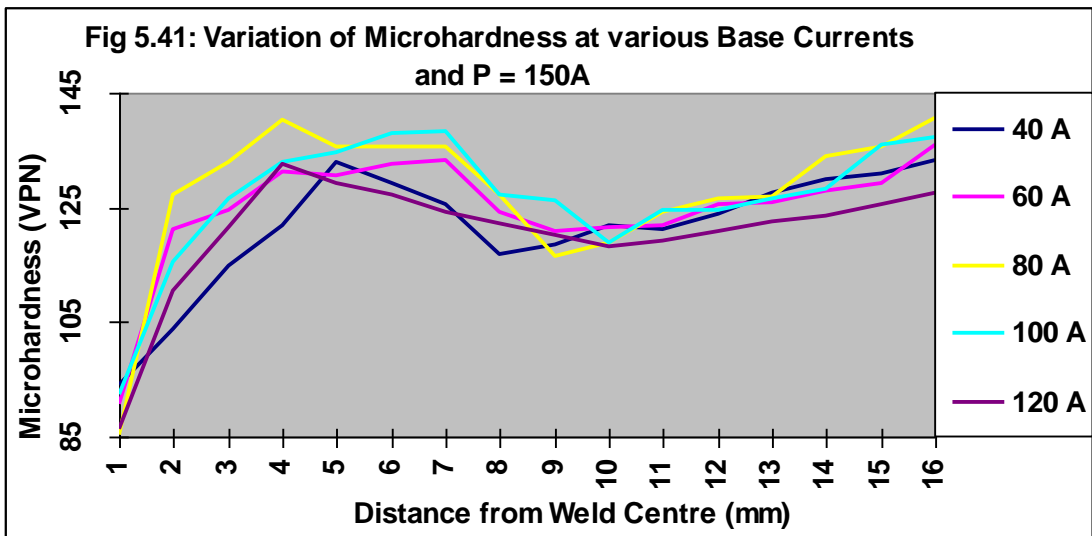
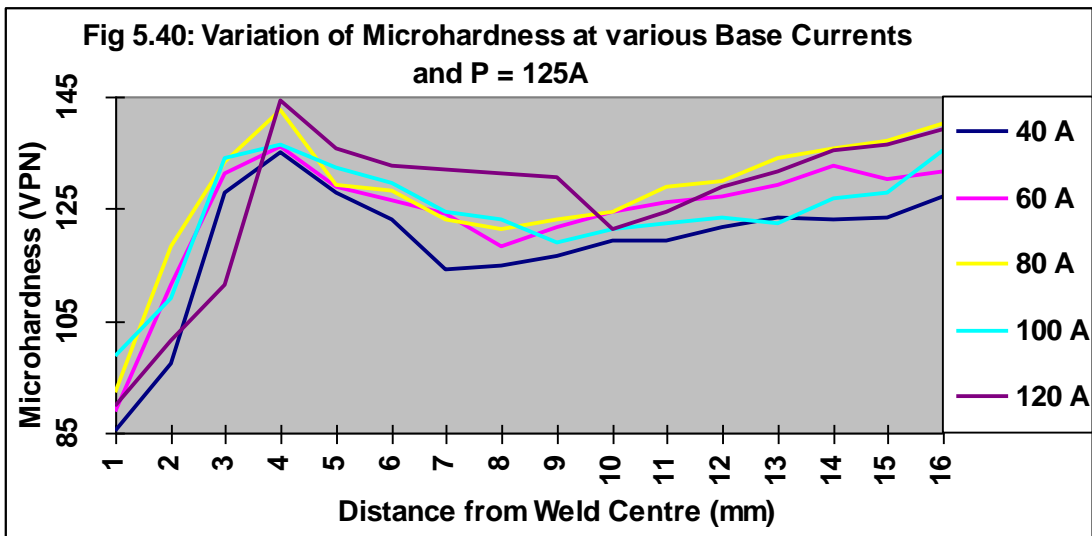
end of HAZ and saturated in unaffected base metal. Similar results were concluded by Borbosa et al [99] and Bradley et al [174].

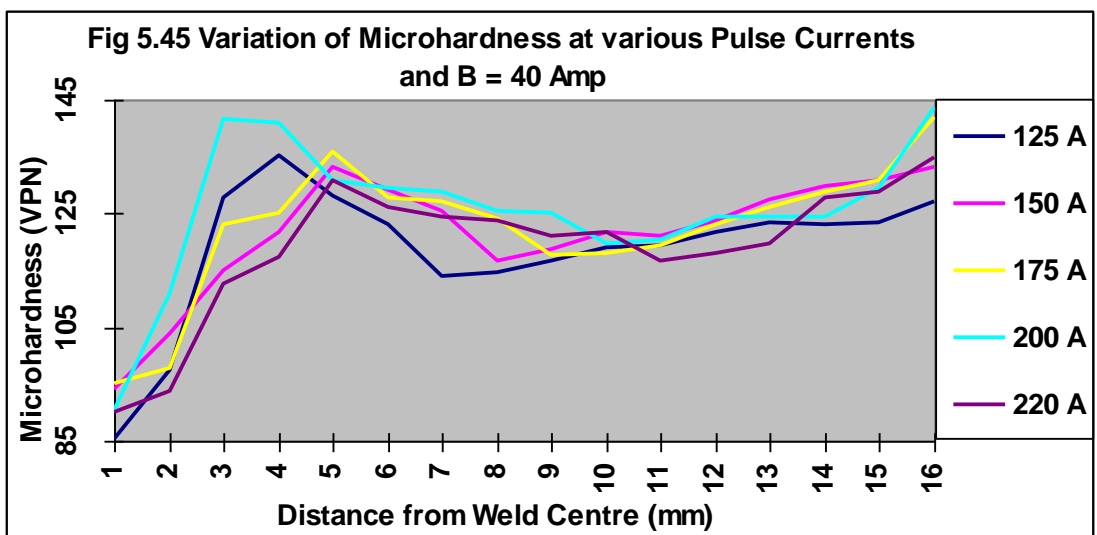
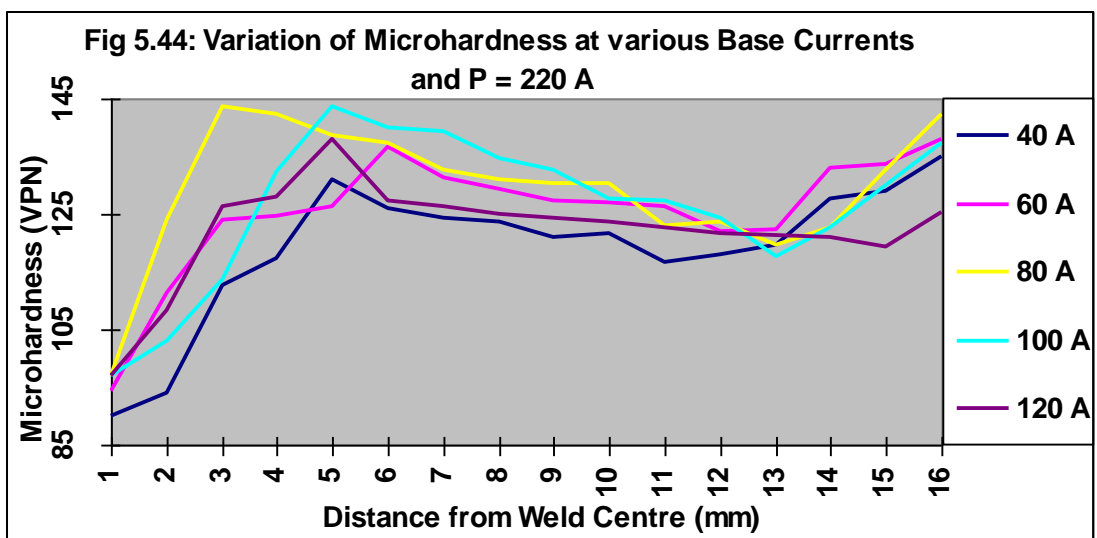
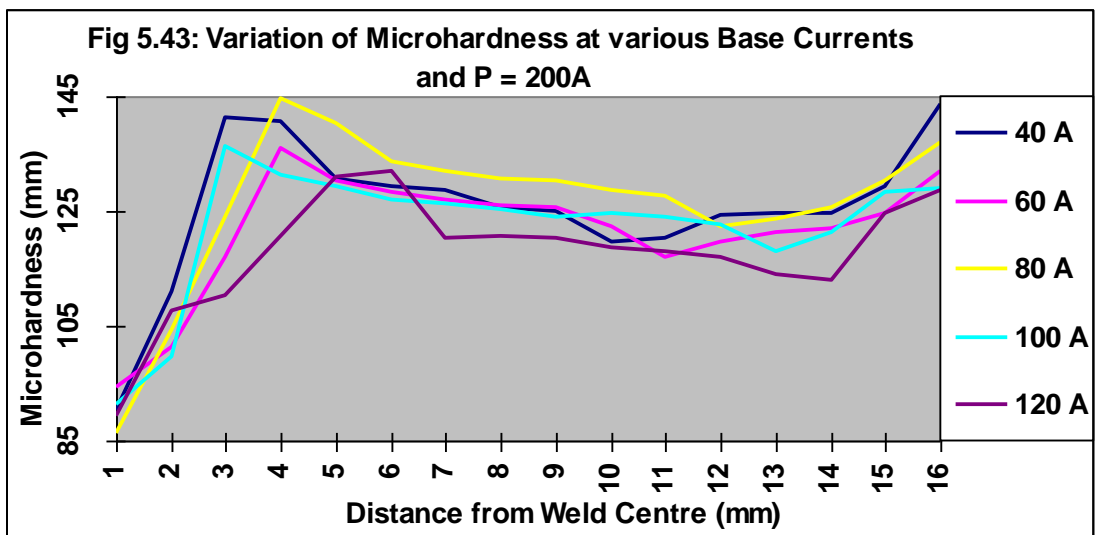


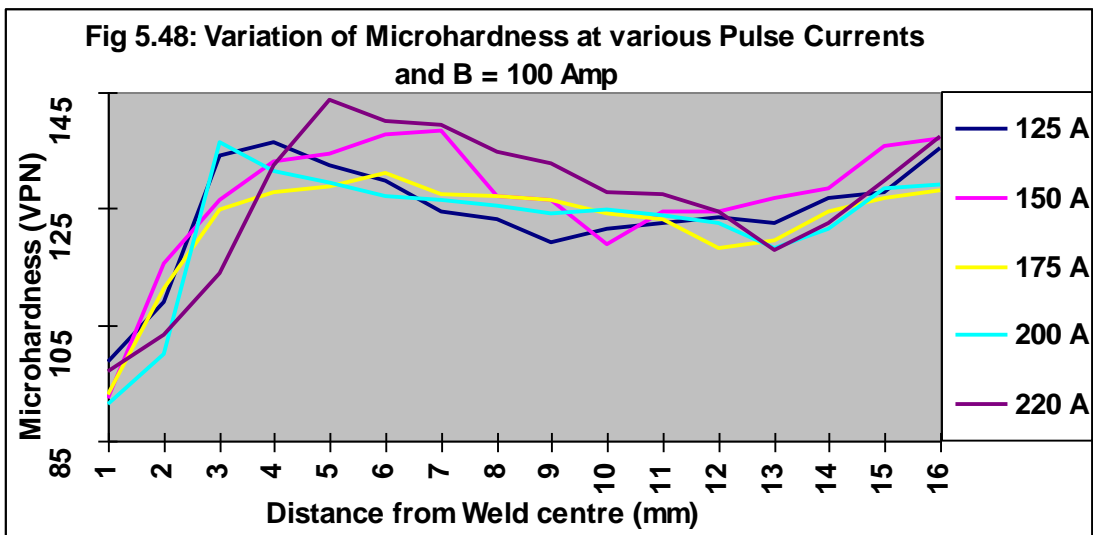
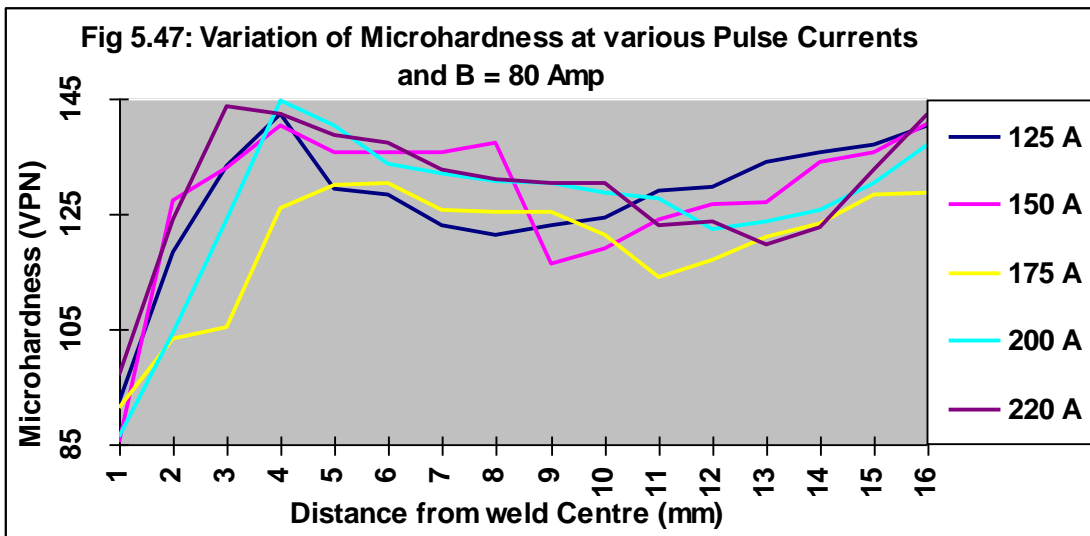
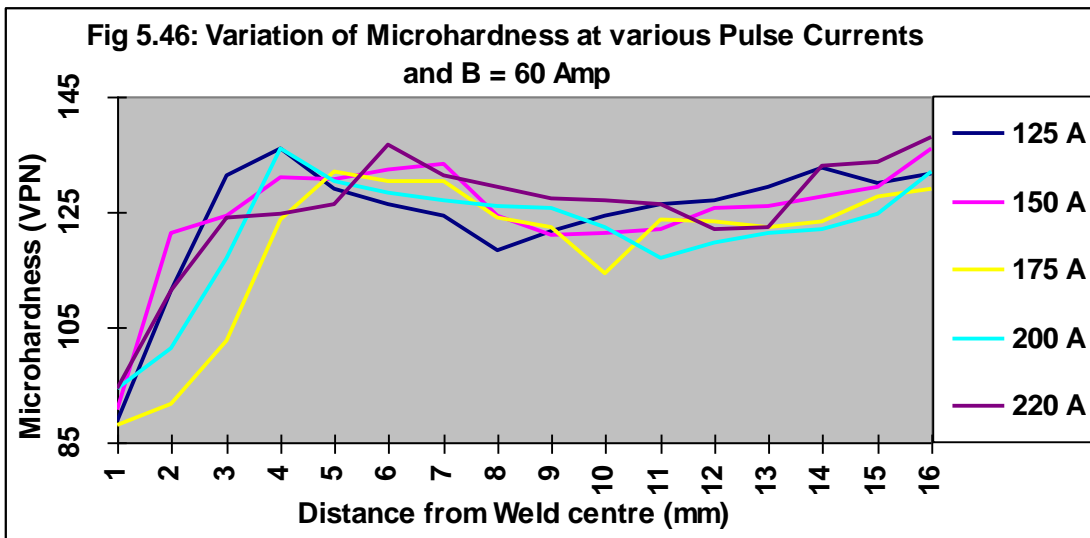


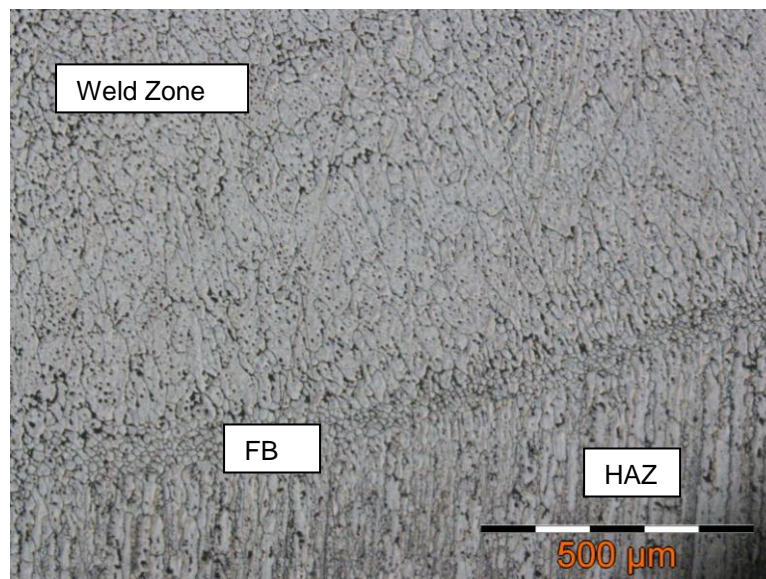
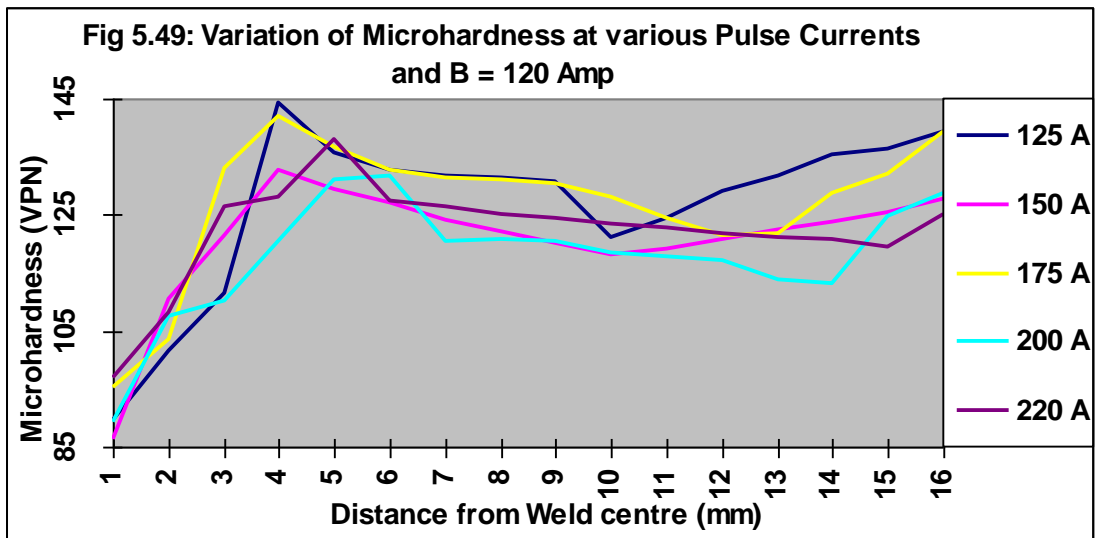






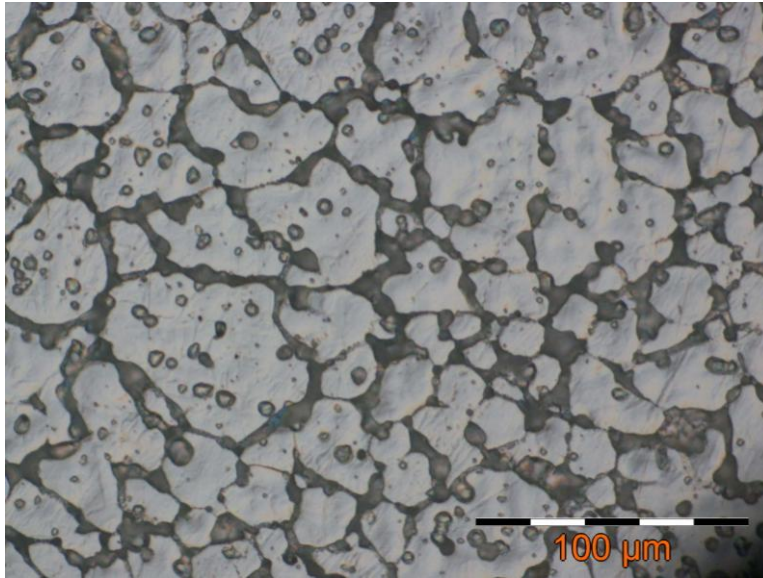






**Fig 5.50: Microstructure of Pulsed Welded Al Alloy 7039**

It is also observed that as we increase the pulse current, base current, pulse duty cycle and pulse frequency, the drop in the microhardness shifts away from the weld centre towards the unaffected base metal. This is due to the increase in heat input as currents, duty cycle and frequencies increase. The heat input should be limited while welding heat treatable alloys because at higher heat input per unit length of weld, the HAZ will be wider and more severe losses of strength takes place as explained / shown in Fig 2.7 [177].



**Fig 5.51: Weld Zone Microstructure (Pulse GTA Welded – AA 7039)**

## **5.4 Experimentation on Aluminium Alloy 6061**

### **5.4.1 Bead Geometry – Experimental Results and Analysis**

The experiments were conducted as per the parameters values decided in table 4.4 and experimental layout in orthogonal array L16 as shown in table 4.5. The results were tabulated in table 5.1. For optimizing the process parameters, three quality characteristics have to be considered for a single characteristic. The weighted response of bead geometry properties is obtained by adding weights to the responses as a single quality characteristic.

In this optimisation, AHP (Analytical Hierarchy Process) was used for analysing the weights of different parameters of weld bead geometry after taking the comparative importance value of each parameter by three experts in the field of welding technology [172]. After calculation of relative importance values, the weights for bead penetration, bead width and bead height are selected as 0.64, 0.254 and 0.106 respectively. The weightage response is tabulated in Table 5.2.

**Analysis of variance** is the most important tool for calculating the responsible factors which significantly affects the bead geometry properties. For determining the significant affecting process parameters, F-test was

performed. The results of ANOVA and the percentage contribution by each of the process parameters are tabulated in Table 5.3. The response graph in Fig 5.52 is drawn from response Table 5.4, to identify the significant levels of each factor.

**Table 5.1: Experimental results for the bead geometry of AA6061**

| Expt No | Penetration (p) mm | Width (b) mm | Height (h) mm | Expt No | Penetration (p) mm | Width (b) mm | Height (h) mm |
|---------|--------------------|--------------|---------------|---------|--------------------|--------------|---------------|
| 01.     | 0.36               | 8.16         | 2.04          | 09.     | 1.46               | 8.42         | 1.83          |
| 02.     | 0.47               | 7.98         | 2.50          | 10.     | 1.21               | 8.33         | 1.62          |
| 03.     | 0.76               | 8.27         | 2.47          | 11.     | 1.02               | 8.65         | 1.70          |
| 04.     | 0.97               | 8.32         | 2.74          | 12.     | 1.05               | 8.41         | 1.86          |
| 05.     | 0.83               | 8.08         | 1.83          | 13.     | 1.00               | 7.93         | 1.66          |
| 06.     | 1.63               | 8.15         | 1.85          | 14.     | 0.64               | 7.70         | 2.41          |
| 07.     | 1.08               | 8.54         | 1.78          | 15.     | 1.97               | 8.46         | 1.67          |
| 08.     | 1.57               | 8.15         | 1.86          | 16.     | 1.82               | 8.51         | 1.94          |

**Table 5.2: Weighted response for the bead geometry of AA6061**

| Expt No | Weighted Response | Expt No | Weighted Response | Expt No | Weighted Response | Expt No | Weighted Response |
|---------|-------------------|---------|-------------------|---------|-------------------|---------|-------------------|
| 01.     | 2.519             | 05.     | 2.778             | 09.     | 3.267             | 13.     | 2.830             |
| 02.     | 2.593             | 06.     | 3.309             | 10.     | 3.062             | 14.     | 2.621             |
| 03.     | 2.849             | 07.     | 3.049             | 11.     | 3.030             | 15.     | 3.587             |
| 04.     | 3.025             | 08.     | 3.272             | 12.     | 3.005             | 16.     | 3.532             |

**Table 5.3: Results of analysis of variance for bead geometry of AA6061**

| Symbol | Welding parameter | Deg of freedom | Sum of square | Mean square | F     | Contributed percentage |
|--------|-------------------|----------------|---------------|-------------|-------|------------------------|
| P      | Pulse Current     | 3              | 0.4063        | 0.1354      | 2.374 | 26.89                  |
| B      | Base Current      | 3              | 0.3683        | 0.1228      | 2.152 | 24.38                  |
| F      | Pulse Frequency   | 3              | 0.0320        | 0.0107      | 0.187 | 02.18                  |
| T      | Pulse Duty Cycle  | 3              | 0.5333        | 0.1778      | 3.116 | <b>35.29</b>           |
| Error  |                   | 3              | 0.1711        | 0.0571      |       | 11.32                  |
| Total  |                   | 15             | 1.5110        | 0.5038      |       |                        |

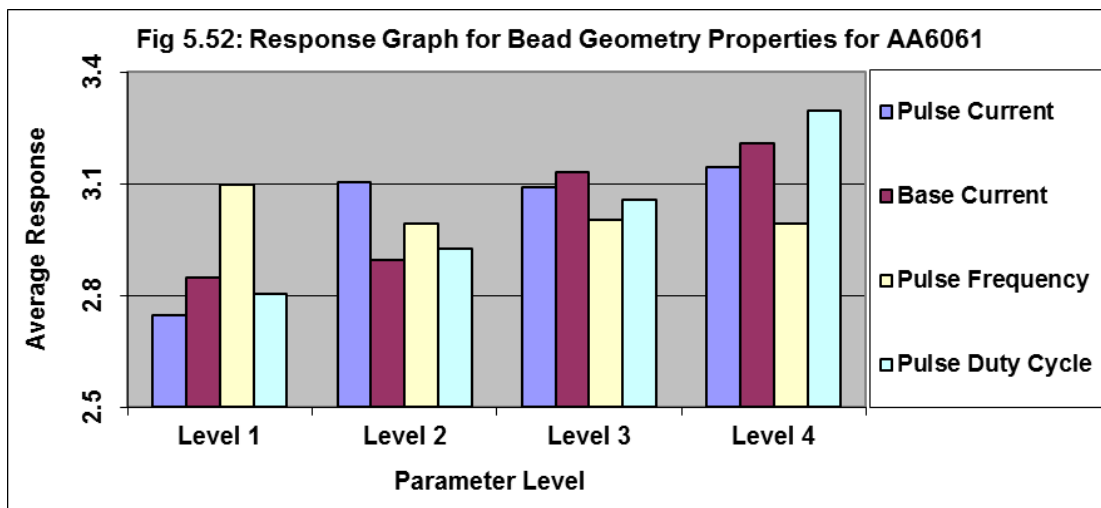
**Confirmation Test:** The optimal level of process parameters were predicted by using the response graph and ANOVA. The process parameters and their levels which affect the weld bead geometry are pulse current at level 4, base current at level 4, pulse frequency at level 1 and pulse duty cycle at level 4. The obtained results were verified by conducting a confirmation test based on results obtained in Table 5.5.

**Table 5.4: Response table for the weld bead properties of AA6061**

| Symbol | Welding parameter | Level 1      | Level 2 | Level 3 | Level 4      |
|--------|-------------------|--------------|---------|---------|--------------|
| P      | Pulse Current     | 2.747        | 3.102   | 3.091   | <b>3.143</b> |
| B      | Base Current      | 2.849        | 2.896   | 3.129   | <b>3.209</b> |
| F      | Pulse Frequency   | <b>3.098</b> | 2.991   | 3.002   | 2.992        |
| T      | Pulse Duty Cycle  | 2.805        | 2.925   | 3.055   | <b>3.297</b> |

**Table 5.5: Confirmation test results for bead geometry of AA6061**

| Optimum Response | Optimal level of process parameters | Penetration (p) mm | Bead width (b) mm | Bead height (h) mm |
|------------------|-------------------------------------|--------------------|-------------------|--------------------|
| Predicted        | P4 – B4 – F1 – T4                   |                    |                   |                    |
| Experiment       | P4 – B4 – F1 – T4                   | 2.01               | 8.72              | 2.77               |



In this investigation, the pulse current of 150 A, base current of 110 A, pulse frequency of 50 Hz and pulse duty cycle of 75% results the maximum values

of bead geometry. The confirmation test conducted with predicted levels of factors proved to be effective and worthy.

On the basis of the results in Tables 5.1 to 5.5 and Fig 5.52, it has been observed that pulse current, base current and pulse duty cycle plays an important role for optimising the weld bead geometries but the parameters pulse current and pulse duty cycle have the maximum contributions i.e. **26.89% and 35.29 %** respectively because higher pulse duty cycle indicates the tendency towards continuous pulse current and results in higher heat inputs which is responsible for deeper penetration and wider weld bead. Also the stirring / agitating nature of the weld pool in pulsed welding produces deeper penetrating beads with better grain refinement in the fusion zone, which directly improves the weld mechanical properties and can be seen in the results of next experimentation.

At the same time at lower pulse frequencies, narrower HAZ and wider fusion zones are achieved which was earlier reported by Omar et al [38]. In this bead geometry optimization, pulse frequency does not play any significant role i.e. 2.18% and similar conclusions were drawn by Yarmuch et al [10].

#### **5.4.2 Mechanical Properties – Experimental Results and Analysis**

In order to remove oil, moisture and oxide layer from base metal, they were thoroughly wire brushed, cleaned with acetone and preheated at 150 °C in the oven before welding. The experiments were conducted as per the parameters values decided in Table 4.4 and experimental layout in orthogonal array L16 as shown in Table 4.5.

Tensile specimens of required dimension as per ASTM E8M were separated out from welded coupon plates [173] and tests were carried out on 400 KN computer controlled Universal Testing Machine. The specimens were loaded at the rate of 1.5 KN/min as per ASTM specifications, so that the tensile specimen undergoes deformation. All specimens finally fail after necking and the load vs displacement profile was recorded. Higher the tensile properties have better quality characteristics.

At the same time for microhardness measurement, samples of transverse cross-section of joint were taken from the weld coupons. The specimens for microstructural characterization were mechanically polished using 220, 320, 400, 600 and 1000 grit waterproof SiC emery papers and alumina grade-II paste. Microhardness tests were carried out on a Leco Digital Microhardness Tester with 50 gf load and 15 second dwell time incorporated with diamond indenter. Final polishing was carried out using 3 and 1  $\mu\text{m}$  diamond paste. To reveal the macrostructures of the welded sample, deep etching technique using 10% HF acid was used. However, for further revealing of microstructures, Keller's reagent was used as etchants. Olympus make metallurgical microscope coupled with Image Analysis system was used for the microstructural characterization.

**Table 5.6: Experimental results for the mechanical properties of AA6061**

| <b>Experiment No</b> | <b>Ultimate Tensile Strength MPa</b> | <b>Microhardness VPN</b> | <b>Elongation Percentage</b> |
|----------------------|--------------------------------------|--------------------------|------------------------------|
| <b>01</b>            | 287.07                               | 83.1                     | 08.12                        |
| <b>02</b>            | 269.96                               | 83.7                     | 13.78                        |
| <b>03</b>            | 267.73                               | 87.3                     | 13.48                        |
| <b>04</b>            | 281.37                               | 85.0                     | 14.14                        |
| <b>05</b>            | 268.68                               | 85.5                     | 16.38                        |
| <b>06</b>            | 267.32                               | 87.8                     | 08.04                        |
| <b>07</b>            | 249.09                               | 95.8                     | 13.60                        |
| <b>08</b>            | 258.26                               | 93.2                     | 13.84                        |
| <b>09</b>            | 261.66                               | 95.6                     | 15.28                        |
| <b>10</b>            | 252.02                               | 88.8                     | 14.24                        |
| <b>11</b>            | 261.66                               | 100.5                    | 17.22                        |
| <b>12</b>            | 256.34                               | 92.7                     | 16.32                        |
| <b>13</b>            | 269.98                               | 89.1                     | 15.78                        |
| <b>14</b>            | 265.35                               | 86.8                     | 14.80                        |
| <b>15</b>            | 261.12                               | 91.5                     | 13.12                        |
| <b>16</b>            | 259.32                               | 94.4                     | 13.80                        |

The results of the mechanical properties – ultimate tensile strength (UTS), microhardness of weld zone and percentage elongation are tabulated in table 5.6; and the reported properties are almost inferior to parent metal. All tensile specimens fractured at weld joint, therefore their mechanical properties correspond to that of weld joint. For optimizing the process parameters, three quality characteristics have to be considered for a single characteristic. The weighted response of mechanical properties is obtained by adding weights to the responses as a single quality characteristic.

**Table 5.7: Weighted response for the mechanical properties of AA6061**

| Expt No | Weighted Response | Expt No | Weighted Response | Expt No | Weighted Response | Expt No | Weighted Response |
|---------|-------------------|---------|-------------------|---------|-------------------|---------|-------------------|
| 01.     | 242.16            | 05.     | 228.27            | 09.     | 224.25            | 13.     | 229.85            |
| 02.     | 228.89            | 06.     | 227.19            | 10.     | 215.44            | 14.     | 225.76            |
| 03.     | 227.67            | 07.     | 214.20            | 11.     | 225.12            | 15.     | 223.07            |
| 04.     | 238.19            | 08.     | 221.10            | 12.     | 219.60            | 16.     | 222.13            |

**Table 5.8: Results of ANOVA for the mechanical properties of AA6061**

| Symbol | Welding parameter | Deg of freedom | Sum of square | Mean square | F     | Contributed percentage |
|--------|-------------------|----------------|---------------|-------------|-------|------------------------|
| P      | Pulse Current     | 3              | 412.47        | 137.49      | 4.501 | <b>52.55</b>           |
| B      | Base Current      | 3              | 166.86        | 55.62       | 1.821 | 21.26                  |
| F      | Pulse Frequency   | 3              | 60.23         | 20.07       | 0.657 | 07.67                  |
| T      | Pulse Duty Cycle  | 3              | 53.65         | 17.88       | 0.586 | 06.84                  |
| Error  | Error             | 3              | 91.64         | 30.55       |       | 11.68                  |
| Total  |                   | 15             | 784.85        |             |       |                        |

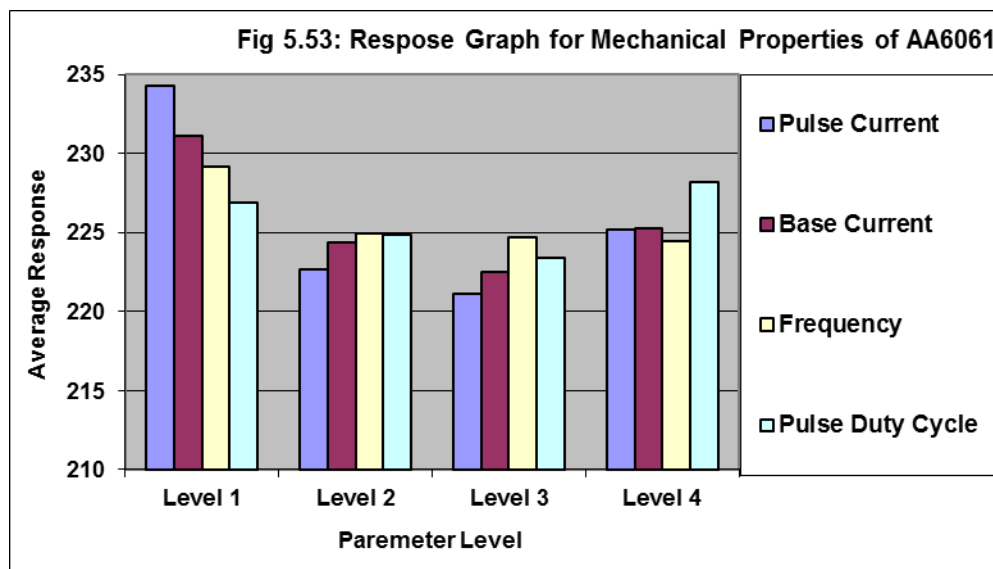
**Table 5.9: Response table for the mechanical properties of AA6061**

| Symbol | Welding parameter | Level 1       | Level 2 | Level 3 | Level 4       |
|--------|-------------------|---------------|---------|---------|---------------|
| P      | Pulse Current     | <b>234.23</b> | 222.69  | 221.10  | 225.20        |
| B      | Base Current      | <b>231.13</b> | 224.37  | 222.52  | 225.26        |
| F      | Pulse Frequency   | <b>229.15</b> | 224.96  | 224.70  | 224.42        |
| T      | Pulse Duty Cycle  | 226.84        | 224.86  | 223.38  | <b>228.18</b> |

In this optimisation, AHP (Analytical Hierarchy Process) was used for analysing the weights of different parameters of mechanical properties after taking the comparative importance value of each parameter by three experts in the field of welding technology [172]. After calculation of relative importance values, the weights for UTS, microhardness and percentage elongation are selected as 0.796, 0.160 and 0.044 respectively. The weightage response is tabulated in Table 5.7.

**Table 5.10: Confirmation test results for the mechanical properties of AA6061**

| Optimum Response | Optimal level of process parameters | UTS MPa | Microhardness VPN | Elongation Percentage |
|------------------|-------------------------------------|---------|-------------------|-----------------------|
| Predicted        | P1 – B1 – F1 – T4                   |         |                   |                       |
| Experiment       | P1 – B1 – F1 – T4                   | 309.33  | 104.5             | 17.24                 |



**Analysis of Variance (ANOVA)** is most important tool for calculating responsible factors, which significantly affects mechanical properties. For determining these effects on process parameters, F-test was performed. Results of ANOVA and percentage contributions by each process parameters are tabulated in Table 5.8. Response graphs (Fig 5.53) are drawn from response table indicated Table 5.9, to identify the significant levels of each factor.

**Confirmation Test:** Optimal level of process parameters was predicted using response graph and ANOVA. Process parameters and their levels which affect mechanical properties are pulse current at level 1, base current at level 1, pulse frequency at level 1 and pulse duty cycle at level 4. The obtained results were verified for the improvement in multiple quality characteristics by conducting a confirmation test based on results obtained in Table 5.10.

ANOVA calculations shown in Table 5.8 and Response Graph in Fig 5.53, shows that pulse current, base current, pulse duty cycle and frequency plays significant role on microstructure and mechanical properties of welded Al alloy 6061, but pulse current plays the maximum role i.e. **52.55 %** because it has direct influence on the tensile properties of the weld joints of AA6061 and also reported earlier by Senthilkumar et al [104] and Ravishankar et al [168]. In this investigation, pulse current of 120A, base current of 80A, pulse frequency of 50Hz and pulse duty cycle of 75% resulted in the maximum values of mechanical properties.

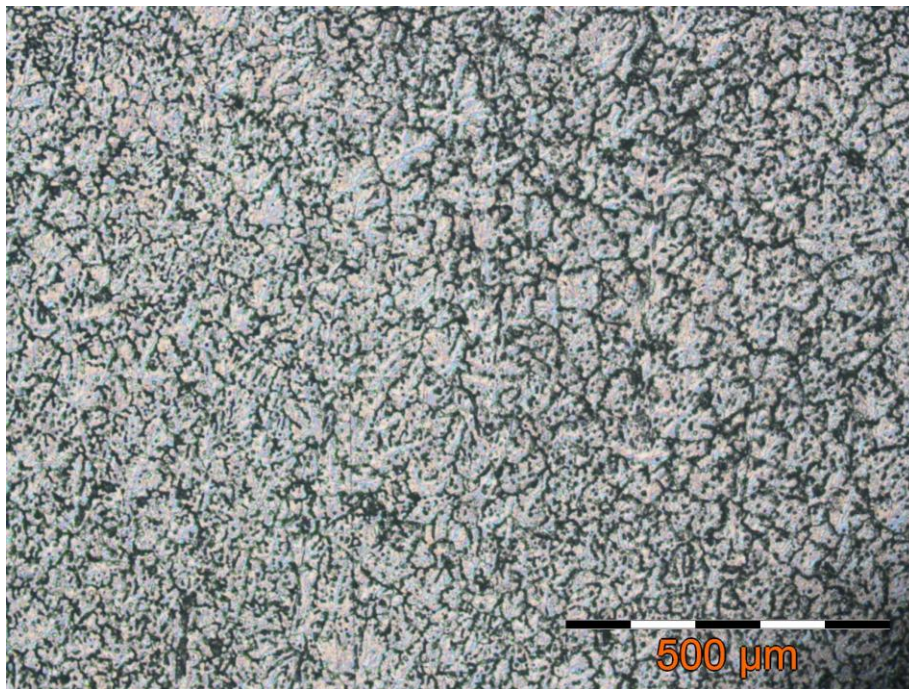
In fusion zone, the weld zone has as-cast structure consisting of a mixture of filler metal and the parent metal as shown in Fig 5.55. The properties of weld depend upon the composition of filler and base metal, the amount of dilution, the quality of the welding process and the rate of solidification. The weld metal dilution (volume fraction of the base metal in the weld bead) was evaluated for the optimized sample (P1-B1-F1-T4) in terms of area fractions (assumed to replace volume fractions as shown in Fig 5.56 and found approximately 62%. In similar manner, the dilution of a welded sample (without pulsing) at 120 A and 50 Hz was evaluated and found around 55%, which is lesser than pulsed welded sample.

$$\text{The dilution D of the weld bead} = \frac{(A+B+C) - (A+C) \times 100}{(A+B+C)}$$

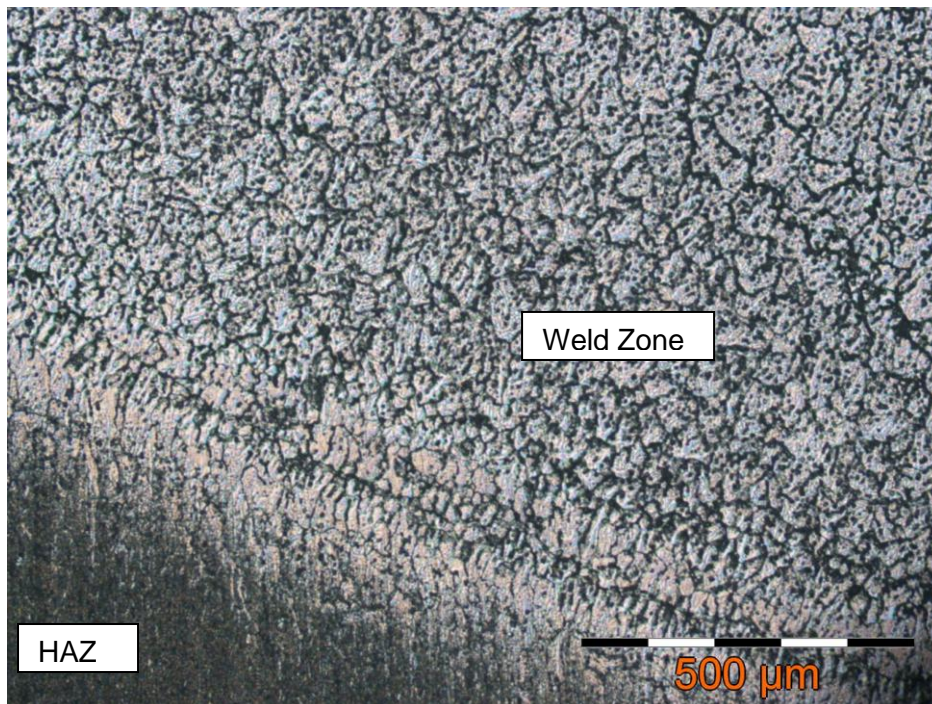
(Where A = area of top and bottom reinforcement, B = area of fused base metal, C = area of weld deposit).

The dilution of weld metal improves in an excellent manner with pulse welding due to agitating / stirring nature of the weld pool. Due to this high dilution

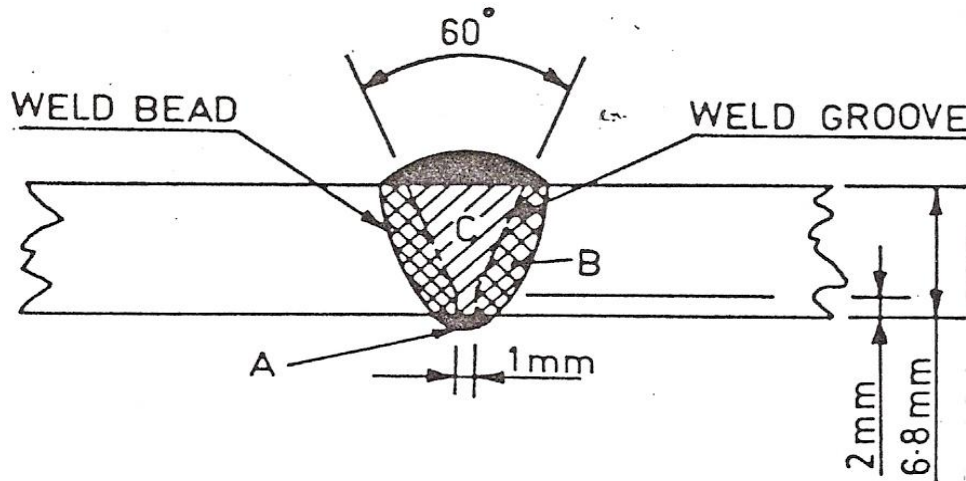
level, non-precipitation hardenable filler deposited functions as precipitation hardenable alloy and because of this reason only the tensile properties are high. The aluminium alloy 6061-T6 is not significantly sensitive to natural ageing.



**Fig 5.54: Microstructures of Weld Zone of GTA welded AA6061**



**Fig 5.55: Microstructures of HAZ and Weld Zone of GTA welded AA6061**



**Fig 5.56: Schematic Diagram of Weld Groove and Bead**

The metallurgical advantages of pulsed current welding are refinement of fusion zone grain size and substructure, reduced width of HAZ, control of segregation etc. Microstructures of optimized sample were characterized by image analysis system and shown in Fig 5.54 and 5.55. From the microstructural characterization it is observed that the pulse parameters play an important role in grain refinement in the fusion zone and development of fine microstructure, which improves the mechanical properties of weld joints and earlier reported by Reddy GM et al [153-155]. When the ratio of heat input per unit length to welding speed increases, the loss of strength in the weld zone as well as in HAZ becomes more severe. The high heat input results in the formation of coarse grains in the weld zone and HAZ as explained in Fig 2.8 and 2.9, which is directly responsible for loss of mechanical properties like tensile strength and microhardness [177].

## **5.5 Experimentation on Aluminium Alloy 6061 with Gas Mixtures**

### **5.5.1 Bead Geometry – Experimental Results and Analysis**

The experiments were conducted as per the parameters values decided in table 4.6 and experimental layout in orthogonal array L25 as shown in table 4.7. The results were tabulated in Table 5.11. For optimizing the process parameters, four quality characteristics have to be considered for a single characteristic. The weighted response of bead geometry properties is obtained by adding weights to the responses as a single quality characteristic.

In this optimisation, AHP (Analytical Hierarchy Process) was used for analysing the weights of different parameters of weld bead geometry after taking the comparative importance value of each parameter by three experts in the field of welding technology [172]. After calculation of relative importance values, the weights for bead penetration, bead width and bead height are selected as 0.64, 0.254 and 0.106 respectively. The weightage response is tabulated in Table 5.12.

**Analysis of variance (ANOVA)** is the most important tool for calculating the responsible factors which significantly affects the bead geometry properties. For determining the significant affecting process parameters, F-test was performed. The results of ANOVA and the percentage contribution by each of the process parameters are presented in Table 5.13. The Response graph in Fig 5.57 is drawn from response Table 5.14, to identify the significant levels of each factor.

**Table 5.11: Experimental results for bead geometry of AA6061 with gas mixtures**

| S. No | Penetration (p) mm | Width (b) mm | Height (h) mm | S. No | Penetration (p) mm | Width (b) mm | Height (h) mm |
|-------|--------------------|--------------|---------------|-------|--------------------|--------------|---------------|
| 01.   | 0.64               | 8.51         | 1.97          | 14.   | 1.15               | 7.81         | 2.06          |
| 02.   | 0.71               | 7.13         | 1.23          | 15.   | 1.10               | 9.30         | 1.79          |
| 03.   | 0.92               | 6.22         | 2.00          | 16.   | 0.75               | 6.81         | 1.68          |
| 04.   | 1.52               | 8.76         | 1.80          | 17.   | 1.71               | 7.62         | 1.80          |
| 05.   | 1.31               | 9.28         | 1.13          | 18.   | 2.20               | 9.68         | 2.39          |
| 06.   | 1.27               | 8.14         | 1.79          | 19.   | 1.02               | 8.91         | 2.24          |
| 07.   | 1.17               | 9.50         | 2.14          | 20.   | 1.58               | 7.76         | 2.03          |
| 08.   | 1.04               | 8.81         | 1.69          | 21.   | 1.05               | 7.81         | 1.86          |
| 09.   | 1.02               | 8.08         | 1.37          | 22.   | 1.75               | 9.84         | 2.17          |
| 10.   | 0.89               | 8.24         | 1.56          | 23.   | 0.82               | 7.44         | 2.01          |
| 11.   | 1.57               | 9.67         | 2.21          | 24.   | 1.29               | 8.63         | 2.16          |
| 12.   | 0.72               | 7.01         | 1.96          | 25.   | 1.34               | 8.24         | 1.82          |
| 13.   | 1.21               | 8.67         | 1.98          |       |                    |              |               |

**Confirmation Test:** The process parameters and their levels which affect the weld bead geometry are pulse current at level 4, base current at level 5, pulse frequency at level 1, pulse duty cycle at level 5 and percentage of Helium at level 4. The obtained result was verified by conducting a confirmation test based on results obtained in Table 5.15.

**Table 5.12: Weighted response for bead geometry of AA6061 with gas mixtures**

| Exp No | Weighted Response | Exp No | Weighted Response | Exp No | Weighted Response | Exp No | Weighted Response |
|--------|-------------------|--------|-------------------|--------|-------------------|--------|-------------------|
| 1.     | 2.774             | 8.     | 3.077             | 15.    | 3.251             | 22.    | 3.843             |
| 2.     | 2.392             | 9.     | 2.848             | 16.    | 2.384             | 23.    | 2.622             |
| 3.     | 2.375             | 10.    | 2.823             | 17.    | 3.215             | 24.    | 2.922             |
| 4.     | 3.383             | 11.    | 3.689             | 18.    | 4.112             | 25.    | 3.138             |
| 5.     | 3.312             | 12.    | 2.445             | 19.    | 3.147             |        |                   |
| 6.     | 3.065             | 13.    | 3.181             | 20.    | 3.191             |        |                   |
| 7.     | 3.382             | 14.    | 2.932             | 21.    | 2.847             |        |                   |

On the basis of the results in Tables 5.11 to 5.15 and Fig 5.57, it has been observed that pulse current, base current, pulse frequency and pulse duty cycle plays an important role for optimising the weld bead geometries but the parameter, percentage of helium in argon has the maximum contribution i.e. **26.52 %** because argon plus helium gas mixtures in combination with pulsing parameters increases the control of heat input and produce better bead geometries in comparison to continuous current welding, which directly improves the mechanical properties of the welds.

Helium has high ionization potential which increases the weld bead penetration for getting better bead geometry and the improvement in bead geometry parameters can be easily seen by comparing the results of Table 5.01 (without gas mixtures) and Table 5.11 (with gas mixtures), and similar results was reported by Reichelt et al [7], Marya et al [8] and Kuk et al [70]. The improvement of mechanical properties by using pulsing parameters with gas mixtures can be seen in the next experimentation.

In this investigation, the pulse current of 195 A, base current of 135 A, pulse frequency of 50 Hz, pulse duty cycle of 90% and 40% of He in argon-helium gas mixture resulted the maximum values of bead geometry. The confirmation test conducted with predicted levels of factors proved to be effective and worthy.

**Table 5.13: Results of ANOVA for bead geometry of AA6061 with gas mixtures**

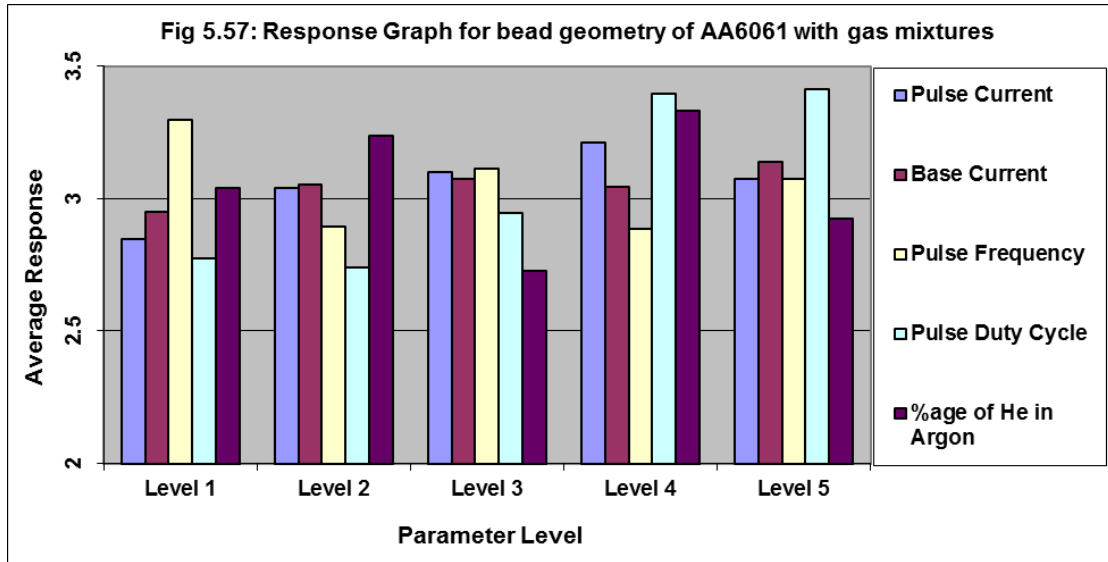
| Symbol | Welding parameter             | Deg of freedom | Sum of square | Mean square | F      | Contributed percentage |
|--------|-------------------------------|----------------|---------------|-------------|--------|------------------------|
| P      | Pulse Current                 | 4              | 0.5796        | 0.1449      | 0.7366 | 12.34                  |
| B      | Base Current                  | 4              | 0.3803        | 0.0951      | 0.4834 | 8.09                   |
| F      | Pulse Frequency               | 4              | 0.9091        | 0.2273      | 1.1553 | 19.35                  |
| T      | Pulse Duty Cycle              | 4              | 0.7964        | 0.1991      | 1.0122 | 16.95                  |
| X      | Percentage of Helium in Argon | 4              | 1.2462        | 0.3114      | 1.5837 | <b>26.52</b>           |
| Error  |                               | 4              | 0.7869        | 0.1967      |        | 16.75                  |
| Total  |                               | 24             | 4.6985        |             |        |                        |

**Table 5.14: Response table for bead geometry of AA6061 with gas mixtures**

| Symbol | Welding parameter             | Level 1      | Level 2 | Level 3 | Level 4      | Level 5      |
|--------|-------------------------------|--------------|---------|---------|--------------|--------------|
| P      | Pulse Current                 | 2.847        | 3.039   | 3.100   | <b>3.210</b> | 3.074        |
| B      | Base Current                  | 2.952        | 3.055   | 3.073   | 3.046        | <b>3.138</b> |
| F      | Pulse Frequency               | <b>3.297</b> | 2.895   | 3.112   | 2.885        | 3.076        |
| T      | Pulse Duty Cycle              | 2.776        | 2.740   | 2.945   | 3.395        | <b>3.413</b> |
| X      | Percentage of Helium in Argon | 3.042        | 3.236   | 2.727   | <b>3.333</b> | 2.926        |

**Table 5.15: Confirmation test for bead geometry of AA6061 with gas mixtures**

| Optimum Response | Optimal level of process parameters | Penetration (p) mm | Bead width (b) mm | Bead height (h) mm |
|------------------|-------------------------------------|--------------------|-------------------|--------------------|
| Predicted        | P4–B5–F1–T5–X4                      |                    |                   |                    |
| Experiment       | P4–B5–F1–T5–X4                      | 2.29               | 10.43             | 2.39               |



### 5.5.2 Mechanical Properties – Experimental Results and Analysis

The experiments were conducted as per the parameters values decided in table 4.6 and experimental layout in orthogonal array L25 as shown in table 4.7. Tensile specimens of required dimension as per ASTM E8M were separated out from welded coupon plates [173] and tests were carried out on 400 KN computer controlled Universal Testing Machine. The specimens were loaded at the rate of 1.5 KN/min as per ASTM specifications, so that the tensile specimen undergoes deformation. All specimens finally fail after necking and the load vs displacement profile was recorded. Higher the tensile properties have better quality characteristics.

At the same time for microhardness measurement, samples of transverse cross-section of joint were taken from the weld coupons. The specimens for microstructural characterization were mechanically polished using 220, 320, 400, 600 and 1000 grit waterproof SiC emery papers and alumina grade-II paste. Final polishing was carried out using 3 and 1  $\mu\text{m}$  diamond paste. To reveal the macrostructures of the welded sample, deep etching technique using 10% HF acid was used. However, for further revealing of microstructures, Keller's reagent was used as etchants.

**Table 5.16: Experimental results for mechanical properties of AA6061 with gas mixtures**

| <b>Experiment No</b> | <b>Ultimate Tensile Strength MPa</b> | <b>Microhardness VPN</b> | <b>Elongation %age</b> |
|----------------------|--------------------------------------|--------------------------|------------------------|
| <b>01</b>            | 256.40                               | 114.1                    | 08.71                  |
| <b>02</b>            | 267.47                               | 112.6                    | 12.94                  |
| <b>03</b>            | 283.36                               | 098.7                    | 10.00                  |
| <b>04</b>            | 288.08                               | 112.5                    | 10.90                  |
| <b>05</b>            | 298.75                               | 112.9                    | 09.70                  |
| <b>06</b>            | 293.76                               | 105.8                    | 07.84                  |
| <b>07</b>            | 290.74                               | 097.8                    | 09.00                  |
| <b>08</b>            | 352.85                               | 110.6                    | 09.08                  |
| <b>09</b>            | 272.12                               | 120.8                    | 09.92                  |
| <b>10</b>            | 386.07                               | 099.2                    | 10.70                  |
| <b>11</b>            | 290.74                               | 109.0                    | 10.00                  |
| <b>12</b>            | 272.63                               | 112.4                    | 10.36                  |
| <b>13</b>            | 282.62                               | 109.3                    | 12.06                  |
| <b>14</b>            | 280.75                               | 100.5                    | 10.86                  |
| <b>15</b>            | 300.95                               | 103.9                    | 08.12                  |
| <b>16</b>            | 300.18                               | 105.7                    | 09.20                  |
| <b>17</b>            | 288.05                               | 107.0                    | 11.30                  |
| <b>18</b>            | 282.42                               | 102.2                    | 09.32                  |
| <b>19</b>            | 290.74                               | 115.4                    | 10.58                  |
| <b>20</b>            | 278.27                               | 101.4                    | 09.90                  |
| <b>21</b>            | 295.69                               | 108.1                    | 10.60                  |
| <b>22</b>            | 293.02                               | 095.6                    | 11.04                  |
| <b>23</b>            | 294.00                               | 102.5                    | 09.62                  |
| <b>24</b>            | 301.50                               | 097.0                    | 10.48                  |
| <b>25</b>            | 310.03                               | 099.5                    | 10.58                  |

**Table 5.17: Weighted response for mechanical properties of AA6061 with gas mixtures**

| Exp No | Weighted Response | Exp No | Weighted Response | Exp No | Weighted Response | Exp No | Weighted Response |
|--------|-------------------|--------|-------------------|--------|-------------------|--------|-------------------|
| 1.     | 185.78            | 8.     | 242.75            | 15.    | 209.69            | 22.    | 203.06            |
| 2.     | 192.57            | 9.     | 197.18            | 16.    | 209.84            | 23.    | 205.33            |
| 3.     | 197.97            | 10.    | 259.82            | 17.    | 203.19            | 24.    | 208.45            |
| 4.     | 206.64            | 11.    | 205.17            | 18.    | 198.26            | 25.    | 214.26            |
| 5.     | 210.99            | 12.    | 195.27            | 19.    | 206.98            |        |                   |
| 6.     | 205.84            | 13.    | 200.65            | 20.    | 195.63            |        |                   |
| 7.     | 202.02            | 14.    | 196.99            | 21.    | 207.98            |        |                   |

**Table 5.18: Results of analysis of variance (ANOVA) for mechanical properties of AA6061 with gas mixtures**

| Symbol | Welding parameter             | Deg of freedom | Sum of square | Mean square | F     | Contributed %age |
|--------|-------------------------------|----------------|---------------|-------------|-------|------------------|
| P      | Pulse Current                 | 4              | 1621.34       | 405.34      | 2.902 | <b>29.31</b>     |
| B      | Base Current                  | 4              | 992.89        | 248.22      | 1.777 | 17.95            |
| F      | Pulse Frequency               | 4              | 611.07        | 152.77      | 1.094 | 11.08            |
| T      | Pulse Duty Cycle              | 4              | 1205.99       | 301.49      | 2.158 | 21.80            |
| X      | Percentage of Helium in Argon | 4              | 541.21        | 135.30      | 0.969 | 09.79            |
| Error  |                               | 4              | 558.79        | 139.69      |       | 10.10            |
| Total  |                               | 24             | 5531.29       |             |       |                  |

**Table 5.19: Response table for mechanical properties of AA6061 with gas mixtures**

| Symbol | Welding parameter             | Level 1 | Level 2       | Level 3       | Level 4       | Level 5       |
|--------|-------------------------------|---------|---------------|---------------|---------------|---------------|
| P      | Pulse Current                 | 198.79  | <b>221.52</b> | 201.54        | 202.78        | 207.82        |
| B      | Base Current                  | 202.92  | 199.22        | 208.99        | 203.25        | <b>218.08</b> |
| F      | Pulse Frequency               | 208.78  | 204.08        | 201.85        | <b>214.87</b> | 203.99        |
| T      | Pulse Duty Cycle              | 195.84  | <b>214.27</b> | 203.65        | 204.92        | 213.79        |
| X      | Percentage of Helium in Argon | 209.97  | 201.49        | <b>213.60</b> | 202.36        | 205.03        |

The results of the mechanical properties – ultimate tensile strength (UTS), microhardness of weld zone and percentage elongation are tabulated in Table 5.16; and the reported properties are almost inferior to parent metal. All tensile specimens fractured at weld joint, therefore their mechanical properties correspond to that of weld joint. For optimizing the process parameters, four quality characteristics have to be considered for a single characteristic. The weighted response of mechanical properties is obtained by adding weights to the responses as a single quality characteristic.

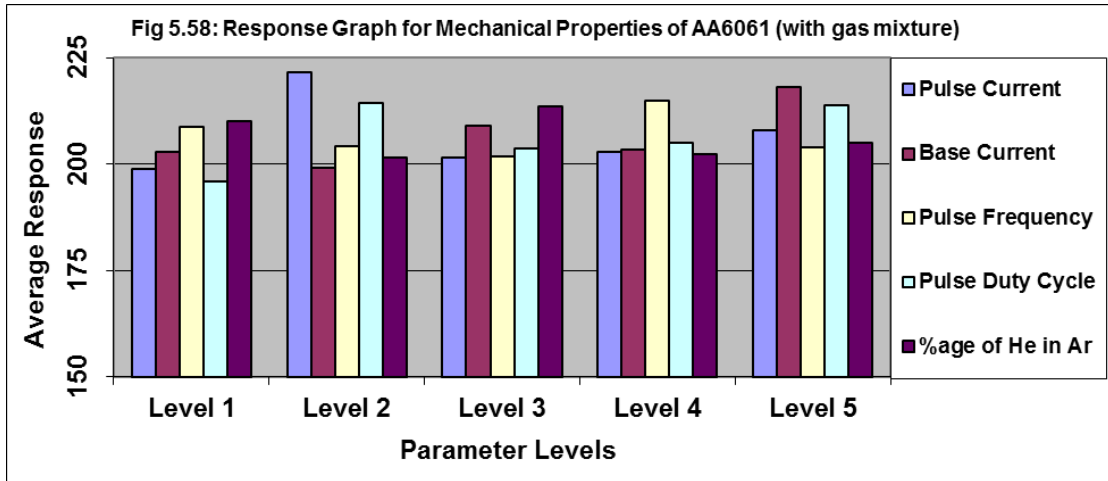
In this optimisation, AHP (Analytical Hierarchy Process) was used for analysing the weights of different parameters of mechanical properties after taking the comparative importance value of each parameter by three experts in the field of welding technology [172]. After calculation of relative importance values, the weights for UTS, microhardness and percentage elongation are selected as 0.796, 0.160 and 0.044 respectively. The weightage response is tabulated in Table 5.17.

**Analysis of Variance (ANOVA)** is most important tool for calculating responsible factors, which significantly affects mechanical properties. For determining these affect on process parameters, F-test was performed. Results of ANOVA and percentage contributions by each process parameters are tabulated in Table 5.18. Response graphs (Fig 5.58) are drawn from response table indicated Table 5.19, to identify the significant levels of each factor.

**Confirmation Test:** Optimal level of process parameters was predicted using response graph and ANOVA. Process parameters and their levels which affect mechanical properties are pulse current at level 2, base current at level 5, pulse frequency at level 4, pulse duty cycle at level 2 and percentage of Helium in Argon at level 3. The obtained results were verified for the improvement in multiple quality characteristics by conducting a confirmation test based on results obtained in Table 5.20.

**Table 5.20: Confirmation test results for mechanical properties of AA6061 with gas mixtures**

| Optimum Response | Optimal level of process parameters | UTS MPa | Microhardness VPN | Elongation %age |
|------------------|-------------------------------------|---------|-------------------|-----------------|
| Predicted        | P2 B5 F4 T2 X3                      |         |                   |                 |
| Experiment       | P2 B5 F4 T2 X3                      | 389.31  | 121.4             | 12.98           |



ANOVA calculations shown in Table 5.18 and Response Graph in Fig 5.58, shows that pulse current, base current, pulse duty cycle, pulse frequency and percentage of He in Ar-He mixture plays significant role on microstructure and mechanical properties of welded Al alloy 6061, but pulse current plays the maximum role i.e. **29.31 %** because it has direct influence on the tensile properties of the weld joints of AA6061 and also reported earlier by Senthilkumar et al [104] and Ravishankar et al [168].

In this investigation, pulse current of 165A, base current of 135A, pulse frequency of 125Hz, pulse duty cycle of 45% and 30% of He with Ar resulted in the maximum values of mechanical properties. Lower microhardness was observed in the weld zone in all samples as earlier explained in experimentation of microhardness analysis.

The HAZ is very important in welding of aluminum alloys, especially in alloys hardened by precipitation (artificial ageing). During artificial ageing in Al-Mg-Si alloys, a high density of fine, needle-shaped  $\beta''$  particles are formed uniformly in the matrix (aluminum,  $\alpha$ ). This precipitate is the dominating hardening phase, which is produced according to the following precipitation sequence:

Super-saturated Solid Solution → Solutes Clustering → GP Zones (spherical)  
→  $\beta''$  (needle) →  $\beta'$  (bar) →  $\beta$

However, since these precipitates are thermodynamically unstable in a welding process, the smallest ones will start to dissolve in parts of the HAZ where the peak temperature has been above the ageing temperature ( $> 160^\circ\text{C}$ ), while the larger ones will continue grow. Close to the weld fusion line full reversion of the  $\beta''$  particles is achieved. At the same time, coarse  $\beta'$  precipitates may form in the intermediate peak temperature range.

The loss of mechanical strength commonly referred to as over-aging in welding of a 6061-T6 Al alloy and it can explain in terms of the precipitation sequence. During welding, however, the base metal adjacent to the fusion line is subjected to a gradient of temperature imposed by the welding thermal cycle. At certain distance from the fusion line, the cooling curve crosses the interval of temperatures between  $383$  to  $250^\circ\text{C}$  in which the  $\beta'$  phase is stable. It is thus the transformation of  $\beta''$  into  $\beta'$  that is responsible of the decrease in hardening of  $\alpha$  matrix due to the incoherence of the  $\beta'$  phase caused by the thermodynamic instability of  $\beta''$  in a welding process.

## **5.6 Experimentation on Aluminium Alloy 7039 with Gas Mixtures**

### **5.6.1 Bead Geometry – Experimental Results and Analysis**

The experiments were conducted as per the parameters values decided in Table 4.6 and experimental layout in orthogonal array L25 as shown in Table 4.7. The results were tabulated in Table 5.21. For optimizing the process parameters, four quality characteristics have to be considered for a single characteristic. The weighted response of bead geometry properties is obtained by adding weights to the responses as a single quality characteristic.

In this optimisation, AHP (Analytical Hierarchy Process) was used for analysing the weights of different parameters of weld bead geometry after taking the comparative importance value of each parameter by three experts in the field of welding technology [172]. After calculation of relative importance values, the weights for bead penetration, bead width and bead height are

selected as 0.64, 0.254 and 0.106 respectively. The weightage response is tabulated in Table 5.22.

**Table 5.21: Experimental results for the bead geometry of AA7039 with gas mixtures**

| S. No | Penetration (p) mm | Width (b) mm | Height (h) mm | S. No | Penetration (p) mm | Width (b) mm | Height (h) mm |
|-------|--------------------|--------------|---------------|-------|--------------------|--------------|---------------|
| 01.   | 0.54               | 7.07         | 1.45          | 14.   | 1.12               | 10.58        | 1.99          |
| 02.   | 0.80               | 7.93         | 1.23          | 15.   | 1.67               | 9.40         | 2.01          |
| 03.   | 2.00               | 9.78         | 1.74          | 16.   | 1.71               | 9.86         | 1.83          |
| 04.   | 1.76               | 9.55         | 1.56          | 17.   | 1.42               | 9.04         | 2.42          |
| 05.   | 2.03               | 10.09        | 1.76          | 18.   | 1.33               | 8.76         | 1.87          |
| 06.   | 0.61               | 7.82         | 1.59          | 19.   | 1.78               | 9.42         | 2.28          |
| 07.   | 0.91               | 8.09         | 1.48          | 20.   | 1.19               | 9.45         | 1.83          |
| 08.   | 1.23               | 9.12         | 1.97          | 21.   | 1.42               | 10.06        | 1.91          |
| 09.   | 1.63               | 9.56         | 1.12          | 22.   | 1.84               | 9.81         | 1.87          |
| 10.   | 1.49               | 9.98         | 2.13          | 23.   | 1.56               | 8.52         | 1.63          |
| 11.   | 1.66               | 9.61         | 1.82          | 24.   | 2.35               | 10.68        | 1.42          |
| 12.   | 0.69               | 9.13         | 1.74          | 25.   | 1.29               | 8.05         | 2.09          |
| 13.   | 1.06               | 9.69         | 1.89          |       |                    |              |               |

**Table 5.22: Weighted response for bead geometry of AA7039 with gas mixtures**

| Exp No | Weighted Response | Exp No | Weighted Response | Exp No | Weighted Response | Exp No | Weighted Response |
|--------|-------------------|--------|-------------------|--------|-------------------|--------|-------------------|
| 1.     | 2.295             | 8.     | 3.313             | 15.    | 3.670             | 22.    | 3.868             |
| 2.     | 2.657             | 9.     | 3.590             | 16.    | 3.793             | 23.    | 3.335             |
| 3.     | 3.949             | 10.    | 3.714             | 17.    | 3.462             | 24.    | 4.367             |
| 4.     | 3.718             | 11.    | 3.696             | 18.    | 3.275             | 25.    | 3.092             |
| 5.     | 4.049             | 12.    | 2.945             | 19.    | 3.774             |        |                   |
| 6.     | 2.545             | 13.    | 3.340             | 20.    | 3.356             |        |                   |
| 7.     | 2.794             | 14.    | 3.615             | 21.    | 3.667             |        |                   |

**ANOVA** is the most important tool for calculating the responsible factors which significantly affects the bead geometry properties. For determining the significant affecting process parameters, F-test was performed. The results of

ANOVA and percentage contribution by each of the process parameters are presented in Table 5.23. Response graph (Fig 5.59) is drawn from response Table 5.24, to identify the significant levels of each factor.

**Table 5.23: Results of analysis of variance for bead geometry of AA7039 with gas mixtures**

| Symbol | Welding parameter             | Deg of freedom | Sum of square | Mean square | F      | Contributed percentage |
|--------|-------------------------------|----------------|---------------|-------------|--------|------------------------|
| P      | Pulse Current                 | 4              | 0.710         | 0.1775      | 0.7346 | 14.38                  |
| B      | Base Current                  | 4              | 1.105         | 0.2763      | 1.1428 | <b>22.37</b>           |
| F      | Pulse Frequency               | 4              | 0.582         | 0.1455      | 0.6020 | 11.78                  |
| T      | Pulse Duty Cycle              | 4              | 1.062         | 0.2656      | 1.0985 | <b>21.50</b>           |
| X      | Percentage of Helium in Argon | 4              | 0.513         | 0.1283      | 0.5308 | 10.39                  |
| Error  |                               | 4              | 0.967         |             |        | 19.58                  |
| Total  |                               | 24             | 4.939         |             |        |                        |

**Table 5.24: Response table for the weld bead properties of AA7039 with gas mixtures**

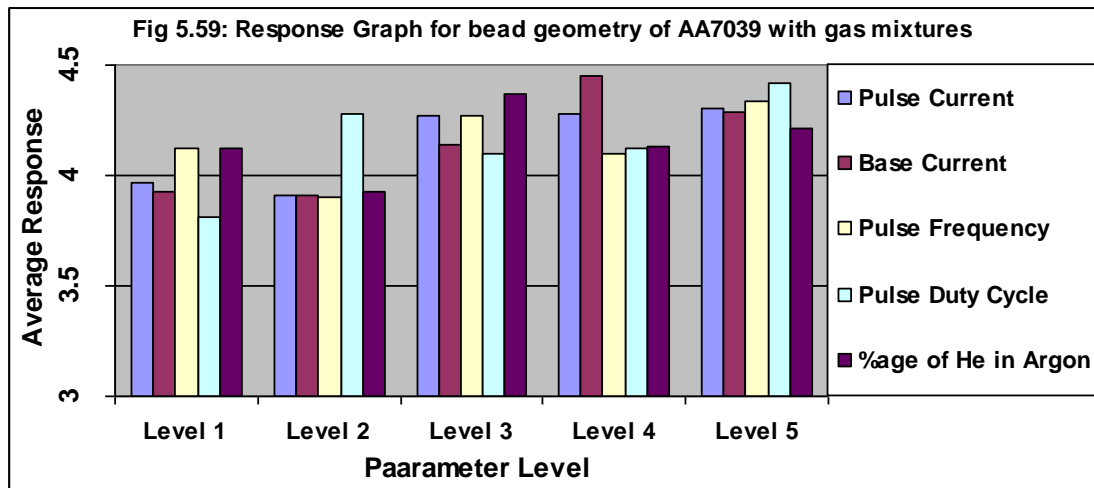
| Symbol | Welding parameter             | Level 1 | Level 2 | Level 3     | Level 4     | Level 5     |
|--------|-------------------------------|---------|---------|-------------|-------------|-------------|
| P      | Pulse Current                 | 3.97    | 3.91    | 4.27        | 4.28        | <b>4.30</b> |
| B      | Base Current                  | 3.93    | 3.91    | 4.14        | <b>4.45</b> | 4.29        |
| F      | Pulse Frequency               | 4.12    | 3.90    | 4.27        | 4.10        | <b>4.34</b> |
| T      | Pulse Duty Cycle              | 3.81    | 4.28    | 4.10        | 4.12        | <b>4.42</b> |
| X      | Percentage of Helium in Argon | 4.12    | 3.93    | <b>4.37</b> | 4.13        | 4.21        |

**Table 5.25: Confirmation test results for the weld bead properties of AA7039 with gas mixtures**

| Optimum Response | Optimal level of process parameters | Penetration (p) mm | Bead width (b) mm | Bead height (h) mm |
|------------------|-------------------------------------|--------------------|-------------------|--------------------|
| Predicted        | P5 -B4 - F5 - T5 - X3               |                    |                   |                    |
| Experiment       | P5 -B4 - F5 - T5 - X3               | 2.32               | 11.55             | 2.87               |

The process parameters and their levels which affect the weld bead geometry are pulse current at level 5, background current at level 4, pulse frequency at level 5, pulse duty cycle at level 5 and percentage of helium in argon at level

3. The obtained result was verified by conducting a confirmation test results obtained in Table 5.25.



On the basis of the results in Tables 5.21 to 5.25 and Fig 5.59, it has been observed that pulse current, base current, pulse frequency, pulse duty cycle and percentage of He in Ar-He gas mixtures plays significant role for optimising the weld bead geometries but the parameter base current and pulse duty cycle have the maximum contribution i.e. **22.37 %** and **21.50 %** respectively because pulsing parameters in conjunction with Ar-He gases increases the control of heat input, which is the most prominent factors for getting highly optimized weld bead geometry.

Helium has high ionization potential which increases the weld bead penetration for getting better bead geometry and the improvement in the weld bead geometry parameters directly improves the mechanical properties of the welds. The improvements in the bead geometry properties by using Ar plus He gas mixtures can be easily seen by comparing the results in Table 5.01 (for AA6061 without gas mixture) and Table 5.21 ((for AA7039 with gas mixtures), and similar results were concluded by Reichelt et al [7], Marya et al [8] and Kuk et al [70].

In this investigation, the pulse current of 210 A, base current of 120 A, pulse frequency of 150 Hz, pulse duty cycle of 90% and 30% of He in Ar-He gas mixture resulted the optimum values of bead geometry. The confirmation test conducted with predicted levels of factors proved to be worthy.

### **5.6.2 Mechanical Properties – Experimental Results and Analysis**

The experiments were conducted as per the parameters values decided in Table 4.6 and experimental layout in orthogonal array L25 as shown in Table 4.7. Tensile specimens of required dimension as per ASTM E8M were separated out from welded coupon plates [173] and tests were carried out on 400 KN computer controlled Universal Testing Machine. The specimens were loaded at the rate of 1.5 KN/min as per ASTM specifications, so that the tensile specimen undergoes deformation. All specimens finally fail after necking and the load vs displacement profile was recorded. Higher the tensile properties have better quality characteristics.

At the same time for microhardness measurement, samples of transverse cross-section of joint were taken from the weld coupons. The specimens for microstructural characterization were mechanically polished using 220, 320, 400, 600 and 1000 grit waterproof SiC emery papers and alumina grade-II paste. Microhardness tests were carried out on a Leco Digital Microhardness Tester with 50 gf load and 15 second dwell time incorporated with diamond indenter. Final polishing was carried out using 3 and 1  $\mu\text{m}$  diamond paste.

To reveal the macrostructures of the welded sample, deep etching technique using 10% HF acid was used. However, for further revealing of microstructures, Keller's reagent was used as etchants. Olympus make metallurgical microscope coupled with Image Analysis system was used for the microstructural characterization.

The results of the mechanical properties – ultimate tensile strength (UTS), microhardness of weld zone and percentage elongation are tabulated in Table 5.26 and almost all properties are inferior to the parent metal. All tensile specimens fractured at weld joint, therefore their mechanical properties correspond to that of weld joint. For optimizing the process parameters, four quality characteristics have to be considered for a single characteristic. The weighted response of mechanical properties is obtained by adding weights to the responses as a single quality characteristic.

**Table 5.26: Experimental results for mechanical properties of AA7039  
with gas mixtures**

| <b>Experiment No</b> | <b>Ultimate Tensile Strength MPa</b> | <b>Microhardness VPN</b> | <b>Elongation Percentage</b> |
|----------------------|--------------------------------------|--------------------------|------------------------------|
| <b>01</b>            | 324.09                               | 113.2                    | 4.42                         |
| <b>02</b>            | 338.53                               | 104.1                    | 7.78                         |
| <b>03</b>            | 328.36                               | 120.6                    | 5.28                         |
| <b>04</b>            | 348.24                               | 103.2                    | 7.32                         |
| <b>05</b>            | 338.53                               | 099.2                    | 7.80                         |
| <b>06</b>            | 339.51                               | 108.5                    | 6.96                         |
| <b>07</b>            | 340.74                               | 107.2                    | 6.58                         |
| <b>08</b>            | 345.91                               | 110.7                    | 6.10                         |
| <b>09</b>            | 342.96                               | 116.3                    | 6.88                         |
| <b>10</b>            | 350.29                               | 104.1                    | 7.52                         |
| <b>11</b>            | 336.10                               | 120.1                    | 7.98                         |
| <b>12</b>            | 308.78                               | 118.1                    | 4.62                         |
| <b>13</b>            | 336.10                               | 117.6                    | 4.08                         |
| <b>14</b>            | 319.88                               | 105.8                    | 5.96                         |
| <b>15</b>            | 344.75                               | 118.4                    | 7.42                         |
| <b>16</b>            | 337.55                               | 103.2                    | 6.00                         |
| <b>17</b>            | 331.60                               | 111.6                    | 5.84                         |
| <b>18</b>            | 347.96                               | 118.7                    | 7.02                         |
| <b>19</b>            | 349.39                               | 119.7                    | 7.22                         |
| <b>20</b>            | 341.60                               | 127.6                    | 6.74                         |
| <b>21</b>            | 335.12                               | 103.2                    | 6.82                         |
| <b>22</b>            | 361.97                               | 106.6                    | 8.42                         |
| <b>23</b>            | 339.22                               | 105.0                    | 7.36                         |
| <b>24</b>            | 340.65                               | 112.8                    | 6.42                         |
| <b>25</b>            | 331.95                               | 117.8                    | 6.94                         |

In this optimisation, AHP (Analytical Hierarchy Process) was used for analysing the weights of different parameters of mechanical properties after taking the comparative importance value of each parameter by three experts

in the field of welding technology [164]. After calculation of relative importance values, the weights for UTS, microhardness and percentage elongation are selected as 0.796, 0.160 and 0.044 respectively. The weightage response is tabulated in Table 5.27.

**ANOVA** is most important tool for calculating responsible factors, which significantly affects mechanical properties. For determining these affect on process parameters, F-test was performed. Results of ANOVA and percentage contributions by each process parameters are tabulated in Table 5.28. Response graphs (Fig 5.60) are drawn from response table indicated Table 5.29, to identify the significant levels of each factor.

**Table 5.27: Weighted response for mechanical properties of AA7039 with gas mixtures**

| Exp No | Weighted Response | Exp No | Weighted Response | Exp No | Weighted Response | Exp No | Weighted Response |
|--------|-------------------|--------|-------------------|--------|-------------------|--------|-------------------|
| 1.     | 225.59            | 8.     | 238.23            | 15.    | 239.78            | 22.    | 247.06            |
| 2.     | 232.24            | 9.     | 238.07            | 16.    | 231.17            | 23.    | 232.84            |
| 3.     | 230.26            | 10.    | 239.26            | 17.    | 229.85            | 24.    | 235.68            |
| 4.     | 237.76            | 11.    | 235.12            | 18.    | 241.74            | 25     | 231.88            |
| 5.     | 230.92            | 12.    | 217.76            | 19.    | 242.89            |        |                   |
| 6.     | 233.91            | 13.    | 233.94            | 20.    | 240.29            |        |                   |
| 7.     | 234..25           | 14.    | 221.27            | 21.    | 229.82            |        |                   |

**Table 5.28: Results of analysis of variance (ANOVA) for mechanical properties of AA7039 with gas mixtures**

| Symbol | Welding parameter             | Deg of freedom | Sum of square | Mean square | F     | Contributed percentage |
|--------|-------------------------------|----------------|---------------|-------------|-------|------------------------|
| P      | Pulse Current                 | 4              | 356.41        | 89.10       | 3.613 | <b>34.46</b>           |
| B      | Base Current                  | 4              | 111.12        | 27.78       | 1.126 | 10.74                  |
| F      | Pulse Frequency               | 4              | 70.82         | 17.70       | 0.718 | 06.85                  |
| T      | Pulse Duty Cycle              | 4              | 148.04        | 37.01       | 1.501 | 14.31                  |
| X      | Percentage of Helium in Argon | 4              | 249.39        | 62.35       | 2.528 | 24.11                  |
| Error  |                               | 4              | 98.65         | 24.66       |       | 09.54                  |
| Total  |                               | 24             | 1034.43       | 258.60      |       |                        |

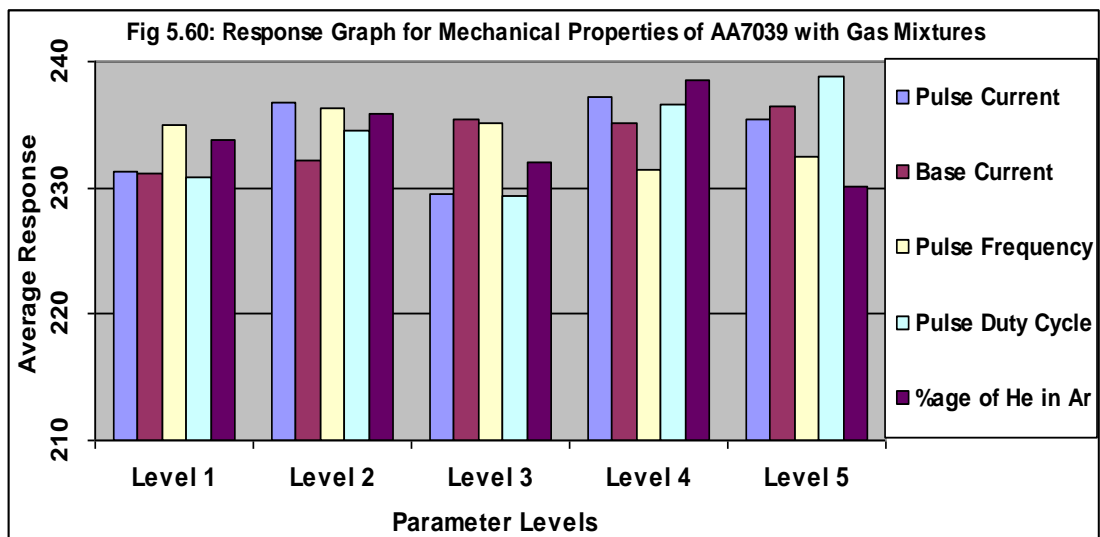
**Table 5.29: Response table for mechanical properties of AA7039 with gas mixtures**

| Symbol | Welding parameter             | Level 1 | Level 2       | Level 3 | Level 4       | Level 5       |
|--------|-------------------------------|---------|---------------|---------|---------------|---------------|
| P      | Pulse Current                 | 231.35  | 236.74        | 229.57  | <b>237.19</b> | 235.46        |
| B      | Base Current                  | 231.12  | 232.23        | 235.40  | 235.13        | <b>236.43</b> |
| F      | Pulse Frequency               | 234.98  | <b>236.33</b> | 235.12  | 231.36        | 232.52        |
| T      | Pulse Duty Cycle              | 230.91  | 234.46        | 229.43  | 236.67        | <b>238.84</b> |
| X      | Percentage of Helium in Argon | 233.83  | 235.81        | 231.99  | <b>238.59</b> | 230.09        |

**Table 5.30: Confirmation test results for mechanical properties of AA7039 with gas mixtures**

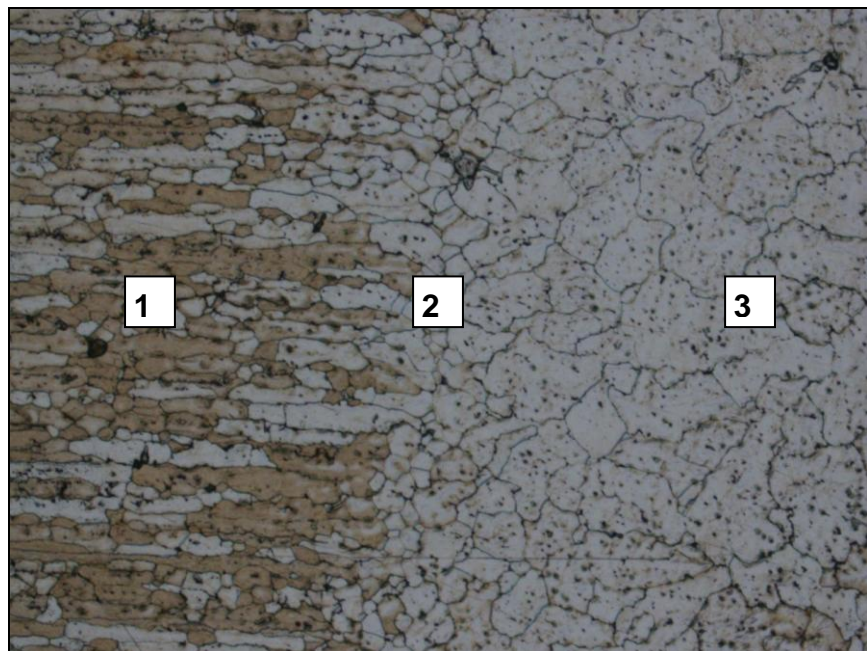
| Optimum Response     | Optimal level of process parameters | UTS MPa | Microhardness VPN | Elongation percentage |
|----------------------|-------------------------------------|---------|-------------------|-----------------------|
| Predicted Experiment | P4-B5-F2-T5-X4<br>P4-B5-F2-T5-X4    | 354.38  | 130.7             | 8.48                  |

**Confirmation Test:** Optimal level of process parameters was predicted using response graph and ANOVA. Process parameters and their levels which affect mechanical properties are pulse current at level 4, background current at level 5, pulse frequency at level 2, pulse duty cycle at level 5 and percentage of Helium in Argon at level 4. The obtained results were verified for the improvement in multiple quality characteristics by conducting a confirmation test based on results obtained in Table 5.30.



ANOVA calculations shown in Table 5.28 and Response Graph in Fig 5.60, shows that pulse current, base current, pulse duty cycle, pulse frequency and percentage of He in Ar-He mixture plays significant role on microstructure and mechanical properties of welded Al alloy 7039, but pulse current plays the maximum role i.e. **34.46 %** because pulse parameters with argon-helium gas mixtures produces better weld bead geometry of deep penetration which directly related with the mechanical properties of weld joints.

In this investigation, pulse current of 155A, base current of 135A, pulse frequency of 75Hz, pulse duty cycle of 90% and 40% of He with Ar resulted in the maximum values of mechanical properties. It has been observed that the overall microhardness in the weld is lower than the parent metal due to as cast nature of the microstructure, which is characterized by coarse grains and lack of strengthening phases.



1. HAZ

2. Fusion Boundary

3. Weld Zone

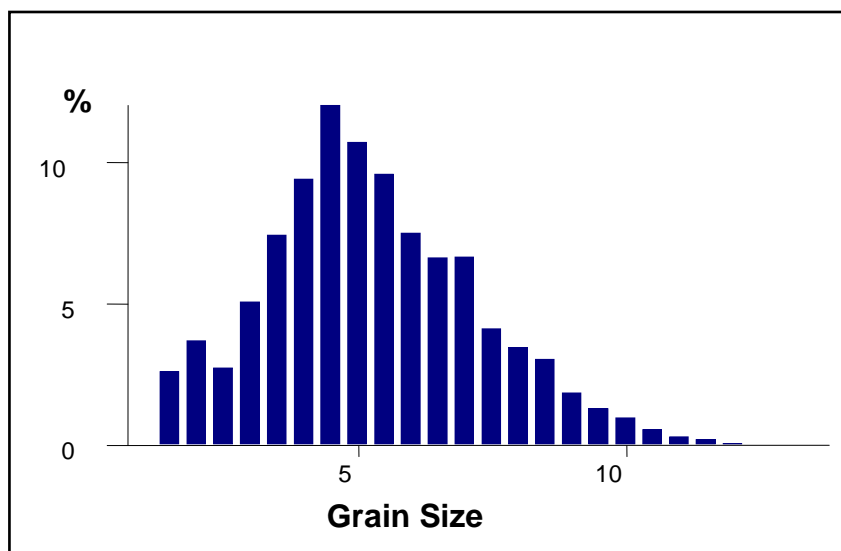
**Fig 5.61: Microstructure of welded AA7039 at HAZ, Fusion Boundary and Weld Zone**

Fig 5.61 shows the microstructure of HAZ, fusion boundary and weld zone of pulsed welded (with gas mixtures) AA7039. Coarse columnar grains of HAZ, fine equiaxed grains of fusion boundary and coarse cellular of weld zone are

clearly visible in this microstructure. Fig 5.62 shows the microstructure of the HAZ of welded AA7039, in which coarse columnar grains are also visible. Grain size analysis was done and plotted in Fig 5.63, which shows that majority of the grains lies in the size of grain size no 3 to 8. Fig 5.64 shows the microstructure of the weld zone, in which coarse grains are clearly visible. The majority of the grains are of grain size no 1 and around 40% grains are in the Grain size no 2 to 5 as shown in Fig 5.65.



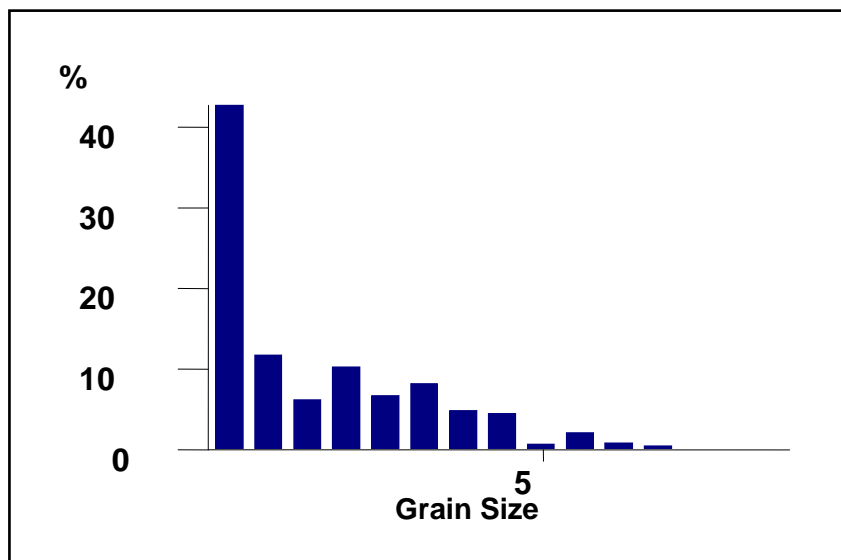
**Fig 5.62: Microstructure of HAZ of welded AA7039 (100x)**



**Fig 5.63: Grain Size (μm) Frequency Distribution of HAZ of welded AA7039**



**Fig 5.64: Microstructure of welded AA7039 at Weld Zone**



**Fig 5.65: Grain Size ( $\mu\text{m}$ ) Frequency Distribution of AA7039 at Weld Zone**

As earlier explained, the coarse grains are very much unfavorable for the mechanical properties of welds, because of this UTS and microhardness of the welded samples are inferior to the base metal. The detailed justification of deterioration of mechanical properties has been explained earlier in the experimentation of variation of microhardness.

## 5.7 Experimentation on Titanium Alloy Grade–5 with Gas Mixtures

### 5.7.1 Bead Geometry – Experimental Results and Analysis

The experiments were conducted as per the parameters values decided in Table 4.8 and experimental layout in orthogonal array L25 as shown in Table 4.7. The results were tabulated in Table 5.31. For optimizing the process parameters, four quality characteristics have to be considered for a single characteristic. The weighted response of bead geometry properties is obtained by adding weights to the responses as a single quality characteristic.

In this optimisation, AHP (Analytical Hierarchy Process) was used for analysing the weights of different parameters of weld bead geometry after taking the comparative importance value of each parameter by three experts in the field of welding technology [172]. After calculation of relative importance values, the weights for bead penetration, bead width and bead height are selected as 0.64, 0.254 and 0.106 respectively. The weightage response is tabulated in Table 5.32.

**Table 5.31: Experimental results for the bead geometry of Ti Alloy Gr–5**

| S. No | Penetration (p) mm | Width (b) mm | Height (h) mm | S. No | Penetration (p) mm | Width (b) mm | Height (h) mm |
|-------|--------------------|--------------|---------------|-------|--------------------|--------------|---------------|
| 01.   | 0.41               | 6.06         | 0.96          | 14.   | 0.91               | 7.74         | 1.18          |
| 02.   | 0.43               | 6.19         | 1.01          | 15.   | 0.88               | 7.02         | 1.08          |
| 03.   | 0.49               | 7.77         | 1.03          | 16.   | 0.82               | 8.18         | 1.72          |
| 04.   | 0.62               | 7.93         | 1.52          | 17.   | 0.77               | 7.68         | 1.06          |
| 05.   | 0.61               | 8.56         | 1.33          | 18.   | 0.92               | 7.67         | 1.52          |
| 06.   | 0.71               | 8.64         | 1.39          | 19.   | 0.98               | 6.62         | 1.25          |
| 07.   | 0.79               | 8.58         | 1.74          | 20.   | 0.73               | 6.80         | 1.30          |
| 08.   | 0.81               | 7.97         | 1.08          | 21.   | 0.86               | 8.17         | 1.44          |
| 09.   | 0.63               | 7.31         | 1.33          | 22.   | 1.02               | 8.14         | 1.22          |
| 10.   | 0.82               | 7.62         | 1.68          | 23.   | 0.81               | 7.63         | 1.44          |
| 11.   | 0.77               | 7.12         | 1.26          | 24.   | 0.87               | 7.14         | 1.14          |
| 12.   | 0.67               | 8.16         | 1.48          | 25.   | 0.99               | 6.64         | 1.06          |
| 13.   | 0.74               | 7.08         | 1.08          |       |                    |              |               |

**Table 5.32: Weighted response for bead geometry of Ti Alloy Grade-5**

| Exp No | Weighted Response | Exp No | Weighted Response | Exp No | Weighted Response | Exp No | Weighted Response |
|--------|-------------------|--------|-------------------|--------|-------------------|--------|-------------------|
| 1.     | 1.904             | 8.     | 2.657             | 15.    | 2.461             | 22.    | 2.850             |
| 2.     | 1.956             | 9.     | 2.402             | 16.    | 2.789             | 23.    | 2.609             |
| 3.     | 2.397             | 10.    | 2.640             | 17.    | 2.560             | 24.    | 2.491             |
| 4.     | 2.574             | 11.    | 2.435             | 18.    | 2.698             | 25     | 2.434             |
| 5.     | 2.706             | 12.    | 2.658             | 19.    | 2.440             |        |                   |
| 6.     | 2.796             | 13.    | 2.386             | 20.    | 2.332             |        |                   |
| 7.     | 2.869             | 14.    | 2.670             | 21.    | 2.778             |        |                   |

**Table 5.33: Results of analysis of variance for bead geometry of Ti Alloy Gr-5**

| Symbol | Welding parameter             | Deg of freedom | Sum of square | Mean square | F      | Contributed percentage |
|--------|-------------------------------|----------------|---------------|-------------|--------|------------------------|
| P      | Pulse Current                 | 4              | 0.0935        | 0.0234      | 2.292  | 06.70                  |
| B      | Base Current                  | 4              | 0.2436        | 0.0609      | 5.971  | 17.46                  |
| F      | Pulse Frequency               | 4              | 0.2929        | 0.0732      | 7.178  | 20.99                  |
| T      | Pulse Duty Cycle              | 4              | 0.2156        | 0.0539      | 5.283  | 15.46                  |
| X      | Percentage of Helium in Argon | 4              | 0.5085        | 0.1271      | 12.463 | <b>36.45</b>           |
| Error  |                               | 4              | 0.0408        | 0.0102      |        | 02.93                  |
| Total  |                               | 24             | 1.3949        | 0.3487      | 33.187 |                        |

**Table 5.34: Response table for the weld bead properties of Ti Alloy Gr - 5**

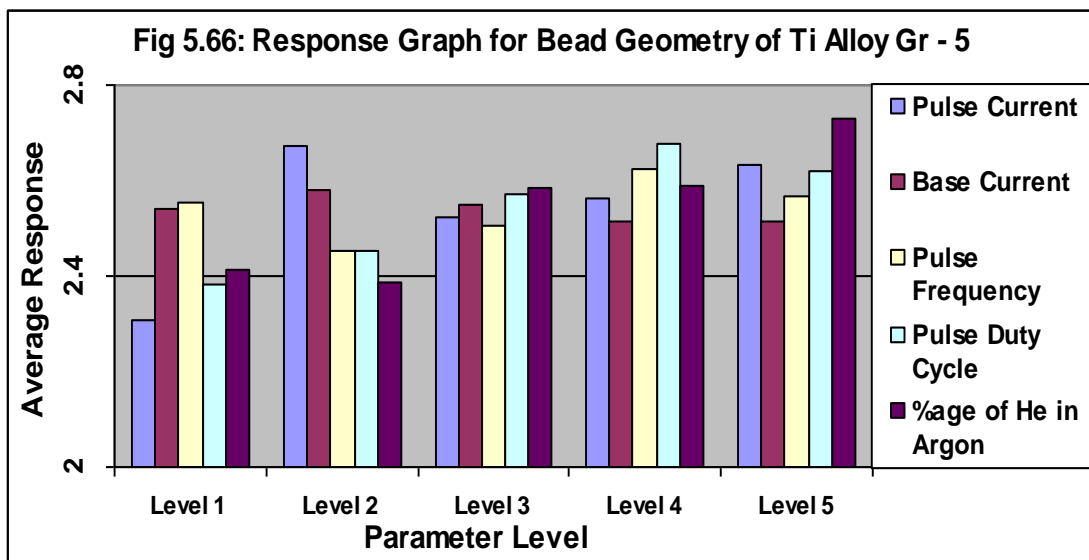
| Symbol | Welding parameter             | Level 1 | Level 2      | Level 3 | Level 4      | Level 5      |
|--------|-------------------------------|---------|--------------|---------|--------------|--------------|
| P      | Pulse Current                 | 2.307   | <b>2.673</b> | 2.522   | 2.564        | 2.632        |
| B      | Base Current                  | 2.541   | <b>2.579</b> | 2.549   | 2.515        | 2.515        |
| F      | Pulse Frequency               | 2.552   | 2.452        | 2.505   | <b>2.622</b> | 2.566        |
| T      | Pulse Duty Cycle              | 2.381   | 2.452        | 2.571   | <b>2.676</b> | 2.618        |
| X      | Percentage of Helium in Argon | 2.415   | 2.385        | 2.583   | 2.588        | <b>2.729</b> |

**ANOVA** is the most important tool for calculating the responsible factors which significantly affects the bead geometry properties. For determining the significant affecting process parameters, F-test was performed. The results of ANOVA and the percentage contribution by each of the process parameters are presented in Table 5.33. Response graph (Fig 5.66) is drawn from Response Table 5.34, to identify the significant levels of each factor.

The optimal level of process parameters were predicted by using the response graph and ANOVA. The process parameters and their levels which affect the weld bead geometry are pulse current at level 2, background current at level 2, pulse frequency at level 4, pulse duty cycle at level 4 and percentage of helium in argon at level 5. The obtained result was verified by conducting a confirmation test results obtained in Table 5.35.

**Table 5.35: Confirmation test results for the weld bead properties of Ti Alloy Gr - 5**

| Optimum Response | Optimal level of process parameters | Penetration (p) mm | Bead width (b) mm | Bead height (h) mm |
|------------------|-------------------------------------|--------------------|-------------------|--------------------|
| Predicted        | P2-B2-F4-T4-X5                      |                    |                   |                    |
| Experiment       | P2-B2-F4-T4-X5                      | 1.04               | 8.71              | 1.77               |



On the basis of the results in Tables 5.31 to 5.35 and Fig 5.66, it has been observed that pulse current, base current, pulse frequency and pulse duty cycle plays an important role for optimising the weld bead geometries but the

parameter, percentage of helium in Ar-He gas mixture has the maximum contribution i.e. **36.45 %** because Ar-He mixture as shielding gas increases the control of heat input. The oscillating nature of current and periodic variations of arc forces in combination of Ar-He gas mixtures produce good quality of weld bead geometry with higher depth to width ratio, which directly influence the mechanical properties of weld joints of Ti alloys.

In this investigation, the pulse current of 110 A, background current of 60 A, pulse frequency of 125 Hz, pulse duty cycle of 70% and 50% of helium with argon resulted in the maximum values of bead geometry. The confirmation test conducted with predicted levels of factors proved to be effective and worthy.

### **5.7.2 Mechanical Properties – Experimental Results and Analysis**

The experiments were conducted as per the parameters values decided in Table 4.8 and experimental layout in orthogonal array L25 as shown in Table 4.7. Tensile specimens of required dimension as per ASTM E8M were separated out from welded coupon plates [173] and tests were carried out on 400 KN computer controlled Universal Testing Machine. The specimens were loaded at the rate of 1.5 KN/min as per ASTM specifications, so that the tensile specimen undergoes deformation. All specimens finally fail after necking and the load vs displacement profile was recorded. Higher the tensile properties have better quality characteristics.

At the same time for microhardness measurement, samples of transverse cross-section of joint were taken from the weld coupons. The specimens for microstructural characterization were mechanically polished using 220, 320, 400, 600 and 1000 grit waterproof SiC emery papers and alumina grade-II paste. Microhardness tests were carried out on a Leco Digital Microhardness Tester with 100 gf load and 15 second dwell time with diamond indenter.

Final polishing was carried out using 3 and 1  $\mu\text{m}$  diamond paste. To reveal the macrostructures of the welded sample, deep etching technique with potassium permanganate and hydrofluoric acid were used. However, for

further revealing of microstructures, kroll solution (H<sub>2</sub>O–100 ml, HF–3 ml and HNO<sub>3</sub>–5 ml) was used as etchants. Olympus make metallurgical microscope coupled with Image Analysis system was used for the microstructural characterization of the weldment.

**Table 5.36: Experimental results for mechanical properties of Ti Alloy Gr – 5**

| <b>Experiment No</b> | <b>Ultimate Tensile Strength MPa</b> | <b>Microhardness VPN</b> | <b>Elongation Percentage</b> |
|----------------------|--------------------------------------|--------------------------|------------------------------|
| <b>01</b>            | 1017.71                              | 368.0                    | 1.22                         |
| <b>02</b>            | 1152.86                              | 347.1                    | 2.00                         |
| <b>03</b>            | 1118.86                              | 335.8                    | 2.38                         |
| <b>04</b>            | 1107.29                              | 364.3                    | 2.58                         |
| <b>05</b>            | 1072.96                              | 352.5                    | 2.66                         |
| <b>06</b>            | 1128.91                              | 349.2                    | 3.56                         |
| <b>07</b>            | 1132.79                              | 341.9                    | 4.06                         |
| <b>08</b>            | 1103.40                              | 352.7                    | 5.08                         |
| <b>09</b>            | 1178.78                              | 331.4                    | 6.32                         |
| <b>10</b>            | 1078.99                              | 342.6                    | 4.32                         |
| <b>11</b>            | 1195.12                              | 358.1                    | 2.74                         |
| <b>12</b>            | 1101.61                              | 344.7                    | 5.84                         |
| <b>13</b>            | 1130.69                              | 328.9                    | 6.92                         |
| <b>14</b>            | 1104.45                              | 368.1                    | 2.86                         |
| <b>15</b>            | 1244.05                              | 342.5                    | 5.64                         |
| <b>16</b>            | 1024.28                              | 351.2                    | 4.54                         |
| <b>17</b>            | 1134.82                              | 344.8                    | 5.52                         |
| <b>18</b>            | 1207.19                              | 325.7                    | 6.36                         |
| <b>19</b>            | 1179.13                              | 336.7                    | 2.60                         |
| <b>20</b>            | 1193.76                              | 329.5                    | 6.86                         |
| <b>21</b>            | 1167.60                              | 347.2                    | 3.00                         |
| <b>22</b>            | 1170.75                              | 345.7                    | 5.66                         |
| <b>23</b>            | 1068.34                              | 350.3                    | 4.98                         |
| <b>24</b>            | 1145.34                              | 347.2                    | 5.02                         |
| <b>25</b>            | 1169.22                              | 324.9                    | 6.50                         |

The results of the mechanical properties – ultimate tensile strength (UTS), microhardness of weld zone and percentage elongation are tabulated in Table 5.36. All tensile specimens fractured at weld joint, therefore their mechanical properties correspond to that of weld joint. For optimizing the process parameters, four quality characteristics have to be considered for a single characteristic. The weighted response of mechanical properties is obtained by adding weights to the responses as a single quality characteristic.

In this optimisation, AHP (Analytical Hierarchy Process) was used for analysing the weights of different parameters of mechanical properties after taking the comparative importance value of each parameter by three experts in the field of welding technology [172]. After calculation of relative importance values, the weights for UTS, microhardness and percentage elongation are selected as 0.796, 0.160 and 0.044 respectively. The weightage response is tabulated in Table 5.37.

**Table 5.37: Weighted response for mechanical properties of Ti Alloy Gr – 5**

| Exp No | Weighted Response | Exp No | Weighted Response | Exp No | Weighted Response | Exp No | Weighted Response |
|--------|-------------------|--------|-------------------|--------|-------------------|--------|-------------------|
| 1.     | 710.15            | 8.     | 757.93            | 15.    | 839.64            | 22.    | 796.53            |
| 2.     | 785.67            | 9.     | 797.57            | 16.    | 709.98            | 23.    | 736.23            |
| 3.     | 762.29            | 10.    | 814.12            | 17.    | 774.71            | 24.    | 781.60            |
| 4.     | 763.07            | 11.    | 754.79            | 18.    | 813.08            | 25.    | 790.10            |
| 5.     | 739.30            | 12.    | 768.12            | 19.    | 798.73            |        |                   |
| 6.     | 772.09            | 13.    | 762.43            | 20.    | 806.12            |        |                   |
| 7.     | 772.52            | 14.    | 814.12            | 21.    | 794.69            |        |                   |

**ANOVA** is most important tool for calculating responsible factors, which significantly affects mechanical properties. For determining these affect on process parameters, F-test was performed. Results of ANOVA and the percentage contributions by each process parameters are tabulated in Table 5.38. Response graph (Fig 5.67) is drawn from response table indicated Table 5.39, to identify the significant levels of each factor.

**Table 5.38: Results of ANOVA for mechanical properties of Ti Alloy Gr–5**

| Symbol | Welding parameter             | Deg of freedom | Sum of square | Mean square | F     | Contributed percentage |
|--------|-------------------------------|----------------|---------------|-------------|-------|------------------------|
| P      | Pulse Current                 | 4              | 5880.84       | 1470.21     | 2.760 | <b>24.48</b>           |
| B      | Base Current                  | 4              | 4234.40       | 1058.60     | 1.987 | 17.63                  |
| F      | Pulse Frequency               | 4              | 5608.92       | 1402.23     | 2.632 | 23.35                  |
| T      | Pulse Duty Cycle              | 4              | 2177.37       | 0544.34     | 1.022 | 09.07                  |
| X      | Percentage of Helium in Argon | 4              | 3987.85       | 0996.96     | 1.872 | 16.60                  |
| Error  |                               | 4              | 2130.74       | 0532.69     |       | 08.87                  |
| Total  |                               | 24             | 24020.12      |             |       |                        |

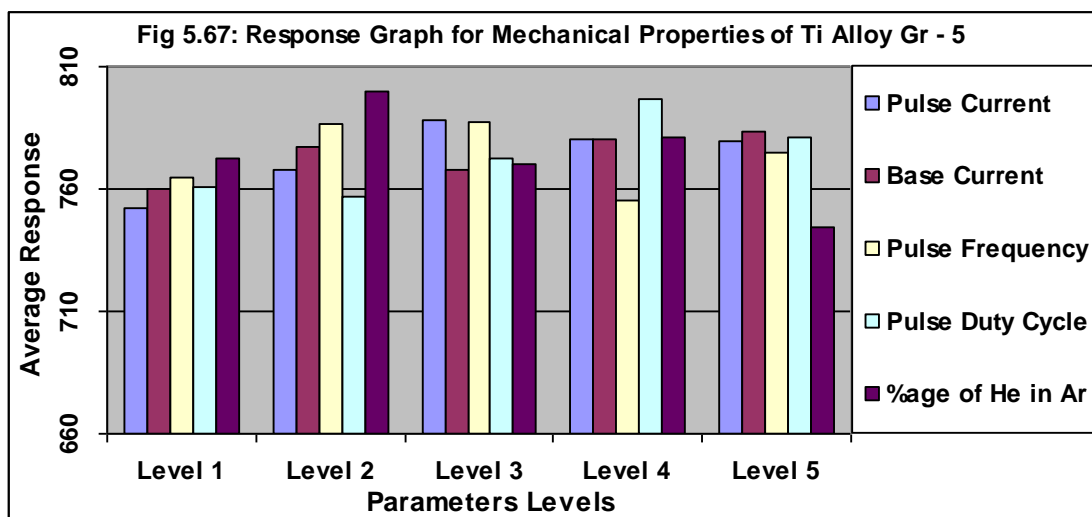
**Table 5.39: Response table for mechanical properties of Ti Alloy Grade – 5**

| Symbol | Welding parameter             | Level 1 | Level 2       | Level 3       | Level 4       | Level 5       |
|--------|-------------------------------|---------|---------------|---------------|---------------|---------------|
| P      | Pulse Current                 | 752.10  | 768.11        | <b>787.82</b> | 780.52        | 779.83        |
| B      | Base Current                  | 760.21  | 776.84        | 767.53        | 780.68        | <b>783.12</b> |
| F      | Pulse Frequency               | 764.53  | 786.47        | <b>787.33</b> | 755.17        | 774.88        |
| T      | Pulse Duty Cycle              | 760.97  | 757.17        | 772.32        | <b>796.60</b> | 781.32        |
| X      | Percentage of Helium in Argon | 772.81  | <b>800.11</b> | 770.19        | 781.19        | 744.09        |

**Table 5.40: Confirmation test results for mechanical properties of Ti Alloy Grade–5**

| Optimum Response | Optimal level of process parameters | UTS MPa | Microhardness VPN | Elongation %age |
|------------------|-------------------------------------|---------|-------------------|-----------------|
| Predicted        | P3–B5–F3–T4–X2                      |         |                   |                 |
| Experiment       | P3–B5–F3–T4–X2                      | 1247.27 | 372.3             | 7.04            |

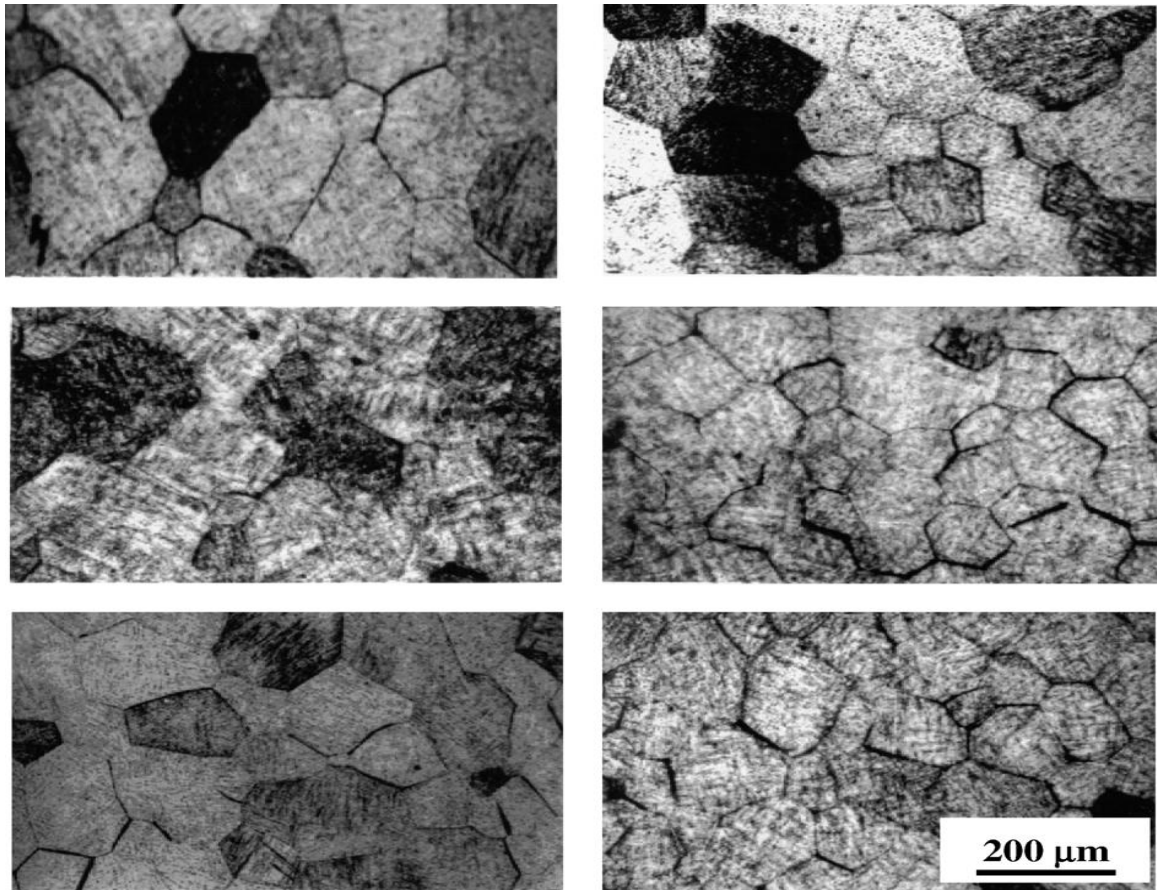
**Confirmation Test:** Optimal level of process parameters was predicted using response graph and ANOVA. Process parameters and their levels which affect mechanical properties are pulse current at level 3, background current at level 5, pulse frequency at level 3, pulse duty cycle at level 4 and percentage of Helium in Argon at level 2. The obtained results were verified for the improvement in multiple quality characteristics by conducting a confirmation test based on results obtained in Table 5.40 and the microstructures of the welded Ti alloy grade-5 are shown in Fig 5.68.



On the basis of the results in Tables 5.36 to 5.40 and Fig 5.67, it has been observed that pulse current, base current and pulse duty cycle plays an important role for optimising the mechanical properties but the parameter, pulse current and pulse frequency have the maximum contribution i.e. **24.48%** and **23.35%** respectively because pulse parameters with Ar-He gas mixtures produces good quality of weld bead which directly affects the mechanical properties of the weld joints. From the results of welded joints of Ti alloys as shown in Table 5.36, it has been observed that tensile strength and microhardness of all samples are greater than the parent metal.

In this investigation, the pulse current of 120 A, background current of 90 A, pulse frequency of 100 Hz, pulse duty cycle of 70% and 20% of helium with argon resulted in the maximum values of mechanical properties. The confirmation test conducted with predicted levels of factors proved to be effective and worthy.

From the microstructures of the fusion zone exhibited in Fig 5.68, it has been observed that the microstructure at the fusion zone of the pulse GTA welded Ti alloy consist of acicular  $\alpha$  and needle like martensite  $\alpha'$ . This has lead to a significant increase in microhardness (upto 372 VHN) in the weld zone and the same was reported by Arenas et al [156]. The welds exhibit equiaxed grain morphology due to the pulsing nature of the current in contrast to the columnar grain morphology in continuous current welding.



**Fig 5.68: Optical micrographs of Ti Alloy Grade-5 at Fusion Zones**

## **Chapter 6**

### **CONCLUSIONS AND SCOPE FOR THE FUTURE STUDY**

#### **A. CONCLUSIONS**

In this experimental study of pulsed GTAW process, it can be concluded from various ANOVA results and weighted response graphs / tables of AA6061, AA7039 and Ti alloy Grade-5 that pulse parameters with argon / argon-helium gas mixtures plays a significant role in optimizing the bead geometry characteristics and mechanical properties of the weld joints. The combined effect of pulse parameters with argon / argon-helium gas mixture increases the control of heat input by oscillating nature of pulse current and periodic nature of the arc forces, which refines the microstructure and improve the weld strength.

#### **6.1 Aluminium Alloy 7039 (Without Pulsing)**

Following conclusions can be drawn after studying the bead geometry and microhardness profile of GTA welded (without pulsing) 6.0mm thick aluminium alloy 7039 in the range of current from 90 to 180 A and frequency of 50 to 200 Hz with 99.99% pure argon shielding gas and sinusoidal AC balanced wave:

- (1) Width of weld bead slightly increases with increase in current at constant frequency i.e. higher heat input and decreases with increase in frequency at constant current due to radiation and convection losses of heat at higher frequencies.
- (2) Penetration of weld bead increases with increase in current and slightly increases with increase in frequency due to increase in heat input.
- (3) The low microhardness of the weld zone can be attributed due to as-cast nature of microstructure with coarse grains and the maximum microhardness is achieved in the fusion boundary due to presence of small equiaxed grains.
- (4) The microhardness reduces in the particular area of the HAZ (normally called as Soft Zone) due to grain coarsening and over-ageing.

## **6.2 Aluminium Alloy 7039 (With Pulsing)**

Following conclusions can be drawn after studying the bead geometry and microhardness profile of pulsed GTA welded 6.0mm thick aluminium alloy 7039 in the range of pulse current from 125 to 220 A, base current from 40 to 120 A, pulse frequency of 50 to 250 Hz and pulse duty cycle from 10 to 90% with 99.99% pure argon shielding gas and sinusoidal AC balanced wave:

(1) The penetration and penetration / width ratio increases with increase in the heat input i.e. pulse parameters like pulse currents, base currents, pulse frequencies and pulse duty cycles, due to agitating / stirring nature of weld pool.

(2) The maximum microhardness is achieved in the fusion boundary because increase in super-cooling promotes the fine equixed grains, which have more grain boundaries and serve as an effective barrier to the movement of dislocations.

(3) The microhardness in the weld centre is lowest because as-cast nature of microstructures and growing of coarse grains.

(4) The microhardness reduces in the particular area of the HAZ (Soft Zone) due to dissolution and coarsening of main strengthening phase.

(5) Cyclic variations of energy heat input in pulse welding produces thermal fluctuations and results for the periodic interruptions in solidification, which refines the microstructure and increase the mechanical properties in comparison to continuous current welding.

## **6.3 Aluminium Alloy 6061**

Following conclusions can be drawn after studying the bead geometry and mechanical properties of pulsed GTA welded 5.0mm thick aluminium alloy 6061 in the range of pulse current from 120 to 150 A, base current from 80 to 110 A, pulse frequency of 50 to 125 Hz and pulse duty cycle from 30 to 75% with 99.99% pure argon shielding gas and sinusoidal AC balanced wave:

(1) The pulse current of 150 A, base current of 110 A, pulse frequency of 50 Hz and pulse duty cycle of 75% results the maximum values of bead

geometry. Pulse frequency does not play significant role in optimizing the bead geometries.

(2) The pulse current of 120A, base current of 80A, pulse frequency of 50Hz and pulse duty cycle of 75% resulted in the maximum values of mechanical properties.

#### **6.4 Aluminium Alloy 6061 with Gas Mixtures**

Following conclusions can be drawn after studying the bead geometry and mechanical properties of pulsed GTA welded 5.0mm thick AA6061 in the range of pulse current from 150 to 210 A, base current from 75 to 135 A, pulse frequency of 50 to 150 Hz, pulse duty cycle from 30 to 90% and 10 to 50 % of helium in argon shielding gas with sinusoidal AC balanced wave:

(1) The pulse current of 195 A, base current of 135 A, pulse frequency of 50 Hz, pulse duty cycle of 90% and 40% of helium with argon resulted in the maximum values of bead geometry.

(2) In this investigation, pulse current of 165A, base current of 135A, pulse frequency of 125Hz, pulse duty cycle of 45% and 30% of helium with argon resulted in the maximum values of mechanical properties.

#### **6.5 Aluminium Alloy 7039 with Gas Mixtures**

Following conclusions can be drawn after studying the bead geometry and mechanical properties of pulsed GTA welded 5.0mm thick AA7039 in the range of pulse current from 150 to 210 A, base current from 75 to 135 A, pulse frequency of 50 to 150 Hz, pulse duty cycle from 30 to 90% and 10 to 50 % of helium in argon shielding gas with sinusoidal AC balanced wave:

(1) The pulse current of 210 A, base current of 120 A, pulse frequency of 150 Hz, pulse duty cycle of 90% and 30% of helium with argon resulted in the optimum values of bead geometry.

(2) The pulse current of 155A, base current of 135A, pulse frequency of 75 Hz, pulse duty cycle of 90% and 40% of He with Ar resulted in the maximum values of mechanical properties.

(3) The overall microhardness in the weld is lower than the parent metal due to as cast nature of the microstructure, which is characterized by coarse grains.

(4) Fusion boundary of welded AA7039 has fine and equiaxed grains of very small size. The HAZ is having coarse grains of larger size, which are the main cause of deterioration of weld joint properties.

## **6.6 Titanium Alloy Grade – 5 with Gas Mixtures**

Following conclusions can be drawn after studying the bead geometry and mechanical properties of pulsed GTA welded 2.5 mm thick Ti Alloy Grade-5 in the range of pulse current from 100 to 140 A, base current from 50 to 90 A, pulse frequency of 50 to 150 Hz, pulse duty cycle from 40 to 80% and 10 to 50 % of helium in argon shielding gas with sinusoidal AC balanced wave:

(1) The pulse current of 110 A, base current of 60 A, pulse frequency of 125 Hz, pulse duty cycle of 70% and 50% of helium with argon resulted in the maximum values of bead geometry.

(2) The pulse current of 120 A, base current of 90 A, pulse frequency of 100 Hz, pulse duty cycle of 70% and 20% of helium with argon resulted in the maximum values of mechanical properties. The welds exhibit equiaxed grain due to the pulsing nature of the current.

## **B. SCOPE FOR THE FUTURE STUDY**

(1) The present study was conducted for pulse parameters; pulse current, base current, pulse duty cycle and pulse frequency. Further experimentation can be done with various welding speeds, arc voltages, AC balance and gas flow rates on AA7039, AA6061 and Ti alloy Gr-5.

(2) Similar study can be done with the new developed series of various aluminium, magnesium and titanium alloys.

## REFERENCES

01. Wareing A. J, "Control of TIG welding in practice", Welding and Metal Fabrication, Nov / Dec 1988, pp 375 – 380.
02. Koi, S and Tsai, M. C, "Thermal analysis of GTAW electrodes", Welding Journal, 1985 64(9), pp 266s – 269s.
03. Viklas, E.P, "Pulsed current and its applications", Welding Journal, 1970, 49(4), pp 255 – 262.
04. Campbell, R.D and Lecoursiere, E.J, "A guide to the use of tungsten electrode for GTAW", Welding Journal, 1995, 74(1) pp 39 – 45.
05. Mukhopadhyay, G. L, "Shielding gases for GMA & GTA welding ", Indian Welding Journal 26 (4), 1993, pp 225 – 230.
06. Ellis, M.B.D and Spiller, K.R, "Gas shielded fusion welding of aluminium alloys", Welding and Metal Fabrication, Nov / Dec 1993, pp 441 – 444.
07. Reichelt, W.R, Evancho, J.W and Hoy, M.G, "Effect of shielding gas on GMA welding of aluminum", Welding Journal, 1980, 59(5) pp 147s – 155s.
08. Marya M, Edwards G.R and Liu S, "An investigation on the effects of gases in GTA welding of a wrought AZ80 magnesium alloy", Welding Journal, 2004, 83(7): pp 203s – 212s.
09. Bob, Y, "Shielding and purging gases: Making the right selection", Welding Journal, 1995 74(1) pp 47 – 49.
10. Yarmuch M.A.R and Patchett B.M, "Variable AC polarity GTAW fusion behavior in 5083 aluminum", Welding Journal, 2007, 86(7) 196s – 200s.
11. Gas tungsten-arc welding', Welding Handbook (AWS 1972, 6th Ed), Section 4, 69.53 – 69.60.
12. Mohamed AA, "Optimization of weld bead dimensions in GTAW of Al-Mg alloy", Materials and Manufacturing Processes, 2001, 16(5), 725 – 736.
13. Qi Y, Ju D, Quan H, and Liying H, "EBW, LBW and GTA Welding of Titanium Sheet", Material Science Engineering, 2000, A280: 177–181.
14. Simpson R.P, "Refinement of Weld Fusion Zones in Alpha-Beta Titanium Alloys", Welding Journal, 1997, 56, 67s.
15. Tarng Y.S and Yang W.H, "Optimization of the Weld Bead Geometry in GTAW by the Taguchi Method", International Journal of Advance Manufacturing Technology, 1998, 14, 549 – 554.
16. Juang S.C and Tarang Y.S, "Process Parameter Selection for Optimizing the Weld Pool Geometry in the TIG Welding of Stainless Steel", Journal of Material Process Technology, 2002, 122: pp 33 – 37.
17. Greenwood, Norman N.; Earnshaw, A. (1997), "Chemistry of the Elements" (2nd ed), Oxford: Butterworth-Heinemann, ISBN 0080379419, pp 217.
18. George J. Binczewski (1995). "The Point of a Monument: A History of the Aluminum Cap of the Washington Monument", JOM 47 (11): 20 – 25.
19. Sanders R.E, "Technology Innovation in aluminium Products", The Journal of the Minerals, 2001, 53 (2): pp 21 – 25.
20. Krebs, Robert E. "The History and Use of Our Earth's Chemical Elements: A Reference Guide" (2nd ed), 2006.
21. Gunther Brandt, Phil Heinz and Litz Dorn, "Pulsed Current GTAW using Transistorized Power sources", Welding and Cutting, June 1985, pp E93 – E96.

22. Janakiram, G.D, Mitra, T.K and Shankar, V, "Microstructural refinement through inoculation of type 7020 Al-Zn-Mg alloy welds and its effect on hot cracking and tensile property", *Journal of Material Process Technology*, 2003, 142 pp 174 – 181.
23. Yang Y.P, Dong P, Zhang J and Tian X, "A hot-cracking mitigation technique for welding High-Strength Aluminum Alloy", *Welding Journal*, 2000, 79(1), pp 9s – 17s.
24. Shore R.J and McCauley R.B, "Effects of porosity on high strength aluminum 7039, *Welding Journal*, 1970, 49(7): pp 311s – 321s.
25. Fujii H, Aoki Y and Nogi K, "Electron Beam, GTAW under microgravity, *Trans, JWRI*, 2001, 30(1): pp 105 – 109.
26. Jonsson P.G, Murphy A.B and Szekely J, "The influence of oxygen additions on argon-shielded GMAW processes", *Welding Journal*, 1995, 74(2), pp 48s – 58s.
27. Onsoien M, Peters R, Olson D.L and Liu S, "Effect of hydrogen in argon GTAW shielding gas: Arc characteristics and Bead morphology", *Welding Journal*, 1995, 74(1), pp 10s – 15s.
28. Senthil Kumar T, Balasubramanian V and Sanavullah M.Y, "Effect of pulsed current TIG welding parameters on tensile properties of AA6061 Aluminium alloy". *Indian Welding Society*, 2005: pp 29 – 39.
29. Balasubramanian M, Jayabalan V and Balasubramanian V, "Optimizing the pulsed current gas tungsten arc welding parameters", *Journal of Material Science and Technology*, 2006, 22(6): pp 821 – 825.
30. Balasubramanian M, Jayabalan V and Balasubramanian V, "A mathematical model to predict impact toughness of pulsed current GTA welded titanium alloy", *Journal of Advanced Manufacturing Technology*, 2008, 35: pp 852 – 858.
31. Balasubramanian M, Jayabalan V and Balasubramanian V, "Developing mathematical model to predict tensile properties of pulsed current GTA welded Ti-6Al-4V alloy", *Material Design*, 2008, 29(1): pp 92 – 97.
32. Kumar Pawan, Kohle K P, Ashutosh Som and Datta C K, "Optimization of Weld Bead Geometry for Pulsed GTAW Process for AA6061 by Taguchi Method" *International Journal of Manufacturing Technology and Industrial Research* 2010, 1(1), pp 39 – 44.
33. Kumar Pawan, Kohle K P, Kolhe P R and Datta C K, "Optimizing pulsed GTAW process parameters for bead geometry of titanium alloy using taguchi method " *Asian Science*, 2009, 4 (1-2), pp 78 – 82.
34. Kumar Pawan, Kohle K P, Ashutosh Som and Datta C K, "Optimization of bead geometry of GTAW Process for AA7039 using Ar + He gas mixtures" *Indian Welding*, 2009, 42 (4), pp 26 – 33.
35. Kumar Pawan and Datta C K, "Optimizing Pulsed GTAW Process parameters for bead geometry of Aluminium Alloy 6061 by Taguchi Method", *International Conference on Advances in Mechanical Engineering*, 2010, pp 397 - 401.
36. Becker, D.W and Adams, C.M, "Investigation of Pulsed GTA Welding parameters", *Welding journal*, 1978, 57(5): 134s to 138s.
37. Backer, D.W and Adams, (Jr.) C.M, "The role of pulsed TIG welding variables in solidification & grain refinement", *Welding journal* 1979, 58 (2): 67s – 75s.
38. Omar, A. A and Lundin, C.D, "Pulsed plasma – Pulsed GTAW arc: A study of the process variables", *Welding journal*, 1979, 58 (4): 97s to 105s.
39. Birman, U.I and Petrov, A.V, "Influence of weld metal solidification pattern on hot cracking during Pulsed GTAW", *Welding Production*, 1971, 06: pp 22 – 25.
40. Vainarman, A.E, "The argon shielded pulsed arc welding of Aluminium alloys". *Automatic Welding*, 1966, 07, pp 56 – 59.

41. Kazakov, Y. V, "Structure and properties of joints made by Pulsed Arc Welding between components of different thickness." *Automatic Welding*, 1969, 08: pp 30 – 32.
42. Bunchinski, V.N and Potapevaskii, A.G, "The pulsed arc welding of Kh 18 NIOT stainless steel". *Automatic welding*, 1965, 14: 34 to 38.
43. Ramesh, V.R, "Some recent innovations in TIG process", *Indian Welding Journal*, 1977, 9 (3): pp 88 to 96.
44. Karnad, S.S, "TIG and Pulsed TIG welding process – Equipments and Controls". *Tool and Alloy steels*, 1984, 18 (8): pp 225 – 231.
45. Balasubramanian V, Jayabalan V and Balasubramanian M, "Effect of current pulsing on tensile properties of titanium alloy", *Materials and Design*, 2008, 29: pp 1459 – 1466.
46. Sundaresan S, Janaki Ram G.D and Madhusudhan Reddy G, "Microstructural refinement of weld fusion zones in alpha-beta titanium alloy using pulsed current welding", *Material Science Engineering A*, 1999, 262: pp 88 – 100.
47. Sacks R.J, "Welding: Principles and Practices", Glencoe, Peoria, IL, 1981.
48. Jackson C.E and Shrubsall A.E, "Control of Penetration and melting ratio with welding technique", *Weld Journal*, 1953, 32(4). pp 172s-178s.
49. Caddle R.N, "The Influence of Physical properties on penetration in arc welding", *Trans of ASME, Journal of Engineering for industry*, 1967, 37(5) pp 328-332.
50. Cary. H.B, "Modern Welding Technology" 2<sup>nd</sup> edn. Prentice Hall, Englewood Cliffs, New Jersey. 1989, pp 120-164.
51. Kolhe K. P and Datta C.K, "Parametric study of SAW on mild steel", *Indian Weld Journal*, 2004, 37 (3 – 4) pp 43 – 53.
52. Gunnert H.V, "Penetrations and Travel Speed in Metal Arc Welding", *Weld Journal* 2001, 27, pp 542.
53. Saedi H.R and Unkel W, "Arc and weld pool behavior for pulsed current GTAW", *Weld Journal*, 1988, 67(11), pp 247s – 255s.
54. Kumar Rakesh, Diltthey Ulrich, Dwivedi D.K and Ghosh P.K, "Thin sheet welding of Al 6082 alloy by AC pulse-GMA and AC wave pulse-GMA welding", *Materials and Design*, 2009, 30(2): pp 306 – 303.
55. Kumar Pawan and Datta C K, "Influence of current & frequency on AA7039 using GTAW Process". *IIW – International Conference*, 2008, pp 997–1002.
56. Gurave H.S. and Stout R.D, "Solidification phenomenon in inert GMAW", *Welding Journal*, 1963, 42 (7) pp 298s – 310s.
57. Gunaraj V and Murugan N, "Prediction of heat-affected zone characteristics in SAW of structural steel pipes", *Welding Journal*, 2002, 81(11) pp 45s- 53s.
58. AWS Welding Handbook, 1976 Vol – 4, 7<sup>th</sup> Ed. Miami Florida, USA pp. 25-33 & 113-187.
59. Rewnwick B.G and Patchett B.M, "Operating Characteristics of the SAW Process", *Welding Journal*, 1976, 55(4) pp 69s – 76s.
60. Quintino. L and Allum C.J, "Pulsed GMAW: Interaction between process parameters – part 1", *Welding and Metal Fabrication*, 1984 (3) pp 85-87.
61. Rothwell A.B and Bonomo F, "Weldability of HSLA steels relation to pipeline welding", Paper presented at AWS 1976, 57 (5) Annual Meeting in St Louis, Missouri.
62. Houldcraft P.T, "Welding process and control parameters", 1997, Cambridge university press, London.
63. Cornu J, "Advanced welding system" Part – 2, IFS publication ltd, UK, 1988, pp 97–123 and 243.

64. Lancaster J.F, "Metallurgy of welding – 4<sup>th</sup> Ed, 1987, London, Allen and Unwin.
65. Konkak P.J and Koons G.F, "Optimization of parameters for two wires AC SAW", *Welding Journal*, 1978, 57(12), pp 367s – 374s.
66. Jenney C.L and O'Brien A, "AWS Welding Handbook – 1", 2001, 9<sup>th</sup> edn.
67. Ko S.H, Choi S.K and Yoo C.D, "Effects of surface depression on pool convection and geometry in stationary GTAW", *Welding Research Supplement*, 2001, 80(2) pp 39s – 45s.
68. Balasubramanian M, Jayabalan V & Balasubramanian V, "Optimizing the Pulsed Current GTAW Parameters to Attain Maximum Impact Toughness", *Materials and Manufacturing Processes*, 2008, 23, pp 69–73.
69. Leitner R.E, McElhinney H, Pruitt E.I, "An investigation of Pulsed welding variables. *Welding Journal*, 52(9), 1973, pp 405s – 410s.
70. Kuk, J.M, Jang, K.C, Lee, D.G and Kin, I.S, "Effects of temperatures and shielding gas mixtures on fatigue life of 5083 aluminium alloy", *Journal of Materials Processing Technology*, 2004, 155 & 156, pp 1408 – 1414.
71. Goyal V.K, Ghosh P.K and Saini J.S, "Analytical studies on thermal behavior and geometry of weld pool in pulsed current gas metal arc welding", *Journal of Materials Processing Technology*, 2009, 209(3): pp 1318 – 1336.
72. Esme U, Kokangul A, Bayramoglu M and Geren N, "Mathematical modeling for prediction and optimization of TIG welding pool geometry", *Metalurgija*, 2009, 48(2): pp 109 – 112.
73. Moulton J.A and Weckman D.C, "Double-sided arc welding of AA5182-O Al sheet for Tailor Welded Blank applications" *Welding Journal*, 2010, 89(1): pp 11s – 23s.
74. Zhang Y.M and Zhang S.B, "Double-sided arc welding increases joint penetration", *Welding Journal*, 1998, 77(6): pp 57s – 61s.
75. Zhang Y.M and Zhang S.B, "Welding aluminum alloy 6061 with the opposing dual-torch GTAW process", *Welding Journal*, 1999, 78(6): 202-s to 206-s.
76. Zhang Y.M, Pan C and Male A.T, "Solidification behavior of Al-Mg aluminum alloy using double-sided arc welding process", *Journal of Materials Science Letters*, 2000, 19(10): 831–833.
77. Zhang Y.M, Pan C and Male A.T, "Improved microstructure and properties of AA6061 weldments using a double-sided arc welding process" *Metallurgical and Materials Transactions A*, 2000, 31(10): 2537–2543.
78. Zhang Y.M, Pan C and Male A.T, "Welding of austenitic stainless steel using a double-sided arc welding process", *Material Science and Technology*, 2001, 17(10): 1280–1284.
79. Zhang Y.M, Zhang S.B and Jiang M, "Keyhole double-sided arc welding process", *Welding Journal*, 2002, 81(11): pp 249s – 255s.
80. Kotecki D.J, Cheever D.L and Howden D.G, "Mechanism of ripple formation during weld solidification", *Welding Journal*, 1972, 51(8): pp 386s – 391s.
81. Renwick R.J and Richardson R.W, "Experimental investigation of GTA weld pool oscillations", *Welding Journal*, 1983, 62(2): pp 29s – 35s.
82. Deam R, "Weld pool frequency: A new way to define weld procedure", *Conference proceedings, 2<sup>nd</sup> International conference on Trends in welding research*, May 1989, Gatlinburg USA, ASM International, pp 967 – 971.
83. Sorensen C.D and Eager T.W, "Modelling of oscillation in partially penetrated weld pools", *Journal of Dynamic Systems, Measurement and Control*, 1990, 112: pp 469 - 474.

84. Xiao Y.Z and den Ouden. G, "A study of weld pool oscillation", *Welding Journal*, 1990, 69(8), pp 289s – 283s.
85. Giridharan P.K and Murugan N, "Optimization of pulsed GTAW process parameters for the welding of AISI 304L stainless steel sheets", *International Journal of Advance Manufacturing Technology*, 2009, 40, 478 – 489.
86. Balasubramanian M, Jayabalan V and Balasubramanian V, "Prediction and optimization of pulsed Current GTAW process parameters to obtain sound weld pool geometry in titanium alloy using Lexicographic method", *Journal of Materials Engineering and Performance*, 2008, 18(7): pp 871 – 877.
87. Matsuda F, et al, "Solidification crack susceptibility of weld metal", *Conference proceedings on recent trends in welding science and technology*, Gatlinburg, USA 1989, pp 127.
88. Katayama S, et al, "Laser weldability of Al alloys", *Conference proceedings on recent trends in welding science and technology*, Gatlinburg, USA, 1989, pp 687.
89. Aluminium and aluminium alloys, *ASM specialty handbook*, ASM international, Materials Park, OH, 1994.
90. Huang, C and Kou, S, "Liquation cracking in full-penetration Al-Cu Welds", *Welding Journal*, 2004, 83(2) pp 50s – 58s.
91. Gupta, R.K and Narayanmurty, S.V.S, "Analysis of crack in aluminium alloy AA2219 weldment", *Engineering Failure Analysis*, 2006, 13, pp 1370 – 1375.
92. Judas J.H and Collins F.R, "Preventing weld cracks in high strength aluminium alloys", *Welding Journal*, 1966, 45, pp 241s – 249s.
93. Guitterez L.A, Neye G and Zschech, "Microstructure, hardness profile and tensile strength in welds of AA6013-T6 extrusions", *Welding Journal*, 1996, 75(4), pp 115s–121s.
94. Mondolfo L.F, "Aluminium Alloys—Structure and Properties", Butterworths, London, 1997.
95. Tveiten Bard Wathne et al, "Fatigue life enhancement of aluminium joints through mechanical and thermal pre-stressing", 2006, 28(12): pp 1667 – 1676.
96. Padmanabham G, Schaper M, Pandey S and Simmchen E, "Tensile and fracture behavior of pulsed GMA welded Al-Cu-Li", *Welding Journal*, 2007, 86(6): pp 147s – 160s.
97. Myhr O.R, Grong H.J, Fjaer H.G and Marioara C.D, "Modeling of the microstructure and strength evolution in Al–Mg–Si alloys during multistage thermal processing", *Acta Materialia*, 2004, 17: pp 4999 – 5008.
98. Gaofeng Fu, Fuquan Tian and Hong Wang, "Studies on softening of heat affected zone of pulsed current GMA welded Al–Zn–Mg alloy", *Journal of Materials Processing Technology*, 2006, 180: pp 216 – 220.
99. Barbosa C, Dille, Delplancke J.L, Rebello J.M.A and Acselrad O, "A microstructural study of flash welded and aged 6061 and 6013 aluminum alloys" *Materials Characterization*, 2006, 57, pp 187–192.
100. Kumar Pawan, Kohle K P and Datta C K, "Process optimization in joining Aluminium Alloy 7039 using TIG Arc welding process" *International Journal of Agricultural Engineering*, 2009, 2(2), pp 202 – 206.
101. Kumar Pawan, Kohle K P and Datta C K, "Influence of pulse parameters on microhardness of welded AA7039 using the GTAW Process". *International Journal of Manufacturing Technology & Research*, 2009, 5 (3 – 4).
102. Kumar Pawan and Datta C K, "Influence of current & frequency on AA7039 using GTAW Process". *IIW – International Conference*, 2008, pp 997–1002.

103. Preston, R.V, Shercliff, H.R, Withers, P.J and Smith, S, "Physically-based constitutive modeling of residual stress development in welding of aluminium alloy 2024", *Acta Mater*, 2004, 52(17), pp 4973 – 4983.
104. Senthilkumar. T, Balasubramanian. V and Sanavullah. M.Y, "Influences of pulse current TIG welding parameters on the tensile properties of AA6061", *Materials & Design*, 2007, 28(7) pp 2080 – 2092.
105. Geoffroy N, Vittecoq E, Birr A, Mestralb F.de and Martinc J.M, "Fatigue behavior of an arc welded Al–Si–Mg Alloy", *Scripta Materialia*, 2007, 57: pp 349 – 352.
106. Luijendijk T. "Welding of dissimilar aluminium alloys", *Journal of Materials Processing Technology*, 2000, 103(7) pp 29 – 35.
107. Gambrell S.C and Kavikondala Kishen, "Contraction ratios in thick aluminium welded joints", *Welding Journal*, 1996, 75(4), pp 109s – 114s.
108. Kumar A and Sundarrajan S, "Optimization of pulsed TIG welding process parameters on mechanical properties of AA 5456 Aluminum alloy weldments", *Materials and Design*, 2009, 30(4): pp 1288 – 1297.
109. Kumar A, Shailesh P and Sundarrajan S, "Optimization of magnetic arc oscillation process parameters on mechanical properties of AA 5456 Aluminum alloy weldments", *Materials and Design*, 2009, 29: pp 1904 – 1913.
110. Koteswara Rao et al, "GTA welded AA2219 alloy using scandium containing fillers – mechanical and corrosion behavior", *Transactions of the Indian Institute of Metals*, 2004, 57(5): pp 451 – 459.
111. Huang Ji-Wu, Yin Zhi-min and Lex Xue-feng, "Microstructure and properties of 7A52 Al alloy welded joint", *Trans. of Non-ferrous Metals, Society of China*, 2008, 18: 804 – 808.
112. Squillace A, De Fenzo A, Giorleo G and Bellucci F, "A comparison between FSW and TIG welding techniques: modifications of microstructure and pitting corrosion resistance in AA 2024-T3 butt joints", *Journal of Materials Processing Technology*, 2004, 152: pp 97 – 105.
113. Owen, R.A, Preston, R.V, Withers, P.J, Shercliff, H.R and Webster, P.J, "Neutron and synchrotron measurements of residual strain in TIG welded Al alloy 2024" *Materials Science and Engineering A346* (2003) 159\_ 167.
114. Balasubramanian V, Ravisankar V and Madhusudhan Reddy. G, "Influences of pulsed current welding and post weld aging treatment on fatigue crack growth behavior of AA7075 joints", *International Journal of Fatigue*, 2008, 30(3), pp 405 – 416.
115. Balasubramanian V, Ravisankar V and Madhusudhan Reddy. G, "Effect of pulsed current welding on fatigue behavior of high strength aluminium alloy joints", *Materials and Design*, 2008, 29(2), pp 492 – 500.
116. Ghosh P.K, and Sharma Vijay, "Chemical composition and microstructure in pulsed MIG welded Al–Zn–Mg alloy", *Journal of Material Transaction*, 1991, 32: pp 145 – 150.
117. Potluri N.B, Ghosh P.K, Gupta P.C and Reddy Y.S, "Studies on weld metal characteristics and their influences on tensile and fatigue properties of pulsed current GMA welded Al–Zn–Mg alloy", *Welding Journal Research Suppl*, 1996, 75, 62s – 70s.
118. Lin, D.C, Wang, T. S and Srivatsan, T.S, "A mechanism for the formation of equiaxed grains of Al - Li alloy 2090", *Material Science Engineering*, 2003, 335 pp 304 – 309.
119. Balasubramanian V, Ravisankar V and Madhusudhan Reddy G, "Effect of pulsed current and post weld aging treatment on tensile properties of argon arc welded high strength aluminium alloy", *Materials Science and Engineering A*, 2007, 459: pp 19 – 34.
120. Kou, S, "Welding Metallurgy", 2nd ed. New York, NY: John Wiley and Sons, 151, 160 – 163 & 303 – 339.

121. Norman, A.F, Drazhner, V and Prangnell, P.B, "Effect of welding parameter on the solidification microstructure of autogenous TIG welds in an Al–Cu–Mg–Mn alloy", *Material Science Engineering A*, 1999, 259, pp 53 – 64.
122. Myhr, O.R, Klokkehaug, S, Fjær, F.G, Grong, O and Klucken, A.O, "Modelling of microstructure evolution and residual stresses in processing and welding of 6082 and 7108 aluminium alloys", *Proc. 5th International Conference on "Trends in Welding Research"*, Atlanta (Georgia), 1998, Published - ASM International (1999), pp. 233-238.
123. Myhr, O.R, Klokkehaug, S, Fjær, F.G, Grong, O and Klucken, A.O, "Modelling of microstructure evolution, residual stresses and distortions in 6082-T6 aluminium weldments", *Welding Journal*, 1998, 77, 286s-292s.
124. Prasad Rao K, Ramanaiah N and Viswanathan N, "Partially melted zone cracking in AA6061 welds", *Materials and Design*, 2008, 29: pp 179–186.
125. Huang C, Kou S and Purins J.R, "Liquation, solidification, segregation and hot cracking in the partially melted zone of Al - 4.5 Cu welds", *Proceedings of Merton C. Flemings Symposium on Solidification Processing*, ed. 2001.
126. Huang C and Kou S, "Partially melted zone in aluminum welds — liquation mechanism and directional solidification", *Welding Journal*, 2000, 79(5): pp 113s – 120s.
127. Huang C and Kou S, "Liquation mechanisms in multicomponent aluminum alloys during welding. *Welding Journal*, 2002, 81(10): pp 211s – 222s.
128. Huang C and Kou S, "Partially melted zone in aluminum welds – planar and cellular solidification", *Welding Journal*, 2001, 80(2): pp 46s – 53s.
129. Huang C and Kou S, "Partially melted zone in aluminum welds – solute segregation and mechanical behavior", *Welding Journal*, 2001, 80(1): pp 9s – 17s.
130. Huang C and Kou S, "Liquation cracking in full – penetration Al-Cu welds", *Welding Journal*, 2004, 83(4): pp 111s – 122s.
131. Huang C and Kou S, "Liquation cracking in partial – penetration aluminium welds", *Welding Journal*, 2003, 82(7): pp 184s – 194s.
132. Srinivasa Rao K, Madhusudan Reddy G and Prasad Rao K, "Studies on partially melted zone in Al–Cu alloy welds—effect of techniques and prior thermal temper", *Materials Science and Engineering A*, 2005, 403: pp 69 – 76.
133. ASM International handbook, "Corrosion of Weldments", 2006 (#05182G). (1–12).
134. Reddy G.M, Gokhale A.A and Prasad Rao K, "Optimization of pulse frequency in pulsed current GTAW of aluminium – lithium alloy sheets", *Journal of Material Science & Technology*, 1998; Vol 14, pp 61–66.
135. Rajesh Manti, Dwivedi D.K & Agarwal A, "Microstructure and hardness of Al-Mg-Si weldments produced by pulse GTAW", *International Journal of Advance Manufacturing Technology*, 2008, 36: 263 – 269.
136. Madhusudhan Reddy G, Gokhale A.A and Prasad Rao K, "Weld microstructure refinement in a 1441 grade aluminium–lithium alloy" *Journal of Material Science*, 1997, 32(15): pp 4117 – 4126.
137. Mohandoss T and Madhusudhan Reddy G and Prasad Rao K, *International Journal for Joining of Materials*, 1998, 98 – 107.
138. Kim H.T and Nam S.W, "Study on the solidification cracking", *Scripta Materialia*, 1996, 34(7), pp 1139 – 1145.
139. G. Madhusudhan Reddy, T. Mohandoss, K. Prasad Rao, *Science and Technology of Welding & Joining*, 2005, 10.

140. Shinoda. T, Ueno. Y and Masumoto. I, "Effects of pulsed welding current on solidification cracking in austenitic stainless steel welds", Trans Japanese Welding Society, 1990, 21 pp 18 – 23.
141. Madhusudan. Reddy. G, "Welding of Aluminium and alloys", In: Proceedings of ISTE summer school on 'Recent Developments in Materials Joining' Annamalai University, 2001.
142. Kou S and Le Y, "Nucleation mechanism and grain refining of weld metal", Welding Journal, 1986, 65: pp 65 – 70.
143. Prasad Rao K, "Fusion zone grain refinement in GTA welds using magnetic arc oscillation and current pulsing", Proceedings of National Conference on Recent Advances in Materials Processing, Annamalai Nagar, India, 2001, pp. 176–196.
144. Pao P.S, Gill S.J and Feng C.R, "On fatigue crack initiation from corrosion pits in 7075 – T7351 aluminium alloy", Scripta Materialia, 2000, 43(5): pp 391 - 396.
145. David SA and Vitek JM, "Correlation between solidification parameters and weld microstructures", International Material Reviews, 1989, 34: pp 213 – 245.
146. Dwivedi D.K, "Influence of modifier and grain refiner on solidification behaviour and mechanical properties of cast Al-Si base alloys", Institution of Engineers (I), 2002, 83: pp 46 – 50.
147. Rao S.R.K, Madhusudhan Reddy G, Kamraj M and Rao K.P, "Grain refinement through arc manipulation techniques in Al-Cu alloy GTA welds", Material Science and Engineering A, 2005, 404: pp 227 – 234.
148. Aidun D.K & Dean J.P, 1999. "Effect of enhanced convection on the microstructure of Al-Cu- Li welds", Welding Journal, 1999, 78 (9) pp 394s – 354s.
149. Linert T.J, Tellwag W.L Jr, Grimmer B.B & Waree R.W, "Friction Stir Welding studies on mild steel, Welding Journal, 2003, 80(8) pp 1s – 9s.
150. Gianetto J.A, Smith N.J & Bowker J.T, "Effect of the composition and energy on the structure and properties of high strength weld metal", Welding Journal, 1992.
151. Mendes da Silva Celina Leal and Scotti Americo, "The influence of double pulse on porosity formation in aluminum GMAW", Journal of Materials Processing Technology, 2006, 171: pp 366 – 372.
152. Grossbeck M.L, King J.F and Hoelzer D.T, "Impurity effects on gas tungsten arc welds in V-Cr-Ti alloys", Journal of Nuclear Materials, 2000, 283 - 287(2): pp 1356 – 1360.
153. Mohandoss T and Madhusudhan. Reddy. G, "Effect of frequency of pulsing in GTA Welding on the microstructure and mechanical properties of titanium alloy welds", Journal of Material Science Lett, 1996, 15: pp 626 – 628.
154. Shelwatker D.A, Madhusudhan Reddy. G and Gokhale A.A, "GTAW studies on similar and dissimilar combinations of Al-Zn-Mg alloy RDE 40 and Al – Li alloy 1441", Science Technology Welding & Joining, 2002, 7(6): pp 352 – 361.
155. Balasubramanian V, Ravisankar V and Madhusudhan. Reddy. G, "Effect of pulsed current and post weld aging treatment on tensile properties of argon arc welded high strength aluminium alloy", Material Science Engineering, 2007, A459: pp19 – 34.
156. Arenas M.F and Acoff V.L, "Analysis of gamma titanium aluminide welds produced by GTAW", Welding Journal, 2003, 82(5): pp 110s – 115s.
157. Choi B.H and Choi B.K, "The effect of welding conditions according to mechanical properties of pure titanium" Journal of Materials Processing Technology, 2008, 201(1-3): pp 526 – 530.
158. Winco K.C, Yung B, Ralph W.B and Lee R. Fenn, "An investigation into welding parameters affecting the tensile properties of titanium welds", Journal of Materials Processing Technology, 1997, 63(1-3): pp 759 – 764.

159. Balasubramanian M, Jayabalan V and Balasubramanian V, "Effect of microstructure on impact toughness of pulsed current GTA welded  $\alpha$ - $\beta$  titanium alloy", *Materials Letters*, 2008, 62: pp 1102 – 1106.
160. Wei Zhou and Chew K.G, "Effects of welding on impact toughness of butt joints in titanium alloy", *Materials Science and Engineering A*, 2003, 347, 180–185.
161. Inoue H and Ogawa T, "Weld cracking and solidification behavior of titanium alloys", *Welding Journal*, 1995, 74(1), pp 21s – 27s.
162. Keshava Murthy and Sundaresan S, "Fracture toughness of Ti-6Al-4V after welding and post weld heat treatment, *Welding Journal*, 1997, 76(2), pp 81s – 91s.
163. Balasubramanian M, Jayabalan V and Balasubramanian V, "Process parameter optimization of the pulsed current argon tungsten arc welding of titanium alloy", *Journal of Material Science Technology*, 2008, 24(3): pp 423 – 426.
164. Balasubramanian M, Jayabalan V and Balasubramanian V, "Effect of pulsed GTAW on corrosion behavior of Ti-6Al-4V titanium alloy", *Materials and Design*, 2008, 29: pp 1359 – 1363.
165. Karimzadeh F, Heidarbeigy M and Saatchi A, "Effect of heat treatment on corrosion behavior of Ti-6Al-4V alloy weldments", *Journal of Materials Processing Technology*, 2008, 206: pp 388 – 394.
166. Wang S.H and Wei M.S, "Tensile properties of GTA weldments in commercially pure Ti, Ti-6Al-4V and Ti-15V-3Al-3Sn-3Cr alloys at different strain rates", *Science and Technology of Welding and Joining*, 2004, 9(5): 415 – 422.
167. Acoff V.L, Thompson R.G, Griffin R.D and Radhakrishanan B, "Effect of post PWHT on Ti-14%Al-21%Nb fusion zone structure and hardness", *Welding Journal*, 1995, 74(1), pp 1s – 9s.
168. Ravishankar, V and Balasubramanian, V, "Influences of pulsed current welding parameters on tensile strength and impact behavior of Al-Mg-Si alloy weldments", *Proceedings of international conference on IMPLAST*, New Delhi, 2003 pp 224 – 232.
169. Roy, R. K, "A primer on taguchi method" Chapter – 6, pp 100 – 142, Van Nostrand Reinhold, 1990.
170. Bryne, D. M and Taguchi, S, "The Taguchi approach to parameter design", *Quality Progress*, Dec 1987, pp 19 – 26.
171. Ross, Philip. J, "Taguchi techniques for quality engineering", McGraw Hill Book Company, New York, 1988.
172. "The Analytical Hierarchy Process" – Mc-Graw Hill, New York, 1980.
173. Annual Book of ASTM Standards (2004). Philadelphia (PA): American Society for Testing of Materials, 2004.
174. Bradley, G. R and James, M. N, "Geometry and Microstructure of MIG and Friction Stir welded Al alloy 5383 – H321", Oct 2000.
175. Qui L, Yang C.L, Lin S.B and Fan C.L, "Effect of pulse current on microstructure and mechanical properties of variable polarity arc weld bead of 2219-T6 Al alloy", *Materials Science and Technology*, 2009, 25(6), pp 739 – 742.
176. "Arc welding of non-ferrous metals", 2011, 4<sup>th</sup> Edition Chapter 2, Kobe Steel Ltd, Japan.
177. Sindo Kou, "Welding Metallurgy", 2<sup>nd</sup> Edition Chapter–14 & 15, pp 343 – 374.